



A computational approach to motivated behaviour and apathy.

Thesis submitted for the degree of Doctor of Philosophy.

Dr Akshay Nair

Institute of Neurology,
University College London.

(2021)

Declaration of Authorship:

I, Dr Akshay Nair, confirm that the work presented in this thesis is my own. Where information has been derived from other sources, I confirm that this has been indicated in the thesis.

Supervisors:

- Prof. Sarah Tabrizi, Head of Department of the Huntington's Research Centre and Joint Head of the Department of Neurodegenerative Diseases, UCL. *(Primary)*
- Prof. Geraint Rees, Dean of the UCL Faculty of Life Sciences and Professor of Cognitive Neurology, Institute of Cognitive Neuroscience, UCL. *(Primary)*
- Dr Robb Rutledge, Principal Research Associate, Max Planck Centre for Computational Psychiatry and Aging, UCL. *(Secondary)*

Acknowledgments:

In completing this work, I am grateful both for the opportunity to embark on a PhD and the support I received throughout it. Firstly, none of this work would have been possible without the many participants who took part in this research, in particular those who carry the HD gene. The engagement of this community with research was both eye opening and humbling. Secondly, I am most indebted to the Wolfson Foundation who kindly funded my fellowship.

In terms of support, I start with my supervisors: Robb Rutledge, Geraint Rees and Sarah Tabrizi. Robb's lab at the Max Planck was a rare opportunity for me to become embedded in the world of computational psychiatry, a theoretical approach which has changed my perspective of mental disorders. Robb himself was always generous with his time and an incisive problem-solver. At critical junctures during my fellowship, Geraint gave me both time and some of the best advice I have received during my time at UCL. Finally, Sarah can only be described as the embodiment of forward momentum. Her encouragement and support will stay with me long after my PhD is complete. What I perhaps am most grateful for is that my supervisors gave me intellectual freedom and encouraged me to develop my own ideas and experiments.

Although the work presented here is my own it would not have been possible without the help of a large number of colleagues, and friends, I met over the last four years. In terms of the Huntington's disease projects presented here I would like to thank Marina Papoutsis for endless imaging and statistical advice, Ahmed Aziz for advice on managing epidemiological data and Adeel Razi for supporting me through the world of dynamic causal modelling. More broadly, I would like to thank all the members of the HD-YAS, team many of whom I count as friends. On the Max Planck side, I would like to thank Bastien Blain for his help throughout my fellowship and the other members of the Rutledge lab who all at various points helped me to solve unexpected problems, usually with coding. I was also lucky enough to supervise two exceptional students during my PhD – Lesley Farrah-Dorwling-Carter and Fei Shang, both of whom helped me in various experiments.

Completing this thesis was at times gruelling and it simply would not have been possible without the endless support of my wife, Lee. The last four years have also seen the arrival of my two beautiful children: Kiran and Aria. Although the culprits responsible for much stolen sleep, this is offset by the boundless energy they bring and joy as we watch them grow. For these reasons I dedicate this work to my family.

Abstract: A computational approach to motivated behaviour and apathy

The loss of motivation and goal-directed behaviour is characteristic of apathy. Across a wide range of neuropsychiatric disorders, including Huntington's disease (HD), apathy is poorly understood, associated with significant morbidity, and is hard to treat. One of the challenges in understanding the neural basis of apathy is moving from phenomenology and behavioural dysfunction to neural circuits in a principled manner. The computational framework offers one such approach. I adopt this framework to better understand motivated behaviour and apathy in four complementary projects.

At the heart of many apathy formulations is impaired self-initiation of goal-directed behaviour. An influential computational theory proposes that "opportunity cost", the amount of reward we stand to lose by not taking actions per unit time, is a key variable in governing the timing of self-initiated behaviour. Using a novel task, I found that free-operant behaviour in healthy participants both in laboratory conditions and in online testing, conforms to predictions of this computational model. Furthermore, in both studies I found that in younger adults sensitivity to opportunity cost predicted behavioural apathy scores. Similar pilot results were found in a cohort of patients with HD. These data suggest that opportunity cost may be an important computational variable relevant for understanding a core feature of apathy – the timing of self-initiated behaviour.

In my second project, I used a reinforcement learning paradigm to probe for early dysfunction in a cohort of HD gene carriers approximately 25 years from clinical onset. Based on empirical data and computational models of basal ganglia function I predicted that asymmetry in learning from gains and losses may be an early feature of carrying the HD gene. As predicted, in this task fMRI study, HD gene carriers demonstrated an exaggerated neural response to gains as compared to losses. Gene carriers also differed in the neural response to expected value suggesting that carrying the HD gene is associated with altered processing of valence and value decades from onset.

Finally, based on neurocomputational models of basal ganglia pathway function, I tested the hypothesis that apathy in HD would be associated with the involvement of the *direct pathway*. Support for this hypothesis was found in two related projects. Firstly, using data from a large international HD cohort study, I found that apathy was associated with motor features of the disease thought to represent direct pathway involvement. Secondly, I tested this hypothesis *in vivo* using resting state fMRI data and a model of basal ganglia connectivity in a large peri-manifest HD cohort. In keeping with my predictions, whilst emerging motor signs were associated with changes in the indirect pathway, apathy scores were associated with connectivity changes in the direct pathway connectivity within my model.

For patients with apathy across neuropsychiatry there is an urgent need to understand the neural basis of motivated behaviour in order to develop novel therapies. In this thesis, I have used a computational

framework to develop and test a range of hypotheses to advance this understanding. In particular, I have focussed on the computational factors which drive us to self-initiate, their potential neural underpinnings and the relevance of these models for apathy in patients with HD. The data I present supports the hypothesis that opportunity cost and basal ganglia pathway connectivity may be two important components necessary to generate motivated behaviour and contribute to the development of apathy in HD.

Impact statement:

Apathy, the loss of motivation and goal-directed behaviour, is one of the most common, disabling and hard to treat symptoms in neuropsychiatry. The aim of this thesis was to develop a better understanding of this disabling symptom using a computational approach. This is a multi-level theoretical framework which can be used to connect psychological constructs, like motivation and apathy, to neural systems via the use of mathematical algorithms to model both brain and behaviour. In particular, I use this approach to study apathy in Huntington's disease (HD). HD is a genetic neurodegenerative disorder associated with motor, psychiatric and cognitive phenotypes. In HD, apathy affects nearly all patients, is found at all stages of the disease and shows a close relationship with disease progression.

I firstly consider a fundamental component of many descriptions of apathy – self-initiation. In this section I draw on computational theories of action initiation based on the concept of *opportunity cost*. Put simply, opportunity cost measures the amount of reward we stand to lose by not taking action. In my thesis, I developed a novel task in which I manipulated opportunity cost while allowing participants free choice over when to take action. In two experiments, I show that opportunity cost invigorates self-initiation for rewarding and non-rewarding tasks. Furthermore, I show for the first time, across two experiments, that sensitivity to changes in opportunity cost predict behavioural apathy scores in younger adults. Pilot data suggests that this task may be useful for understanding apathy in HD too.

Learning optimal behaviour is a key component of motivated behaviour and heavily involves the striatum, a part of the brain affected by HD. Leveraging this fact, in a separate experiment I completed an fMRI study investigating whether differences in learning from making gains or avoiding losses were different in healthy HD gene carriers, 25 years from disease onset. As predicted from RL models of striatal function, in this experiment I showed that HD gene carriers showed a bias toward gain versus loss learning in task fMRI data. Using computational modelling, I show this may be related to the coding of learnt value in HD gene carriers. This represents the earliest functional imaging difference between gene carriers and healthy controls.

In the final two chapters, I turn more squarely to apathy in manifest HD. Based on empirical findings and theoretical models, I hypothesised that apathy in HD may be driven by the involvement of the direct basal ganglia pathway – one of the key subcortical pathways controlling cortical activation. Although challenging to quantify directly, I found support for this hypothesis by making predictions of two types of data – epidemiological and resting state neuroimaging data. Firstly, I show for the first time in a large epidemiological dataset of HD patients that apathy is associated with motor signs associated with the involvement of the direct pathway. Secondly, using a sophisticated analysis pipeline I show that apathy in HD is associated with altered connectivity of the direct pathway, in a model of the basal ganglia circuitry in resting state fMRI data. Both of these results are also novel for the field.

By adopting a computational framework, I developed hypotheses by considering motivated behaviour and apathy across computational, algorithmic and neural implementation levels. The data I present suggests that opportunity cost may be an important computational variable in timing self-initiated behaviour and individual sensitivity to opportunity cost may predict motivational status. Furthermore, I argue that basal ganglia function and connectivity are an important component of the neural system underpinning motivated behaviour and disruption of basal ganglia function may contribute to the development of apathy in HD. It is my hope that these new insights improve our understanding of motivated behaviour and eventually lead to better, much needed, novel therapies for neuropsychiatric patients with apathy.

Table of Contents

LIST OF FIGURES:	11
LIST OF TABLES	12
CHAPTER 1: INTRODUCTION	13
1.1 OVERVIEW:	13
1.2 WHAT IS APATHY?	16
1.3 MOTIVATED BEHAVIOUR AS THE “MAXIMISATION OF NET REWARDS PER UNIT TIME THROUGH SELF-INITIATED ACTIONS”:	20
1.4 REINFORCEMENT LEARNING AS A FAMILY OF ALGORITHMS WELL SUITED TO MODELLING MOTIVATED BEHAVIOUR.....	22
1.5 THE INTERSECTION BETWEEN RL AND COGNITIVE NEUROSCIENCE	26
1.6 HD – CLINICAL FEATURES:.....	27
1.7 APATHY IN HD:	29
1.7.1 <i>Apathy in HD: epidemiology</i>	29
1.7.2 <i>Apathy in HD: cognitive and computational correlates</i>	30
1.7.3 <i>Apathy in HD: human neuroimaging</i>	30
1.7.4 <i>Apathy in HD: conclusion and hypotheses</i>	31
1.8 HYPOTHESIS 1: LOSS OF SENSITIVITY TO OPPORTUNITY COST CONTRIBUTES TO APATHY IN HD	33
1.9 HYPOTHESIS 2: THE RATIO OF DISRUPTION TO THE DIRECT, <i>VERSUS</i> INDIRECT, PATHWAY CELLS OF THE STRIATUM DRIVES A PROPORTION OF THE APATHY SEEN IN HD	36
1.9.1 <i>Huntington’s disease – aetiology:</i>	37
1.9.2 <i>Neuropathology of HD</i>	38
1.9.3 <i>Cortico-striatal connectivity</i>	41
1.9.4 <i>Dopamine receptors in the striatum</i>	42
1.9.5 <i>Striatal pathways and loops</i>	43
1.9.6 <i>RL models of the striatal function:</i>	46
1.9.7 <i>Implications for motivated behaviour and apathy in HD</i>	48
1.10 CONCLUSION:.....	51
CHAPTER 2: METHODS	53
2.1 COHORTS:	53
2.1.1 <i>Huntington’s Disease Young Adult Study (HD-YAS):</i>	54
2.2 APATHY SCALES:.....	57
2.2.1 <i>Apathy and Motivation Index (AMI):</i>	58
2.2.2 <i>Apathy Evaluation Scale:</i>	58
2.2.3 <i>Baltimore apathy scale (BAS):</i>	59
2.2.4 <i>Problem-Behaviour Assessment – Apathy:</i>	59
2.2.5 <i>A note on the measurement of apathy in HD</i>	60
2.3 fMRI PRINCIPLES:.....	60
2.3.1 <i>What does fMRI measure?</i>	61
2.3.2 <i>The BOLD signal:</i>	62
2.3.3 <i>fMRI pre-processing:</i>	64
2.4 CONCLUSION:.....	67
CHAPTER 3: STAYING HUNGRY - OPPORTUNITY COST DETERMINES FREE OPERANT ACTION INITIATION LATENCY AND BEHAVIOURAL APATHY SCORES	68
3.1 ABSTRACT:.....	68
3.2 INTRODUCTION:	69
3.2.1 <i>When should I act?</i>	69
3.2.2 <i>When as a decision problem with an optimal solution:</i>	70
3.2.3 <i>Choice of action latency – a gap in the theoretical market</i>	71
3.2.4 <i>Predictions from the opportunity cost theory</i>	74

3.2.5 'Motivation' as a function mapping outcome to utility	75
3.2.6 Data presented in this chapter:	75
3.3 METHODS:.....	76
3.3.1 Samples:.....	76
3.3.2 Questionnaire data:	76
3.3.3 Experiment (3) - Huntington's patients:	77
3.3.4 In-lab task description:	78
3.3.5 Changes for online version:.....	80
3.3.6 Changes to task for HD version:	80
3.3.7 Outcome measures:	81
3.3.8 Statistical analysis:.....	81
3.4 RESULTS:	83
3.4.1 Increased opportunity cost invigorates action initiation for rewarding actions:.....	84
3.4.2 Opportunity cost invigorated non-rewarding actions in healthy participants	85
3.4.3 Individual sensitivity to opportunity cost manipulation predicted task performance	86
3.4.4 Individual sensitivity to opportunity cost predicted behavioural apathy scores in younger adults	87
3.4.5 Individual sensitivity to opportunity cost predicted apathy scores in pilot cohort of patients with manifest HD.....	89
3.4.6 Computational modelling:	91
3.5 DISCUSSION:	92
3.6 CONCLUSION:.....	99
3.7 SUPPLEMENTARY MATERIAL	100
CHAPTER 4: ABERRANT STRIATAL VALUE REPRESENTATION IN HUNTINGTON'S DISEASE GENE CARRIERS 25 YEARS BEFORE ONSET	101
4.1 ABSTRACT:.....	101
4.2 INTRODUCTION	102
4.3 METHODS:.....	106
4.3.1 Participant details:	106
4.3.2 Task description:	107
4.3.3 Behavioural and computational analysis:.....	108
4.3.4 MRI acquisition:	110
4.3.5 Functional imaging pre-processing:	111
4.3.6 Principles to modelling with a General Linear Model.....	111
4.3.7 Dealing with the problem multiple comparisons.....	113
4.3.8 General Linear Models used and statistical details	115
4.3.9 Region of interest approach for replication analysis:	115
4.3.10 Region of interest for reward bias analysis:.....	117
4.3.11 Structural imaging processing:	118
4.4 RESULTS:	120
4.4.1 Sample demographics:.....	120
4.4.2 Task performance	122
4.4.3 Computational modelling of behaviour	124
4.4.4 Robust activation of fronto-striatal regions associated with task	125
4.4.5 Left ventral striatal reward bias at cue onset in gene carriers	127
4.4.6 Ventral striatal reward bias seen in striatal response to model-derived value estimates.....	128
4.4.7 More robust response to loss cues in controls:	129
4.4.8 Neural reward bias not correlated with disease burden score:	130
4.5 DISCUSSION	131
4.6 CONCLUSIONS	134
CHAPTER 5: RELATIONSHIP BETWEEN DISTINCT MOTOR SIGNS AND APATHY IN HUNTINGTON'S DISEASE: CLUES TO MECHANISM.	137
5.1 ABSTRACT:.....	137
5.2 INTRODUCTION:	138
5.3 METHODS:.....	141

5.3.1 Participants:	141
5.3.2 Statistical analysis with mixed effects models:	141
5.4 RESULTS:.....	145
5.4.1 Sample characteristics:	145
5.4.2 Relationship between apathy in HD and motor signs	146
5.4.3 Finger tapping speed and apathy	147
5.4.4 Cognitive processing speed and apathy:	147
5.4.5 Discussion:	148
5.4.6 Conclusion:.....	152
5.4.7 Supplementary figures:	153
5.4.8 Model (1) diagnostics: square root apathy and motor signs.....	153
5.4.9 Model (2) diagnostics: square root apathy and finger tapping.....	153
5.4.10 Model (3): square root apathy and processing speed.....	154
CHAPTER 6: IMBALANCED BASAL GANGLIA CONNECTIVITY IS ASSOCIATED WITH MOTOR DEFICITS AND APATHY IN HUNTINGTON'S DISEASE: FIRST EVIDENCE FROM HUMAN IN VIVO NEUROIMAGING	155
6.1 ABSTRACT:.....	155
6.2 INTRODUCTION:	157
6.3 METHODS:.....	162
6.3.1 Sample:	162
6.3.2 Clinical outcomes:	162
6.3.3 MRI data acquisition:	163
6.3.4 MRI pre-processing:	163
6.3.5 Analysis of resting state data:.....	164
6.3.6 Resting state fMRI modelling with GLM:	165
6.3.7 Dynamic causal modelling and specification of the connectivity matrix	167
6.3.8 Parametric empirical Bayes (PEB)	172
6.3.9 Hypothesis testing with Bayesian model reduction.	174
6.4 RESULTS:	176
6.4.1 Sample demographics:.....	176
6.4.2 Average connectivity parameters show a network suppressing motor cortex activity.....	178
6.4.3 Altered connectivity in components of the indirect pathway associated with total motor score.....	179
6.4.4 Altered connectivity in components of the direct pathway connectivity associated with apathy in gene carrier cohort.....	180
6.5 DISCUSSION:	181
6.6 CONCLUSIONS:.....	185
6.7 SUPPLEMENTARY ANALYSIS:	186
CHAPTER 7: CONCLUSIONS:.....	191
PUBLICATIONS:	197
REFERENCES:	198
CHAPTER 8: APPENDIX.....	214
8.1 HD-YAS ELIGIBILITY CRITERIA.....	214
8.1.1 Inclusion criteria	214
8.1.2 Exclusion criteria.....	214
8.2 TRACKON ELIGIBILITY CRITERIA	215
8.2.1 Inclusion Criteria.....	215
8.2.2 Exclusion Criteria.....	215

List of Figures:

FIGURE 1-1: PROCESS FOR GENERATING GOAL-DIRECTED BEHAVIOUR REPRODUCED FROM LEVY AND DUBOIS (2006).....	18
FIGURE 1-2: EXAMPLE OF SUB-COMPUTATIONS THAT MUST BE PERFORMED OPTIMALLY IN ORDER TO MAXIMISE NET REWARDS.....	21
FIGURE 1-3: APATHY IN HD SHOWS A CLOSE RELATIONSHIP WITH DISEASE PROGRESSION.	29
FIGURE 1-4: DIAGRAM OF NEUROPATHOLOGICAL VONSATTEL GRADING SYSTEM FOR HD SEVERITY.....	38
FIGURE 1-5: EFFECT OF HD ON FIBRE ABUNDANCE IN DIRECT AND INDIRECT PATHWAY.....	40
FIGURE 1-6: DIRECT AND INDIRECT PATHWAY CONNECTIVITY AND EFFECTS OF OPTOGENETIC STIMULATION.....	43
FIGURE 2-1: A. SCHEMATIC REPRESENTATION OF THE HRF	63
FIGURE 3-1: OVERVIEW OF FISHERMAN GAME DESIGN:	78
FIGURE 3-2: OPPORTUNITY COST INVIGORATES REWARDING ACTIONS:.....	84
FIGURE 3-3: OPPORTUNITY COST INVIGORATES NON-REWARDING ACTIONS.....	85
FIGURE 3-4: CORRELATION BETWEEN INDIVIDUAL SENSITIVITY TO ENVIRONMENT MANIPULATION (SUBJECT-LEVEL ENV. BETA FROM MIXED MODEL) AND THE DIFFERENCE IN MEAN LOG LATENCY OF ROD FIXING.	86
FIGURE 3-5: SENSITIVITY TO OPPORTUNITY COST CORRELATES WITH APATHY.....	87
FIGURE 3-6: HD TASK RESULTS (A) MEAN LATENCY OF HD GROUP (N = 19) PERFORMING THE FISHERMAN TASK (B) RELATIONSHIP BETWEEN PRICE BETA AND CLINICAL APATHY (AS MEASURED BY AES).	90
FIGURE 3-7: SCREENSHOT FOR SMARTPHONE ADAPTATION OF FISHERMAN GAME.....	98
FIGURE 3-8: EACH PARTICIPANT'S SPEARMAN CORRELATION CO-EFFICIENT BETWEEN THE MEAN LOG LATENCY WITHIN EACH RATIO AND THE RATIO FROM THE TASK. PLEASE NOT THAT IN THIS CASE, THE RATIO IS INVERSELY CORRELATED WITH THE OPPORTUNITY COST.	100
FIGURE 4-1: REINFORCEMENT LEARNING TASK WITH GAIN AND LOSS DOMAINS WAS PERFORMED BY SUBJECTS.	107
FIGURE 4-2: MODEL COMPARISON OF COMPETING COMPUTATIONAL MODELS.....	110
FIGURE 4-3: MASKS FOR REWARD RESPONSE REGIONS OF INTEREST USED FOR REWARD BIAS ANALYSIS.	117
FIGURE 4-4: DEPRESSIVE SCORES AND CAUDATE VOLUMES BY GROUP.....	121
FIGURE 4-5: BOTH GROUPS PERFORMED TASK WELL, WITH NO GROUP DIFFERENCES A.....	122
FIGURE 4-6: COMPUTATIONAL MODEL PARAMETER ESTIMATES BY GROUP AND VALENCE.	124
FIGURE 4-7: NEURAL ACTIVATION IN RESPONSE TO CHOICE (A-C) AND OUTCOME (D-F) IN TASK.	126
FIGURE 4-8: LEFT VENTRAL STRIATUM BETA VALUES FOR REWARD BIAS CONTRASTS, BY GROUP.	127
FIGURE 5-1: RELATIONSHIP BETWEEN APATHY IN HD AND FOUR COMMON MOTOR SIGNS (N = 2608).	146
FIGURE 5-2: SUPPLEMENTARY FIGURE SHOWING THE DISTRIBUTION OF THE RESIDUALS FROM THE LINEAR MODEL ASSESSING THE RELATIONSHIP BETWEEN APATHY AND MOTOR SIGNS.	153
FIGURE 5-3 SUPPLEMENTARY FIGURE SHOWING THE DISTRIBUTION OF THE RESIDUALS FROM THE LINEAR MODEL ASSESSING THE RELATIONSHIP BETWEEN APATHY AND FINGER TAPPING	153
FIGURE 5-4: SUPPLEMENTARY FIGURE SHOWING THE DISTRIBUTION OF THE RESIDUALS FROM THE LINEAR MODEL ASSESSING THE RELATIONSHIP BETWEEN APATHY AND COGNITIVE PROCESSING SPEED.....	154
FIGURE 6-1: SUMMARY OF THE RESTING STATE fMRI ANALYSIS PIPELINE USED IN THIS STUDY	164
FIGURE 6-2: REGION OF INTEREST LOCATIONS FOR AN EXAMPLE SUBJECT:.....	165
FIGURE 6-3: EXAMPLE SUMMARY TIMESERIES FROM FOUR ROIS FROM ONE PARTICIPANT.	167
FIGURE 6-4: SCHEMATIC OF THE DCM A-MATRIX USED IN THIS STUDY.....	168
FIGURE 6-5: THIS MODEL GENERATES SIMPLIFIED REPRESENTATIONS OF THREE PATHWAYS OF INTEREST – THE DIRECT, INDIRECT AND HYPER-DIRECT PATHWAY.	169
FIGURE 6-6: A. SPREAD OF APATHY SCORES IN THE PERI-MANIFEST HD COHORT AS MEASURED BY THE BALTIMORE APATHY SCALE.	177
FIGURE 6-7: SCHEMATIC SHOWING THE AVERAGE PARAMETER VALUES IN THE MODELLED NETWORK, ACROSS ALL 94 HD SUBJECTS, FOR BETWEEN NODE CONNECTIONS.	178
FIGURE 6-8: ASSOCIATION BETWEEN INTER-NODE CONNECTIVITY PARAMETERS AND (A) TOTAL MOTOR SCORE AND (B) BALTIMORE APATHY SCORE.	179
FIGURE 6-9: AVERAGE COUPLING ESTIMATES SHOW AN ACTIVE INHIBITION OF M1 IN HD GENE CARRIERS AND CONTROLS	186
FIGURE 6-10: ASSOCIATION BETWEEN INTER-NODE CONNECTIVITY PARAMETERS AND TOTAL MOTOR SCORE – INDIVIDUAL PARAMETER ESTIMATES SHOWN FOR EACH HD PARTICIPANT. R REPRESENTS CORRELATION	

COEFFICIENT. SIGNIFICANT CORRELATIONS OCCURRED IN THE SAME PATHWAYS IDENTIFIED USING HIERARCHICAL MODELLING.....	187
FIGURE 6-11: ASSOCIATION BETWEEN INTER-NODE CONNECTIVITY PARAMETERS AND APATHY SCORES SHOWING INDIVIDUAL PARAMETER ESTIMATES FOR EACH HD PARTICIPANT. R REPRESENTS CORRELATION COEFFICIENT. SIGNIFICANT CORRELATIONS OCCURRED IN THE SAME PATHWAYS IDENTIFIED USING HIERARCHICAL MODELLING.....	188
FIGURE 6-12: CUMULATIVE FRAMEWISE DISPLACEMENT (SUM OF FRAMEWISE DISPLACEMENT (FWD IN MM)) DURING SCANS WAS NOT SIGNIFICANTLY DIFFERENT BETWEEN CONTROLS AND HD GENE CARRIERS ($p > 0.05$). WITHIN GENE CARRIER COHORT, FWD SHOWED MILD CORRELATION WITH MOTOR SCORES ($r = 0.37$, $p < 0.01$) HOWEVER NO CORRELATION WITH APATHY SCORES ($p > 0.05$).	189

List of Tables

TABLE 1-1: MECHANISTIC SUB-TYPES OF APATHY AND THE PROPOSED NEUROANATOMICAL CORRELATES BY LEVY AND DUBOIS (2006).....	19
TABLE 3-1: DEMOGRAPHICS FOR PARTICIPANTS INCLUDED IN THE IN-LAB, EXPERIMENT (1), AND THE ONLINE REPLICATION, EXPERIMENT (2).	83
TABLE 4-1: SAMPLE DEMOGRAPHICS:	120
TABLE 4-2: REPLICATION ANALYSIS AT CUE PRESENTATION ACROSS BOTH GROUPS:	125
TABLE 4-3: REPLICATION ANALYSIS AT OUTCOME PRESENTATION ACROSS BOTH GROUPS:.....	125
TABLE 5-1: SAMPLE CHARACTERISTICS INCLUDING CHANGE IN CLINICAL VARIABLES USED IN THE MODEL BETWEEN FIRST AND LAST AVAILABLE VISIT.	145
TABLE 6-1: SAMPLE DEMOGRAPHICS	177
TABLE 6-2: COMPARISON OF BASELINE CONNECTIVITY PARAMETERS IN THE MOTOR NETWORK IN GENE CARRIERS AND CONTROLS.....	190

Chapter 1: Introduction

“I just feel like a light-bulb has gone off. I want to do things, but I just don’t seem able to get myself going. I feel like I can’t be bothered. I do try...I say all the right things to get myself going but it doesn’t seem to work. Some days I can’t really get out of bed. I just sit and watch people from my window. [...]”

Apathy, as described by a patient in the Huntington’s Disease Neuropsychiatry Clinic at the National Hospital for Neurology and Neurosurgery, London.

1.1 Overview:

Amelia Earhart is quoted as saying “the most difficult thing is the decision to act, the rest is merely tenacity [...]”. At the heart of this quote, and I would argue at the heart of apathy, is the fundamental challenge of deciding to take unprompted goal-directed action. Where Ms Earhart’s motivation led her to become the first solo female pilot to traverse the Atlantic, for patients with severe apathy, the loss of motivation can lead to a profound self-neglect, loss of independence and the breakdown of their relationships (Van Duijn et al., 2010; Konstantakopoulos et al., 2011; Starkstein et al., 2006). Not only is apathy serious but it is also a highly prevalent and transdiagnostic neuropsychiatric symptom. In neurology, apathy is common in many patient groups including those with cerebrovascular disease, demyelinating conditions such as multiple sclerosis (MS) and many neurodegenerative conditions, such as Parkinson’s disease (PD) and Alzheimer’s disease (AD) (Le Heron et al., 2019). In psychiatry, apathy is common in affective disorders, such as major depression, and psychotic disorders, such as

schizophrenia (Foussias and Remington, 2010; Husain and Roiser, 2017; Salamone et al., 2015a; Treadway et al., 2012).

Schizophrenia is an interesting case study of the problems facing patients with apathy. Bleuler (1950), who coined the term ‘schizophrenia’, believed that apathy was a central feature of this condition, writing “the patients [...] no longer have the urge to do anything either of their own initiative or at the bidding of another” (Bleuler, 1950). As the definition of schizophrenia developed, apathy fell into the class of “negative symptoms” and has consistently been associated with morbidity and functional decline (Andreasen, 1982; Fervaha et al., 2014; Foussias and Remington, 2010). Despite this, many of the dominant theories of schizophrenia have largely focussed on the emergence of positive symptoms – delusions and hallucinations (Friston et al., 2016a; Howes and Nour, 2016; Kapur, 2003). Therapeutically, there are also now many efficacious antipsychotic medications for the treatment of positive symptoms of schizophrenia; however, there are few treatment options to offer patients with schizophrenia who present with apathy (Huhn et al., 2019; Krause et al., 2018; Salamone et al., 2015a). This divergence between the impact of apathy and our ability to treat this disabling symptom in schizophrenia is a common theme in almost all clinical populations.

It is important to highlight that apathy is not only a clinical phenomenon. Motivational levels in the general population vary. Put simply, we are not all Emilia Earhart. Many individuals and organisations seek to boost motivation and are aware that low motivation results in lost productivity. In 2017, Gallup estimated the cost to U.S. companies of employees who were not motivated or engaged in their work to be between \$960 billion and \$1.2 trillion per year (Wigert et al., 2017). At the extreme end of the motivational spectrum, healthy individuals can also be classed as being apathetic (Ang et al., 2017). Importantly, apathy in the healthy population shares key characteristics of the apathy seen in clinical populations. In both populations, behaviourally apathetic individuals often feel that their motivation is ‘low’, they find it hard to self-initiate, actions feel more effortful and taxing activities no longer seem ‘worth it’ (Ang et al., 2017).

Apathy therefore occurs in a wide range of cohorts in neurology, psychiatry and in the general population with similar characteristics seen across groups. Although apathy in most conditions is poorly

understood, the widespread occurrence of apathy across groups suggests that insights into this disabling symptom may be gained from adopting a transdiagnostic theoretical framework. Using such an approach, observations or hypotheses from one group may be meaningfully applied to another.

The central aim of this thesis was to use such a transdiagnostic approach to develop hypotheses to explain why apathy is so common in Huntington's disease (HD). HD is a genetic neurodegenerative condition that causes a complex neurological, psychiatric and cognitive phenotype (Bates et al., 2015; McColgan and Tabrizi, 2018). Amongst this complex presentation, apathy in HD occupies a unique position. Apathy has the highest prevalence of the many psychiatric features of HD (van Duijn et al., 2014). Apathy in HD is the most sensitive psychiatric feature associated with clinical onset and disease progression (Martinez-Horta et al., 2016; Tabrizi et al., 2013). Much like schizophrenia, despite the associated prevalence and morbidity, our understanding of apathy in HD is poor and treatments are limited (Krishnamoorthy and Craufurd, 2011).

In order to use a transdiagnostic approach to build hypotheses to apply to HD, I required a flexible theoretical framework which could account for observations from patients with neurological lesions, psychiatric patients and explain the variance of motivation seen in the general population. To this end, I adopted a *computational approach* to apathy and motivated behaviour in this thesis.

An early proponent of this approach was Marr (1982). In the book 'Vision', Marr described the formulation of visual processing at three complementary levels of description – computational, algorithmic and implementation levels (Marr, 1982). At the computational level the principle aim is to determine the specific problem the system is trying to solve. Once this computational problem has been defined the algorithmic level describes how this computation could be achieved – in terms of inputs, outputs and algorithms. Finally, when considering implementation, we can ask how these higher-level constructs can be physically realised at the neural level.

A computational approach is not therefore simply the use of mathematical models in cognitive science but a multi-level theoretical framework to bridge higher level concepts to neural structures and processing. Importantly, each level of the hierarchy should be informed by the levels above or below

it. For example, while a highly sophisticated algorithm may recapitulate behaviour well, such an algorithm could not fit within a computational approach unless there is some neural basis for its implementation. For the purposes of understanding psychiatric symptoms and disorders therefore a computational approach is particularly powerful (Huys et al., 2016; Nair et al., 2020). Psychological theories and constructs can be used to inform the computational level of these models whereas information about neural dysfunction or lesions, seen in disease states, can inform the implementation level. Sitting in between is the algorithmic level whose parameters and functions can be used to bridge these two levels of explanation and explain some aspects of variance in performance.

In this chapter, I will describe the principal hypotheses that I have developed using a computational approach to study apathy, both in healthy populations and patients with HD. Before presenting these hypotheses, I will summarise and synthesise relevant background material. Given the multi-layered nature of the computational approach, I have drawn from a wide range of different sources. I will begin by outlining prominent formulations of apathy and ask how these inform the top level of a computational theory of motivated behaviour, the computational level. I will ask what the computational goal of motivated behaviour is and how answering this question can be used to operationalise the study of apathy. I will summarise key formulations about the nature of clinical apathy and propose an extension to these formulations to address the computational goal of motivated behaviour. I will then outline how algorithms from reinforcement learning (RL) can be used to model motivated behaviour and how I have used RL models in this thesis (Sutton and Barto, 2018). I will then review in greater detail the problem of apathy in HD and the hypotheses that I test. In this thesis I principally ask: (1) What factors determine the timing of un-prompted action initiation and how are these factors related to apathy? (2) What role do striatal pathways play in the expression of motivated behaviour and the development of apathy?

1.2 What is apathy?

Before framing apathy within a computational framework, I will first describe how a succession of key theoretical formulations over the last thirty years have shaped our understanding of apathy. One of the

first, and most influential, conceptualisations of apathy was put forward by Marin (1991). Marin argued that apathy was, at its core, a loss of motivation (Marin, 1991). His operational definition of motivation drew on work by Atkinson (Atkinson, 1964). Motivation was defined as a “superordinate concept” that sought to explain the “direction, vigour and persistence of an individual’s actions”. Marin argued that loss of interest or emotion alone was not sufficient to constitute apathy. Rather, these cognitive and emotional features must be seen in conjunction with diminished goal-directed behaviour. Marin further argued that apathy could both be a symptom of an existing condition or a separate syndrome. As an example, Marin argues that reduced motivation in the context of acute depression would be considered a symptom because the loss of motivation was secondary to the “dysphoria” of depression. The loss of goal-directed behaviour is found in the presence of marked emotional distress. By comparison, he argues that descriptions of loss of motivation following psychotic depression may be more in keeping with a syndrome of apathy. Such patients may not present with, or experience, depressive symptoms but rather show a lack of “initiative” and “vital impulse”. In both of these examples, the primary disorder is depression, however, in Marin’s formulation, apathy appears primary in the latter case whereas secondary to dysphoria in the first case. Similarly, later in dementias when there is significant cognitive impairment apathy represents a symptom secondary to a marked cognitive failure in attention and planning. However, apathy is also present early in many dementias, such as Huntington’s disease, before significant cognitive impairment and as such, an apathy syndrome may be an early neuropsychiatric complication. Marin’s formulation of apathy was highly influential. Leaning heavily on the outline proposed by Marin (1991), Starkstein *et al* (2001) and later Robert (2009) proposed a set diagnosed criteria for the syndrome of apathy with loss of motivation being a cardinal feature (Mann, 1991; Robert *et al.*, 2009; Starkstein *et al.*, 2001). Based on Marin’s formulation, the widely used Apathy Evaluation Scale (AES) and Lille Apathy Rating Scales (LARS) were developed. (Marin *et al.*, 1991; Sockeel *et al.*, 2006).

Although influential, the Marin formulation of apathy and the role of “motivation” in its definition was not without critics (Levy and Dubois, 2006a). In a challenge to the Marin formulation of apathy, Levy and Dubois (2006) argued that it was unnecessary to rely on the ‘blurred and inhomogeneous’

psychological construct of motivation to define apathy. They observed that apathy was often inferred by clinicians and carers based on an observable change in the patient's behaviour. As such, they argued that apathy should be viewed as an observable behavioural syndrome. In place of motivation, they reframed apathy as a quantitative reduction in self-generated voluntary goal-directed behaviour from some baseline level of performance. They proposed a chain of cognitive events that would be required to produce goal-directed action (Fig. 1-1). Impairment in this chain of events, at any stage, would result

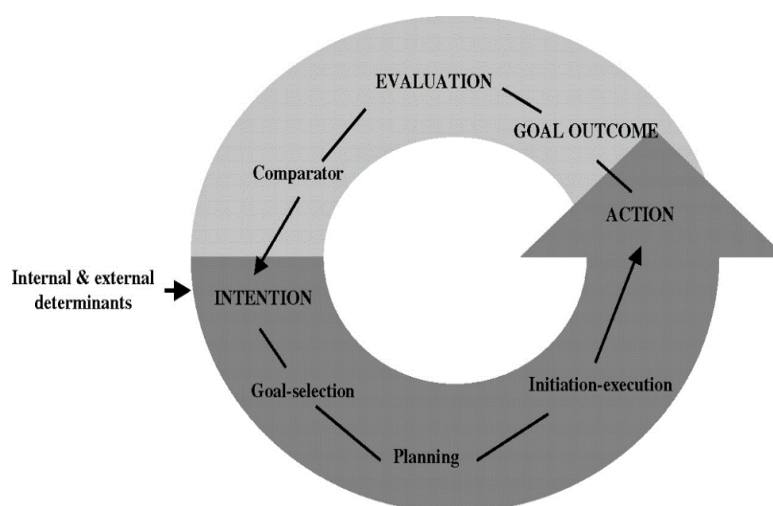


Figure 1-1: Process for generating goal-directed behaviour reproduced from Levy and Dubois (2006)

in loss of goal-directed behaviour causing apathy. Based on lesion localisation in neuropsychiatric populations, Levy and Dubois argued that the neural structures which performed the steps of this chain fell largely within the prefrontal-basal ganglia circuits. They proposed that disruption of specific locations within these circuits resulted in three specific subtypes of apathy - namely emotional-affective, cognitive deficits and auto-activation deficits.

Emotional-affective apathy was characterised as a failure to form appropriate connections between emotions and behaviour leading to reduced responsiveness to action outcomes. Levy and Dubois (2006) argued that emotions provide the motivational “value” for action. In order to enact actions appropriately, patients must also successfully execute a number of cognitive functions – such as being able to retain information, plan action and change course of action as needed. Failure in these ‘cognitive’ aspects of motivated behaviour result in cognitive apathy or cognitive “inertia”. Finally, Levy and Dubois described apathy secondary to failures in “auto-

activation”. In this form of apathy, patients struggle to self-initiate the thoughts and behaviours necessary to have goal-directed behaviour – they have a “mental emptiness”. Based on a detailed review of the neurological literature, they went on to propose neuroanatomical correlates of each sub-type of apathy centred around different prefrontal-basal ganglia loops (as described in Table 1-1).

Deficit sub-type	Proposed anatomical correlates
Emotional-affective	Orbital and medial PFC and limbic striatum
Cognitive	Dorsolateral PFC and basal ganglia nuclei in the cognitive loop
Auto-activation	Medial PFC, large frontal lobe lesions and frontal white matter, limbic/cognitive striatum.

Table 1-1: Mechanistic sub-types of apathy and the proposed neuroanatomical correlates by Levy and Dubois (2006).

Although Levy and Dubois do not use the term motivation in their definition, it should be recalled that Marin (1991) described motivation as an overarching concept which included all processes that determined the “direction, vigour and persistence of an individual’s actions” and not the qualia of motivation itself. As such, it could be argued that the steps outlined by Levy and Dubois (2006) in Fig. (1-1) may all fall under the umbrella of “motivational” processes. Furthermore, both formulations overlap in their emphasis of the loss of self-initiated goal-directed behaviour and that lesions of fronto-subcortical loops are highly likely to generate apathy. Where both formulations are however limited, from the point of view of a computational framework for motivated behaviour, is the limited discussion of the relevance of normal motivated behaviour for the study of apathy, and perhaps more fundamentally – addressing what computational problem motivated behaviour is trying to solve.

In a recent paper Le Heron *et al* (2018) made significant theoretical advances to address these limitations (Le Heron et al., 2018a). Le Heron and colleagues focus on apathy “as reduced motivation

for self-initiated goal-directed behaviour”. By overlapping brain regions associated with apathy in a wide range of neurological disorders they highlight two key regions reliably associated with apathy in a range of lesion models – the dorsal anterior cingulate and the ventral striatum. They also highlight other, less consistently involved areas including regions such as the insula, orbitofrontal cortex and dorsolateral prefrontal cortex. Having identified a possible circuit for motivated behaviour they ask why these regions are so consistently involved in apathy. I will not repeat their review and argument here but will summarise as follows. The ACC and VS appear to show relevant activity across three critical aspects of motivated behaviour: (1) choosing whether to act, (2) persisting with that action and (3) learning from outcomes of those actions. In each of these components, they cite evidence that the ACC in particular, although also the VS to some extent, show activity representing the integration of costs and benefits. In the numerous studies cited, the costs involved in motivated behaviour include the anticipated effort of the necessary action, cognitive effort and determining whether other, better, options are worth pursuing. On the basis of this evidence, Le Heron and colleagues conclude that apathy can be thought of as a failure in “cost-benefit” occurring during, at least, one of their three components of motivated behaviour. Finally, Le Heron and colleagues explicitly set out to build a transdiagnostic framework for apathy by interpreting the lesions to brain regions in light of our understanding of their function in non-clinical populations. As such, the focus shifted from specific pathologies to higher level cognitive processes and how diseases disrupt them.

1.3 Motivated behaviour as the “maximisation of net rewards per unit time through self-initiated actions”:

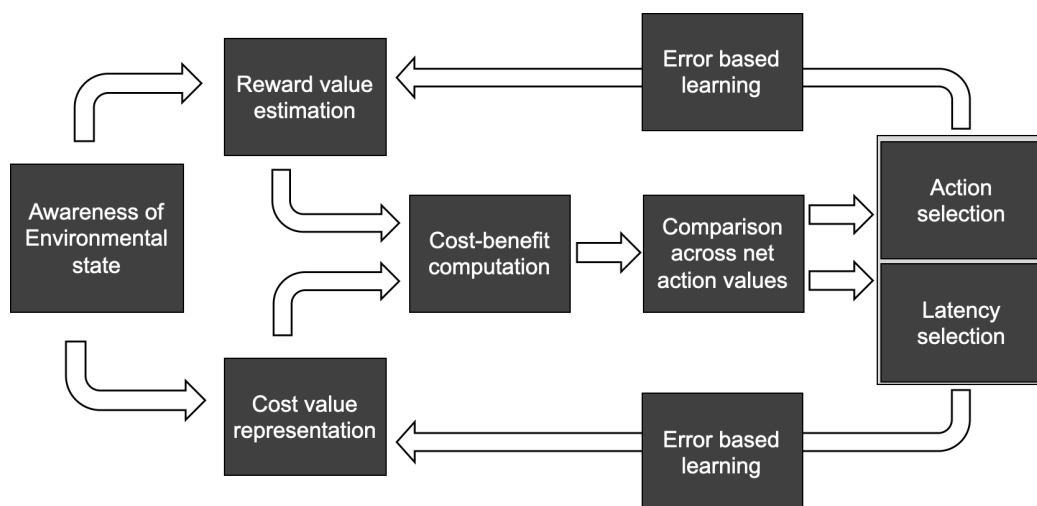


Figure 1-2: Example of sub-computations that must be performed optimally in order to maximise net rewards.

Adapted from Levy and Dubois (2006) and Le Heron (2018).

The neurocognitive approach outlined by Le Heron and colleagues closely resembles a computational framework for motivated behaviour; however, a few points remain outstanding. Although cost-benefit analysis may be *what* the network outlined by Le Heron *et al* (2018) does, this does not explain *why* the network performs this function. At the highest, computational, level it is important to define the overarching goal of the system. If cost-benefit integration is what this system does, then it seems likely that it is performing these functions to maximise net benefits, or net rewards. Indeed it is often the assumption of reward-effort paradigms that participants act to maximise net reward (Bonnelle et al., 2015, 2016; Klein-Flügge et al., 2015, 2016). Importantly, however, all of the above formulations of apathy have highlighted the critical role of timely self-initiated goal directed behaviour in apathy. Therefore, I propose that a working computational goal motivated behaviour is *the maximisation of net rewards per unit time through self-initiated actions*.

This working definition of motivated behaviour makes explicit the *why* of motivated behaviour. In keeping with previous work, this overarching aim can only be achieved by completing a number of sub-computations optimally. Example sub-functions are shown in Fig. (1-2). For example, motivated agents must accurately appraise both rewards and costs and be able to complete cost-benefit evaluation. They must then be able to choose the action or goal with the highest net reward value reliably and execute with appropriate timing. Defined in this way, apathy can be viewed as marked reduction in net reward per unit time achieved by an individual interacting with their environment. Diseases with gross

anatomical lesions may cause apathy through significant disruption to one or more underlying sub-computations, whereas disorders lacking gross lesions may drive apathy through a shift in algorithmic parameters governing the necessary computations. Finally, variance in these parameters may explain natural variation in motivated behaviour in healthy populations in controlled settings. Under this approach, apathy and reductions in motivated behaviour lie along a continuum. “Clinical apathy” would be hypothesised to exist at some extreme of this spectrum whereby a failure of the above processes leads to functional impairment – for example impaired social or occupational function and in extreme cases activities of daily living. It should be further noted that apathy and motivated behaviour viewed in this way overlaps with other symptoms in psychiatry – in particular anhedonia. Anhedonia is defined as “consistently and markedly diminished interest or pleasure in almost all daily activities” and is has a motivational component in that patients may no longer seek out pleasure (Husain and Roiser, 2017). As described by Marin, untangling apathy from anhedonia, clinically, may be dependent on the primacy of symptoms – anhedonic patients may experience a loss of motivated behaviour secondary to a loss of pleasure. In this sense, apathy may be considered a broader concept – defining the process of connecting awareness of reward to attainment of reward through action and anhedonia offers one mechanism of disruption to this pathway, through impaired pleasure.

This working definition of motivated behaviour and apathy also places some restrictions on suitable algorithms that can be used to model this form of behaviour. Suitable algorithms must seek to optimise behaviour based on expected future rewards. For ecological validity, these algorithms must also not rely on a complete model of the world but instead build such models from experience and adapt behaviour based on feedback in the form of reward or costs. Finally, to achieve this computational goal of motivated behaviour, algorithms must not only describe how actions are chosen but also, when.

1.4 Reinforcement learning as a family of algorithms well suited to modelling motivated behaviour

Reinforcement learning (RL) is branch of machine learning that sits alongside ‘supervised learning’ techniques, such as regression, and ‘unsupervised learning’ techniques, such as clustering algorithms

(Sutton and Barto, 2018). Supervised learning techniques rely on being provided a labelled set of training data from which to draw extrapolations about unseen data. On the other hand, unsupervised learning can be used to infer the hidden structures in unlabelled data (P. Murphy, 1991). By comparison, the goal of RL is not necessarily to build a model or understanding of the environment but to maximise a numerical value known as ‘reward’ that a decision making agent, such as a robot, animal or human, earns through interactions with an environment (Sutton and Barto, 2018). Formally, the interplay between agents and environments is modelled as a Markov Decision Process (MDP) (Doya and Kimura, 2013; Puterman, 2005; Sutton and Barto, 2018). In MDPs, the environment is made of distinct states (S) and the decision-maker is aware of which state they are in. They transition from one state to another state by taking actions (A) and transitions between states are probabilistic in nature. In MDPs, the probability of encountering future states only depends on the current state the agent is in, not the precise history of previously visited states (Puterman, 2005). As an agent moves through an environment in this manner, they encounter rewards (R) for moving between states. While the agent may know what state they are in, the probability of receiving a reward in a given state and the transition matrix that governs the relationship between states, is not known to the agent. Agents continue through the environment in this manner (S, A, R, S, A...), encountering and collecting rewards until they enter a terminal or absorbing state (in a finite MDP).

Depending on the distribution of rewards in the environment, states within an environment can be thought of as having different values. These state values ($V(S)$) are based not only on the rewards immediately available from that state, but also the value of all future states which may be encountered from that state onwards. The state values can therefore guide a decision maker’s choice of action – it is preferable to move towards states with estimated higher values because of the higher long-term yield of rewards. As actions affect which future states the agent will encounter and therefore the amount of reward, actions themselves can be thought of as having action values (Q-values). As MDPs may be very large, or contain loops, the projected future reward which is used to estimate a state or action value may become intractably large. To overcome this, future rewards are often discounted in a temporal manner (Sutton and Barto, 2018).

The goal of RL algorithms is to find the optimal solution to MDPs - to maximise the amount of reward an agent extracts from an environment. By learning and estimating state or action values, RL algorithms alter the mapping of which actions to take in each state in order to maximise reward - the decision maker's policy (or π). Example policies include a 'greedy' policy in which the agent simply chooses the action with the highest future expected reward value (Sutton and Barto, 2018). This strategy is risky. If the agent has not sufficiently explored the environment the current 'best' action may actually be sub-optimal. Because they do not know the true state or action values in the MDP, but rather hold estimates based on their experience, the truly best option may not yet be apparent. Agents must therefore weigh exploiting this option against exploring the environment further by choosing other actions. To overcome this limitation, two other commonly used policies include ' ϵ -greedy', whereby actions of lower value are chosen with a small (ϵ) probability, and a 'softmax' action selection rule whereby the probability of choosing an action is determined by its value relative to other action and a noise parameter (Daw, 2009).

There are broadly two forms of RL – model-based and model-free RL (Dayan and Niv, 2008; Doll et al., 2012) . In model-based methods, the agent may estimate a model of the world – including the transition probabilities between states and the probability of a reward in a state. Using these estimates of the environment, model-based RL can unfurl projections of future states in order to plan decisions. This approach has the downside of being resource heavy as, for example, agents are not only required to recall states, but the nature of the relationships between those states. Also, if the model of the environment itself is wrong, this can lead to poor outcomes. Alternatively, model-free methods do not build models of the environment – instead they focus on holding and updating estimates of state or action values.

One highly influential algorithm used to update such value in model-free RL values is temporal difference learning (TDL) (Sutton, 1988; Sutton and Barto, 2018). Using TDL, after progressing a specific number of time steps forward in the environment, the agent uses the feedback it has gained, in the form of reward, to update its value estimates for states. The difference between the reward actually received by the agent and its own estimate value for that state or action is called the TDL prediction error (δ).

Let us consider a simple example in which the environment is composed of a linear sequence of states. With every time step the agent can only take one action, with probability of 1, and moves to the next state, again with probability of 1, terminating at state ‘T’. As described above, state values are not simply determined by the amount of reward available in that state, but the reward value of states which can be encountered from that state on (discounted in a temporal manner using a discount factor of γ). In this simple example, mathematically, the value of the first state in the environment can therefore be expressed as follows:

Equation (1-1):

$$\begin{aligned} V(S_1) &= \sum_{i=1}^T \gamma^{i-1} (r_i|S_1) = (r_1|S_1) + \gamma(r_2|S_2) + \gamma^2(r_3|S_3) + \gamma^3(r_4|S_4) \dots + \gamma^{T-1}(r_T|S_T) \\ &= (r_1|S_1) + \gamma((r_2|S_2) + \gamma(r_3|S_3) + \gamma^2(r_4|S_4) \dots) \\ &= (r_1|S_1) + \gamma V(S') \end{aligned}$$

Where $(r_t|S_t)$ represents the immediate reward received in that state, and $\gamma(r_{t+1}|S_t)$ represents that discounted reward that will be received in the next time step, and so on. When collapsed, the state value equations becomes simply the reward plus the discounted value of the next state.

It is worth highlighting this simple reconfiguration of the state value equation above:

Equation (1-2):

$$0 = (r_1|S_1) + \gamma V(S') - V(S_1)$$

This rearrangement highlights that there is no difference or ‘error’ between the sum of the reward received in that state and the discounted value of the next states and the ‘true’ state values ($V(S_t)$).

While learning, RL algorithms do not know ‘true’ state values. As such, until convergence, agents using TDL to learn state values, hold estimated state values (\hat{V}). These estimates are potentially wrong, leading to the *temporal difference prediction error* (δ) (Niv, 2007; Sutton, 1988):

Equation (1-3):

$$\delta = (r_t | S_t) + \gamma (\hat{V}(S')) - \hat{V}(S_t)$$

By using this error signal, agents can update their value estimates to more accurately reflect the true reward yield they can expect from that state or from taking that action. The degree to which estimates are updated based on another parameter, the learning rate (α) is as follows:

Equation (1-4):

$$\hat{V}(S_t) \leftarrow \hat{V}(S_t) + \alpha \delta$$

As described above, learning from error and adapting behaviour in response to rewards is a key component of motivated behaviour. Likewise, learning from error is critical in RL because it can be used to update the agent's estimations for the value of certain states, or actions, and therefore be used to update the agent's policy – what actions to take in which states.

The aims of RL and the working goal of motivated behaviour that I have proposed above are therefore well aligned. In both cases, the overarching goal of behaviour is to maximise rewards through initiation and optimisation of actions made by the decision maker.

1.5 The intersection between RL and cognitive neuroscience

A key link between RL and cognitive neuroscience was the seminal finding that dopamine neurons in the VTA showed changes in phasic activity which could be modelled and predicted by a TDL RL algorithm (Schultz, 2015; Schultz et al., 1997). There is also now considerable evidence that RL, both model-free and model-based, can be used to model, and fit, a range of human behaviour relevant to motivated behaviour in particular learning of value, costs and action selection (Daw et al., 2006, 2011; Hauser et al., 2017; O'Doherty et al., 2004, 2003). Furthermore, latent variables from RL models, such as the TDL prediction error and expected value, parametrically correlate with BOLD signals in areas highly relevant to apathy such as the prefrontal cortex, the cingulate cortex and the striatum (Chase et al., 2015; Garrison et al., 2013; Rutledge et al., 2010). Despite these successes, RL has a number of caveats and I will describe four here (Dayan and Niv, 2008). Firstly, MDPs themselves are simplified

models of the environment and although RL may find optimal solutions to MDPs, these can only be seen as approximate solutions to ecological behaviour. Secondly, most RL algorithms are derived from the machine learning literature and are often agnostic to brain structure or function. Furthermore, RL algorithms rely on repeated exposure to a problem and can be slow to learn and adjust behaviour, especially for complex MDPs. These requirements may limit the translational potential as animals and humans rarely have the luxury of repeated exposure to determine optimal behaviour. It should be noted however that Botvinick *et al* (2019) have argued that recent advances in RL, such as episodic deep RL and meta-RL may overcome some of these limitations and offer richer insights than the RL algorithms they supersede (Botvinick et al., 2019). Finally, it is important to note that RL is not the only modelling framework which has been applied to computational models of brain and behaviour. Other algorithms, such as Bayesian modelling or biophysically realistic neural network models for example, also describe many aspects of motivated behaviour (Frank, 2011; Frank and Badre, 2012; Friston et al., 2014a; Pezzulo et al., 2018). For the purposes of the questions I pursue however, I did not believe that these alternative, often more complex, modelling approaches yielded sufficiently distinct predictions to those generated by RL models. As such, RL seemed an appropriate algorithmic framework on which to build the hypotheses I pursue here.

I use RL models in two ways in this body of work. Throughout the thesis, RL algorithms serve as explicit generative hypotheses about behaviour and, in some instances, neural activity. As such, I have used these algorithms to make behavioural (Chapter 3&5), and neural, predictions (Chapter 4&6). Secondly, I used RL algorithms to quantitatively fit to data yielding individual parameter estimates which can be used to test hypotheses, such as comparison across groups (Chapter 4). Fitted variables from these algorithms have also been used to probe functional neuroimaging data.

Having laid out the theoretical framework that guided my work in this thesis, I will now describe the problem of apathy in HD with a review of the literature and how I have used this computational framework to develop and test relevant hypotheses.

1.6 HD – clinical features:

Clinically, HD is characterised by a progressive neurological, psychiatric and cognitive phenotype (McColgan and Tabrizi, 2018). HD patients show a complex movement disorder characterised by a range of features such as chorea bradykinesia, dysarthric speech, oculomotor dysfunction, poor coordination and an abnormal gait (Dorsey et al., 2013). The clinical ‘onset’ of HD is defined as the emergence of unequivocal motor signs of the conditions (Huntington Study Group., 1996). Typically, in adult onset cases, hyperkinetic features such as chorea form the dominant clinical picture early in the disease whereas hypokinetic features and rigidity occur later in the illness (Ross et al., 2014a). As the disorder progresses, motor dysfunction gives rise to increased rigidity, dystonia and impaired swallowing. Inexorably, patients with HD end up bedbound and completely dependent for care. Alongside these motor features HD causes a dementia syndrome (Dumas et al., 2013). Patients show progressive worsening of cognitive abilities in a range of domains weighted towards ‘executive’ dysfunction. Typically, impairments are found in domains such as planning, attention, cognitive flexibility, emotion recognition and psychomotor slowing (Papoutsi et al., 2014; Paulsen and Long, 2014; Ross et al., 2014a; Stout et al., 2011).

Almost all patients with HD also develop psychiatric features (van Duijn et al., 2014; Eddy et al., 2016). In his seminal monograph on ‘Familial Chorea’ in 1872, George Huntington noted that patients with familial chorea had “the tendency to insanity” (Huntington, 1872). Common psychiatric manifestation in HD also includes depression, anxiety including the development of obsessions, compulsivity, personality change, irritability, aggression and of particular focus in this thesis, apathy (Eddy et al., 2016; Ghosh and Tabrizi, 2018; Paoli et al., 2017). Fig. (1-3B) shows the prevalence of common psychiatric symptoms in a large cohort of patients with HD at varying stage of the disease, reproduced with permission from van Duijn (2014). It is also estimated that 20% of patients with HD will experience suicidal ideation and 5-10% of HD patients will die by suicide (Kachian et al., 2019).

1.7 Apathy in HD:

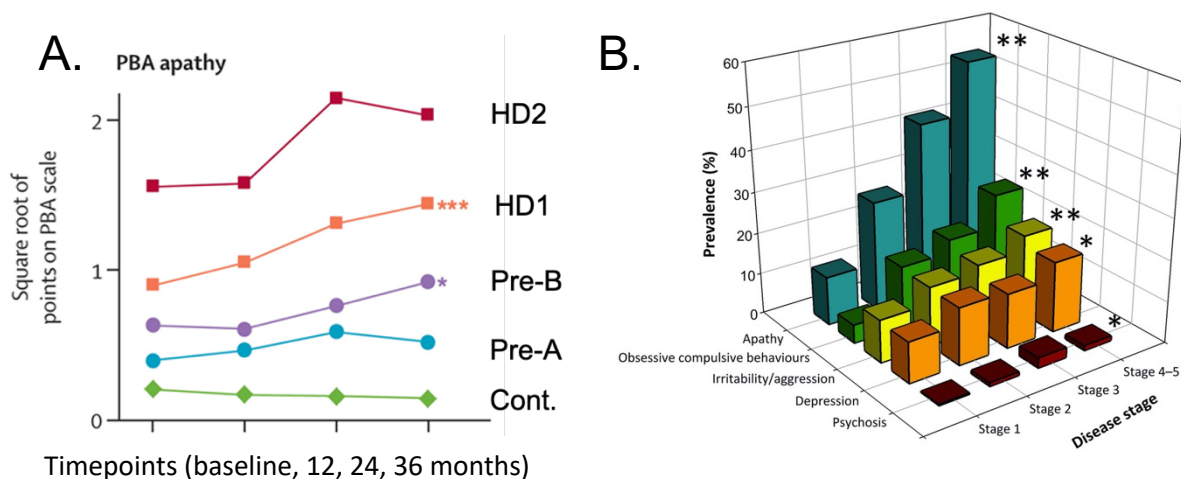


Figure 1-3: Apathy in HD shows a close relationship with disease progression. A. Tabrizi et al (2013) found that of all neuropsychiatric markers, apathy progressed significantly in both patients with early HD (HD1) and pre-manifest participants closer to disease onset (Pre-B). B. van Duijn et al (2014) also showed that apathy was the most prevalent psychiatric symptom in HD and increased in proportion with disease stage. Legend A: PBA (Problem Behaviour Assessment Scale), HD (manifest HD patients), Pre-A and Pre-B (premanifest HD patients, < 10.8 years to onset and >10.8 years to onset respectively) Legend B: Disease stages were defined according to the Total Functional Capacity (TFC) score: Stage 1=TFC score 13-11, Stage 2=TFC score 10-7, Stage 3=TFC score 6-3, Stage 4=TFC score 2-1, Stage 5 =TFC score 0.

1.7.1 Apathy in HD: epidemiology

Apathy and HD have an intimate relationship. Firstly, apathy is very common in patients with HD. In a study of 1993 patients with HD from the REGISTRY study, van Duijn *et al* (2014) reported that moderate to severe apathy was found in approximately 30% of patients. By comparison depression, irritability and obsessional symptoms were found in 13% of patients (van Duijn *et al.*, 2014). In a related study, Martinez-Horta *et al* (2016) reported apathy was common even in premanifest gene carriers (Martinez-Horta *et al.*, 2016). For those within the preHD-A group, greater than 10.8 years from estimated motor onset, 23% reported apathy, however, this figure rose to 62% of the preHD-B groups, those within 10.8 years from onset. By comparison, apathy was only reported in 2% of controls in this study. This corresponded to an odds-ratio (OR) of 15.2 for developing apathy in the preHD-A cohort and an OR of 88 for the preHD-B cohort. Alongside this prevalence, numerous studies have shown that apathy is strongly associated with disease progression. As shown in Fig. (1.3B), van Duijn *et al* (2014) found a strong relationship with the stage of HD and the prevalence of apathy. Thompson *et al* (2012) also report that in a longitudinal study almost all HD patients showed some degree of apathy and that apathy showed the strongest progression over time (Thompson *et al.*, 2012). These findings lead the

authors to conclude that “the neuropsychiatric syndrome of apathy appears to be intrinsic to the evolution and progression of HD”. This relationship between HD and apathy is also seen in pre-manifest cohorts. As described above, Martinez-Horta *et al* (2016) described a significantly increased prevalence of apathy in the preHD-A and preHD-B cohorts of their study. In the longitudinal deep phenotyping study, TRACK-HD, only apathy showed a significant increase in the preHD-B cohort over the three visits (Fig. (1-3A)). For patients with HD, not only is apathy itself disabling but it has been shown to be associated with increased functional and cognitive decline, unemployment, reduced independence and suicidality (Andrews *et al.*, 2020; Banaszekiewicz *et al.*, 2012; Fritz *et al.*, 2018; Honrath *et al.*, 2018; Jacobs *et al.*, 2018; Kachian *et al.*, 2019; Sellers *et al.*, 2020; Sousa *et al.*, 2018a).

1.7.2 Apathy in HD: cognitive and computational correlates

Despite the prevalence of apathy in HD and its associated comorbidities, relatively little is known about why patients with HD develop apathy. Cognitively, apathy in HD has been associated with poorer global cognitive function, impaired executive function, and impaired emotion recognition (Andrews *et al.*, 2020; Baudic *et al.*, 2006; Kempnich *et al.*, 2018; Sousa *et al.*, 2018a). More recently, McLauchlan *et al* (2019) reported that manifest patients with HD and apathy persisted longer in a tapping task in which they were competing against a rigged computer opponent (McLauchlan *et al.*, 2019). In this task, the computer opponent always won more points and participants were required to determine whether they continued racing or quit the task. HD patients persisted longer than controls and those with HD apathy persisted with the task the longest. Contrary to these findings, Heath *et al* (2019) reported that apathy was associated with earlier exiting in a progressive ratio task although, it should be noted that this association was only found when authors combined data from both HD patients and controls (Heath *et al.*, 2019). To my knowledge no associations between apathy and computational parameters have been made in HD.

1.7.3 Apathy in HD: human neuroimaging

With regard to human neuroimaging, although data relating to apathy has emerged in recent years it is not consistent. Using the TRACK-HD data, Scahill *et al* (2013) and Baake *et al* (2018) found no associations between apathy severity and change in grey matter volume (GMV), white matter volumes (WMV) or volume of subcortical structures (Baake *et al.*, 2018a; Scahill *et al.*, 2013). By comparison, Martínez-Horta *et al* (2018) describe apathy severity associated with loss of grey matter volume in a range of cortical and subcortical regions, including the dorsal ACC, caudate and putamen; however strongest associations were found only in the amygdala and superior temporal lobes (Martínez-Horta *et al.*, 2018a). Using ^{18}F -FDG PET to assess for metabolic changes associated with severity of apathy, this group also found strongest reductions in tracer uptake associated with apathy in the Supplementary Motor Area (SMA), ACC and areas of the prefrontal cortex (Martínez-Horta *et al.*, 2018a). Similar conflicting findings are reported in analysis of white matter tracts. Using DTI, Delmaire *et al* (2013) found an association between apathy and fractional anisotropy (FA) in the rectus gyri, however using the TRACK-HD data, Gregory *et al* (2015) reported no significant changes in FA and apathy (Delmaire *et al.*, 2013; Gregory *et al.*, 2015a). More recently De Paepe *et al* (2019) reported that higher mean diffusivity (MD), but not FA, in the right fronto-striatal tract (FST) and the right uncinate fasciculus (UF) were associated with overall apathy scores in a cohort of HD patients (De Paepe *et al.*, 2019). They also showed that right FST MD was associated with cognitive apathy whereas right UF MD was associated with auto-activation deficits. It should be noted however, that only the association between right UF MD and apathy remained significant once demographic confounds were added to the model. I am unaware of any task fMRI changes associated with apathy in HD; however, using resting state fMRI (rsfMRI) McColgan *et al* (2017) report increased functional connectivity associated with apathy in a network that includes a range of nodes including the caudate, frontal pole, precuneus and parietal lobes (McColgan *et al.*, 2017a).

1.7.4 Apathy in HD: conclusion and hypotheses

Given current evidence it is challenging therefore to summarise imaging correlates of apathy in HD and very few common strands emerge. Perhaps unsurprisingly, given the poor understanding of the pathophysiology of apathy in HD, treatments for apathy in HD are sorely lacking (Eddy et al., 2016). Recently Gelderblom *et al* (2017) reported that bupropion, a noradrenergic and dopaminergic reuptake inhibitor, did not alleviate apathy in the only randomised control trial (RCT) for HD apathy (Gelderblom et al., 2017). Translational research therefore offers little consistent evidence to explain why patients with HD develop apathy.

I therefore focused on three consistent epidemiological observations regarding apathy and HD to guide the hypotheses I test in this thesis. Firstly, apathy in HD is very prevalent - affecting nearly all patients. Secondly, there appears to be a robust link between apathy and disease progression, even in early HD. Finally, apathy is common even in early stages of the disease. Given these observations, it seems plausible that apathy in HD is driven by a core disease process, one which is likely to occur in nearly all patients, from early disease and progress reliably. Furthermore, based on the emphasis placed by many formulations of apathy on self-initiated behaviour, to further restrict the search space of potential hypotheses I pursued the idea that apathy in HD may be driven by impaired self-initiation perhaps overlapping with the process driving bradykinesia in HD, which is also common in HD. Based on these observations I pursued two related hypotheses in this thesis.

Firstly, where bradykinesia is the slowing of movements, under the working definition I propose above, apathy is a marked reduction in net reward per unit time achieved by an individual interacting with their environment. I hypothesised that at an algorithmic level, apathy in HD is driven by impaired representation of variables that drive optimal free-operant action initiation. More specifically, based on extensions to RL theory, I hypothesised that one such candidate variable is *opportunity cost* – the amount of reward that can be lost per unit time through inaction (Niv et al., 2005, 2007).

Secondly, based on a range of empirical evidence and RL models that I will describe shortly, I argue that the gradual disruption and loss of the *direct* basal ganglia pathway is a candidate disease process to drive apathy in HD. As I will discuss in detail below, although initially conceptualised as playing a role in motor control, the direct and indirect basal ganglia pathway is believed to play roles in goal-

directed behaviour. I will also describe evidence that these pathways are highly susceptible to damage in HD and the ratio of damage between the direct and indirect pathways changes over the time course of the disease. I argue that not only could the emergence of apathy in HD reflect the ratio of damage across these pathways, but that long before clinical onset, the ratio of damage between these pathways may have significant implications for some of the sub-computations of motivated behaviour such as learning.

I will conclude this chapter by describing these two principal hypotheses in more detail. Before I do so, I would like to highlight one important caveat. As I described above, motivated behaviour and apathy are complex constructs made up of a number of sub-processes and are likely to involve many brain regions. HD likewise is a complex disease, with a range of neuropsychiatric features and affecting almost all of the brain in terminal stages. As such, it is highly unlikely that one computational process or one pathophysiological process drives apathy in HD. I therefore do not propose that the hypotheses I have outlined above are the sole drivers of apathy in HD, especially as the disease progresses. I do argue however, that the hypotheses that I developed may explain several clinical and epidemiological features associated with apathy in HD and therefore, they could play an important role in the development of apathy in these patients.

1.8 Hypothesis 1: Loss of sensitivity to opportunity cost contributes to apathy in HD

In most ecological settings, prompts that guide the timing of action initiation are rare. In free-operant behaviour therefore, a critical decision problem is when to take unprompted action. In terms of harvesting rewards from an environment, when to act is as important as determining how to act. Impaired or slow self-initiation of goal-directed behaviour is also a central behavioural hallmark of many apathy formulations (Le Heron et al., 2018a; Levy and Dubois, 2006a; Marin, 1991). Despite the critical importance of the timing of self-initiated behaviour, both to free-operant behaviour and apathy, very few computational models describe the algorithmic factors which drive self-initiation.

As I described above, decision making problems can be modelled as MDPs and optimally solved using RL. Typically, MDPs are framed in discrete time steps and taking an action moves the agent onto the next time step (Sutton and Barto, 2018). There is no scope for actions to take different lengths of time or for agents to dwell within states. This is clearly an important limitation when considering that our goal is to study ecological and free-operant behaviour. To address these limitations, semi-MDPs (SMDPs) can be used to model continuous time discrete-event problems – such as deciding when to take an action (Sutton et al., 1999). In SMDPs, discrete actions are still chosen however, they can take variable amounts of time to complete. In these cases, the transition time associated with an action becomes an important feature as it governs when an agent moves from one state to another. Within this framework, during these transitions' agents do not earn rewards and therefore transition times have an important role in determining long run sum of future rewards.

This, however, raises another challenge – in very large environments or environments with states connected as loops, the sum of future rewards can become intractably large. In many RL formulations therefore, one approach to simplifying this mathematical problem is to discount future rewards in a temporal fashion – rewards further away are more heavily discounted as we saw earlier. An alternative formulation, which is critical to the extension of RL models to free operant settings, is average-reward reinforcement learning (Daw, 2013; Mahadevan, 1996; Niv, 2007; Sutton and Barto, 2018). In this form of RL, the performance of a policy is not based on total rewards earned but rather the average reward earned per time step (\bar{R}). In this branch of RL, state values are termed *differential state values* (Mahadevan, 1996; Niv, 2007; Niv et al., 2005). They are calculated by comparing the reward gained from a state to the average reward earned across the environment, based on the current policy plus the sum of future expected reward.

By combining these two modelling techniques, SMDPs and average reward RL, Niv *et al* (2007) proposed an extended RL model in which agents could optimally decide their choice of free-operant action latency through an awareness of the average net reward per unit time available in the environment. This model will be explained in detail in Chapter 3, however, in brief, during extended

latencies between actions, the agent is not accruing rewards. Therefore, in environments with a high average reward rate, longer latencies are costlier in terms of rewards forgone or ‘opportunity cost’.

Opportunity costs, therefore, drive an animal to initiate rewarding behaviour more quickly. To offset this balance, Niv *et al* (2007) also introduced a vigour dependent cost which increased as latency decreased (Niv *et al.*, 2007). Niv’s model is also therefore a good example of the incorporation of effort costs into RL. By balancing these two costs, animals could choose to maximise the net rate of reward they received in an environment. At the implementational level, Niv *et al* (2007) proposed that tonic dopamine levels may code the average reward term in their model. As such, the invigorating effects of dopamine supplementation are modelled as increasing the average reward rate which drives up opportunity cost (Salamone *et al.*, 2015b; Walton and Bouret, 2019). The same mechanism explains invigoration associated with motivational states. For example, hungry animals may not only eat faster but they move faster and complete non-rewarding actions, like grooming, faster (Hull, 1943; Niv, 2007; Niv *et al.*, 2005). This invigoration is predicted by the opportunity cost theory because hunger increases the subjective reward value of food. This increases average reward in the environment resulting in higher *opportunity cost*. Because the opportunity cost applies to all states all actions are invigorated.

This normative model of action initiation outlines the algorithmic factors which determine the latency with which we self-initiate and is therefore highly relevant to apathy. I hypothesised that variation in behavioural apathy in the healthy population may be driven by differences in experienced opportunity cost. In HD, I hypothesised that, perhaps secondary to the same disease process driving bradykinesia, the coding of opportunity cost is disrupted.

In order to test these hypotheses however, I needed to demonstrate that key predictions from this model applied to normal human behaviour. Although highly influential there is limited evidence that people adapt their choice of action latencies in free operant settings in response to changes in opportunity cost (or conform to other predictions from Niv’s model). There is also no clear evidence linking opportunity cost to motivational status in healthy human participants. If disruption to opportunity cost sensitivity contributes to the development of apathy in HD, the computational framework would predict that

variance in opportunity cost sensitivity in control populations should also be correlated with motivational status.

I test these hypotheses in Chapter 3 in three independent experiments using a novel behavioural paradigm that I developed entitled “The Fisherman Game”. Alongside finding evidence supporting the main behavioural predictions from Niv’s model, I find that there is a relationship between sensitivity to opportunity cost in younger healthy participants and behavioural apathy. I also show that this relationship also extends to patients with HD, with sensitivity to changes in opportunity cost predicting clinical apathy scores in a pilot cohort of patients with HD. I will also describe collaborative work that I have been involved with, in which this task was modelled using an average reward RL model.

1.9 Hypothesis 2: The ratio of disruption to the direct, *versus* indirect, pathway cells of the striatum drives a proportion of the apathy seen in HD

For the remainder of this chapter I focus on the second line of questioning that I pursued in this thesis – given the clinical, computational and epidemiological observations described above, what is the neural basis of apathy in HD? As a reminder, there is the limited consistent translational evidence to explain the emergence of apathy in HD. Based on epidemiological evidence it appears that the process driving apathy should fulfil the following criteria: (1) very common – occurring in nearly all patients at some stage, (2) common even in early stages of the disease and (3) shows a tight connection with disease progression. Furthermore, as I outlined above, given the importance of timely self-initiated behaviour in formulations of apathy – the neural mechanism driving apathy in HD may impact the ability to self-initiate, perhaps by disrupting the coding of opportunity cost or overlap with the process driving bradykinesia. As I shall outline below, based on work in neuropathology, physiology and computational neuroscience, I argue that one possible mechanism which meets these criteria is the progressive involvement of medium spiny neurons (MSNs) within the striatum which form the direct basal ganglia pathway. Beyond apathy however, I argue that the relative involvement of the direct and indirect pathway has implications for motivated behaviour in HD, perhaps decades before onset.

I will outline my review of the literature which has led me to form these hypotheses. Firstly, I will describe the aetiology and pathology of HD in greater detail with a particular focus on the impact on the striatum and related structures. I will then present the recent evidence which suggests that activity of cells in the striatal pathways places an important role in the expression of motivated behaviour before discussing the implications of RL models of striatal function for motivated behaviour in HD.

1.9.1 Huntington's disease – aetiology:

HD is a genetic neurodegenerative condition caused by a CAG triplet repeat expansion in the *huntingtin* gene resulting in a toxic gain-of-function mutation (Bates et al., 2015; MacDonald et al., 1993). The normal function of huntingtin protein, and the role of its CAG repeat sequence, remains under investigation; however, there is a fascinating association between the presence and length of the triplet expansion in the HTT gene and neural complexity in evolution (Zuccato et al., 2010). Sea urchins have 2 CAG repeats in the huntingtin gene, zebrafish have four, mice have seven, dogs have ten and rhesus macaques have 15 repeats (Zuccato and Cattaneo, 2016). By comparison, on average the CAG expansion size in humans is typically between 17 and 19 repeats with some geographical variation (Kremer et al., 1994). Over 40 CAG repeats results in fully penetrant HD cases. Fewer than 26 repeats is considered normal, between 26-35 repeats poses risks of expansion for future generations and between 36-39 repeats shows reduced penetrance (Bates et al., 2015). Aside from diagnostic value, HTT CAG length also explains approximately 60% of the variance in clinical age of onset with higher repeat lengths associated with lower age of onset (Djoussé et al., 2003; Lee et al., 2012). Age and CAG length can therefore be used to estimate time to onset in pre-manifest HD gene carriers.

It is not the focus of this chapter to detail the intracellular effects of mutant huntingtin, however, they include disrupted synaptic transmission, impaired axonal transport, transcription irregularities, mitochondrial dysfunction and ultimately cell death (Bates et al., 2015). Like many proteins affected in neurodegenerative diseases, mutant huntingtin is widely expressed, however, certain cells such as the medium spiny neurons (MSNs) of the striatum are particularly susceptible to damage (Schulte and Littleton, 2011).

1.9.2 Neuropathology of HD

The striatum is the input node to the basal ganglia and consists of the caudate, putamen and ventrally, the nucleus accumbens. In both neuropathology and structural neuroimaging, loss of striatal volume is a canonical finding in HD (Scahill et al., 2017; Vonsattel et al., 2011; Waldvogel et al., 2015; Wilson et al., 2018a). The Vonsattel staging system for HD is based on the visible changes to the curvature of the ventricular facing wall of the caudate. As the disease progresses, the normally convex ventricular surface gradually flattens and eventually becomes concave in severe disease due to the loss of neurons (see Fig. 1.4).

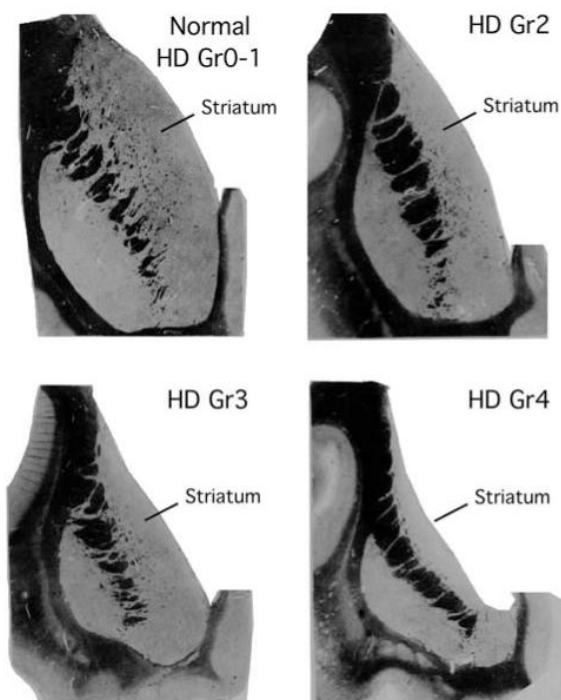


Figure 1-4: Diagram of neuropathological Vonsattel grading system for HD severity. Curvature of ventricular aspect of caudate determines staging. As the stages of disease progress, the normal convex protrusion of the striatum into the ventricle flattens and eventually becomes concave. Reproduced with permission from Reiner et al (2011)

The striatum is an anatomically diverse structure and the effect of HD is not evenly distributed across the various cell types, compartments and axes of the striatum (Calabresi et al., 2014a; Crittenden and Graybiel, 2011; Rüb et al., 2015). Firstly, at a macroscopic level, HD has been shown to affect dorsal striatum earlier and more severely than the ventral striatum (Waldvogel et al., 2015). Despite this ‘dorso-ventral’ gradient of cell loss is extensively distributed in the striatum in early HD. Von Sattel

reports that in Grade 1 HD, the tail and body of the caudate are noticeably smaller as compared to controls, although with a “normal appearance” (Vonsattel et al., 2011). Although there is sparing of the nucleus accumbens even late into the disease, at Grade 1 there is a 50% reduction in cell count in the head of the caudate. By grade 4, the caudate and putamen have lost 95% of neurons (Vonsattel et al., 2011).

γ -aminobutyric acid (GABA) expressing MSNs account for 90-95% of the striatum with interneurons, expressing both GABA and acetylcholine accounting for the remainder (Kawaguchi et al., 1995; Lanciego et al., 2012). MSNs have highly arborized dendritic trees capable of receiving and integrating inputs from a number of inputting connections (Kreitzer, 2009). MSNs within the striatum can be classified based on their protein/receptor expression and the targets of their efferent connections (Reiner and Deng, 2018). Based on this classification MSNs in the striatum fall into four categories: (1) those expressing dopamine-1 receptor (D1-R) and substance P (SP) that project to the globus pallidus internal segment (GPi); (2) D1/SP expressing MSNs which project to the substantia nigra pars reticulata; (3) dopamine-2 receptor (D2) and enkephalin (Enk) expressing MSNs which project to the globus pallidus external segment (GPe); and finally, (4) MSNs which project to the substantia nigra pars compacta (SNpc) – some of which co-contain SP and ENK (Reiner and Deng, 2018). As I will describe in more detail below, the D1/SP neurons which project to GPi and to SNpr form what is known as the *direct pathway* and D2/Enk expressing neurons form what is known as the *indirect pathway*.

Added to this, MSNs also fall into two ‘compartments’ – striosomes and matrix (Crittenden and Graybiel, 2011; Graybiel, 2000). Crittenden & Graybiel (2011) describe the striosomal compartment as forming “labyrinthine, interconnected structure” surrounded by the much larger matrix compartment which is estimated to make up to 80% of the striatum (Crittenden and Graybiel, 2011). Both striosome and matrix compartments are composed of D1- and D2- expressing MSNs however, it is thought that only striosomal MSNs project to the SNpc.

Although striatal atrophy is the hallmark of HD, not all MSNs are equally vulnerable to the disease. In a quantitative immunohistochemistry study, Deng *et al* (2004) compared the loss of striatal MSN subpopulations using a range of control and HD cases (Deng et al., 2004). By staining axons projecting

to the GPi and GPe, Deng *et al* (2004) found that even in Grade 1 HD, D2/ENK cell loss was already substantial ($33.6\% \pm 7.2\%$ of control levels). The degree of early involvement of these cells was so severe early in disease that the authors did not find convincing evidence of progressive involvement as the disease progressed until the final disease stage. By comparison, reduced staining of D1/SP cells, projecting to GPi, was also present in early disease but less severe – $70.9\% \pm 4.1\%$ of control levels at grade 1. These cells showed approximately 10% per stage reduction through stages 2 and 3. By stage 4, both populations showed significant loss – ENK staining down to $\sim 4\%$ of control levels and SP staining down to 7%. These data are shown in Fig. (1-5) and are consistent with a range of studies, using immunohistochemistry to label cells and ligand binding to identify changes in receptor expression (Reiner and Deng, 2018).

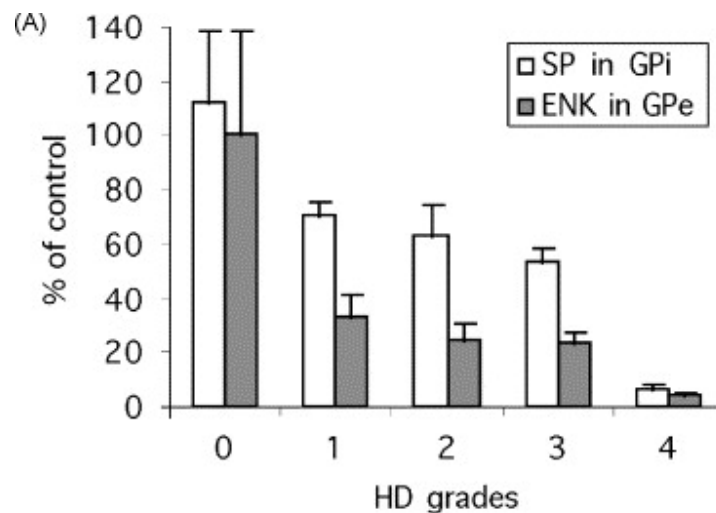


Figure 1-5: Effect of HD on fibre abundance in direct and indirect pathway. Reproduced with permission from Deng (2004): “The fibre abundance for each target area for each HD case was expressed as a percent of control fibre abundance. The mean per cent abundance (\pm S.E.M.) for each HD grade are separately graphed for SP and ENK in the pallidum”

MSNs with projections to the substantia nigra are also affected in HD, however, the data appear less consistent. Deng *et al* (2004) find that D1/SP neurons projecting to the SNpr in particular show vulnerability to the disease process in HD with a similar pattern of loss to the D2/Enk neurons with marked loss from grade 1. By comparison, as summarised by Reiner and Deng (2018) receptor binding studies which show marked loss of D2-R in GPe and relatively preserved D1-Rs in GPi at Grade 1, consistent with the data above, show only a modest loss of 20% D1-R in the SNpr. In these studies, significant D1-R loss in both GPi and SNpr are seen in Grades 2-3. Similarly, MSNs projecting to the

dopaminergic SNpc are also affected by HD, however, it is unclear whether these neurons are affected differently from those projecting to SNpr (Tippett et al., 2007). It appears that these neurons emerge from the striosomes of the striatum and Tippett *et al* (2007) report that loss of these MSNs may be associated with psychiatric disturbance in HD.

These studies demonstrate that the D1/SP MSN loss in HD, in particular those projecting to GPi, shows some of the characteristics that I outlined above which may make this a candidate disease process for the development of apathy. Firstly, striatal MSNs are highly susceptible to HD and direct pathway MSNs are likely to be affected in all patients with HD. Secondly, these cells may be affected in early disease, to some degree. Thirdly, it seems that these cells are progressively affected as the disease advances.

1.9.3 Cortico-striatal connectivity

The striatum receives inputs from the cortex, the thalamus and mid-brain dopamine nuclei and sends outputs to deeper basal ganglia structures. Cortico-striatal connectivity occurs in a topographic manner (Haber, 2016). This pattern of connectivity means the ventral striatum and nucleus accumbens are heavily innervated by the prefrontal cortex. By comparison dorsal regions receive afferents from sensorimotor cortex. Early models of cortico-striatal connectivity argued that there were five functionally segregated cortico-striatal loops: a ‘motor,’ ‘oculomotor’, a ‘dorsolateral prefrontal’, a ‘lateral orbitofrontal’ and ‘limbic’ circuit (Alexander et al., 1986; DeLong and Wichmann, 2009a). There is now growing evidence to suggest that the striatum and basal ganglia act as a point of integration across these loops (Averbeck et al., 2014; Haber, 2016; Tziortzi et al., 2014).

Alongside the glutamatergic cortico-striatal connections, the cells of the striatum receive dopaminergic projections from two midbrain nuclei, the ventral tegmental areas (VTA) and substantia nigra pars compacta (SNpc) (Arias-Carrián et al., 2010; Haber, 2016). Connections from these two nuclei form the mesolimbic and nigrostriatal pathways, with the former projecting to the ventral striatum and the latter projecting to the dorsal striatum. Interestingly, the connections between the striatum and midbrain do not appear to be unidirectional like those of the cortico-striatal connections. There appears to be

reciprocal connectivity between the striatum and these midbrain DA nuclei (Haber, 2016; Haber et al., 2000). Furthermore, these reciprocal connections do not form closed loops. Starting ventrally, striato-midbrain connections are thought to extend into regions of the DA producing midbrain which project more dorsally in what Haber *et al* (2000) argues form an ‘ascending loop’ (Haber et al., 2000). As such, ventral striatal activity may influence more dorsal striatal activity via the midbrain dopamine.

The striatum is therefore not only the recipient of neural signals from brain regions performing critical computations for motivated behaviour, but it may also serve a role in the integration of information from different cortical loci to co-ordinate goal-direct behaviour.

1.9.4 Dopamine receptors in the striatum

As described above, based on dopamine receptor expression, MSNs fall broadly into two populations (Graybiel, 2000). One class of MSNs contain primarily express ‘D1’ dopamine receptors and the other express ‘D2’ receptors. These two broad classes of MSNs are thought to be expressed throughout the striatum, including ventral regions (Yager et al., 2015). The differential expression of D1 and D2 receptors across these two populations is a critical feature of striatal biology with implications for the hypotheses presented in this thesis. Both D1 and D2 receptors are metabotropic, G-protein coupled receptors that have the opposite effect on the intracellular availability of cyclic adenosine monophosphate (cAMP) (Beaulieu et al., 2015). Downstream DA-receptor activation has a net effect on MSN excitability - with D1-R activation increasing excitability of MSNs to cortical stimulation and D2-R activation reduces MSN excitability (Surmeier et al., 2007). It is also thought that both types of MSN can undergo long term changes in synaptic plasticity, long term potentiation (LTP) and depression (LTD), in response to dopaminergic signalling (Cerovic et al., 2013; Shen et al., 2008, 2015; Surmeier et al., 2007).

These findings suggest that cortico-striatal synaptic strength can be modulated both in the short-term, through changes in excitability, and in the long-term, through changes in plasticity. Critically, however, the overall effect that dopamine has on net striatal activity is dependent on the ratio of D1 to D2 receptors and therefore, the relative sizes of the respective MSN populations.

1.9.5 Striatal pathways and loops

D1- and D2-expressing MSNs form two pathways that emerge from the striatum that have opposing effects on cortico-thalamic activity. The D1/SP expressing MSNs form what is known as the direct pathway, also known as the striato-nigral pathway, and D2/ENK MSNs form what is known as the indirect pathway, or the striato-pallidal pathway (Albin et al., 1989; DeLong, 1990a; DeLong and Wichmann, 2009b).

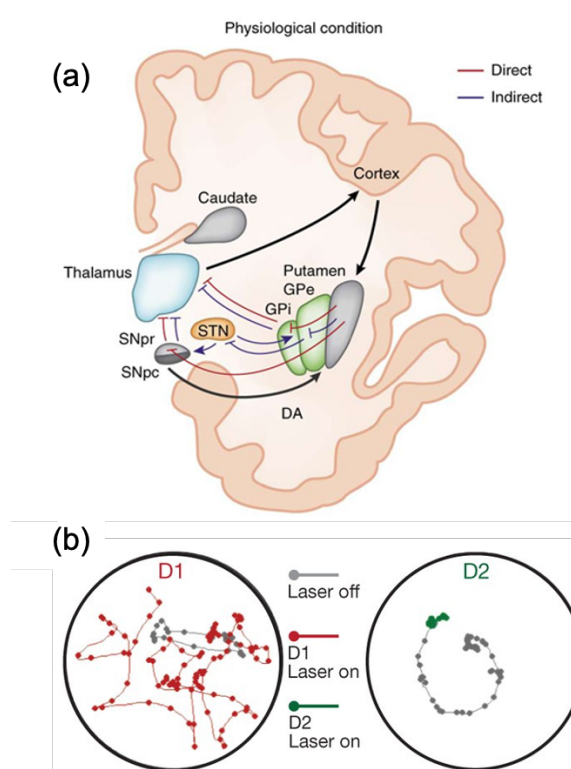


Figure 1-6: Direct and indirect pathway connectivity and effects of optogenetic stimulation (a) Direct and indirect pathway connectivity reproduced with permission from Calabresi et al (2015). These pathways for polysynaptic connections from the striatum to the thalamus (b) The effect of optogenetic stimulation of the direct (D1) pathway and indirect (D2) pathway from Kravitz et al (2010), reproduced with permission. In this figure, grey dots represent mouse location every 300ms before laser is initiated, red dots indicate position with direct pathway stimulation and green dots indicate position with indirect pathway stimulation over the same time period.

The Fig. 1.6A shows a simplified schematic of these two pathways from Calabresi *et al* (2015). The direct pathway, consisting of D1-expressing MSNs has the net effect of disinhibiting the thalamus and exciting the cortex. Direct pathway MSNs from the striatum form inhibitory connections with regions that exert an inhibitory control over the thalamus - globus pallidus internal segment (GPi) and the

substantia nigra par reticulata (SNpr), thereby causing thalamic activation (Graybiel, 2000). In comparison, D2-expressing MSNs of the indirect pathway have the net effect of inhibiting thalamocortical activity. Indirect pathway MSNs from the striatum inhibit cells in the globus pallidus externa (GPe). This inhibition of GPe disinhibits the subthalamic nucleus (STN). The disinhibited STN excites the two inhibitory output nuclei of the basal ganglia, the GPi and SNpr, leading to thalamic inhibition and subsequently, cortical inhibition (Deniau et al., 2007; Graybiel, 2000).

It was proposed, based on the circuitry described above, that these pathways are also functionally opponent in their control over movement (Albin et al., 1989; DeLong, 1990b). The direct pathway activation resulted in movement, and conversely, it was hypothesised that indirect pathway activation resulted in reduced movement. Indeed, this theory was in part developed to explain how loss of indirect pathway neurons in HD contributed to hyperkinesia. Recently a series of experiments, using pathway specific ablation, dysfunction and optogenetics activation, have yielded *in vivo* largely supportive evidence of this functional opponency model in mice (Bateup et al., 2010; Freeze et al., 2013; Kravitz et al., 2010). For example, Fig. (1.6B) from Kravitz *et al* (2010) shows an example optogenetic stimulation of MSNs in the dorsomedial striatum. Stimulation of direct pathway MSNs elicited less freezing, more self-initiation of movement and greater persistence with ambulation – key components of motivated behaviour. Conversely indirect pathway MSNs activation resulted in increased freezing, reduced self-initiation of movement and reduced persistence with movement. Data from this study supports the role of these pathways not only in movement but also movement initiation and persistence – key steps set out above in the generation and completion of motivated behaviour.

Beyond movement, other studies have now demonstrated that these pathways play a role in other important aspects of motivated behaviour namely decision making and learning. In a follow up optogenetic study, Kravitz *et al* (2012) developed a system in which sensitive switches activated optogenetic stimulation of either the direct or indirect pathway neurons. The mice, with optogenetic probes *in situ* were then free to roam within an environment containing one of these switches or an inactive switch. Using this set-up, they demonstrated that direct pathway activation, in the dorsal striatum, resulted in significant bias towards that touchpad, whereas the opposite was seen with indirect

pathway activation. The biases in the dorsal striatum, induced on the first day of testing transferred over to the next testing day and lasted longer for the positive bias induced by direct pathway activation. These effects were not due to motor change or dopamine receptor activation. Beyond the dorsal striatum, Hikida *et al* (2010) showed that inhibition of direct pathway activation in the nucleus accumbens reduced reward learning whereas inhibition of the indirect pathway inhibited avoidance learning.

Despite this evidence, and perhaps not unsurprisingly, this two, opponent and independent pathway model is over simplistic. Firstly, it has been shown that additional pathways, not accounted for in the original models, exist such as thalamo-striatal back projections and a direct effect of the cortex on the STN (Nambu *et al.*, 2002). This cortico-STN, or ‘hyper-direct’, pathway leads to inhibition of cortical activity. Aside from these additional pathways, the independence of these two pathways has also been challenged. Interneurons in the striatum are thought to facilitate interactions between MSNs and outside of the striatum connections between these two pathways are seen (Calabresi *et al.*, 2014a). Functionally, these pathways may also not be separate. Using a method that allowed in-vivo observation of pathway activation during free movement Cui *et al* (2013) found that both the direct and indirect pathway activity increased at action initiation and were both relatively less active at rest (Cui *et al.*, 2013).

As summary to this section and central to the hypotheses tested in this thesis are the following points. Firstly, MSNs in the striatum largely fall within two categories, those expressing D1- and D2-receptors. Cortical afferents to these MSNs are topographically arranged meaning that these cell types are involved in the processing of not only motor information, but information salient to valuation and motivation. These striatal cell types form the basis of direct and indirect pathways in the basal ganglia which can, respectively, increase and decrease the vigour and initiation of free operant behaviour. Dopamine plays a critical role in controlling the excitability of these cells’ types – both in the short term and in the longer term by modulating synaptic plasticity. Finally, as dopamine is only capable of exerting these effects via its receptors the net effect of dopamine in the striatum is physiologically equivalent to the ratio of these receptor subtypes, and therefore, the ratio of MSN populations.

1.9.6 RL models of the striatal function:

As described above, one of the principal findings that bridges RL algorithms with neuroscience was the observation that in a conditioning paradigm, phasic activity of DA neurons in the VTA could be predicted based on the TDL prediction error (δ) (Schultz et al., 1997). This result has been replicated numerous times using a range of techniques (Day 2007, Hart 2014, Kim 2012, Steinberg 2013, Hamid 2015). In humans numerous functional MRI (fMRI) studies have shown that ventral and dorsal striatal activity correlates with fitted prediction error signals (Daw et al., 2006; Garrison et al., 2013; McClure et al., 2003; O'Doherty et al., 2004, 2003; Pessiglione et al., 2006; Rutledge et al., 2010).

The topographical connectivity of the striatum and the presence of prediction errors both ventrally and dorsally in the striatum, especially in instrumental conditioning, drew a comparison between the ventro-dorsal organisation of the striatum and a common RL algorithm known as the 'actor-critic' model (Chakravarthy et al., 2010; Collins and Frank, 2014; Joel et al., 2002; O'Doherty et al., 2004).

In the actor-critic algorithm the agent is thought of as having two components, 'critic' and the 'actor' which update value estimates and policy in tandem (Collins and Frank, 2014; Joel et al., 2002; Sutton and Barto, 2018). The actor takes actions based on a policy. Despite taking the actions however, the actor itself has no information regarding the outcome of its choice of action – it does not see the reward, or any state or Q-values. Instead, the critic module learns state-values. The critic, however, has no ability to determine the policy. These two components only communicate via the TDL δ computed by the critic. Alongside, being used by the critic to update its state-value estimates, δ is used to directly influence in the actor's policy. For example, the actor may choose an action based on a probabilistic policy such as the softmax. The δ computed by the critic are passed onto the actor, however, instead of changing state-values or Q-values, δ is used to directly influence the probability of choosing an action. An alternative, less formal, example may be that of parent trying to guide the behaviour of a young child. The child may act in 'exploratory' ways without fully realising the consequences of their action and may get this feedback from their (possibly frustrated) parent. While the parent can offer praise and critique based on their appraisal of the situation, it is the child who needs to update their behaviour.

Over time, it is the hope of all agents using actor-critic RL, and indeed frustrated parents, that this interaction leads to an optimal behavioural policy.

What is not accounted for in traditional actor-critic models is the presence of the two main pathways in the striatum. A positive prediction error, coded by a rapid and transient increase dopamine levels, will have antagonistic effects on the direct and indirect pathway. To address these limitations of standard actor-critic models, Collins and Frank (2014) proposed an extended actor-critic framework called ‘‘Opponent Actor Learning’’ (OPAL). In this model, ventral striatum acts as the critic. It learns state values using TDL, as described above, and updates these values based on prediction errors (δ). This prediction error was passed onto two separate actor modules, termed ‘Go’, G , and ‘No-Go’, N . Biologically, these actors were thought to represent the cortico-striatal synaptic weights of the direct and indirect pathway respectively. In their model, the value of the actors was updated according to these update rules:

Equation (1-5):

$$G_a(t + 1) = G_a(t) + [\alpha_G G_a(t)] \times \delta_t$$

$$N_a(t + 1) = N_a(t) + [\alpha_N N_a(t)] \times -\delta_t$$

Under these update rules, following an action ‘a’, both actors receive the same TDL δ from the critic however, for the ‘Go’ actor, the value of action ‘a’, G_a , is increased by a positive δ and for the No-Go actor, the value of action ‘a’, N_a is decreased by a positive δ . The reverse is true for negative δ . In this manner, the model simulates the effect of D1- and D2- cells respectively. As firing rates cannot be negative, both actor weights are constrained to be positive. It is also worth noting that in this model, the learning rate (α) for each actor is multiplied by the current weight of the actor itself - $\alpha_G G_a(t)$ for example. In this way three-factor Hebbian learning is also incorporated. Presynaptic activity from the cortex determines the action value being learned, dopamine modulation is signalled by the δ and post-synaptic activity represented by the actor weights (α_G and α_N). The choice between actions is made using a softmax policy as previously described, however, the overall action value entered into the softmax (Act_a) is computed as the linear sum of the Go ($G_a(t)$) and NoGo ($N_a(t)$) actor weights:

Equation (1-6):

$$Act_a(t) = \beta_G G_a(t) - \beta_N N_a(t)$$

The role of tonic dopamine is modelled in the β values which effectively modulate the current striatal pathway weights. β_G and β_N are inversely related such that when high tonic DA is simulated β_G is high and β_N is low and the opposite is true when dopamine levels are depleted. Reaction times are modelled as being inversely proportional to the net action value so long as this value exceeds a threshold for Go versus No-Go pathway activity.

Collins and Frank (2014) use this striatal RL model to simulate a range of behaviours, including instrumental conditioning, effort-based decision making and free-operant action initiation. Like other more biophysically realistic models of striatal function, the central message of OPAL is that the role dopamine plays in learning and effort-based decision making, within the mesolimbic circuitry, is contingent on the functioning of the striatal pathways and importantly the ratio of activity within these pathways (Frank et al., 2004; Franklin and Frank, 2015).

It is clear that for patients with HD, these models have significant implications. As described above, not only are both of these pathways affected in HD but the degree of their respective involvement evolves over the course of the disease with D2/Enk cells of the indirect pathway being affected earlier than the cells of the direct pathway. Based on OPAL, similar models, and the empirical evidence I have outlined above I developed two further hypotheses which I have tested in this thesis.

1.9.7 Implications for motivated behaviour and apathy in HD

Firstly, given the early involvement of the indirect pathway in HD, models like OPAL would predict that in early HD learning associated with negative prediction errors would be impaired. In these models, negative prediction errors influence learning and action selection by increasing the weight of the indirect pathway ($N_a(t)$) driving selection away from that action. With loss or dysfunction in the indirect pathway, it may be predicted that patients with early HD may struggle to learn in settings dependent on negative prediction errors, such as learning to avoid loss. In keeping with this hypothesis, using an

instrumental conditioning paradigm, Palminteri *et al* (2012) showed that HD gene carriers within 10 years from onset were better at learning from gains than from losses. Using computational modelling, they fit an RL model to the data and found that this bias towards gain learning was driven by poorer choices in the loss frame. Building on this work, in Chapter 4, I describe a task fMRI study I completed with HD gene carriers approximately 25 years from onset. Hypothesising early dysfunction in the indirect pathway, I predicted that either in the behavioural data, or in the functional imaging data, that we would find a similar bias in learning towards gains as compared to losses. Comparing data from 35 gene carriers 25 years from onset and 35 well matched young adult controls, I find evidence that striatal activity in the gene carrier groups does show a bias towards gain learning as compared to loss learning and in post-hoc analysis, that this effect may be driven by impaired representation of the value of loss predicting cues. Not only are these findings in keeping with Palminteri's work, they represent the earliest functional imaging difference detected between HD gene carriers and matched controls. This chapter is also an example of the multiple levels of computational analysis – aside from presenting behavioural and model-free fMRI results, I fit RL models to the behavioural data and use variables from these models to probe the neural data and test computationally derived hypotheses.

In the final two chapters I present analyses to test my principle hypothesis regarding apathy in HD – that progressive direct pathway involvement drives a proportion of the apathy seen in HD. As we have seen, it is thought that as HD progresses the direct pathway becomes increasingly involved. Based on empirical evidence, OPAL and similar models of striatal function predict that the loss of the direct pathway not only prevents actions from being reinforced in learning tasks but that actions are less likely to be taken overall or taken with increased latency. These models also predict that the loss of the direct pathway would lead to reduced sensitivity to tonic changes in dopamine levels which, as described above, are predicted to carry the environment opportunity cost.

Finding evidence to support this hypothesis was challenging as there are few validated measures of *in vivo* direct and indirect pathway function. In the first of two related chapters, Chapter 5, I adopt an indirect approach. Based on the functional opponency of the direct and indirect pathways, it is argued that the loss of the indirect pathway drives the development of chorea in HD whereas the loss of the

direct pathway drives the development of bradykinesia in HD. Based on my hypothesis I predicted therefore that apathy in HD would be found to a greater degree in patients with HD who present with bradykinesia as compared to those who present with chorea. Using a large representative dataset from the multinational ENROLL-HD data (n = 2608) dataset, I found that, as predicted, higher bradykinesia scores were associated with higher apathy and the reverse relationship was found for chorea.

Although encouraging, this work only provides indirect evidence in support of my hypothesis. In the final data chapter, Chapter 5, I attempt to address this hypothesis using *in vivo* neuroimaging data. As described above, the direct and indirect pathway alter the activity within the thalamus. Within neuroimaging, this form of causal connectivity is known as *effective connectivity*. By using dynamic causal modelling (DCM), a Bayesian framework for estimating effective connectivity from resting state fMRI data, Kahan *et al* (2014) reported changes in the connectivity of the direct and indirect pathway in a small cohort of patient with Parkinson's disease (n = 12) undergoing deep brain stimulation of the STN (Kahan *et al.*, 2014a). Based on this work, Adeel Razi and I developed an updated protocol to use spectral DCM for resting state data to determine the effective connectivity within the direct and indirect pathways of 94 peri-manifest HD gene carriers from the TRACK-ON HD study. In this study, I tested two hypotheses. Firstly, although it is hypothesised that indirect pathway changes are associated with the onset of motor signs in HD, there is no *in vivo* neuroimaging data to support this. Secondly, as described above, we asked whether direct pathway changes were associated with the development of apathy in this cohort of peri-manifest HD patients. To test these hypotheses, as described in Chapter 5, we used a fully automated Bayesian procedure allowing associations between clinical measures and connectivity parameters to emerge *de novo* from the data. Using this approach, we found very strong evidence (posterior probability > 0.99) to support both of our hypotheses. Firstly, more severe motor signs in HD were associated with altered connectivity in the indirect pathway and by comparison, apathy scores were associated with changes in the direct pathway component of our model. Given the immense complexity of basal ganglia circuitry and the relatively poor resolution afforded by *in vivo* human neuroimaging, I cannot claim that these results are a direct proof of my hypothesis however,

they do suggest that changes in functional connectivity within specific parts of the basal ganglia circuitry may contribute to the development of apathy in HD.

1.10 Conclusion:

In this chapter I have sought to lay out the theoretical computational framework from which I have approached the problem of motivated behaviour and apathy. Using this approach, I developed hypotheses to explain why patients with HD develop apathy by considering the computational, algorithmic and implementational levels. I have used a range of methods and cohorts in this thesis and so each chapter contains a detailed methods section. I have also included a Methods chapter which describes the cohorts used, how apathy is measured in this thesis and principles of functional MRI data acquisition and pre-processing.

In the first data chapter, Chapter 3, I will present the development of my task, ‘The Fisherman Game’, to test some of the principle predictions from the opportunity cost model of vigour selection. In this chapter I present data from three independent experiments and demonstrate the opportunity cost influences free-operant action initiation and correlates with apathy scores, particularly in younger adults.

I then present data from a task fMRI study in a cohort of HD gene carriers 25 years from onset. In this study, I show that neural activation in the ventral striatum of HD gene carriers shows a ‘reward bias’ that may be driven by impaired representation of loss predicting cues. These findings are in keeping with early dysfunction in the indirect striatal pathway. In this chapter, I fit a computational model to behavioural data, extract parameters and use this to complete group comparison. I also replicate canonical findings from the computational literature in this study – such as the correlation between ventral striatal activity and the reward prediction error.

In the final two chapters I seek to build evidence that direct pathway involvement contributes to the development of apathy in HD. In Chapter 4, I analysed data from 2608 patients with HD and find that motor signs believed to be associated with direct pathway involvement, such as bradykinesia, are associated with increased apathy severity whereas chorea, believed to be associated with indirect

pathway involvement, is associated with reduced apathy severity. Finally, in Chapter 5, I developed a novel analysis technique to assess whether clinical features in HD are associated with changes in direct and indirect pathway connectivity. By analysing resting state fMRI study using DCM, I find that increased severity of motor signs and apathy are associated with changes in the indirect and direct pathway components of our model respectively, in a peri-manifest cohort of HD patients (n = 96).

Apathy remains a disabling and poorly understood symptom of a range of neuropsychiatric syndromes. As a medical student, I remember interviewing patients with schizophrenia and was struck not by their psychotic features but the impact that negative symptoms, such as apathy, has on their lives. As a working psychiatrist, I have now frustratingly seen apathy disable patients under my care with schizophrenia, depression, Alzheimer's disease and, of course, Huntington's disease. More broadly, therefore, the aim of my thesis was to advance our understanding of apathy and motivated behaviour with the hope that such advances may lead to much needed treatments.

Chapter 2: Methods

Over the following four data chapters, I have used a variety of methods to address the hypotheses set out in the Introduction. Each of the following chapters has an extended Methods section laying out the specific methodology used. In this Chapter, I describe in more detail three broader aspects of the methods used: (1) the cohorts used, (2) apathy scales and (3) principles of fMRI research.

To begin, I will describe the three Huntington's Disease (HD) studies from which I have either recruited patients or used available data for Chapters 4-6, namely, the HD Young Adult Study (HD-YAS), ENROLL-HD and TRACK-ON HD respectively. In Chapter 2, I collected a separate cohort of healthy participants, for in-person and online behavioural testing, and a small cohort of manifest HD patients across three separate experiments. These cohorts and their recruitment are described in detail in Chapter 2. Following on from a description of the cohorts I will describe the apathy scales used in this thesis – the Apathy and Motivation Index (AMI), the Apathy Evaluation Scales (AES), the problem-behaviour assessment (PBA) and finally, the Baltimore Apathy Scale. In the final section of this chapter, I will describe the principles of functional magnetic resonance imaging (fMRI) in more detail. In Chapters 4 and 6, I used task and resting state fMRI respectively with different approaches to analysis in both and so each chapter contains a detailed description of the relevant data analysis. Here, I limit the discussion to the principles of fMRI data acquisition and pre-processing.

2.1 Cohorts:

2.1.1 Huntington's Disease Young Adult Study (HD-YAS):

During my fellowship I was part of the study team for the HD-YAS study. The aim of HD-YAS was to identify the earliest features associated with carrying the HD gene (Scahill et al., 2020). HD-YAS was cross sectional, completed at a single site (London, UK) with a case-control design. The study adopted a deep-phenotyping approach. Participants underwent extensive cognitive and neuropsychiatric assessments followed by detailed brain imaging using multiple MRI sequences including structural imaging, resting state fMRI and diffusion imaging. On the second day of their two-day visit participants also underwent a lumbar puncture for analysis of cerebrospinal fluid (CSF). Blood samples were also taken on both days. Full inclusion and exclusion criteria for HD-YAS may be found in Chapter 8 (the Appendix). In summary participants with no significant neurological, psychiatric or medical history between the ages of 18-40 were recruited into the study. HD gene carriers were required to have a CAG expansion of greater than or equal to 40 and no diagnostic motor features of HD. By virtue of their age and CAG length, HD-YAS gene carriers were also required to have resulting "disease burden score" (DBS) of less than or equal to 240 (Mason et al., 2018). DBS is calculated as follows:

Equation (2-1):

$$\text{DBS} = \text{age} \times (\text{CAG} - 35.5)$$

As described in the Introduction the combination of age and CAG length, such as in the DBS, can be used in HD to provide an estimate of the age of clinical diagnosis (Langbehn et al., 2010). In HD-YAS, the DBS cut-off of 240 was used. This equated to an approximate cut-off of 18 years from onset using a well-established predictive model known as the Langbehn model (Langbehn et al., 2004, 2010). In HD-YAS, confirmation of genetic status was gained from local genetics departments and with repeat sequencing as part of the study. Control participants were selected either from controls with no family history of HD or controls with a family history of HD and a negative genetic test. In total 64 young HD gene carriers, with a mean time to onset of 23.6 years, were recruited into HD-YAS, along with 67 close matched gene-negative controls (Scahill et al., 2020).

As part of the study team, I was involved primarily in consenting and completing medical assessments for the larger YAS study. It was from this cohort I also recruited participants into the task fMRI study presented in Chapter 4 (“Gains and Losses”). For this sub-study, I recruited 35 gene carriers and 35 gene negative participants who completed a reinforcement learning task in the MRI scanner while fMRI data was collected. Demographics and further details for this sub-cohort are described in Chapter 4.

The results of the larger HD-YAS study are reported in Scahill *et al* (2020). In summary, there were no significant differences in cognitive or psychiatric assessment in this cohort. Of the neuroimaging measures, only brain putamen volumes were different between groups; however, this did not correlate with time to onset. By comparison, CSF neurofilament light chain and YKL-40 biomarker were found to be elevated in the gene carrier cohort and correlated with time to onset suggesting that these CSF biomarkers may be particularly sensitive in HD.

TRACK-ON HD

In Chapter 6, I use resting state fMRI data collected from the TRACK-ON longitudinal cohort study (Klöppel *et al.*, 2015). TRACK-ON itself was a follow-on longitudinal study to the TRACK-HD study which was a prospective observational study aimed at establishing biomarkers for HD and its progression (Tabrizi *et al.*, 2011, 2012, 2013). TRACK-HD recruited 123 controls, 120 premanifest HD participants and 123 early HD participants in Stages 1&2. Data for TRACK-HD was collected across 4 sites (London (UK), Leiden (Netherlands), Paris (France), and Vancouver (Canada) and similar to HD-YAS included extensive cognitive, psychiatric and motor assessments alongside blood samples and neuroimaging. TRACK-ON HD was developed as an extension to TRACK-HD to study compensation in the premanifest cohort – the ability of some participants to maintain motor and cognitive performance despite the presence of brain atrophy. Data for TRACK-ON was collected at three annual time points between 2012-2014 at the same four sites. Alongside neuroimaging data participants completed a battery of brain MRI measures including volumetric MRI, task and resting state fMRI and diffusion

weighted imaging (DWI). Participants also underwent extensive cognitive, motor and psychiatric assessment.

As described in Kloppel *et al* (2015), the baseline cohort included 106 premanifest HD gene carriers (females 54; mean age \pm SD: 42.8 ± 9.1), 22 early HD patients (females 15, mean age \pm SD: 45.2 ± 7.9), and (3) 111 age- and sex-matched controls (females 67, mean age \pm SD: 48.1 ± 10.7). Of these, 79 controls and 102 pre-manifest participants were previous participants of TRACK-HD (with some pre-manifest participants now classed as HD participants). An additional 33 controls and 30 pre-manifest participants were also recruited. Most pre-manifest and control participants were also in TRACK-HD. As compared to HD-YAS, premanifest patients were required to have a DBS of ≥ 250 , which approximated to ≤ 15 years from predicted onset, and a TMS of ≤ 5 at recruitment. Participants were aged 18-65 years and other inclusion and exclusion criteria were similar to HD-YAS (see Chapter 8: Appendix). For my analysis in Chapter 6, I used resting state fMRI data from the final time-point in TRACK-ON to maximise variance in motor scores. The demographics for this cohort are detailed in Chapter 6.

ENROLL-HD:

In Chapter 5, I completed an analysis using data from the ENROLL-HD study to determine whether a pattern of association was found between apathy in HD and specific motor and cognitive features.

ENROLL-HD is a worldwide observational study and “clinical research platform” (Landwehrmeyer *et al.*, 2017). The aims of ENROLL-HD are threefold – firstly, to establish a worldwide database of patients with HD for rapid recruitment to further studies in particular drug studies; secondly to collect regular standardised assessments of participants; and finally, to compare the care of HD patients worldwide. The study aims to recruit one-third of all affected individuals with HD globally and as such has broad inclusion and exclusion criteria. HD gene carriers at any stage of their condition may be recruited, including pre-manifest individuals assuming that they or their legal representative can give informed consent. Controls may be recruited from participants who are tested and found to be gene

negative, family controls who are not directly related to the patient (such as a spouse) and community controls – participants unrelated to a HD family and who did not grow up in a household with HD. Participants may undergo genotyping as part of the study. Patients with a non-HD choreic movement disorders are excluded. Likewise controls with history of major central nervous system disorder are also excluded. Aside from these few restrictions, ENROLL-HD therefore captures a very representative HD sample.

At each visit a range of core data are collected from each participant including standardised assessments of motor function, cognition, functional capacity and psychiatric symptomatology, including apathy (as discussed below). The core motor assessment uses the well validated Unified Huntington's Disease Ratings Scale 99 (UHDRS '99) providing a measure of chorea, bradykinesia, oculomotor function, dysarthria, dystonia, gait, and postural stability (Mestre et al., 2018). Psychiatric symptoms are measured using the Problem Behavioral Assessment Short Version (PBA-s) which measures the frequency and severity of a range of psychiatric symptoms including apathy (Mestre et al., 2016). Finally, the core cognitive assessments include Categorical Verbal Fluency Test, Symbol Digit Modality Test and Stroop Colour and Word Reading Test. Full details of the ENROLL study can be found on the freely available protocol (https://enroll-hd.org/enrollhd_documents/Enroll-HD-Protocol-1.0.pdf).

Data from ENROLL is released periodically after significant increases in sample size and therefore sample sizes are dependent on when the data is requested. At the time of analysis for Chapter 5, I was able to access data from 2608 patients with manifest HD for my analysis. The demographics of that cohort are outlined in Chapter 5.

2.2 Apathy scales:

In the following section I will briefly describe the principal measurements of apathy used in this thesis. Each data chapter is based on a different cohort as described above and therefore apathy measurements vary based on suitability and availability. In this thesis, four measures of apathy are used – the Apathy

and Motivation Index (AMI), the Apathy Evaluation Scale (AES), the Baltimore Apathy Scale and the apathy sub-scale from the PBA-S.

2.2.1 Apathy and Motivation Index (AMI):

In Chapter 3, I report results from two experiments conducted on young healthy adults to determine the relationship between opportunity cost and apathy. The AMI, a relatively new scale, was developed specifically for the assessment of distinct apathy subtypes in healthy people (Ang et al., 2017). The AMI was adapted from the Lille Apathy Rating Scale (LARS), an apathy scale commonly used in Parkinson's disease (Sockeel et al., 2006). A preliminary 51-item questionnaire was developed and questions were adapted for healthy participants. After an exploratory factor analysis to examine the latent structure of this preliminary 51-item questionnaire, it was determined that a three-factor structure accounted best for the data, broadly falling into themes of behavioural activation (BA), social motivation (SM) and emotional sensitivity (ES) (Ang et al., 2017; Bonnelle et al., 2015). The BA item broadly centred around self-initiation of actions, SM related to willingness to engage socially and ES reflects strength of feelings of positive and negative emotional states. The six highest loading items from each of these three apathy sub-types were retained for the 18-item Apathy and Motivation Index (AMI). This factor analysis was completed on 505 participants with a follow-up confirmatory analysis completed on 479 participants recruited online. SM was found to correlate with both BA and ES however BA and ES were not significantly correlated. Each item on the AMI is scored from 0-4 with a higher score indicating more apathy and total scores can range from 0 – 72.

2.2.2 Apathy Evaluation Scale:

As described in the Introduction, the Apathy Evaluation Scale (AES), which is one of the most commonly used clinical apathy scales, draw heavily from Marin's formulation of apathy (Marin, 1991; Marin et al., 1991). The AES consists of 18-items scored on a 4-point Likert scale with scores ranging from 18-72, with higher scores indicating more severe apathy. The AES has been used as a measure of apathy in a range of neurodegenerative disorders including Alzheimer's disease, Parkinson's disease and Huntington's disease (Clarke et al., 2007; Sousa et al., 2018b; Starkstein et al., 2001). The AES is

available in self-, carer and clinician rated versions and for my pilot study in Chapter 2 the self-rated version was chosen. It has been shown that the self-rating and carer rating of apathy using the AES are highly correlated (Baake et al., 2018b; Mason and Barker, 2015). AES contains sub-scales for cognitive, emotional and behavioural ‘auto-activation’. In HD total AES has been used as a measure of apathy in clinical trials. Although the AES has been validated in a range of disorders, no validation has been completed in HD and as such there are no established cut-offs for clinically significant apathy – cut-off scores range from 30 – 41.5 (Camacho et al., 2018).

2.2.3 Baltimore apathy scale (BAS):

TRACK-ON HD as described above included a self-reported apathy scale described by Chatterjee *et al* (2005) (Chatterjee et al., 2005) . The BAS was developed based on expert opinion and comprises 14 items which Chatterjee *et al* (2005) describe as capturing different dimensions of apathy. Unlike the AMI or AES, no clear sub-types of apathy are identified within the scale. Each item is scored from 0-3 with scores ranging from 0 to 42, with higher scores indicating higher apathy. The interrater agreement between patient and carer rated apathy were highest when cognitive impairment was minimal, as would be the case in a study like TRACK-ON HD. Chaterjee *et al* (2005) describe using a median split to categorise patients as being apathetic or not – this equated to a patient rated score of greater than 15 however to my knowledge this cut-off has not been validated.

2.2.4 Problem-Behaviour Assessment – Apathy:

As described above the problem behaviour assessment (PBA-S) forms a core part of the ENROLL-HD assessment which is completed annually. The PBA-S is completed as a semi-structured interview and includes measures of depressed mood, low self-esteem, anxiety, suicidality, aggression, irritability, perseveration, compulsive behaviour, delusions, hallucinations, and apathy. For each item the interviewer rates both the severity and frequency between 0 and a maximum of 4. For severity 0 represents the absence of apathy, whereas 4 represents marked impairment with the following description given:

“no longer performs any household tasks, even if prompted repeatedly; never initiates activities, and displays no interest in hobbies or pastimes; markedly impoverished speech, rarely initiates new topics of conversation except in relation to own needs; active choices limited to selecting TV programmes to watch, and perhaps switching on or changing channel to do this”.

The PBA-S is performed with carers present where possible however, this is not necessary, and no separate carer rating is possible. The interviewer may use prompts to assess the severity of apathy. Craufurd *et al* (2001) considered an apathy score of 2 or higher to be clinically significant (Craufurd *et al.*, 2001). Although the most limited apathy scale used in this thesis, the PBA-apathy scale has been shown to correlate with the total AES (Naarding *et al.*, 2009).

2.2.5 A note on the measurement of apathy in HD

Given the burden of apathy in HD it perhaps surprising that a common theme which runs through the paragraphs above is the lack of validation or consistency of scales used in various studies. This problem was recently reviewed by Camacho *et al* (2018). Alongside advocating for more research, they concluded that the study of apathy in HD may benefit from diagnostic standardisation, validation of apathy cut-off scores and methodological consistency across studies. While it was not the aim of this thesis to address these issues, they are relevant for the work presented here. I am aware that the lack of standardisation of apathy measures across the data Chapters represents a limitation hampering comparison across the studies I present.

2.3 fMRI principles:

To conclude this chapter, I will briefly summarise the principles of fMRI signal acquisition and data pre-processing. I use task and resting state fMRI data in Chapter 4 and 6 respectively. Here, I will summarise key principles which underlie the methodological details described in those chapters. The fundamentals of fMRI signal are drawn from a number of recent and excellent overviews, and reviews,

of functional imaging (Drew, 2019; Hillman, 2014; Jenkinson, 2018; Penny et al., 2007; Poldrack et al., 2011; Soares et al., 2016).

2.3.1 What does fMRI measure?

When a human head is placed within the strong magnetic field of an MRI machine, hydrogen nuclei, predominantly found in water, act like tiny bar magnets and begin to align with the direction of this field (called B_0 , with the axis of B_0 called the z-axis). As a result of this forced alignment, these protons demonstrate a precession around the z-axis at a frequency known as the Larmor frequency. The frequency of this precession for a proton is the strength of the magnetic field in Tesla multiplied by 42.58 MHz, for example, making the Larmor frequency within a 3 Tesla (3T) scanner approximate 128Mhz.

Through the use of “RF (radiofrequency) coils” within a scanner, it is possible to generate a further small magnetic oscillation by applying a radiofrequency pulse at the Larmor frequency to knock protons out of their z-axis alignment by causing resonance. These RF coils are aligned perpendicular to the main B_0 field. Excitation from these coils drives two processes. Firstly, the magnetic axis of the hydrogen atoms to tilt into the X-Y plane and secondly, the hydrogen atoms to come into phase with the pulse and surrounding hydrogen atoms. This means when the RF pulse is removed, protons will drift back into magnetic alignment with B_0 and de-phase in the X-Y axis. These two processes are governed by two timing parameters – T1 and T2 respectively. T1 determines how quickly a proton regains aligned magnetization in the z-axis. This is typically over seconds. T2 on the other hand determines the rate at which protons in the X-Y plane de-phase from one another; typically, this is in the scale of milliseconds. One of the key principles governing signal detection in MRI is that the T1 and T2 parameters of hydrogen atoms found in the brain vary depending on the tissue type in which they are found. Using this principle it is possible to develop contrast in the signal between tissue types by changing length of time of two key imaging parameters – the repetition time (TR) and the echo time (TE). The TR governs how frequently tissue is excited whereas the TE governs how soon after the excitation the signal is measures. Based on these parameters, images can be produced to amplify the

contrast between tissues based on either T1 or T2 properties within the brain. For example, T1 weighted imaging, typically used in structural MRI, uses short TR and short TE with the resulting image primarily determined by the T1 properties of the brain structures. By comparison long TR and long TE values are used for T2 weighted images, where images are predominantly affected by difference in tissue T2 signal.

For the purposes of fMRI, it is worth expanding on the T2 signal. As described above, T2 is a property of underlying tissues; however, the T2 signal received is also influenced by local field inhomogeneities. The effect of these field inhomogeneities on T2 signal results in a signal known as T2*. When producing T2 weighted imaging “spin-echo” sequences can be used to mitigate the effect of T2* however, for the purposes of fMRI this value is critical. This is because the oxyhaemoglobin is less paramagnetic than deoxyhaemoglobin and as such, increased oxygenated blood reduces the T2* signal loss as compared to deoxygenated blood. Scan sequences sensitive to T2* therefore offer a measurement of blood oxygenation level dependent (BOLD) inhomogeneities in magnetic field.

Before discussing BOLD in more detail, it is worth noting spatial resolution in MRI is generated by the use of gradient coils. These coils subtly alter the B_0 magnetic field strength in three axes such that at any point within the scanner bore, the B_0 strength is subtly different. This means that the Larmor or resonant frequency of hydrogen in different spatial locations is also different, enabling targeted and systematic excitation of the brain. By applying a RF pulse within a specific band of frequencies which correspond to a range of spatial locations along the z-axis, brain slices can be scanned. Data can then be collected in slices either sequentially or using an interleaved design.

2.3.2 The BOLD signal:

Although nomenclature would suggest that fMRI measures brain function, BOLD is a phenomenon driven by changes in the neuro-vasculature and concentrations of deoxyhaemoglobin (Ogawa et al., 1990). The relationship between BOLD and neuronal activation is complicated and not yet fully resolved. Firstly, BOLD is not a measure of oxygen consumption but rather the measure of the over-compensatory oxygenation which follows localised reductions in oxygenated haemoglobin after

increased neural activity (Attwell and Iadecola, 2002; Raichle, 1998). As a result, BOLD lags behind neural activity and peaks 5-7 seconds after brief stimulation with more complex dynamics associated with prolonged or frequent stimulation (Hillman, 2014; Hirano et al., 2011; Martindale et al., 2005). For this reason, in task fMRI designs, as in Chapter 4, care must be given to the timing of specific stimuli to ensure that their respective BOLD signal can be accurately resolved. The shape of the BOLD signal can be modelled as a haemodynamic response function (HRF). In fMRI analysis, the HRF can be convolved with the design matrix for the experiment to yield predicted BOLD responses of a brain region were showing a stimulus driven activity. This can then be compared to signals gathered across the brain to identify which voxels show task relevant activity. Example HRFs following single and repeated stimulation are shown in Fig. 2-1A and B.

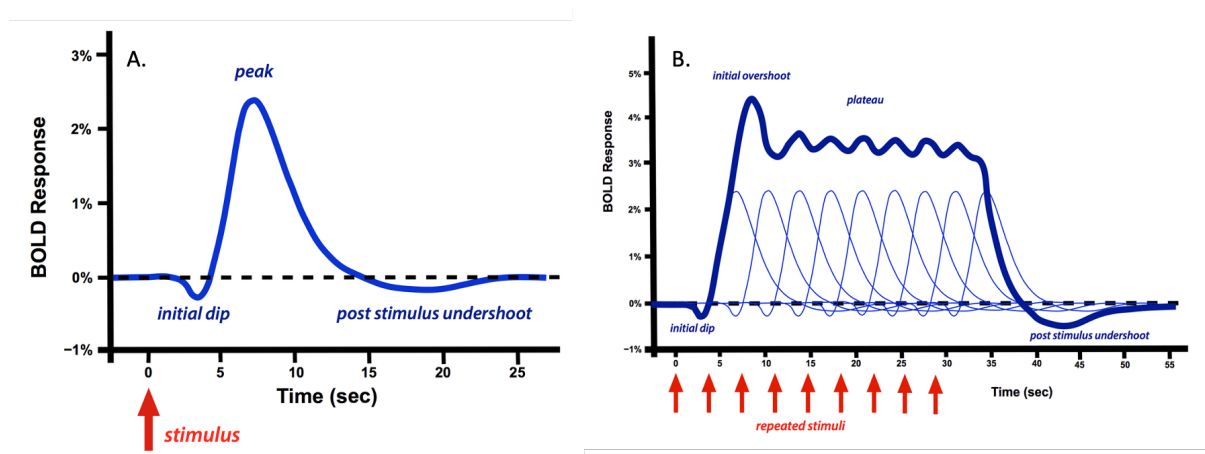


Figure 2-1: A. Schematic representation of the HRF in a single voxel in response to a single, brief stimulus. Plot shows percentage change in BOLD following stimulus presentation. Initially dip in BOLD is followed by a larger overshoot corresponding to over-oxygenation of the brain region following activity. This occurs several seconds after the initial response. B. Shows the HRF estimated in a voxel responding to repeated stimuli. Due to the long duration of the BOLD signal, relative to stimulus onset, the BOLD signal does not have time to reset resulting in a plateau effect as BOLD responses sum. Courtesy of Allen D. Elster, MRIquestions.com (an excellent free neuroimaging resource).

The process explaining how neural activity leads to vascular change and thus BOLD is not yet fully understood and beyond the scope of this Chapter. Current evidence suggests that a range of processes including cell signalling pathways, pericytes, astrocytes, other glial cells and vascular endothelial factors are involved in this neurovascular coupling (Drew, 2019; Hillman, 2014). Given the vascular origin of the BOLD signal, it is not possible to separate neuronal activity through BOLD meaning increased activity in excitatory and inhibitory neurons both results in increased BOLD. Furthermore,

the neuronal property most closely related to BOLD appears to be local field potentials, representing the sum of synaptic inputs and intrinsic neuronal processing, although spiking activity is also correlated (Heeger et al., 2000; Logothetis et al., 2001; Mukamel et al., 2005). In resting state fMRI, further cautions have been raised as the neurovascular coupling models associated with task fMRI may not apply and neuronal-vascular correlations may be weaker (Drew, 2019). In summary, although BOLD offers a non-invasive and safe functional MRI measure numerous questions hang over its meaning.

2.3.3 fMRI pre-processing:

An fMRI dataset itself is four dimensional with T2* weighted images acquired at various co-ordinates (or voxels) throughout the brain stretching over the time of the scan. As described above, by using the differences in Larmor frequencies as a result of gradient coils, images themselves are collected in brain slices by controlling the activation sensitivity. This means that slices of brain activity are not measured across the brain at the same time leading to the need to correct for slice timing in fMRI pre-processing for event-related designs. Another important step in pre-processing is to account for geometric distortions due to magnetic field inhomogeneities. This may be done in two ways, both applied in this thesis. The first is to collect data in a manner which reduces field artifacts in regions of interest and the second is to measure “field maps”. As described in the Introduction, the reward processing network of the brain includes the orbitofrontal brain regions (OFC). The OFC is particularly sensitive to signal dropout in fMRI data acquisition due to the proximity to the sinuses of the skull. Substances of very different densities - air, bone and water for example, interact with the magnetic field of the scanner creating complex variations in the magnetic field known as susceptibility gradients. When these susceptibility gradients interact with the scanner magnetic field, it is possible that the magnetic field gradient experienced in a specific location is not as intended by the scanner. This results in signal drop-out. In plane susceptibility gradients can affect the TE, affecting signals in the phase-encoding direction whereas perpendicular, or through plane, gradients can interfere with the magnetic gradient used to determine the “slice”. In the latter case, susceptibility could mean that regions of the slice are not appropriately excited. Weiskopf et al (2006) and colleagues presented a solution to this problem by

optimising a range of acquisition parameters including the slice tilt, direction of phase encoding and Z-shimming (Weiskopf et al., 2006). Changing slice orientation alters the degree to which susceptibility gradients interact with the phase encoding which may reduce signal dropout. Similarly, altering the direction of phase encoding may reduce susceptibility artifacts otherwise parallel to the phase-encoding direction. Finally, Z-shimming involves adding a further gradient pulse to the sequence to try and counteract the effects of the susceptibility gradients perpendicular to the phase-encoding direction. In Chapter 4, I use an optimised fMRI sequence which aims to minimise distortion and signal drop-out in the OFC, and other reward processing areas. based on these principles, as outlined in Weiskopf (2006). Beyond these measures, it is also possible to account for magnetic distortions by “unwarping” fMRI images. This involves taking capturing the distortions to the magnetic field by acquiring “field maps”. These can then be used to un-deform the images (Penny et al., 2007).

Another source of error in fMRI data may come from motion. If a participant moves during the scanning sequence, inaccurate brain activation patterns are likely to be detected. In some cases, such as real-time fMRI prospective motion correction is possible whereby motion is captured through the use of additional hardware during the scanner (Zaitsev et al., 2017). Alternatively, retrospective motion correction may be applied after images have been collected. This procedure was used in this thesis. In this pre-processing step, the images are realigned with each other such that they are consistently orientated in space. During this process of realignment, motion parameters in six directions are stored and can be used later to regress out nuisance fMRI signals which may actually be residual motion artefact.

After fMRI images from a participant are un-warped, slice-time corrected and realigned to each other, they now need to be aligned with other participants in the study to allow for comparison and group statistics. This is a challenge not least because each subject will most likely have different head shape and dimensions. The solution is the process of normalisation to a standard template. These templates are in essence a “canonical brain” in which location and sizes of brain regions are fixed. In order to run group statistics, neuroimaging data from individual subjects is squeezed or stretched through non-linear

transformations into this standard space. A commonly used template space is that of the Montreal Neurological Institute (MNI). The commonest MNI template is known as the MNI152 (Mandal et al., 2012). This is an average structural brain image from 152 subjects aligned through non-linear transformation to produce a template. Following registration into MNI space each subject's brain shares the same location co-ordinate system meaning, for example, each participant's ventral striatum should be at the same approximate co-ordinates. This also confers the benefit that in standard space, brain atlases may be defined. Discrete atlases parcellate the brain into discrete regions such that each voxel is allocated in only one region. By comparison probabilistic atlases express the probability of voxel being within a specific brain region. These standardised atlases can be used to define regions of interest to restrict analysis or to use as masks. Another advantage is that once in standard space, co-ordinates from published papers may be used to seed regions of interest to investigate for shared activity across studies. In Chapter 4 I used the transformation into MNI space to compare activity in my task with previously published results to demonstrate comparable task activation. Furthermore, I used a discrete anatomical mask of the striatum to limit the voxels in which I performed hypothesis testing. In Chapter 6 by comparison, I used a probabilistic atlas of sub-cortical structures to extract timeseries from a basal ganglia network.

The final step in pre-processing fMRI is to smooth the data. Smoothing blurs the image by changing each voxel's value to the weighted average of surrounding voxels. In effect this reduces the spatial resolution however, smoothing improves the image's signal to noise ratio (Soares et al., 2016). Smoothing also compensates somewhat for differences in registration to standard space and for inter-subject variability. During image analysis, smoothing reduces the number of independent observations within the fMRI dataset (by purposefully spatially correlating voxels) and allows for the use of random field theory (Brett et al., 2003; Penny et al., 2007). These analytical considerations are discussed in more detail in Chapter 4. The degree to which an image is smoothed according to a Gaussian smoothing kernel whose width is defined by the "Full Width at Half Maximum (FWHM)".

Chapters 4 and 6 include fMRI data and analysis however their approaches are quite different. Chapter 4 involves the use of task fMRI to probe the neurocomputational processes engaged in reinforcement learning. The statistical approach in this Chapter 4 is primarily couched in classical statistics with the use of the general linear model to estimate experimental effects. By comparison, Chapter 5 involves resting state fMRI and a Bayesian analytical framework. Although both Chapters involved data acquired and pre-processed as above, they diverge significantly with respect to further analysis. As such, each of these Chapters has a detailed Methods section, not only outlining the details but also the underlying analytical principles.

2.4 Conclusion:

In this Chapter I have aimed to cover broader methodological considerations which apply across the remainder of this thesis. What follows are four data Chapters testing the principal hypothesis laid out in the Introduction namely: (1) Loss of sensitivity to opportunity cost contributes to the development of apathy in HD, and (2) The ratio of disruption to the direct, versus indirect, pathway cells of the striatum drive a proportion of the apathy seen in HD. Each chapter is largely self-contained and includes a separate Methods section to accompany this Chapter.

Chapter 3: Staying Hungry - Opportunity cost determines free operant action initiation latency and behavioural apathy scores

3.1 Abstract:

In free operant settings, deciding *when* to act is as critical as deciding *how* to act. The factors determining when we self-initiate behaviour are poorly understood yet, may be of significant social and clinical importance. Reduced or slowed self-initiated action is a hallmark of behavioural apathy. Using a novel behavioural paradigm, I demonstrate, and replicate in two independent studies, that the choice of free operant action initiation latency is influenced by changes in *opportunity cost*, the amount of reward that could be lost per unit time. Furthermore, I demonstrate in two independent studies that, in younger adults, sensitivity to changes in opportunity cost when determining choice action initiation latency predicts behavioural apathy scores. I also show that sensitivity to changes in opportunity cost predicts clinical apathy scores in a pilot study of patients with Huntington's disease (HD). Taken together, these studies demonstrated that opportunity cost is an important variable in determining our free-operant behaviour. Furthermore, better understanding of the neural basis of opportunity cost may offer some insights into the mechanisms driving apathy.

3.2 Introduction:

In free operant, or self-initiated behaviour, a key decision is the timing of action initiation – should you act now or later? Although many psychological experiments adopt a trial-by-trial design, in most ecological settings prompts are rarely available to guide the timing of our actions. As compared to decisions which involve choosing between multiple competing options, the factors determining our choice of self-initiated action latency are less well understood but may have considerable social and clinical importance.

As described in the Introduction, apathy is a common psychological phenomenon found in both general and clinical populations. In the general population, variance in apathy and motivation levels are thought not only to contribute to academic and work performance but also to health-related outcomes like weight control and later life frailty (Ayers et al., 2017; Desouza et al., 2012; Katzell and Thompson, 1990; Kusurkar et al., 2013). Clinically, apathy is a common neuropsychiatric symptom found in a range of disorders such as schizophrenia, Parkinson’s Disease, Alzheimer’s disease and Huntington’s disease (HD) (Le Heron et al., 2017; Husain and Roiser, 2017; Krishnamoorthy and Craufurd, 2011). In these populations, clinical apathy is commonly associated with reduced self-care, functional decline and the need for external support (Van Duijn et al., 2010; Konstantakopoulos et al., 2011; Pagonabarraga et al., 2015; Starkstein et al., 2006). Apathy is therefore important for both economic and clinical reasons. The concept of apathy is multifaceted with descriptions of behavioural, social, cognitive and emotional apathy in the literature (Ang et al., 2017; Marin, 1991; Robert et al., 2009; Starkstein, 2000). Here, I focus on a core behavioural feature associated with apathy – impairments in the timing of self-initiated goal-directed behaviour.

3.2.1 *When should I act?*

This component of goal-directed behaviour falls largely within descriptions of ‘behavioural apathy’. Marin (1991) and Starkstein (2000) described a ‘dependency on prompts’ as a tell-tale, even diagnostic, feature of apathy (Marin, 1991; Robert et al., 2009; Starkstein, 2000). Levy and Dubois (2006) went

further and placed the quantitative reduction in self-generated behaviour seen in apathy at the heart of their formulation (Levy and Dubois, 2006b). Implied within this quantitative reduction of self-generated behaviour described by Levy and Dubois (2006) is the prolongation in the latency between self-generated actions.

This aspect of behaviour is often described as *vigour* (Niv et al., 2007). Within the literature however, vigour has come to represent both the frequency of action initiation and the force with which those actions are taken. As such, several studies investigating vigour consider the concept of effort discounting – the trade-off between a reward and the exertion of a percentage of one’s maximum effort to ascertain that amount of reward (Le Bouc et al., 2016; Le Heron et al., 2018b; Treadway et al., 2012). Such studies typically have a trial-by-trial design with each trial offering a different effort to reward ratio. The focus of these studies is the integration of cost and reward in deciding which actions to take. Previous work with these designs has shown that apathy in healthy individuals affects probability of accepting effortful options, may be related to effort sensitivity and on a neural level, influence the activity of regions such as the Supplementary Motor Area (SMA) and the cingulate (Bonnelle et al., 2015, 2016; Klein-Flügge et al., 2016).

While related, this chapter is not focussed on the decision problem of whether an action is ‘worth’ the effort or not, but rather, *when* an action should be undertaken if unprompted. Awareness of total effort and reward associated with a decision may be useful in determining which actions to take, however, assuming these values do not change with time, they may not be useful in determining *when* that action is initiated. When using the term vigour in this chapter I am therefore referring to the free-operant response rate.

3.2.2 *When* as a decision problem with an optimal solution:

As described in the introduction, a prominent theoretical framework for modelling decision making problems is to consider such problems as *Markov Decision Processes (MDPs)* (Daw, 2013; Huys et al., 2014; Puterman, 2005). Briefly, as a reminder, within such a framework decision making agents (such as animals, humans or computer programmes) transition from one *state* to another *state* within an

environment by taking *actions* (Sutton and Barto, 2018). The transitions between states are probabilistic in nature and critically for MDPs, the probability of entering a future state is only dependent on the current state and not the history of previously visited states – this is the *Markov property*. As agents move through an environment in this manner, they encounter rewards until they enter a terminal or absorbing state. Depending on the distribution of rewards in the environment, states within an environment are thought of as having different *values*. These state values are based on the rewards immediately available in that state and the value of future states which may be encountered from that state onwards. If a decision maker can compute these state values, they can optimise their choice of actions to maximise their long-term haul of rewards as they traverse the environment. This mapping of which actions to take in each state is called the decision maker's *policy*. Changes in a decision maker's behaviour can be viewed as a change in their policy based on their knowledge of the world.

Framing decision problems as MDPs is advantageous for several reasons. Firstly, MDPs have optimal solutions which can be determined through a range of mathematical techniques such as dynamic programming and reinforcement learning (RL) (Schultz, 2015; Sutton and Barto, 2018). In particular, RL has been used extensively as a model of animal and human decision making and learning (Niv et al., 2007; Palminteri et al., 2012; Pessiglione et al., 2006; Schultz, 2015; Schultz et al., 1997). Furthermore, these mathematical models serve as explicit theoretical models of the generative processes driving behaviour and cognition. Therefore, if they recapitulate or predict behaviour successfully, variables contained within these models may have deeper psychological or neural significance. As many previous studies have shown, including one of the studies I describe in a later chapter, latent variables from these models, such as the reward prediction error, correlate with brain activity in a range of tasks and populations (Chowdhury et al., 2013; Nickchen et al., 2016; Noonan et al., 2012; Pessiglione et al., 2006; Rothkirch et al., 2017; Rutledge et al., 2010; Voon et al., 2011).

3.2.3 Choice of action latency – a gap in the theoretical market

Despite the extensive use of this theoretical framework to model trial-by-trial behaviour in which subjects choose between a discrete range of options, very little work has focussed on the use of these models in the study of free operant behaviour. Niv *et al* (2007) addressed this theoretical gap, and

extended this framework, by proposing that the choice of free operant action initiation latency could also be viewed as a decision problem with an optimal solution. In their computational model, the decision maker chooses not only which action to pick but *when* to take an action. To choose the optimal latency with which to act, Niv *et al* (2007) argued that the decision maker must have computed the *average reward rate*. This variable encodes the amount of reward, on average, that is available in the environment, per unit time. An awareness of this reward rate allows the decision maker to calculate the amount of reward which could be lost if action initiation is delayed – put simply, the cost of sloth. By weighing this *opportunity cost* against the energetic or *vigour cost* of acting too rapidly, the decision maker can derive an optimal latency that maximises their net rewards over a period. Critically, this theory explicitly applies to free operant action initiation. Within this extended framework, every action latency is seen as a decision which can be performed optimally. Prompts are not required to engender action as, immediately after the last action is completed, the decision maker begins to accrue opportunity cost which drives them to act. In algorithmic form, this theory is described as follows:

Equation (3-1):

$$V^*(S) = \max_{a, \tau} \left\{ p_r(a, \tau, S)U_r - C_u(a, a_{prev}) - \frac{C_v(a, a_{prev})}{\tau} - \bar{R}^*\tau + \sum_{S' \in S} p(S'|a, \tau, S)V^*(S') \right\}$$

The optimal value in the current state, $V^*(S)$, is achieved by choosing the best action, a , and latency, τ . For simplicity let us consider a scenario, in which there is only one possible action. Let us also assume that the decision maker is in a recurrent state such that after completing the action (a), the decision maker is returned to the same state (S). The expected value of the reward encountered in that state is given by $p_r(a, \tau, S)U_r$ where $p_r(a, \tau, S)$ is the probability of receiving the reward given the action (a), latency (τ) and state (S) and U_r is the subject utility of that reward. C_u in Eq. (1) represents a fixed latency independent cost of acting.

In this scenario, the optimal state value is determined solely by the decision maker's choice of latency (τ). Assuming the probability of reward is not influenced by the latency, the latency (τ) influences the state value via two key, antagonistic, components of the equation: $\frac{C_v}{\tau}$ and $\bar{R}^*\tau$. C_v , represents a constant

– the ‘cost of vigour’. Longer latencies result in smaller vigour costs (as given by: $\frac{C_v}{\tau}$). However, in this equation longer latencies incur a cost based on the average reward rate (\bar{R}) which reflects the net rewards available per unit time. Longer latencies effectively increase the amount of reward lost per unit time, the opportunity cost ($\bar{R}\tau$). It should be noted in this equation, the opportunity cost is determined by the *optimal* reward rate achievable by the decision maker (as given by $\bar{R}^*\tau$).

A key insight, imbedded within the Niv *et al* (2007) formulation and Eq. (1), is that the average reward (\bar{R}^*) is a global variable encountered in every state. The value of every state encountered by the decision maker is calculated as the difference between the expected value of the reward encountered in that state ($p_r(a, \tau, S)U_r$) and the average reward (\bar{R}^*), calculated across all states. Within the “average reward RL” literature this state value is termed the *differential (or relative) value* of the state (Mahadevan, 1996). This feature of the *average reward* formulation is of value to the study of motivation because, Niv *et al* (2007) argue, it explains the phenomena of ‘general invigoration’. Animals in motivational states, such as hunger or thirst, show an invigoration to complete activities, including non-rewarding activities (Hull, 1943; Niv et al., 2005). Under the opportunity cost model, this is explained because hunger increases the utility of food. When completing other tasks, the hungry animal still incurs the high opportunity cost ($\bar{R}^*\tau$) for longer action latencies as a result of the increased utility for food engendering a shift to faster action latencies. As a further example, let us now reconsider the one-state ergodic example that I described above. Instead of encountering only one state, let us say that with a small probability after taking an action in state 1 (S1) the agent transitions to state 2 (S2). Unlike S1 in which the agent is rewarded however, assume that there is no reward available in S2 but by taking an action the agent can transition back to S1. In this case, carrying the average reward variable into S2 can be used to determine how fast to execute the action to return to S1. Where there is a low average reward, actions in both S1 and S2 will be slowed.

In their paper, Niv *et al* (2007) used this model to successfully recapitulate the choice of latencies with which animals complete a range of free operant tasks. Despite this, there is currently limited evidence to suggest that in a free operant setting, human participants adapt action latencies based on *opportunity cost*. Furthermore, despite the relevance of this theory to impaired self-initiation seen in apathy, no

studies have investigated whether the influence of opportunity cost on action latencies predicts behavioural apathy score.

3.2.4 Predictions from the opportunity cost theory

To address these gaps in the literature, I developed a novel within-subject behavioural paradigm that to test key predictions from the opportunity cost theory. Firstly, I predicted that participants in a free-operant setting would rapidly adapt their choice of action latencies based on opportunity cost and that higher levels of opportunity cost would encourage action initiation. Within the above framework in a new state, with a higher potential reward rate ($\overline{R^*}$) – longer latencies are costlier, and participants should choose to act faster, even when unprompted. Secondly, I also predicted that high opportunity cost would invigorate the completion of non-rewarding actions, like the general invigoration seen in hungry animals. Time spent in non-rewarding states should be invigorated by high opportunity cost as this signal should carry into these states. Finally, given that difficulties with self-generated action initiation are a hallmark of behavioural apathy, I predicted that sensitivity to changes in opportunity cost within a task would predict apathy scores. In popular culture, it is perhaps no coincidence that ‘stay hungry’ is a common motivational slogan. This slogan conveys the idea that maintaining the reward value of a goal, as if one is deprived of it, is critical for motivated behaviour. As described above, within the opportunity cost framework, this ‘hunger’ or motivation may drive a high subjective reward value, or utility, and increases the opportunity cost of time resulting in more frequent action initiation across all states, even those with poor reward rates. As such, it may be predicted that in a task in which opportunity cost was manipulated, the choice of action latency in motivated individuals would be less sensitive to changes in opportunity cost. Their motivated status confers an exaggerated opportunity cost of time making them less sensitive to fluctuations in reward rate within a task. By comparison, if apathy reflects a ‘satiated’ state characterised by a relatively low sense of opportunity cost, this theory predicts that such participants will only choose to emit actions more frequently when opportunity cost is highest.

3.2.5 ‘Motivation’ as a function mapping outcome to utility

In making these predictions, I share the operational definition of motivation espoused in Niv’s thesis as being a function mapping outcomes to their utility (Niv, 2007). I hypothesise that the phenomena of ‘motivational state’, in part, reflects differences in the transformation of outcomes harvested from the world into subjective utility. This function of motivation not only therefore shapes the value of available options, but also determines the subject’s opportunity cost of time. Under this hypothesis therefore, motivation effectively exerts some control over the probability distribution of action latencies that participants are able to choose from.

3.2.6 Data presented in this chapter:

I report evidence from three related experiments each utilising a novel behavioural task that I developed - the ‘Fisherman Game’. Firstly, in an in-lab within subject study I show that in free operant settings, healthy participants adapt their action initiation latencies for rewarding and non-rewarding actions in accordance with the opportunity cost theory. I then replicate these effects in a second independent study in which the task was developed for online use in healthy participants. Secondly, I found that, in these two studies, the sensitivity of action latency choice to changes opportunity cost predicts behavioural apathy scores in the younger adult population. Finally, I show that sensitivity to opportunity cost also predicted clinical apathy scores in a pilot cohort of patients with Huntington’s disease (HD) – a neurodegenerative disease with high apathy prevalence.

In these three experiments I was the academic lead in terms of task and study design. However, I am indebted to two excellent students who ran two of the studies described below under my supervision, Ms. Lesley Farrah-Dorwling Carter and Ms. Fei Shang. Where appropriate, work they performed is credited and their contributions are indicated by their respective initials, LFDC and FS. I also acknowledge valuable discussion with my colleague Ritwik Niyogi who is modelling the data. As this work is not my own, I have not included in this thesis, however, the submitted paper is available as a pre-print (at PsyArXiv: 10.31234/osf.io/d9pgz) and I summarised our findings here for interest.

In addition, I have included in the supplementary section of this chapter data from an earlier pilot task in which, as opposed to making explicit the reward rate, participants were required to emit free-operant responses while the reward rate changed in the background. This task was a precursor to the Fisherman task described below however may be of interest.

3.3 Methods:

3.3.1 Samples:

Experiment (1) - In-lab participants:

Twenty-one younger adult participants were recruited into the first in-lab study. Participants had no known psychiatric history and were not taking any psychotropic medication. The maximum payment for taking part in the experiment was £5. Participants who felt that they struggled with motivation were encouraged to sign up to the study, but participants were not excluded or pre-screened on apathy ratings. This study was approved by the UCL ethics committee (3450/002) and testing was completed in the Max Planck Centre for Computational Psychiatry and Aging, UCL.

Experiment (2) - Online participants

Adult participants (aged 18-65) were recruited from the Prolific online testing portal (<https://prolific.ac/>). 100 participants were recruited. All participants were asked to confirm that they had no history of neurological or psychiatric illness. Participants were not pre-screened by apathy status. Participants were told maximum payment for taking part in the experiment was £5 however due to the nature of online testing participants also received an hourly payment of £5 per hour from Prolific. This study was approved by the UCL ethics committee (12365/002). Participants completed the task remotely. The task itself was hosted on the Gorilla portal (<https://gorilla.sc/>).

3.3.2 Questionnaire data:

In Exp. (1), the in-lab participants completed two questionnaires after finishing the task – the Apathy and Motivation Index (AMI, min: 0 max: 4 with subscales for behavioural, emotional and social

apathy), a validated questionnaire designed to measure apathy in control populations, and the Hospital Depression and Anxiety Scale (HADS, min: 0 max: 21 per scale with total max: 42), a brief self-reported screen tool for assessing depressive and anxiety symptoms (Ang et al., 2017; Stern, 2014). AMI was scored such that higher scores represent higher apathy levels. In Exp (2), the same questionnaires were collected once the task was complete. Given the focus of our experiment, our primary outcome for these experiments was the behavioural apathy score from the AMI.

Based on the correlation co-efficient between price betas and apathy scores as described below, *post-hoc* using G*power, the estimated power achieved in experiment 1 (for an alpha rate of 0.05) was 90.3%. For experiment 2 we assumed a 50% weaker effect online, and to achieve a power of 80% I calculated that we would need 82 participants, however accounting for dropouts associated with online studies we aimed to recruit 100. Post hoc, we found a stronger than expected correlation between price beta and apathy however only in the younger cohort. Based on power calculation, the achieved power in this analysis was 96.6%.

3.3.3 Experiment (3) - Huntington's patients:

We (LFDC and I) recruited 19 manifest patients with HD (mean age 50.4 +/- 8.6, 47% female, Stage 1-2, median total functional capacity 12, range 7-13). These patients were identified from the ENROLL-HD database (Landwehrmeyer et al., 2017). We included, participants between 18 and 65 years old who were not actively depressed, not suffering from an acute psychiatric condition and not taking 3 or more psychotropic drugs. Participants who were more advanced than Stage 2 of the disease or taking part in interventional studies were excluded. As with previous studies, patients who felt they struggled to motivate themselves were encouraged to take part however participants were not screened based on apathy scores. Of the 291 participants identified in the ENROLL-HD database, 73 manifest patients were screened for this study. 29 of these participants were excluded due to ongoing severe physical ill health or acute psychiatric disorder. 44 patients were contacted to take part. Of these, 19 patients meet our inclusion and exclusion criteria and were recruited to this study. These participants completed the Apathy Evaluation Scale (AES, min-max: 18-72). The total AES has previously been validated in HD as a measure of clinical apathy and self-reported apathy on this scale correlates closely with carer

reported apathy. Total AES score has been used to measure apathy in HD and was used as an outcome measure in this pilot study. Participants also completed the AMI as described above. Demographics, anxiety and depression scores (as measured by the Hospital Anxiety and Depression Scale) and performance on symbol digital modality test (SDMT; total correct in 90 seconds) were also collected and controlled for in a linear regression model. To account for relevant motor impairment, the maximum number of keyboard taps in 13 seconds was recorded during the task. All patients provided informed consent and ethical approval for this study was granted by the London – Queen’s Square ethics committee (05/Q0512/74). Testing was completed in Royal London Hospital for Integrative Medicine. Unlike other studies, participants were not paid based on performance.

3.3.4 In-lab task description:

All participants played the task that I designed called the ‘Fisherman Game’. Participants were told that they would play as a fisherman earning money, in fictional yen ¥, by catching fish. To catch fish participants had to press the down arrow key on a keyboard. This action required minimal effort and the force of tapping was not relevant to outcome. Every time they pressed down, they ‘caught’ a fish. The amount of yen earned for each fish was displayed on the screen next to a fish icon. This value changed every 12-13 seconds and was drawn at random from a set of 6 numbers ranging from ¥0.1 to ¥2.5 [0.1, 0.3, 0.7, 1.2, 1.8 and 2.5]. When the price changed participants also heard a bell to alert them to the change in price to minimise effects of poor attention. One block consisted of 12 changes in price. Following each block, participants were given a self-paced rest.

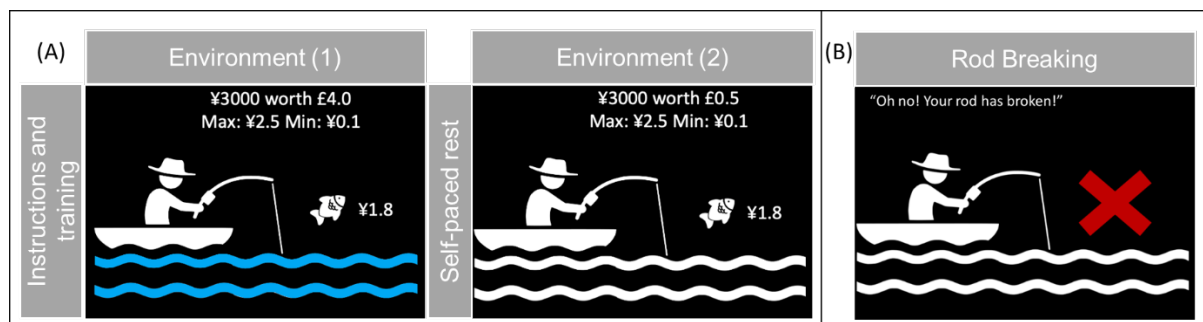


Figure 3-1: Overview of Fisherman Game design: Following assessment of maximum tapping speed, instructions and training, participants completed two counterbalanced environments in which they earned ¥ for fish caught with key presses: high value and low value environment indicated by the monetary value of ¥3000 (£4 or £0.50) and the colour of the water (blue water representing high value and white water representing low value). When not pressing to catch fish, nothing on screen prompted action. To register that a fish was caught, the angle of the fish graphic changed by 45°. A bell sounded each time

the price for fish changed. Information regarding environments and range of fish prices was present on screen at all times. The price of the fish changed every 12-13 seconds and prices were randomly drawn from a set of 6 prices ranging from ¥0.1 - ¥2.5 per fish. Each price was seen four times in an environment and the order of prices was the same in both environments but randomly generated for each participant. (B) Six times in each environment, the participant's 'fishing rod' broke. To fix it they were required to repeatedly tap an alternative button, for no immediate reward a fixed number of times. While the rod broke, no price was displayed on screen, instead participants saw a large red cross which decreased in size with every tap. Time within the task was not stopped while the rod was being fixed.

Participants were told that they would play the fisherman game in two 'environments' each containing two blocks, as described above. Participants were told that in one environment earning ¥3000 would result in payment of £4.00 out of a possible £5.00. In the other environment, they were told earning ¥3000 would only result in a payment of £0.50 out of a possible £5.00. The order of the environments was counterbalanced between subjects and all subjects knew that they would have to play both environments before starting the game. The change in fish price and the change in the environmental value represent the two opportunity cost manipulations in this study.

Finally, to assess whether the change in opportunity cost in each environment invigorated participants, a non-rewarding action was included into both environments of the game. Within the game participants were told their fishing rod may break randomly during the game. To fix the rod, participants were told to tap the right arrow key on the keyboard five times. On the screen, rod breaking was indicated by a red cross which reduced in size with each successive tap. Importantly, rod fixing yielded no additional yen or fish and at the time the rod broke the current price of fish was not displayed. The only value of fixing the rod quickly was to be able to return to collecting fish. The fishing rod broke at three times per block at fixed intervals that differed by block. When the rod broke, time in the task was not stopped. The order of price changes and timings of the rod breaking was identical between the two environments. The task structure and design are shown in Fig. (3.1).

Before starting the experiment, participants read detailed instructions on all aspects of the task including a trial of catching fish for 20 seconds whilst the price changed and a trial of fixing the rod. They also completed a maximum tapping speed assessment over 12 seconds so that participants were aware of their maximum tapping performance before starting the task. When playing the task, on-screen information displayed the current value of ¥3000 in pounds, the maximum and the minimum price of fish. The environment also indicated the colour of the water on screen (see Fig. 3.1). As this task was

designed to test the timing of self-generated or free operant behaviour and not reaction times, nothing displayed on the screen prompted action. To register the catching of the fish, the fish graphic flipped by 45°; however, when the participant did not press, there was no change to the visual display except for the stochastic price changes. Participants were told to go as fast or as slow as they wanted throughout the experiment. The task itself lasted approximately 20 minutes. The task was designed and implemented in Cogent 2000, a psychological toolbox for MATLAB.

3.3.5 Changes for online version:

The task online was almost identical to the one described above. The task was coded by FS in JavaScript and hosted on Gorilla (<https://gorilla.sc/>). The only differences were that the prices changed every 13 seconds with no jitter. Secondly, the number of taps required to fix the rod was increased to 8. At the beginning of the experiment online participants read through the same detailed instructions as the in-lab version. They completed a brief training in which they were instructed to tap for 26 seconds during which the price changed after 13 seconds. All participants were then asked binary (True/False) questions about the task to test understanding. Finally, all participants underwent a sound check to ensure that they could hear the bell when the price changed. The sound check involved correctly identifying three animal sounds. Participants who failed the sounds check ($n = 4$) were immediately excluded. Aside from the 4 participants who were excluded for failing the sound check, 4 participants were excluded due to errors with data at rod breaking (missing data or >42 latencies suggesting an error for those participants). A further two participants tapped very slowly (less than 1 tap per second on average) and were excluded due to lack of data. In total therefore 90 participants were included in the online sample.

3.3.6 Changes to task for HD version:

The HD version of the task was identical to the version described for Experiment (1) however, an additional self-paced break was introduced into each round to minimise the effect of fatigue.

3.3.7 Outcome measures:

Variable of interest in this study was the latency between two successive actions calculated as the difference in timestamps of two button presses. Price at the time of the action initiation, environment and the number of actions pressed per round were recorded. Each latency is therefore considered a decision made by the participant. Latencies for fishing and rod breaking were recorded.

3.3.8 Statistical analysis:

Basic task metrics were first established to assess the effect of the environmental manipulation of opportunity cost. The number of actions initiations were compared, within subject, between the high and low opportunity cost environments.

Action initiation latencies were calculated as the difference between when two key presses were recorded. Outliers were removed from latency data using median absolute deviation (MAD) technique. This outlier removal technique is robust to the presence of outliers and has been recommended for use with latency data (Leys et al., 2013). Using this approach is defined as data point that is greater than 3 median absolute deviations from the median (where $MAD = \text{median}(|Y_i - \text{median}(Y)|)$). Outliers were removed from the raw latency data for each subject in each environment. Latencies were then log transformed for use in linear regression models.

To determine the effect of the environment on rod fixing, the mean log transformed rod fixing latency in each environment was compared using a paired t-test. In the online cohort, the first and last latency recorded for all subjects during rod fixing were removed due to timing errors associated with the change of graphics.

To summarise the effects of our two opportunity cost manipulations, price and environment, at a group level a linear mixed regression model was created. These models are hierarchical in nature, allowing the estimation of effects at the group level, as *fixed effects* whilst also specifying that the data is clustered by subject. As each subject may differ in their sensitivity to opportunity cost these were modelled at the subject level as *random effects*. As such, these models are capable of summarising experimental effects at a group level whilst also estimating individual sensitivities to opportunity cost.

The log transformed latencies were specified as the dependent variable in our model. The fixed effects level included three variables: (1) current price, (2) the environment (low or high as a dummy variable) and (3) the number of taps the subject had performed in the environment. The number of taps captured any linear drift in latencies. Each of these effects was also estimated as random slopes at the subject level alongside a subject specific intercept. Using Bayesian Information Criterion (BIC) to compare models, this complete model resulted in the lowest BIC in Exp. (1) as compared to simpler, nested models with fewer random effects. Linear mixed models were fit in MATLAB 2017a using the **fitlme** function. Models were estimated by fitting an unstructured variance-covariance matrix using a restricted maximum likelihood (REML) fit method. Subject level slopes for price and environment were used as individual measures of sensitivity to our two manipulations of opportunity cost.

We also asked whether these individual sensitivities to opportunity cost were indicative of apathy scores. In Exp. (1), we built a linear regression model to determine whether individual sensitivity to opportunity cost predicted behavioural apathy scores whilst controlling for demographics (age and gender) and symptoms of depression and anxiety (from the HADS score). In Exp (2), the online replication study had a wider age range as compared to the first and we did not find as strong a relationship with apathy as in the first study (see Results). As aging has previously been shown to have an effect of reward-based decision making, *post hoc* we asked whether age influenced the relationship between opportunity cost sensitivity and apathy. Based on the results from the first experiment, we predicted that the effect would be strongest in the ‘younger adults’ demographic group (age 18-35) and we divided our cohort in Exp. (2) into young adults (age 18-35) and older adults (age 35-65).

In the clinical study (Exp. 3), we measured clinical apathy using the Apathy Evaluation Scale. Total scores on this scale have been validated as a clinical measure of apathy in HD. In this analysis, we controlled for confounds related to HD namely cognitive performance measured using the SDMT and motor impairment by controlling for maximum tapping speed with the finger used in the task. The use of psychotropic medications was also controlled for as a dummy variable indicating the use of either antipsychotics, antidepressants or tetrabenazine.

3.4 Results:

The results for the in-lab experiment (Exp. (1)) and the online replication (Exp. (2)) in healthy adults are presented first in tandem, followed by the results of Exp. (3) in HD patients.

Cohort description:

	Experiment 1 (n = 21)	Experiment 2 (n = 90)
Age	22.5 +/- 2.9 (min: 19, max: 32)	38.6 +/- 10.6 (min: 21, max 63)
Gender (F%)	76.2%	51.7%
AMI total	1.4 (+/-0.43)	1.55 (+/- 0.5)
Behavioural AMI	1.6 (+/- 0.88)	1.64 (+/- 0.8)
HADS total	13.7 (+/-7.2)	12.67(+/- 6.8)

Table 3-1: demographics for participants included in the in-lab, Experiment (1), and the online replication, Experiment (2).

Table (3-1) shows the demographic details for participants in Exp. (1), in-lab, and Exp. (2), the online replication study. Although no explicit age range was specified for Exp. (1), other than between 18-65, all subjects fell within the younger adult age range between 18-35. By comparison, online in Exp (2) a wider age range of participants was collected as described in Table 1. Participants were not pre-screened by apathy scores however participants who struggled with motivation were encouraged to take part. Exp. (1) took place under laboratory conditions whereas Exp. (2) was completed online using the Gorilla and Prolific testing platforms.

3.4.1 Increased opportunity cost invigorates action initiation for rewarding actions:

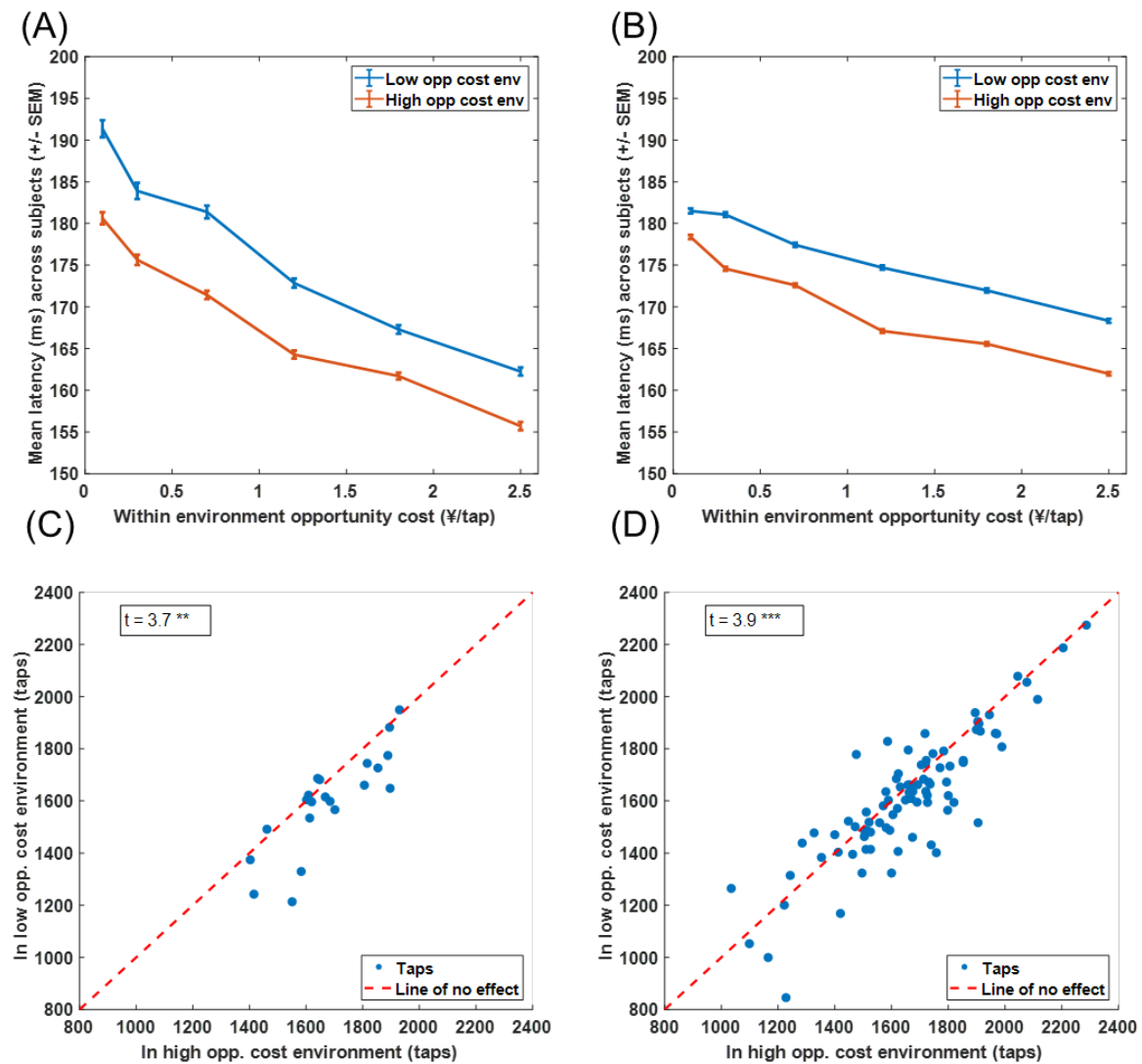


Figure 3-2: Opportunity cost invigorates rewarding actions: (A-B) In both lab-based (A) and online (B) experiments, increased opportunity cost (manipulated by more lucrative environment and higher price for fish) produced the predicted reductions in the chosen latency of free-operant action initiation. Mean chosen latency is plotted by price (¥/tap) and environment (+/- SEM) for (A) Exp. (1) in-lab sample and (B) Exp. (2) online replication sample. (C-D) Higher opportunity cost was associated with more self-initiated action initiation (i.e., more taps) during the fixed environment duration in subjects in both (C) Exp. (1) in-lab and (D) Exp. (2) online replication. Graphs show the number of taps performed by each subject in each environment (low vs. high opportunity cost) as blue dots. Line of no effect is shown as a dashed red line. We predicted more free operant action initiation in the environment associated with higher opportunity cost (i.e., more points below than above the line). ** $p < 0.01$ *** $p < 0.001$

Between the high value environment, in which ¥3000 was worth £4.00 as compared to £0.50 in the low value environment, there was a significant increase in the number of actions subjects initiated as shown in Fig. (3.2) in both the in-lab (3.2C, $t(20) = 3.7$, $p = 0.0013$) and online replication (3.2D, $t(89) = 3.9$, $p < 0.001$).

The effect of opportunity cost on average latencies is shown in Fig. (3.2A&B). I used mixed linear models to summarise group level effects of both opportunity cost manipulations on action latency. I found that participants in both Exp. (1) and Exp. (2) adapted their action latencies with respect to opportunity. For both price (Exp. (1): $\beta = -0.056$, CI: -0.07 to -0.03, $p < 0.001$, Exp. (2): $\beta = -0.039$, CI: -0.05 to -0.03, $p < 0.001$) and environment (Exp. (1): $\beta = -0.049$, CI: -0.08 to -0.01 $p = 0.001$, Exp 2: $\beta = -0.041$, CI: -0.06 to -0.02, $p < 0.001$), as opportunity cost increased action initiation latency decreased. There were also significant fatigue related drifts in latencies (Exp. (1): $\beta = 6.9 \cdot 10^{-5}$, CI: $4.8 \cdot 10^{-5}$ to $8.8 \cdot 10^{-5}$, $p < 0.001$, Exp. (2): $\beta = 4.0 \cdot 10^{-5}$, CI: $3.1 \cdot 10^{-5}$ to $4.9 \cdot 10^{-5}$, $p < 0.001$) in both experiments.

3.4.2 Opportunity cost invigorated non-rewarding actions in healthy participants

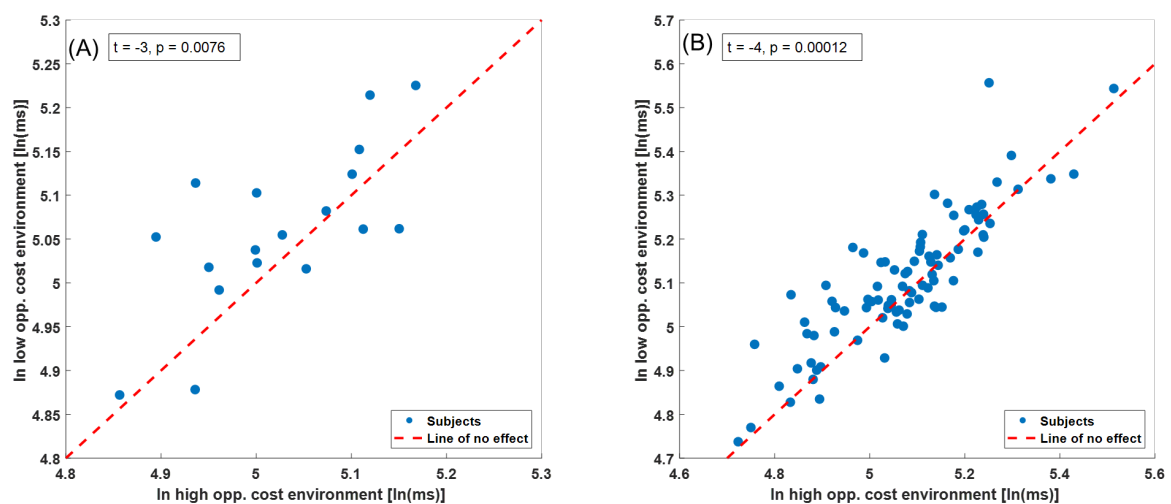


Figure 3-3: Opportunity cost invigorates non-rewarding actions. We found that higher opportunity cost environments led to faster rod-fixing, an action of 0 reward value in both environments, in both A. Exp (1) in-lab ($n = 21$) and B. Exp (2) online replication ($n = 90$). Graphs show mean log latencies of rod fixing in both environments. Line of no effect is shown as a dashed red line. We predicted that most dots will lie above this line indicating slower action initiation in the low value environment.

Higher levels of opportunity would be predicted to have an invigorating effect on non-rewarding actions. In this task, the participants' fishing rod broke during the task. They were required to press a different button to fix the rod and continue collecting rewards. No immediate reward was available for fixing the rod, meaning the latency of rod fixing is driven by the opportunity cost in each environment. In keeping with our predictions participants in both studies showed longer mean latency times in rod

fixing in the low value environment as compared to the high value environment (Exp (1) - Fig 4A, $t(20) = -3.0$, $p = 0.0076$, Exp (2) – Fig 4B, $t(89) = -4.0$, $p < 0.001$).

3.4.3 Individual sensitivity to opportunity cost manipulation predicted task performance

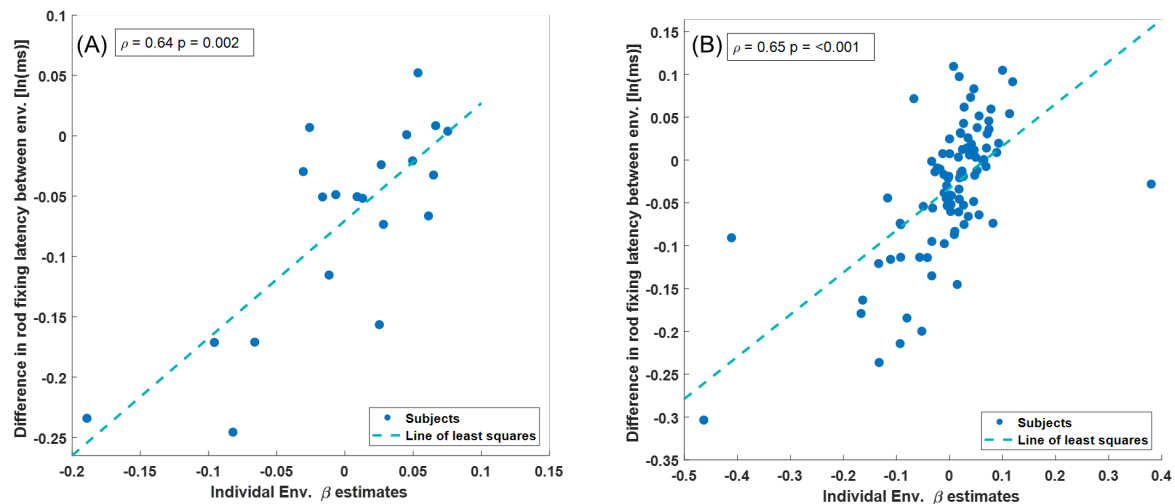


Figure 3-4: Correlation between individual sensitivity to environment manipulation (subject-level env. beta from mixed model) and the difference in mean log latency of rod fixing. Blue dots show individual participants and dashed blue lines show line of least square for A. Exp (1) in-lab sample ($n = 21$) and B. Exp (2) Online replication ($n = 90$).

Individual sensitivity to the environmental manipulation estimated from the linear mixed model strongly correlated with differences in actions initiated between environments (Exp 1: $\rho = 0.96$, $p < 0.001$, Exp 2: $\rho = 0.71$, $p < 0.001$) and difference in mean log rod fixing latencies (Exp 1: $\rho = 0.64$, $p = 0.002$, Exp 2: $\rho = 0.65$, $p < 0.001$, Fig. (3.4)) in both experiments. This analysis was completed to verify the model and make explicit that the rod-fixing effect was driven by the effect of environment.

3.4.4 Individual sensitivity to opportunity cost predicted behavioural apathy scores in younger adults

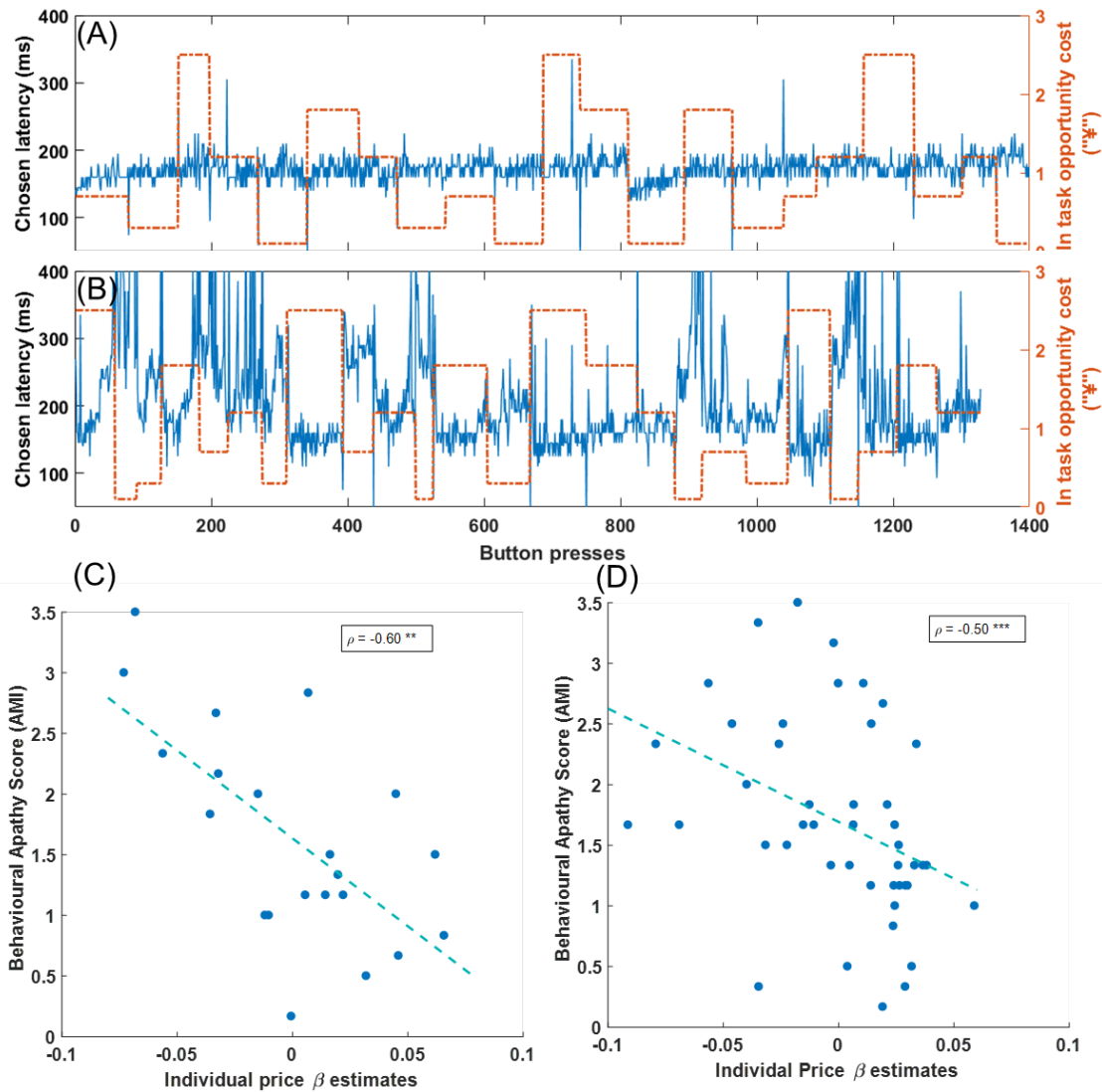


Figure 3-5: Sensitivity to opportunity cost correlates with apathy: Example timeseries from the task as performed by a participant with low behavioural apathy (A – bAMI: 0.83) and a participant with high behavioural apathy (B – bAMI: 3.5) in Exp. (1). Blue timeseries shows the chosen latency for a given button press and orange lines indicate the current fish price. Changes in fish price signal change in opportunity cost, here in the low value environment in both examples. Highly motivated individuals like the participant in (A) showed relatively little sensitivity to change in opportunity cost. By comparison, the example apathetic individual in (B) showed a negative relationship between action latency and opportunity cost. (C-D) Relationship between behavioural apathy scores measured by bAMI and opportunity cost sensitivity (subject-level price beta from linear mixed model) in C. Exp. (1), in-lab (n = 21) and D. Exp. (2), online younger adults (up to 35 years, n = 45). Behavioural apathy scores were significantly associated with opportunity cost sensitivity in both lab ($r = -0.60$ $p = 0.004$) and online samples ($r = -0.50$, $p = 0.0005$). ** $p < 0.01$ *** $p < 0.001$

All participants completed the Apathy Motivation Index (AMI) which is a well validated scale for the assessment of apathy in healthy participants (Ang et al., 2017). The AMI has three distinct subcategories

– behavioural apathy, social apathy and emotional apathy. As this task was designed to assess the effect of opportunity cost on free operant action initiation, I hypothesised sensitivity to opportunity cost would predict behavioural apathy score – more specifically, those with the highest apathy would show the strongest inverse relationship with price.

Fig (3.5A&B) shows the raw timeseries from two participants in Exp. (1). In this figure, the blue lines show the participants, chosen action latencies in the low value environment while the superimposed orange lines show the opportunity cost as signalled by ‘fish price’ changes throughout the task. By comparing these two plots, the choice of action latency by the highly motivated individual was relatively insensitive to the changes in opportunity cost (Fig. 3-5A) as compared to the highly apathetic individual (Fig. 3-5B). The highly apathetic individual shows a stronger negative relationship between action latency and signalled opportunity cost i.e. as opportunity cost within the task reduced, this individual’s chosen action latency increased.

To further explore this relationship a linear regression model was used to assess whether a participant’s sensitivity to opportunity cost, either price or environment, could predict behavioural apathy scores. In these models I controlled for age, gender, anxiety and depression scores. In Exp (1), although both measures of opportunity cost sensitivity predicted apathy at an uncorrected level (Price GLM: $\beta = -11.5$, $t = -3.1$, $p = 0.002$, $F(5,15) = 9.3$, $p < 0.001$, Environment GLM: $\beta = -5.2$, $t = -2.2$, $p = 0.04$, $F(5,15) = 5.5$, $p = 0.004$), only price sensitivity significantly predicted behavioural apathy after using a Bonferroni correction to account for the two tests ($p < 0.025$). In this experiment, price sensitivity predicted neither social apathy ($\beta = -2.8$, $t = -0.7$, $p = 0.49$) nor emotional apathy ($\beta = -5.7$, $t = 1.3$, $p = 0.21$) as measured by the sAMI and eAMI respectively.

I sought to replicate this relationship between apathy and opportunity cost sensitivity independently in Exp (2) however, when including the entire cohort, I found that price sensitivity did not significantly predict behavioural apathy scores (Price GLM: $\beta = -3.4$, $t = -1.7$, $p = 0.08$, $F(5,83) = 9.99$, $p < 0.001$, $R^2 = 37.6\%$) controlling for covariates as described above. As compared to Exp. (2), all participants in Exp 1, ‘in-lab’, fell within the ‘younger adult age’ bracket, namely between 18-35 years. Given that

aging has been shown to play a role in reward-based decision making in a range of studies, we (FS and I) completed a *post-hoc* analysis dividing the cohort into younger (age: 18-35, n = 45) and older working age adult cohorts (age: 36-65, n = 45) predicting that we would replicate the relationship between bAMI and price sensitivity in the younger adult cohort. Post-hoc we found that there was a significant price*age interaction ($\beta = 0.52$, $t = -2.2$, $p = 0.03$). Replicating the results from Exp (1), we found that price sensitivity from this task predicted strongly bAMI scores in younger adults after correcting for demographics, anxiety and depression scores (Price GLM: $\beta = -9.9$, $t = -3.2$, $p = 0.003$, $F(5,39) = 5.7$, $p < 0.001$, $R^2 = 42.2\%$). The relationship between price betas and bAMI in both experiments is shown in Fig (3-5C and 3-5D). In keeping with our *post-hoc* hypothesis – the relationship between price sensitivity and apathy was not seen in the older adults cohort, aged 35-65 (Price GLM: $\beta = 3.0$, $t = -1.2$, $p = 0.25$, $F(5,38) = 8.0$, $p < 0.001$, $R^2 = 51.3\%$). Also replicating results from Exp (1), price sensitivity did not predict sAMI ($\beta = -6.2$, $t = -1.8$, $p = 0.074$) or eAMI ($\beta = -1.2$, $t = -0.48$, $p = 0.64$) scores in the younger adult cohort online.

In summary therefore, in these experiments, the sensitivity of young adults to adapt their free operant choice of action initiation latency in response to changes in opportunity cost within the task predicted behavioural apathy scores.

3.4.5 Individual sensitivity to opportunity cost predicted apathy scores in pilot cohort of patients with manifest HD

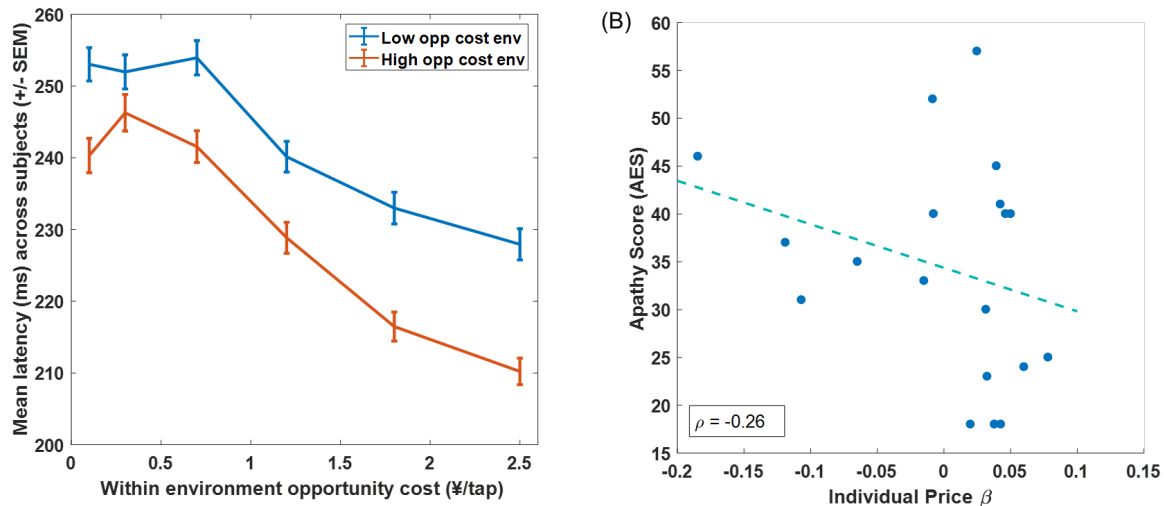


Figure 3-6: HD task results (A) mean (+/- SEM) latency of HD group (n = 19) performing the Fisherman task (B) relationship between price beta and clinical apathy (as measured by AES).

Apathy is a common and disabling symptom in Huntington's disease, an adult onset neurodegenerative population. Despite its prevalence, apathy in HD is poorly understood. Based on the results described above we (LFDC and I) asked whether sensitivity to opportunity cost in our task predicted clinical apathy scores in the HD cohort. A cohort of 19 patients with manifest HD completed the fisherman game. At a group level, HD patients adapted their action latencies with respect only to price but not environment (Price: $\beta = -0.04$, CI: -0.074 to -0.011, $p = 0.007$, Env: $\beta = -0.04$, CI: -0.15 to 0.07, $p = 0.47$). As price changes more often and is more salient, the lack of group level effect of environment may reflect cognitive impairment in HD which affects attention and working memory. Alternatively, the environment manipulation may simply be less sensitive however future work can evaluate this.

Individual price sensitivities for these patients were then used in a regression model to predict apathy scores. Unlike previous experiments, price beta values did not predict bAMI in this cohort however, this scale has not been validated as a measure of clinical apathy in HD. By comparison, the Apathy Evaluation Scale has been used as a measure of apathy in HD and was also used in this study as the dependent variable. Sensitivity to opportunity cost, as a result of the price manipulation, predicted AES apathy scores in the HD cohort (Price GLM: $\beta = -70.6$, $t = -2.7$, $p = 0.02$, $F(7,11) = 9.83$, $p < 0.001$) controlling for the effects of demographic and clinical confounds namely, age, gender, cognitive

impairment measured using the SDMT, depression, anxiety scores and maximum tapping speed of the finger used in the experiment. HD results are shown in Fig 3-6.

3.4.6 Computational modelling:

I have led the work presented above, in terms of design of the task, project co-ordination and analysis. As described in the introduction, the motivation for the task was based on the average reward RL model presented by Niv *et al* (2007). To complete the above project, I have worked with my colleague Dr. Ritwik Niyogi, an expert in average-reward RL, to model the above data, however, I cannot claim this work as my own and therefore I do not include it in this thesis. Instead, I will summarise the findings of this work here and interested readers may find the paper, currently as a pre-print on PsyArXiv (DOI: 10.31234/osf.io/d9pgz)

In brief, the task was modelled as a “real-time cost-benefit decision-making problem, in which subject’s trade-off the opportunity cost of time against the energetic cost of acting quickly” using an average reward RL framework. Each price-by-environment combination was considered to be a separate state and for each participant a “reward sensitivity” parameter and a “vigour cost” parameter was fit, as per Equation (1) above. The modelling focused on the two younger adult studies. We (RN, RR and I) found, and replicated in both studies, that reward sensitivity in our model correlated with apathy in both Exp. (1) ($\rho = 0.62$, $p = 0.008$) and Exp. (2) ($\rho = 0.52$, $p = 0.0009$). As I described in the introduction, I hypothesised that motivated individuals could be thought to react as “hungry” participants – that is, they were predicted to perform the entire task as if opportunity cost was high. By comparison their apathetic, or “satiated” peers, would only be able to generate faster latencies when the opportunity cost was highest. Within the computational model, the reward sensitivity parameter determines the degree of change in subjective utility experienced by the participants going from low to high opportunity cost states. As such, this finding meant that, as predicted, the most apathetic younger adults in both studies experienced the greatest change in experienced opportunity cost of time within our task.

3.5 Discussion:

Ecological behaviour is largely free-operant in nature. We decide not only what action to take but when to take it. When unprompted by the environment, choosing the appropriate action initiation latency is critical in determining how much reward we harvest from the environment. In this series of behavioural experiments, I show with a novel behavioural task that healthy participants rapidly adapt their choice of free-operant action initiation latencies in response to changing opportunity cost, the amount of reward that could be lost per unit time. I found that participants show an invigoration for actions which are not immediately rewarding when overall opportunity cost is high. Furthermore, I found that, in two independent studies, individual sensitivity to opportunity costs predicted behavioural apathy scores in younger adults. I go on to show that in a pilot sample of patients with HD, sensitivity to opportunity costs predicts clinical apathy scores. Taken together these results suggest that awareness of opportunity cost contributes to our choice free operant action initiation latency. Interestingly, there is significant inter-individual variance in sensitivity to opportunity cost between participants which may be, in part, driven by apathy scores.

These findings have potentially important implications for the study of motivation and apathy. I sought to address the problem of *when* we should initiate actions. One of the hallmarks of apathy is reduced self-initiated goal-directed behaviour with apathetic individuals and patients struggling to act in an unprompted manner or do so with prolonged latency. I believe that this work suggests that an awareness of the amount of reward, which is lost per unit time as a result of inaction, may be a critical computational variable in determining when an unprompted action is initiated. For a given price-environment pairing in our task, actions of any latency are rewarded equally. However, longer latencies in our task are costlier to participants due to forgone reward, the opportunity cost. Furthermore, when there is no immediate reward, as in the case of rod-fixing, participants must determine their chosen latency based on the overall opportunity cost in the environment they are in. As compared to effort-based decision-making tasks, I do not modulate effort in this design and require participants to commit only minimal effort in the form of a button press to earn rewards. As such, faster actions are no costlier

in terms of effort in the high versus low opportunity cost settings and yet I found significant within subject changes in chosen latency indicating the role of opportunity cost in this free operant behaviour.

I also found that sensitivity to these changes in opportunity cost predicted apathy scores in younger adults. These results suggest that younger apathetic adults, require higher levels of opportunity cost to generate faster action initiation than their non-apathetic peers. Although this effect was replicated in two studies, it is important to highlight that the effect of aging was identified *post hoc*. Although I predicted a relationship between opportunity cost and apathy, I did not *a priori* predict that this relationship would be influenced by aging. In our study, older apathetic adults were not more sensitive to opportunity cost and this finding needs more investigation. It is known that aging influences a range of factors which may be relevant such reward-based decision making and temporal discounting (Chowdhury et al., 2013; Green et al., 1999; Rutledge et al., 2016). Furthermore, the nature of apathy may change as a result of aging – for example, it may be that apathy in younger adults is a more homogenous construct with a closer relationship with opportunity cost than apathy in older adults. These results are interesting and future planned work will investigate this.

In younger adults, variance in symptoms of behavioural apathy may be driven by variance in the neural representation of opportunity cost. Although I do not probe the biological basis of opportunity cost, theoretical work and recent empirical work *in vivo* animal work proposes that mesolimbic dopamine may signal the value of engaging in work, or the “perceived opportunity cost of sloth” (Hamid et al., 2015; Niv et al., 2005, 2007). Based on this work and results presented here, it may be predicted that younger apathetic participants given L-DOPA may show a greater change in behaviour in this task than younger motivated participants.

Finally, I found that in a pilot study, apathetic patients with HD were most sensitive to opportunity cost, like the younger adult populations. Apathy is very common in HD and is closely associated with disease progression as described in Chapter 1. Striatal degeneration, dopaminergic dysregulation and changes in the availability of striatal dopamine receptors occurs in HD and these changes may alter the coding of opportunity cost in HD patients and its influence on action initiation (Chen et al., 2013; Reiner and Deng, 2018; Waldvogel et al., 2015).

In two previous studies it has been shown that in a trial by trial odd-one-out paradigm, participants modulate reaction times based on experimentally controlled average reward rates confirming a key prediction from the opportunity cost theory (Beierholm et al., 2013; Guitart-Masip et al., 2011). As compared to the results presented above however, these studies did not test whether opportunity cost drives the choice of action latency in free operant settings. Secondly, the reaction times recorded in these experiments not only accounts for vigour of response but also cognitive decision-making time. Incorrect answers lead to no payment and therefore reaction times may also have been influenced by subjects wanting to avoid a speed-accuracy trade-off. Experimenters also actively constrained the reaction times to be less than 500ms and included a time constraint of 400ms in 20% of trials to encourage faster reactions. By comparison, in my task participants were unprompted to act, did not need to make any choices, there was no speed-accuracy trade-off and the tasks involved minimal cognitive load. Finally, these studies are limited in that the reward rate is not made explicit to participants. In their designs, reward rate slowly undulated over the course of the experiment decorrelated from immediate reward. While elegant, this design required the authors to make assumptions about how subjects learned the environmental reward rate. Performance therefore could have been driven by differences in learning as opposed to be driven by the background reward rate. In my task design, I attempted to circumvent this issue by making the opportunity cost explicit throughout the task. Participants therefore did not need to learn any salient variable to decide how quickly to act and were extensively trained.

To my knowledge, the experiments reported here also represent the first reported association between the latency of self-initiated actions in response to changes in opportunity cost and apathy scores. However, three recent studies are of note. Kos *et al* (2017) reported no significant relationship between the timing of self-initiated behaviour and apathy scores in younger adults, aged between 18-40. Aside from the use of a different apathy scale, our tasks differ in several important ways. The task used by Kos *et al* (2017) invoked a trial-by-trial design in which participants chose to press one of two buttons, at their own pace, after a cue. This was contrasted with a condition in which participants were instructed to react as fast as possible to a cue and a condition in which participants made no choice and did not

press either button. As compared to my task, this task prompted action using cues. Secondly, there was no clear opportunity cost on which to base latency decisions. Finally, alongside motor initiation, participants were required to make a choice between two equivalent options and therefore, the measured latency included both decision-making time and action latency time. Muhammed *et al* (2018) report a series of experiments in which participants were asked to modulate their saccade velocity in a trial-by-trial design. Across all three experiments, participants were instructed to act fast or slow and then were required to self-initiate saccades at the appropriate velocity. In the first experiment, no reward was offered for achieving the instructed saccade velocity. In the second, participants were financially rewarded at three different levels for achieving the desired velocity and in the last experiment, participants were financially punished for not achieving the desired speed. Aside from demonstrating that saccade velocity could be self-modulated, this study found that participants most capable of modulating their saccade velocity had higher apathy scores however this effect was only seen in the first experiment. Although the designs of our studies differ considerably, I believe the results presented here are largely in keeping with these findings. In this study I describe an association between behavioural apathy and the degree of change in action latencies - participants with higher behavioural apathy were more susceptible to changes in the externally cued reward rate. In keeping with this, apathetic individuals in the first experiment by Muhammed *et al* (2018) seemingly did not adapt their action velocities in the absence of externally cued rewards however, apathetic individuals in the other two experiments did. As new participants were recruited across the three experiments presented by Muhammed *et al* (2018) however, it is not possible to determine whether change in the ability to modulate saccade velocity, from the first experiment to the second experiment, predicted apathy scores. I would predict that a within subject change between Exp. (1) and Exp. (2) as reported by Muhammed *et al* (2018) may also predict apathy scores. It is important to note however, Muhammed *et al* (2018) do not report a relationship between action initiation latency and apathy, but rather the extent to which participants are able to control velocity of movement was correlated with apathy. More recently, Heath *et al* (2019) found that breakpoints in a touch-screen version of a progressive ratio task correlated significantly with apathy scores in a study that included both HD patients and healthy controls. The progressive ratio task used in this study required participants to complete a basic cognitive task , ‘select

the odd-one-out', repeatedly. Participants could choose to quit at any stage or complete the maximum 432 trials. Participants were reward after 4, then 8, then 16 and finally 32 selections. There were three levels of reward - £1, 20p and 4p. Firstly, was no clear penalty for acting slower within the task – the 432 trials could be completed over any length of time without a reward penalty and therefore, there was no opportunity cost within the task. Secondly, although earlier break points may reflect the relative opportunity cost of carrying on with the experiment as compared to moving on from the task to a different activity, which may have included leaving the clinic for HD patients in this study, this effect not controlled. Finally, it is important to note that in this study apathy correlations were only reported when both samples were collapsed into one group – it appears that break points in this task does not predict apathy scores in either sample when analysed separately.

Aside from studies on vigour, the opportunity cost framework bears some resemblance to the foraging framework, especially the Marginal Value Theorem (Charnov, 1976). In foraging literature, the marginal capture rate represents the average amount of reward, minus effort costs, per unit time is available within a *patch* (Charnov, 1976; Wallis and Rushworth, 2013). If this marginal capture rate for a patch drops below the average for the environment, the animal should choose to move on, incurring an unrewarded travel time. It has been suggested by Le Heron *et al* (2019) that such a framework may have relevance for apathetic symptoms in that failure to calculate the true environmental *capture rate* may lead to apathetic individuals spending time inefficiently in activities which are not rewarding (Le Heron *et al.*, 2019). To date, I am unaware of associations between foraging tasks and apathetic symptoms however, there are some similarities with my task and the concept of foraging. Given the similarities between the capture rate and the average net reward rate, the opportunity cost manipulations in this task – price and environment may engage the same processes as foraging tasks, such regions of the anterior cingulate (Kolling *et al.*, 2012). I show in Exp. (1) and Exp. (2) participants chose faster latencies in fixing the rod in the high versus low value environment. Although this effect can be explained as invigoration secondary to high levels of opportunity cost, a similar behaviour may be predicted within the foraging framework. As the reward rate during rod fixing is zero, the foraging literature would suggest that participants may aim to move on from this patch quickly, relative to the

average reward in the environment. Equally, although there is no travel time in this task, the time spent between actions effectively incurs the same cost as travelling between patches. Viewed in this way, the fact that participants overall chose shorter latencies in the face of high opportunity cost could be equivalent to choosing shorter travel times in foraging tasks when there is a high capture rate.

This study has several strengths. Firstly, the task encourages free operant action initiation without adopting a trial by trial design. As such, the task shares a key characteristic with ecological behaviour in that there are no prompts to guide the timing of actions. Secondly, by making explicit the current reward rate the behavioural differences I report are unlikely to be driven by differences in participant learning rates. Furthermore, changes in opportunity cost were signalled with salient visual and auditory stimuli to minimise the impact of attentional difference. As a result of these design elements I feel that variance in the behaviour observed is driven by primarily by variance in the sensitivity of individuals to externally cued opportunity cost. Following on from the first experiment, I also sought to independently replicate our results by running the experiment online. By adopting this approach, and replicating the main results, I sought to avoid effects driven by any recruitment bias associated with in-lab cognitive testing. I also demonstrated that this task can be meaningfully applied to clinical populations, including those with motoric impairment, however the apathy relationship in HD requires follow-up work in larger studies.

I would also like to highlight a few potential limitations. Within the theoretical model, the optimal rate of reward ($\overline{R^*}$) - represents the optimal *net* reward rate, including vigour costs. Therefore, choice of faster latencies, theoretically represents the effect of both reward sensitivity and vigour costs. Here I demonstrate that as the reward rate is changed during the task, participants adapt their latencies accordingly. Within subject, only reward rate was modulated in this task however between subject, variance in both reward sensitivity and vigour cost may explain the apathy relationship. I did not independently modulate the vigour cost; however, I would predict that these results may be driven by differences in reward sensitivity primarily. Firstly, the vigour cost term in the original formulation is different from 'fatigue'. Where fatigue would be expected to scale with the number of actions performed, this is not true of vigour cost. Every action, taken with the same latency, accrues the same

vigour cost, irrespective of whether it is the first or hundredth action. As such given that the task involved simply pressing a keyboard key, for which there was no travel or reach time, and force was not relevant to outcome, it is likely that the absolute vigour cost for each key press is likely to be very small. Future work may which to modulate vigour cost, however, should do so without influencing the time taken to complete the action and secondly avoid a speed accuracy trade-off. It may also be argued that the action used in this study was relatively so simple that it may not translate into more complex of energetic action such as walking. Beyond the apathy data, I collected no measures of free movement speed with which to correlate task performance, although this is work I hope to conduct in the future. It should also be noted that recent work has shown the vigour of movements may be a personal ‘trait’ as opposed to dependent on that value of energetic cost of particular action being performed. Reppert

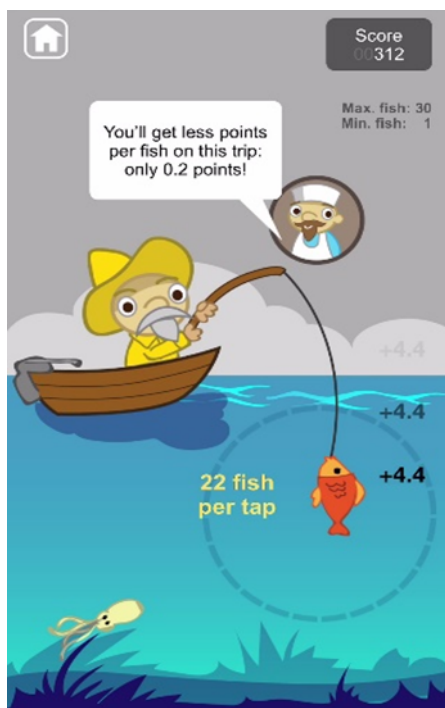


Figure 3-7: Screenshot for smartphone adaptation of fisherman game.

et al (2018) show that head movement velocity and arm reach velocity are very strongly correlated, for the same rewarding outcome, despite the obvious differences in energetic cost. Based on these findings, and the findings between task performance and apathy in my work I would predict that task performance strongly predict free movement – as measured by movement data. This task has been developed for smartphone and this platform will enable us to test these hypotheses (Fig. 3-6).

I also note that in this task, only price sensitivity predicted apathy and not environmental sensitivity despite both being

the task design, the environment manipulation was used to test some of the fundamental predictions from the model; however, as compared to the price manipulation the environmental manipulation had one level, as opposed to six different prices. As such, this may be limited the interindividual variance in the effect of environment. Secondly, relative to price, the environment was a less salient manipulation. It changed once during the task and was only cued visually. By comparison, the price changed frequently and was associated with an auditory signal. As

such, participants may have attended less to the environmental opportunity cost manipulation resulting in weaker than expected effects.

It should also be noted that although participants showed an invigoration for rod fixing, this effect is not precisely same as the general invigoration described by Niv *et al* (2007). Firstly, the rod fixing is not goal-independent and secondly, participants did not choose when to fix the rod. As such rod-fixing differs from, for example, drinking water more quickly when hungry. An alternative design would have been to introduce an optional additional action into the task for which participants were rewarded with some non-monetary reward however, standardising the choice of this option across participants and environments was hard to achieve. I would also argue, that despite the difference between rod-fixing and invigoration as described by Niv *et al* (2007), participants in this study lose time to collect rewards much like hungry animals who choose to drink as opposed to look for food. As such, rod-fixing in this study is invigorated for the same reasons, namely due to the increased opportunity cost between the two environments. Finally, the sample size for the clinical experiment was small. As such, I view these results as pilot data - indicating that this task is tolerable in patients with apathy and motoric impairment however follow-up work is required to assess the relationship between task performance and apathy.

3.6 Conclusion:

In conclusion, using a novel task I find that opportunity cost is likely to be an important determinant in the choice of free operant action initiation latencies in healthy participants. I find, for the first time, a link between sensitivity to opportunity cost and symptoms of apathy in general and clinical populations. These results suggest that better understanding how opportunity cost is coded in the brain and how it affects action initiation may also allow us to better understand symptoms of apathy.

3.7 Supplementary Material

In this section I will briefly describe a pilot study I conducted early in my fellowship. Unfortunately, I do not currently have access to the data however here I will describe the design of that study and show some of the results I generated at the time taken from my log of previous results. Overall a similar pattern of responding was seen to that described in the Fisherman.

In this task participants were told that they could earn up to £5 by tapping the down key on the keyboard. They were told that they would be paid based on the number of points they accumulated. They were also informed that the number of taps needed to earn one extra point would change over the course of the experiment however they were not aware of when the changes occurred. On the screen was simply the text displaying number of points earned. There were 6 fixed ratios each lasting 11 seconds requiring 1, 3, 7, 12, 18, or 25 taps to gain one point. Each ratio was seen four times. Unlike the fisherman, there were no cues signalling a change in ratio and on screen was simply the score. For this pilot I recruited 17 participants.

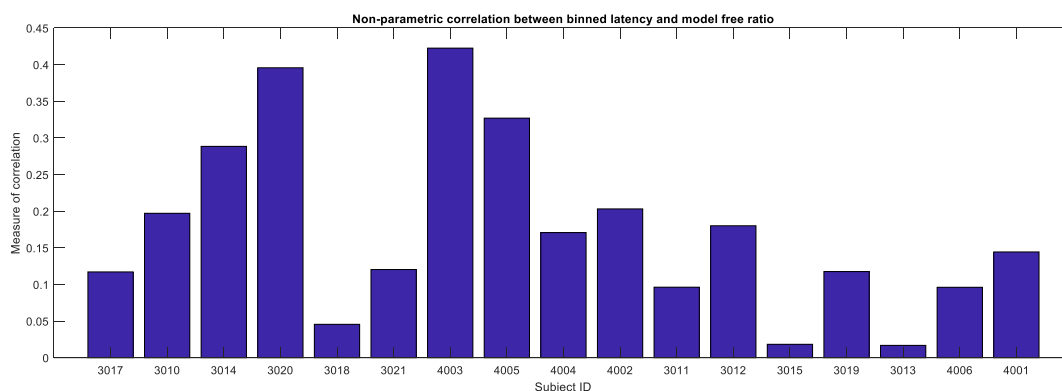


Figure 3-8: each participant's Spearman correlation co-efficient between the mean log latency within each ratio and the ratio from the task. Please note that in this case, the ratio is inversely correlated with the opportunity cost.

As shown in Fig 3-8 across the participants, I found a positive correlation between the free-operant response latency and the hidden ratios in the task. This represents the same effect seen in the fisherman task as the higher the ratio, the lower the opportunity cost. Unfortunately, in this pilot I did not collect bAMI data to test the association between the correlation coefficients and bAMI. I would predict that participants with the lowest correlation would have the lowest bAMI scores.

I chose to move on from this design because, although this task was unstimulating and offered no prompts to action throughout, I wanted to remove minimise effects driven by differences in learning.

Chapter 4: Aberrant striatal value representation in Huntington's disease gene carriers 25 years before onset

4.1 Abstract:

Huntington's disease (HD) is a devastating genetic neurodegenerative condition typically manifesting clinically in the fourth or fifth decade. With the advent of genetic therapies there is increased need to identify the earliest changes associated with carrying the HD gene. Using computational fMRI, I found that, in comparison to matched controls, gene carriers 25 years from motor onset showed exaggerated striatal responses to gain- as compared to loss-predicting stimuli in a reinforcement learning task. Using computational analysis, I also found group differences in striatal representation of stimulus value. These represent some of the earliest functional imaging differences between gene carriers and controls. Behaviourally gene carriers, 9 years from predicted onset, have shown enhanced learning from gains as compared to losses. Importantly, no group differences in behaviour, or caudate volumes. This data suggests a therapeutic window exists whereby HD-related functional neural changes are detectable 25 years before predicted onset.

4.2 Introduction

As argued in the Introduction, motivated behaviour may be considered the sum of a number of sub-processes that must be performed optimally in order to maximise net rewards (Le Heron et al., 2018a; Levy and Dubois, 2006a). In the last chapter, the focus was on the timing of self-initiated actions - *when* we initiate actions and not which actions we choose. More specifically, I presented data from a series of experiments in which I investigated the role *opportunity cost* plays in the self-initiation of actions and its relationship with apathy (Niv, 2007). In this chapter, I move away from the issue of timing, instead focusing on another sub-component of motivated behaviour - learning. In particular this chapter primarily focuses on a form of learning known as *instrumental conditioning*. This form of learning describes the behavioural adaptation seen when feedback, either positive or negative, is given following an action to either increase or decrease the probability of repeating that action (Staddon and Cerutti, 2003). As described by Le Heron *et al* (2018), learning from the outcome of actions is considered a key component of motivated behaviour (Le Heron et al., 2018a). In my working definition of motivated behaviour, maximising rewards requires taking optimal actions which can only be learnt based on feedback. The literature on this form of behavioural adaptation is extensive and is frequently modelled using reinforcement learning, both to better understand the behaviour itself and to probe the neural mechanisms (Daw, 2013; Daw and Tobler, 2013). In this Chapter, I build on this literature to ask a highly clinically relevant question – could aberrant instrumental conditioning be one of the very early consequences of carrying the HD gene?

As described in the Introduction, HD is caused by a CAG triplet repeat expansion in the *huntingtin* gene (Bates et al., 2015; MacDonald et al., 1993). The length of this expansion is proportional to the age of onset of motor signs which typically starts between the ages of 40 to 50 (Langbehn et al., 2010). Although unequivocal motor features of HD are first seen at this point, neural atrophy and cognitive deficits are present earlier, in the premanifest phase (Ross et al., 2014b; Stout et al., 2011; Tabrizi et al., 2011). Given that disease related changes occur before clinical diagnosis and with the disease

modifying drugs for HD currently under investigation, an open question remains – what are the earliest changes associated with carrying the HD gene (Tabrizi et al., 2019; Wild and Tabrizi, 2017)?

HD is characterised by a range of cognitive deficits particularly in fronto-executive functions such as attention, processing speed, set-shifting and emotion recognition (Dumas et al., 2013; Paulsen, 2011; Snowden, 2017). Underlying these cognitive deficits is neuronal atrophy or dysfunction secondary to *mutant huntingtin (mHTT)* expression. In particular, the medium spiny neurons (MSNs) within the striatum, especially those within the indirect pathway, are highly susceptible to the HD disease process (Calabresi et al., 2014a; Niccolini and Politis, 2014; Waldvogel et al., 2015). In recent years, it has also become clear that the striatum is a key node in learning to maximise rewards (Crittenden and Graybiel, 2011; Graybiel and Grafton, 2015; Haber, 2011, 2016; Wilson et al., 2018b). In keeping with these findings, differences in reward processing tasks have been found in HD gene carriers, both in the manifest disease and in the pre-manifest phase up to 10 years before onset (Enzi et al., 2012; Nickchen et al., 2016; Palminteri et al., 2012; Perry and Kramer, 2015; van Wouwe et al., 2016).

Maximisation of rewards is central to the working computational definition of motivated behaviour that I proposed in the Introduction to this thesis. Learning to maximise rewards, however, requires symmetrical, and optimal, performance in learning to both gain rewards and to avoid losses. Although these two processes involve different brain regions, both have been shown to activate the striatum (Daniel and Pollmann, 2014; Liu et al., 2011; Pessiglione et al., 2006). This is perhaps expected as many computational models place the striatum at the centre of behavioural policy adaptation which must occur in both pursuing gains, and avoiding losses (Collins and Frank, 2014; Franklin and Frank, 2015; Joel et al., 2002). Furthermore, striatal activity associated with both gains and losses is predicted by computational models of striatal function such as Opponent Actor Learning (OPAL), described in the Introduction, that focus on the roles of the *direct* and *indirect* pathway in behavioural adaptation (Collins and Frank, 2014; Franklin and Frank, 2015). These opponent pathways comprise MSNs that show differential expression of dopamine receptors, with D1 receptors preferentially expressed on direct pathway cells and D2 receptors expressed on indirect pathway cells (Macpherson et al., 2014). Models like OPAL argue that the net result of this physiological asymmetry is that as the value of an

action is learnt through dopamine-mediated error signals, cortico-striatal synaptic weights and activity within the direct and indirect pathway represent the value of taking or avoiding an action, respectively.

These models are relevant for probing early dysfunction in HD for two reasons. Although gross striatal atrophy is found in HD, the distribution of cell loss across the direct and indirect pathways is not the same (Albin et al., 1992; Deng et al., 2004; Waldvogel et al., 2015). In particular, MSNs within the indirect pathway are affected more than those within the direct pathway. If these cells contribute to avoidance it may be predicted that loss avoidance may be impaired in HD (Zalocusky et al., 2016). Intriguingly Palminteri *et al* (2012) reported that behaviourally, premanifest HD gene carriers approximately 9 years from onset showed such a ‘reward bias’ in learning. In their study, premanifest gene carriers showed better learning from gains as compared to losses, with computational modelling suggesting that this effect was mediated by noisier decision making in the loss frame. (Palminteri et al., 2012). Given the early involvement of the striatal indirect pathway in HD and the proposed role this pathway plays in learning from losses, such an asymmetry between gain and loss learning, or “reward bias”, may be predicted as an early change associated with carrying the HD gene (Albin et al., 1992; Collins and Frank, 2014; Deng et al., 2004; Hikida et al., 2010, 2013; Waldvogel et al., 2015; Zalocusky et al., 2016).

On this basis, I asked whether a ‘reward bias’, or asymmetry between gain and loss learning could be one of the earliest functional imaging features associated with carrying the HD gene. To address this question, I undertook an fMRI study in which young healthy HD gene carriers predicted to be 25 years from clinical diagnosis, based on CAG length and age, completed a RL task to gain rewards and avoid losses. Compared to well matched control participants, I asked whether there was evidence of an asymmetry between gain and loss learning, in the HD gene carriers either at a behavioural level or in the corresponding fMRI signal. I looked for such a reward bias in fronto-striatal regions of interest (ROIs) at both cue and outcome presentation and used computational modelling to better understand the findings.

I would like to note that while I led this study in terms of study design, implementation, coding and analysis, this work formed a sub-study within the larger HD Young Adults Study (HD-YAS) (Scahill

et al., 2020). I am indebted to the members HD-YAS study team for recruitment of the cohort described in this chapter and for data collection. I am also indebted to Dr Robb Rutledge for frequent advice on the execution of this study and to Dr Steve Fleming for providing openly available fMRI analysis code from which I was able to learn a tremendous amount. Last and no means least, I am incredibly grateful for the participation of the young HD gene carriers in this study. Although their genetic mutation undoubtedly hangs over them, at this stage in their life it would be easy to continue in the belief that the effects of the gene have not yet started. By taking part in a study like HD-YAS, these participants confronted this denial head-on. In doing so, they demonstrated a bravery and maturity for which I am most grateful.

Please also note, this Chapter has been accepted, in edited format, for publication in *Biological Psychiatry: Cognitive Neuroscience and Neuroimaging* (Nair *et al* 2021).

4.3 Methods:

4.3.1 Participant details:

The study sought to detect some of the earliest signs of carrying the HD gene. To achieve this, 35 HD gene carriers and 35 matched controls who did not carry the HD gene completed this study. All participants were aged between 18-40 years old. Gene carriers were required to show no diagnostic motor features of HD (diagnostic classification score < 4), have a CAG repeat size ≥ 40 and a disease burden score (DBS) of ≤ 240 indicating these patients are approximately 20 years from onset. Control participants were required to have no known family history of HD or have been tested for HD and not found to be at genetic risk. Exclusion criteria included substance abuse, the use of any medications to treat HD, unstable dose of antidepressants in the past 30 days and significant medical or psychiatric history. Groups were matched for age, gender, highest education level and handedness. Both groups underwent neurological examination by experienced HD clinicians to confirm the absence of gross motor signs associated with HD. Participants underwent a cognitive assessment including the National Adult Reading Test as a measure of premorbid intelligence and core cognitive measures sensitive to change in HD. These included the Symbol Digit Modality Test (total correct in 90s), Stroop word and colour reading (total correct in 45s) and verbal category fluency (scored as unique responses in 60s). Demographics for both groups can be found in Table (1). This study was approved by the Bloomsbury Research ethics committee (16/LO/1323). Sample sizes were chosen *a priori* based on data from Palminteri (2012) on the assumption that the pre-manifest group would show a greater reward bias than the controls however this effect of 50% less than reported by Palminteri (assuming the same standard deviation in both groups). Using G*Power 3.1, it was estimated that sample size of 32 was required in both groups to achieve an alpha rate of 0.05 and a power of 0.9. I did not however see a group difference in behaviour how do report a group differences in ROI betas. Using a post-hoc power calculation for the one-tailed test in ROI betas, with sample size of 35 in each group and an alpha level of 0.05, I estimate a post-hoc power of 83% with an effect size $d = 0.63$ (medium effect).

4.3.2 Task description:

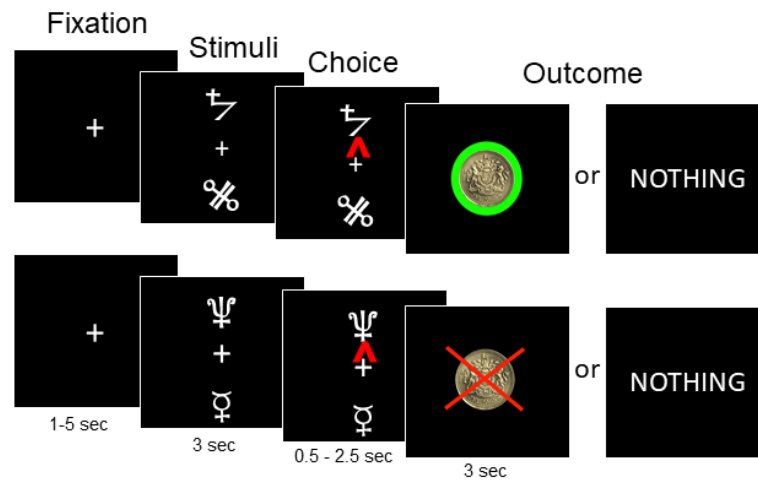


Figure 4-1: Reinforcement learning task with gain and loss domains was performed by subjects. Participants were presented initially with a fixation cross. This was replaced by two abstract symbols. Participants saw three such abstract pairs – a ‘gain pair’, ‘loss pair’ and ‘neutral pair’. Using a button box in their right-hand participants were instructed to press the button to choose the top symbol or withhold their response for 3 seconds to choose the lower symbol. Their choice was displayed with a red marker before the outcome was revealed. In the gain pair, one symbol was associated with reward with a probability of 0.8 and the other with a probability of 0.2. Similarly, in the loss pair, one symbol was associated with losing reward with a probability of 0.8 and the other with a probability of 0.2. Reward in the gain condition was signified with a picture of £1 with a green halo and loss signified with red cross through the £1. Alternatively, participants saw the word ‘Nothing’. In the neutral condition, participants saw an empty disc or the word ‘Nothing’. Timings for transition are shown in the figure and described in Methods.

The task used in this study was identical in design to that described by Pessiglione *et al* (2006) and Palminteri *et al* (2012) to allow for comparison between results (Palminteri *et al.*, 2012; Pessiglione *et al.*, 2006) and shown in Fig 4-1. Compared to previous research, it is important to note that participants were not paid for study participation or for performance. In summary, participants completed a reinforcement learning task in which the aim was to maximise rewards by learning to choose the best symbol from a pair of abstract symbols displayed on the screen. One of the symbols was associated with a “better” outcome with a probability of 0.8 and the other symbol was associated with the same outcome with a probability of only 0.2. Participants saw three pairs of such symbols corresponding to the three conditions – gain, neutral and loss. With the gain frame the better outcome was to win fictional money (£1) as compared to earning no reward. In the loss frame, participants could either receive no reward or lose £1. In the neutral conditions, both outcomes yielded no reward. In the gain condition if

participants won, they saw a high-resolution image of a £1-coin with a green surrounding halo. If they lost, they saw the same £1-coin image with a red cross superimposed over it indicating they had lost money. In both gain and loss conditions the alternative outcome was to see the word ‘Nothing’ appear on the screen. In the neutral condition the two outcomes were either an empty grey disc the same size as the pound coin or the word ‘Nothing’. Stimuli were placed above and below a central fixation cross. To choose the upper stimulus participants were required to make a ‘Go’ response and press a button on an fMRI compatible button box using their right hand. Alternatively, to choose the lower symbol participants withheld response for 3 seconds. Symbol position was random in each trial, so position and value were orthogonal. After either a button press or 3 second delay period, choice was displayed for a jittered interval ranging from 0.5 – 2 seconds drawn from an exponential distribution. Outcome was then displayed for 3 seconds followed by a jittered inter-trial interval (ITI) ranging from 2-6 seconds drawn from an exponential distribution.

Participants were shown each pair of stimuli 30 times with a total of 90 choices per run. Participants completed two runs in the scanner lasting on average 12-14 minutes each. Prior to completing the task in the scanner, participants were given instructions and carried out one run of the task outside of the scanner to familiarise themselves with the task. In the scanner, instructions were repeated before the task began.

4.3.3 Behavioural and computational analysis:

Behaviour from both runs was concatenated and a reinforcement learning model of behaviour was fit to the subject data across the two runs. Percentage correct was determined by the number of times a subject chose the best symbol in the gain and loss pairs. The difference between the percentage correct in gains and losses was used to compute the ‘reward bias’ term. Differences between groups were tested using either a ‘ranksum’ test, or independent t-tests where appropriate after assessment of data distribution, with Z and t-statistics reported respectively. For all t-tests, the degree of freedom was 68 ($n_1 + n_2 - 2$). All behavioural analyses were completed in MATLAB R2017a.

Behaviour was modelled using a standard Q-learning model, combining a Rescorla-Wagner learning model with a softmax action selection mechanism. The value of the chosen option (Q) was updated for the next trial ($i+1$) by updating its current estimated value with the prediction error (δ) multiplied by the learning rate (α) (Sutton and Barto, 2012):

Equation (4-1):

$$Q_{a(i+1)} = Q_{a(i)} + \alpha * \delta_{(i)}$$

The prediction error term was calculated as follows:

Equation (4-2):

$$\delta_{(i)} = reward_{(i)} - Q_{a(i)}$$

where $reward_{(i)}$ represents the outcome following choice. Outcome values were 1 for gaining money, 0 for nothing and -1 for losing money. Action selection was modelled using the softmax function in which probability of choosing action is determined as follows:

Equation (4-3):

$$P_a(t) = \frac{e^{Q_a(t)*\beta}}{\sum_{i=1}^n e^{Q_i(t)*\beta}}$$

Using this action selection rule, the probability an action is chosen is based both on its relative value to the other option and a computational term, β , which represents choice stochasticity. Initial Q values for both symbols for gain domain choices were set at 0.5 and -0.5 for loss domain. This reflects the fact that participants have knowledge about each symbol valence before experiencing outcomes due to their experience with the other symbol pairs. Parameters were fit to maximize the likelihood of the participant's choice using the *fmincon* function (alpha bounded between 0 and 1, inverse beta bounded between 0 and 100). The search was initiated at multiple (40) random start points in parameter space to avoid local minima. Goodness of model fit is reported with McFadden's pseudo- R^2 calculated as $1 - \log$ likelihood of the model divided by \log likelihood of null model (in which choices are determined by chance). There were moderate significant correlations between learning rate and temperature ($r = 0.62$ ($p < 0.01$) in gains and $r = 0.63$ ($p < 0.01$) in losses).

This model reinforcement learning model provided good model fits for both gains and losses (McFadden's pseudo- $R^2_{\text{gain}} = 0.65 \pm 0.27$, pseudo- $R^2_{\text{loss}} = 0.48 \pm 0.25$) with no difference in fits between the groups for either gains or losses ($Z_{\text{gains}} = 0.81$, $p = 0.42$, $Z_{\text{losses}} = -0.83$, $p = 0.40$). Furthermore, comparing this model to a three-parameter model (including a reward multiplier term) and models in which the initial q value (q_0) was both 0 and treated as a free parameter, the model described above performed best in terms of model comparison based on summed BICs across participants and valences (Fig 4-2). Go and No-Go response in gain and loss conditions was approximately 50% as expected and not significantly different between groups and was not considered further ($p_{\text{gains}} = 0.8$, $p_{\text{losses}} = 0.1$).

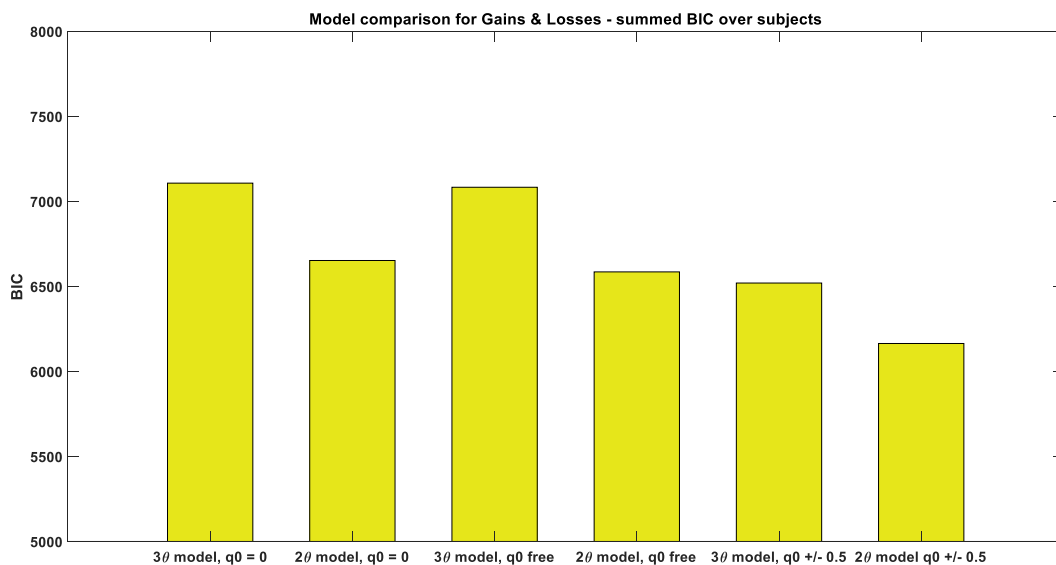


Figure 4-2: Model comparison of competing computational models. 3 parameter model included a reward magnitude as described in Palminteri et al (2012). $q_0 = 0$, q_0 free and $q_0 \pm 0.5$ describe models in which q_0 for both stimuli was initialised as 0 in gain and loss conditions, q_0 was treated as a free parameter and when q_0 was initialised +0.5 in the gain frame and -0.5 in the loss frame. The 2-parameter model with q_0 initialised at +0.5 in the gain frame and -0.5 was the winning model in the model comparison, scoring the lowest BIC score (2θ model, $q_0 \pm 0.5$). This model was used in the main analysis.

4.3.4 MRI acquisition:

Functional imaging data were collected using a standard 2D EPI sequence on a 3T Siemens Prisma system. A sequence optimised to minimise drop-out in regions near the striatum, OFC and amygdala, was used (Weiskopf et al., 2006). Physiological monitoring of heartbeat and breathing were recorded

for 31 of 35 participants. Excluding participants with missing physiological monitoring did not influence results (Supplementary Table 1). Each volume contained 48 slices with a 3mm^3 resolution. Volume TR was 3.36 seconds with a slice tilt of -30 degrees, a Z-shim of -0.4 and ascending slice acquisition order. T1 weighted images were collected for structural alignment and volumetric analysis. The 3D T1-weighted sequence was an optimised MPRAGE protocol, with an echo time (TE) of 3.34ms and a repetition time (TR) of 2530ms. The inversion time was 1100ms, and the flip angle was 7 degrees. The field of view was $256 \times 256 \times 176\text{mm}$, with 1mm isotropic voxels. Parallel imaging acceleration (GeneRalized Autocalibrating Partial Parallel Acquisition, GRAPPA, acceleration factor (R)=2) was applied along with 3D distortion correction and pre-scan normalisation. Following the task, field maps were acquired for unwarping.

4.3.5 Functional imaging pre-processing:

Standard EPI pre-processing steps were taken. Images were processed using SPM12. Images were unwarped using acquired field maps, slice-time correction to the middle slice, corrected for motion, and then warped into Montreal Neurological Institute (MNI) template space and spatially smoothed with a Gaussian kernel of 6-mm. All raw images following unwarping and warping to standard space underwent manual quality check. Please see Methods for more details on functional imaging and pre-processing.

4.3.6 Principles to modelling with a General Linear Model

A GLM approach was used to model the fMRI data. In brief, the GLM is an approach for modelling BOLD signal as a function of a set of explanatory variables, or regressors. As implied, this is a linear modelling approach and such that the overall BOLD activity is considered to be a function of the linear sum of regressors alongside some residual error. Furthermore, each regressor is scaled or multiplied by a parameter, or *beta* (β). Typically, as in the case of this experiment, there are multiple variables which are believed to govern the fluctuations seen in the BOLD signal and as such the GLM is an example of

multiple linear regression. For example, a GLM with three regressors is given by the following equation:

Equation (4-4):

$$Y = X_1 \beta_1 + X_2 \beta_2 + X_3 \beta_3 + \varepsilon$$

Where Y is the observed data, in this case the BOLD timeseries, X_{1-3} are the explanatory variables such as task events and β_{1-3} represent the scaling variable for each explanatory variable to best explain data Y. ε represents the residual error – the discrepancy between the model and data. The β s are estimated to minimise the residual error of the model. Explanatory variables can be grouped in matrix commonly called the design matrix. In fMRI, this linear model is applied to model the BOLD fluctuations in *each* voxel throughout the brain, a *mass univariate* analysis (Penny et al., 2007). This means that for each voxel a β parameter is estimated for each explanatory variable.

To test hypotheses, using these β values, statistical tests can be applied at each voxel. For the most part, in this Chapter I refer to ‘contrasts’ which are user specified weights that can be applied to each β in the GLM. Typically, contrast weight takes one of three numbers, 0, 1 and -1. For example, when the contrast weight is set to for only one beta value is set to ‘1’ (and 0 to the rest), this is the equivalent of asking whether that beta value has a mean above zero. If the contrast value ‘1’ is applied to one β value, say β_1 , and ‘-1’ is applied to another, say β_2 , this is the equivalent of asking whether mean of β_1 is greater than that of β_2 . These contrasts are used to generate statistics, such as the t-statistic, which quantifies the degree of the tested difference whilst also accounting for how much uncertainty, or variance, there is around this difference. The t-values, alongside the degree of freedom, can be used to estimate the p-value – the chance of observing the estimated difference, or greater, under the null hypothesis (Jenkinson et al., 2018; Penny et al., 2007).

4.3.7 Dealing with the problem multiple comparisons

As these tests are being performed at every voxel, a huge number of statistical tests are being carried out resulting in a very high likelihood of false positive results. In this Chapter, the risk of false positive is mitigated in two ways. Firstly, as the aim of this experiment is not exploratory with regards to the neural activation associated with the task, I have limited all analyses to only a handful of small brain regions which are based either on co-ordinates in independent literature or defined using stringent statistical thresholds. This type of analysis is known as a region of interest (ROI). The other approach used in this chapter is that of correcting for multiple comparisons across the whole brain using family wise error correction.

From the size of the test statistic, such as the t-value described above, it is possible to calculate the probability of observing an effect of that size under the assumptions of the null hypothesis. Classically we adopt a significance level, or α , of 0.05. If the probability of the test-statistic, p-values, falls below the alpha level, the result is considered significant. However, an alpha value of 0.05 implies that we would consider events (such as a t-value above a threshold) to be significant if they would only occur, as a false positive, one in twenty times under the null hypothesis. It is therefore clear to see that this is challenging for occasions when we are simultaneously run multiple tests, of a *family of tests*. For example, running 100000 tests with an alpha of 0.05 would effectively tolerate 5000 false positive results. In the case of fMRI this would mean saying that 5000 voxels were significant activated in response to a task condition when in fact, there was no true associated activity. We therefore need to perform a family-wise correction of our tolerated threshold for statistical significance (Lindquist and Mejia, 2015; Penny et al., 2007). The new threshold should minimise the chance of seeing any false positives across any of the family of tests. As will be described below, in this analysis I use two forms of family wise error correction – the Bonferroni correction and random field theory. The Bonferroni correction is conceptually easy to understand – we simply adjust our accepted threshold for significance by dividing our alpha by the number of tests (or members of the family) we have run. This is an extremely conservative correction and runs the risk of generating false negatives. I use Bonferroni

correction in this chapter to set such a conservative threshold when assessing for group differences in the fMRI betas derived from ROIs. The second family wise error correction that I use once in this analysis is based on random field theory (RFT).

I will provide a brief summary of the problems encountered when analysing fMRI data, why RFT is needed and how it is used to solve the multiple comparison problem. Aside from the fact the Bonferroni is highly conservative, that approach assumes that each test is independent. This is not the case in fMRI because brain regions take up multiple voxels and their activity is likely to be highly correlated. Secondly as described above and in the Methods chapter, fMRI data undergoes Gaussian smoothing during pre-processing, blurring the image and altering voxel values based on surrounding values. Therefore, even with 100000 voxels in a scan, each voxel is not an independent observation. In this setting a Bonferroni correction would not be an appropriate correction. In brief, how RFT solves this problem is by modelling the topography of the smoothed statistical maps (Brett et al., 2003; Penny et al., 2007). Instead of considering each voxel independently, RFT considers the topography of the map and the number of peaks of voxels, within the statistical maps which rise above a given threshold. In order to threshold these peaks of activation, RFT describes the data in terms of resolution elements (RESELS) which depends both on the number of voxels and the smoothing that the data has undergone. Once the number of RESELS has been calculated, RFT can be used to determine, for a given statistical threshold, how many peaks of voxels may be expected to exceed that threshold. This property is known as the *Euler Characteristic* (Brett et al., 2003). At high thresholds, the expected Euler Characteristic falls between 0 and 1 giving the probability of finding a peak above the chosen threshold. In other words, at high thresholds the Euler Characteristic approximates the probability of making a family-wise error. As such, we can use RFT to set the statistical threshold for peaks within our map to be that which gives an expected Euler Characteristic of less than 0.05. Beyond peak level inference it is also possible to ask what the probability is of seeing *clusters* of voxels within the data by defining a cluster extent. In this manner a similar p-value based on RFT can be computed which expresses probability of seeing clusters with k or more voxels, above a certain present within the statistical map above a specific

threshold. The caveat to this approach is that while the voxel-wise approach defines precisely the spatial location of peaks within the data, an entire identified cluster must be considered significant.

4.3.8 General Linear Models used and statistical details

More specifically in this analysis at the participant level, a General Linear Model (GLM) was constructed with cue onsets and outcome onsets as regressors of interest. Cue onsets were subdivided by valence and whether the button was pressed or not (i.e. regressors for gain cues were Gain-Go and Gain-NoGo). A second GLM was built for each subject for the computational model-based fMRI analysis containing the cue and reward onsets. The model derived Q-values and RPE from the computational model above were then used as parametric modulators at the time of choice and outcome respectively. As no group differences in parameter estimates were found (see results), individual Q-value regressors and RPE regressors were estimated from each subject's choice behaviour using the mean learning rate parameters across the whole group ($n = 70$, $\alpha_{\text{gain}} = 0.122$, $\alpha_{\text{loss}} = 0.220$). This fixed effects procedure has been used in multiple previous studies and is argued to be a more robust approach for computational fMRI (Rothkirch et al., 2017; Schonberg et al., 2007; Wilson and Niv, 2015).

At the second level, GLMs including group membership alongside covariates of age, gender and handedness were estimated for model-free and model-based contrasts specified at the first-level. The results of these second-level GLMs were imported into the MarsBAR (MARSeille Boîte À Région d'Intérêt) for ROI analysis in which mean GLM parameter (beta) estimates within regions of interest were used to either confirm replication of previous results or to test my hypotheses.

4.3.9 Region of interest approach for replication analysis:

To confirm replication of previously reported results using this task I assessed the significance of parameter estimates within spherical regions of interest defined from previously reported results. I

created 6mm spherical masks seeded at [+/- 12 10 -10] for left and right ventral striatum, [+/-30 28 -6] for bilateral insula and [-1 27 -18] for medial PFC (Pessiglione et al., 2006; Schmidt et al., 2014) . Based on previous work, I assessed activity in these regions for the contrasts Gain Cue > Neutral Cue, Loss Cue > Neutral Cue, Win Money > Lose Money, Lose Money > Win Money. Using computational fMRI, I assessed activity in these regions for Q-values and Reward Prediction error. A single Q-value regressor in this analysis (across gains and losses). Similarly, it should also be noted that the reward prediction error regressor includes prediction errors in both gains and losses – not just gain frames. The Q value regressor tracks the learned value of the chosen option across the task being positive in the gain choices and negative at losses choices. As such, correlated neural activity should increase in the gain frame and decrease in the loss frame, with the extent of activity change predicted by the computational model. Likewise, the RPE regressor is positive for reward outcomes and negative for loss outcomes. Neural activity which correlates with this regressor should show opponent activity with respect to reward as compared to losses. Medial PFC activity is predicted to correlate with the Q value regressors whereas striatal and medial PFC activity is expected with respect to RPE. The insula has been shown to track the inverse of these parameters – with increased activity associated with punishment prediction errors. To replicate these effects, a GLM with cue and reward onsets was built with parametric modulation with the inverse of the RPE computational regressors. No exploratory whole brain group differences are assessed. For the purposes of illustration only, neural activation is shown at an uncorrected threshold of $p < 0.001$ with a cluster extent threshold of $k = 10$.

4.3.10 Region of interest for reward bias analysis:

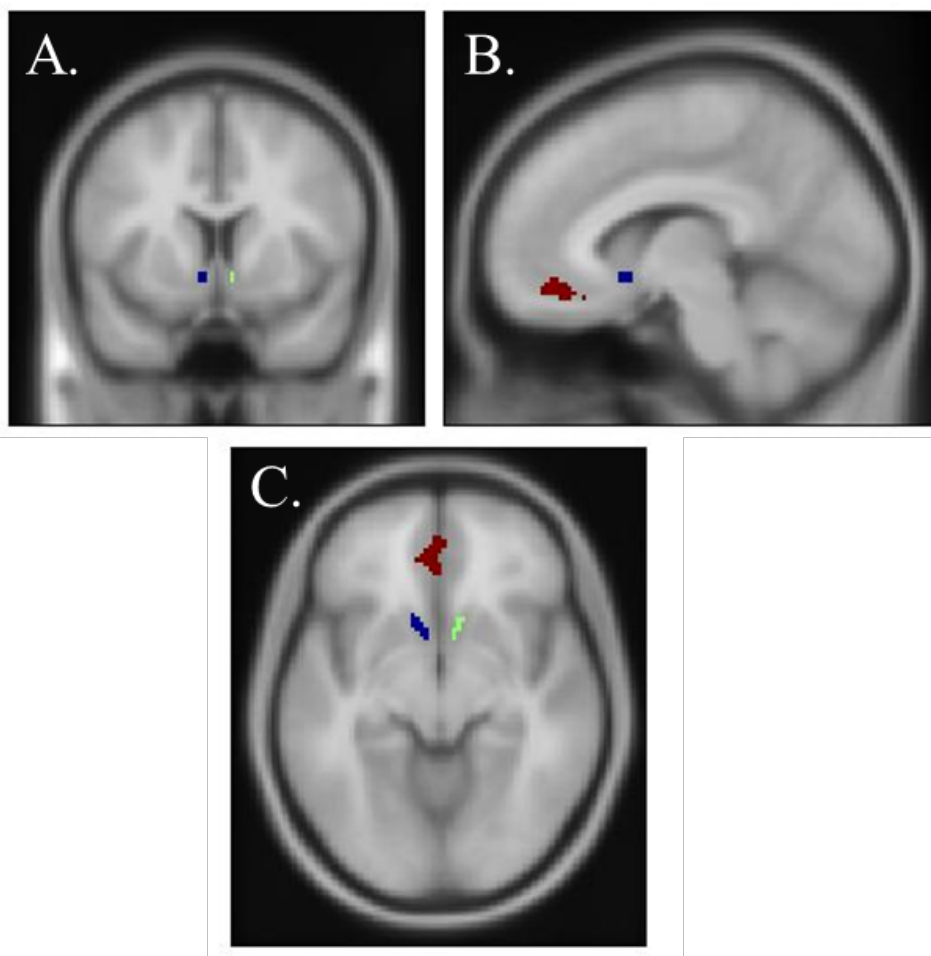


Figure 4-3: Masks for reward response regions of interest used for reward bias analysis. Masks used as task-derived regions of interest which showed reward responsiveness – greater activity in response to winning money as compared to losing money or gain versus loss cue presentation. Clusters were formed from voxels which survived FWE correction across the whole brain at a threshold of $p < 0.05$ across both groups ($n = 70$) in either contrasts. Striatal clusters were identified only in the Win > Lose money contrast. Blue ROI is the left ventral striatum; green ROI is the right ventral striatum and red ROI is the medial PFC superimposed on T1 image A. shows the coronal slice through the striatal ROIs, B. shows the sagittal slice showing left VS and medial PFC and C. shows the axial slice containing all three ROIs.

To determine fronto-striatal regions that showed a “reward bias”, task derived regions of interest were derived from shared activity across both groups in the contrasts Winning Money (in gain frame) > Losing Money (in loss frame) or Gain > Loss predicting cue presentation after whole brain voxel-wise correction at FWE $p < 0.05$ with a minimum cluster extent of 10. Clusters in the left and right striatum and prefrontal cortex were identified in the Win > Lose contrast whereas only a cluster in the prefrontal cortex was found in the Gain > Loss cue contrast. These clusters were extracted using the MarsBAR toolbox in SPM, combined and were used for my region of interest analysis. Striatal clusters were

bounded within the anatomical masks defined by Automated Anatomical Labelling Atlas for the left and right caudate. These ROIs are not biased to group differences and reflect relevant regions that show a ‘reward bias’ during the task – voxels showing increased activity in rewards or reward predicting cues as compared to losses or loss predicting cues. As previous work in both HD patients and with this task suggests lateralisation of fMRI signal, left and right striatal clusters were kept separate (Enzi et al., 2012; Pessiglione et al., 2006). Confirmatory analysis was then performed using the appropriate independent 6mm spherical ROIs described above. Second-level GLMs were imported into MarsBAR and average parameter (beta) values within each ROI were estimated by participant, corrected for effects of age, gender and handedness. These mean parameter estimates were compared across groups using the contrast Gene Carrier > Controls. As reward bias may be seen at stimulus or outcome presentation, Gain Cue > Loss Cue contrast and Win Money > Lose Money contrast were compared between groups for each of the three regions of interest. To correct for multiple comparison across these six tests, a stringent Bonferroni threshold of $p < 0.008$ was considered significant as described above.

A complementary computational fMRI analysis was then used to assess whether neural correlates of Q-value or reward prediction error differed by group. As above, analyses were performed in MarsBAR using the contrast Gene Carrier > Control for each of the three ROIs, with a threshold of $p < 0.008$ considered significant.

4.3.11 Structural imaging processing:

I must highlight that I did not complete the structural imaging analysis and it is described by my colleague Dr. Eileanoir Johnson as follows:

“All T1-weighted scans passed visual quality control checks for the absence of significant motion or other artefacts before processing. Bias correction was performed using the N3 procedure. An automated segmentation procedure, Multi-Atlas Label Propagation with Expectation-Maximisation based refinement (MALP-EM), was used to measure caudate volume (Ledig et al., 2015). All settings were applied using default parameters, except for the inclusion of a brain mask for each participant based on a previously generated whole-brain region derived from semi-automated delineation. MALP-EM has

been validated for use in HD.(Johnson et al., 2017) A validated semiautomated segmentation procedure performed via Medical Image Display Analysis Software (MIDAS) was used to generate volumetric regions of total intracranial volume (TIV) (Freeborough et al., 1997; Malone et al., 2015). Caudate volume was adjusted for TIV using the formula:

Equation (4-5):

$$Caudate_{adjusted} = \frac{TIV_{mean}}{TIV_{individual}} \times caudate_{individual}$$

Whereby:

$Caudate_{adjusted}$ = adjusted caudate volume for the participant

TIV_{mean} = mean TIV for whole cohort

$TIV_{individual}$ = TIV for the participant

$Caudate_{individual}$ = raw caudate volume for the participant

All scans and regions underwent visual quality control by experienced raters to ensure that there were no scan artefacts or errors in the delineation of brain regions. No scans or segmentations failed after visual quality control.”

4.4 Results:

4.4.1 Sample demographics:

<i>n = 35 in both groups</i>	Gene Positive	Gene Negative	
Age	29.4 (+/- 5.7)	30.5 (+/- 5.2)	p = 0.41 ^(a)
Gender (F/All)	19/35	20/35	p = 0.81 ^(b)
Handedness (R/All)	30/35	32/35	p = 0.70 ^(b)
NART	102.2 (+/- 6.9)	103.4 (+/- 8.3)	p = 0.52 ^(a)
Depressive scores	32.2 (+/-8.60)	34.6 (+/- 7.4)	p = 0.22 ^(a)
Adjusted caudate volumes (mls)	7.27 (+/- 0.75)	7.42 (+/- 0.67)	p = 0.40 ^(a)
Median UHDRS motor scores (max)	0 (5)		
CAG	41.8 (+/- 1.2)		
DBS	185.0 (+/- 33.5)		

Table 4-1: Sample demographics: Sample demographic for both groups showing that the cohort were well matched at recruitment for age, gender, and handedness. Groups were matched for intelligence as measured by the National Adult Reading Test (NART) and depressive symptoms. Groups were in the normal range for depressive symptoms measured on the Zung Depressive Scale (<50). Caudate volumes adjusted for Total Intracranial Volume (TIV – see Methods) were also not significantly different between groups. DBS: disease burden score. UHDRS: Unified Huntington Disease Rating Scale^(a) signifying the use of independent t-test, ^(b) signifying the use of Chi-square test

We (myself and the HD-YAS team) recruited 35 gene carriers and 35 gene negative control participants.

The groups were closely matched for age, gender and handedness and there were no differences in NART scores or depressive symptoms (Table 4-1 and Fig. 4-4).

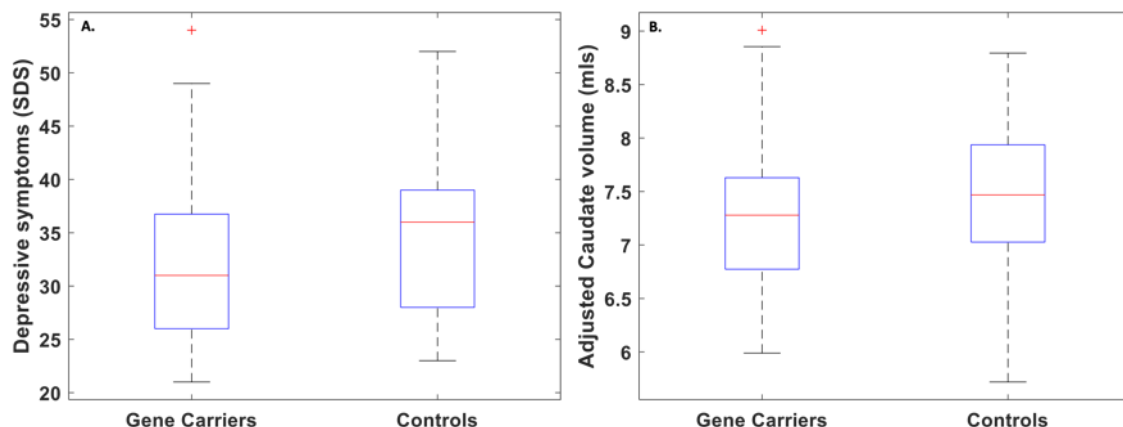


Figure 4-4: Depressive scores and caudate volumes by group. (A) Depressive scores as recorded by the Zung Depression Scale (SDS). Scores < 50 are considered to be in the normal range with scores 50-59 indicating possible mild depression. No difference was seen between groups ($t = -1.2$, $p = 0.22$). (B) Caudate volumes adjusted by total intracranial volume (see methods) showed no significant atrophy between groups ($t = -0.84$, $p = 0.40$)

The groups also did not differ on core cognitive tests sensitive to HD - Stroop word ($t = -1.33$, $p = 0.19$) and Stroop colour reading ($t = -1.06$, $p = 0.29$), SDMT ($t = -0.43$, $p = 0.67$) and verbal fluency ($t = -1.58$, $p = 0.12$). No significant caudate atrophy was seen in the gene carrier group (Table 1 and Fig 4-4). The gene carrier group had an average CAG length of 41.8 (± 1.2) with the estimated years to onset of 26.1 (± 5.5) years based on the Langbehn formula (Langbehn et al., 2010). The median Unified Huntington's Disease motor score in this group was 0 with a max of 5 indicating this group was definitely premanifest.

4.4.2 Task performance

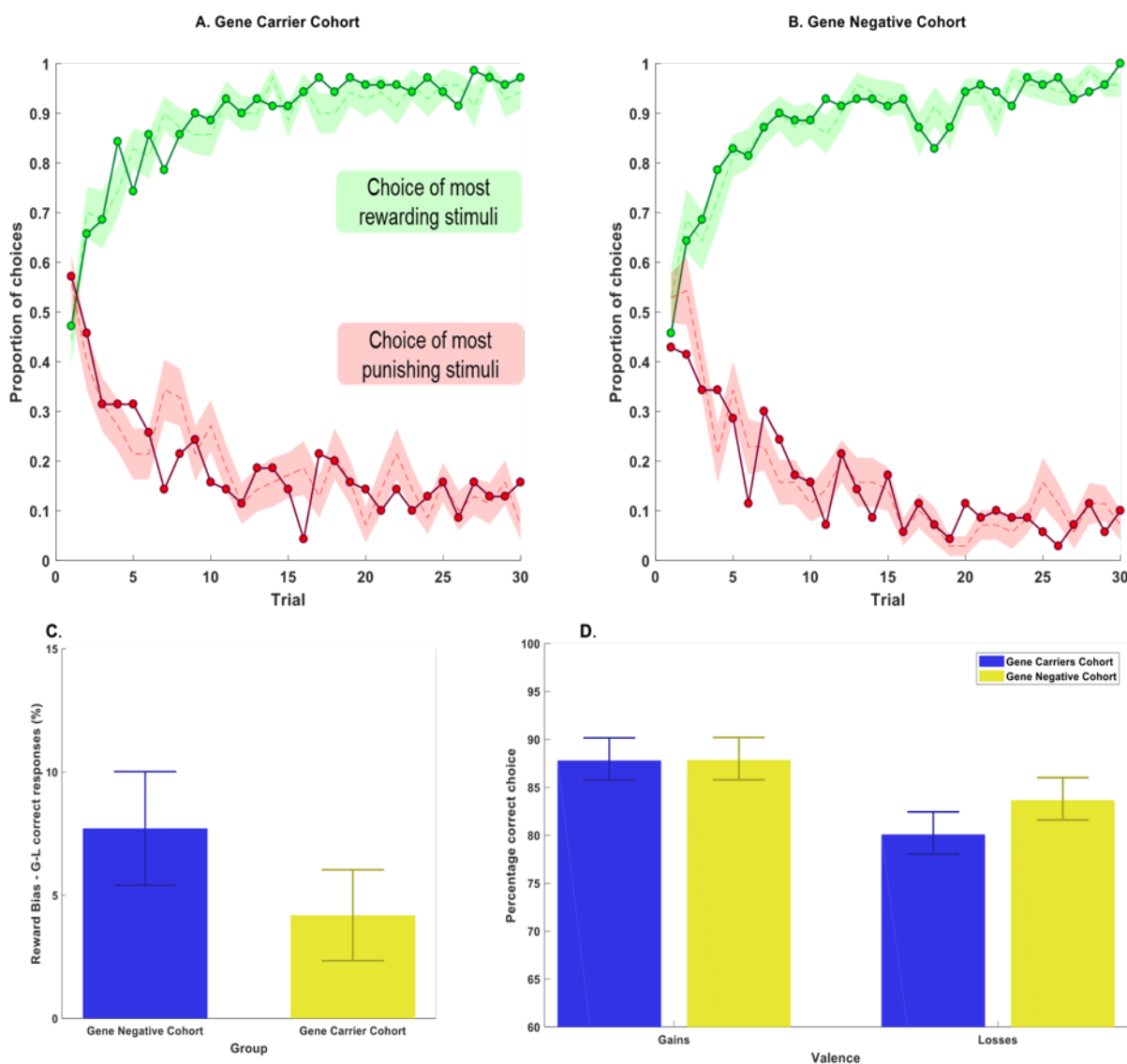


Figure 4-5: Both groups performed task well, with no group differences. A. HD gene carriers ($n=35$) and B. control ($n=35$) groups learned to choose the most rewarding symbol in the gain trials and avoid the most punishing symbol in the loss trials. Mean participant choice data shown by the dashed lines with shaded regions showing \pm S.E.M., green for gains and red for losses. The connected dotted green and red lines show mean computational model performance for gains and losses respectively showing computational model predicted behaviour well in both groups. C. Both groups showed marginally better performance in the learning from gains than losses with small positive 'reward bias' (percentage correct in gains minus loss). D. Percentage correct in gain and losses by group. Bars show mean correct with error bar showing S.E.M. No significant group differences were observed in these metrics.

Participants completed an established reinforcement learning task in which they had to learn to choose between pairs of abstract stimuli (Palminteri et al., 2012; Pessiglione et al., 2006). Three sets of abstract stimuli were presented corresponding to gain, loss and neutral conditions. In the gain condition, choice of one stimulus was associated with a reward with 80% probability and the other with only 20% probability. Likewise, in the loss frame, one stimulus lead to loss of reward with 80% probability whereas the other stimulus was associated with a loss with only 20% probability. In the neutral pair, both stimuli were associated with neither gain nor loss. Participants made responses with a button press using their right hand (see Methods for more details). Both groups learnt to choose the most rewarding symbol and avoid the most punishing symbol (as shown in Figure 4-5A&B).

Both groups also showed more correct responses for gains than losses (Gene carriers: $t = 3.35$, $p = 0.002$; Gene negative: $t = 2.27$, $p = 0.03$) however, this effect was not significantly different between the groups ($t = 1.19$, $p = 0.28$, Fig. 2A). There were no differences in the percentage correct in either gains or losses between groups ($Z_{\text{gains}} = -0.11$, $p_{\text{gains}} = 0.91$, $Z_{\text{losses}} = -0.73$, $p_{\text{losses}} = 0.46$, Fig. 2B).

4.4.3 Computational modelling of behaviour

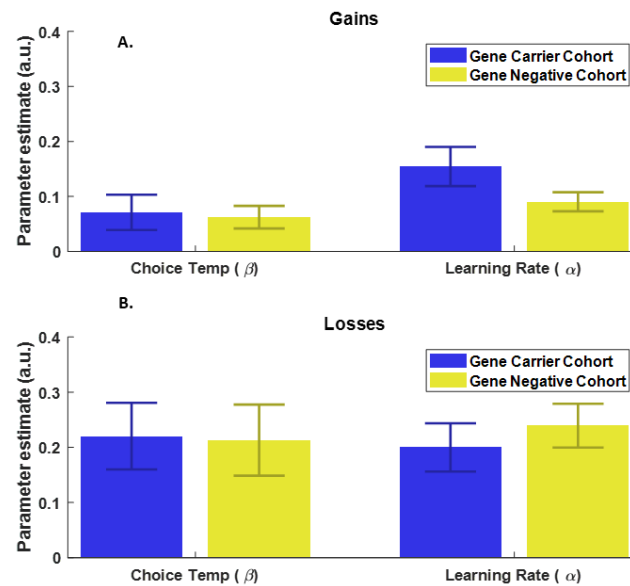


Figure 4-6: Computational model parameter estimates by group and valence. Average parameter estimates for Q-learning model (mean +/- S.E.M.) for each group in A. Gains and B. Losses – no significant group differences were seen.

Average group-wise parameter estimates from a Q-learning model are shown in Fig. (4-6). There were no significant parameter differences between the groups in either gains or losses (α_{gain} : $Z = -1.22$, $p = 0.22$, β_{gain} : $Z = -0.41$, $p = 0.68$, α_{loss} : $Z = -1.29$, $p = 0.19$, β_{loss} : $Z = -0.47$, $p = 0.20$). These results demonstrate that gene carriers over two decades before onset show no robust behavioural differences compared to matched controls. Post-hoc, it appeared as though the gene negative cohort showed a greater difference in learning rates between gains and losses. Using an ANOVA analysis, testing for the main effects of group, valence and their interaction on learning rates, I found only a significant main effect of valence ($F = 9.74$, $p = 0.002$) however no effect of group ($p = 0.89$) or group*valence ($p = 0.99$). This was also true of the noise parameter with only a significant effect of valence ($F = 7.47$, $p = 0.007$) but no effect of group or the interaction ($p = 0.73$ and $p = 0.15$ respectively).

4.4.4 Robust activation of fronto-striatal regions associated with task

As shown in Tables (4-2 & 4-3), using spherical ROIs defined from existing literature, neural activity was seen in fronto-striatal circuits in association with task performance and consistent with previously reported literature across both groups.

<i>n</i> = 70	Gain > Neutral Cue	Loss > Neutral Cue	Q-value
Left VS	t = 3.61, p < 0.001	t = 4.76, p < 0.001	t = -0.018, p = 0.5
Right VS	t = 5.77, p < 0.001	t = 6.77, p < 0.001	t = -0.014, p = 0.51
Medial PFC	t = 2.75, p = 0.004	t = -1.71, p = 0.95	t = 5.61, p < 0.001
Bilateral insula	t = 1.22, p = 0.11	t = 6.33, p < 0.001	Not tested

Table 4-2: Replication analysis at cue presentation across both groups: Table describes the one-sided t-statistic and corresponding p value testing whether activity in ROIs, defined from existing literature, was positively associated with contrast at cue presentation. VS represent ventral striatum and PFC represent prefrontal Cortex. Df for all tests 69.

<i>n</i> = 70	Win > Lose Money	Lose > Win	Reward Prediction error
Left VS	t = 5.67, p < 0.001	Not tested	t = 3.96, p = 0.001
Right VS	t = 6.19, p < 0.001	Not tested	t = 3.37, p = 0.006
Medial PFC	t = 5.52, p < 0.001	Not tested	t = 5.54, p < 0.001
Bilateral insula	Not tested	t = 5.47, p < 0.001	t = -6.02, p < 0.001 ^a

Table 4-3: Replication analysis at outcome presentation across both groups: Table describes the one-sided t-statistic and corresponding p-value testing whether activity in ROIs, defined from existing literature, was positively associated with contrast at outcome presentation. VS represent ventral striatum and PFC represents prefrontal cortex. a Insula activity positively associated with the punishment prediction error. Df for all tests 69.

Bilateral ventral striatum activity was seen in response to gain and loss cues as compared to neutral cues, reflecting learned stimulus value. Ventral striatal activity was also associated with the reward

prediction error. Medial prefrontal cortex activity correlated with positive stimulus valence, the Q-value regressor and reward prediction error. Bilateral insula activation was associated with loss cue onset and the punishment prediction error. Fig. 4-7 shows task activity at whole brain level across both groups at a liberal threshold for illustration purposes only.

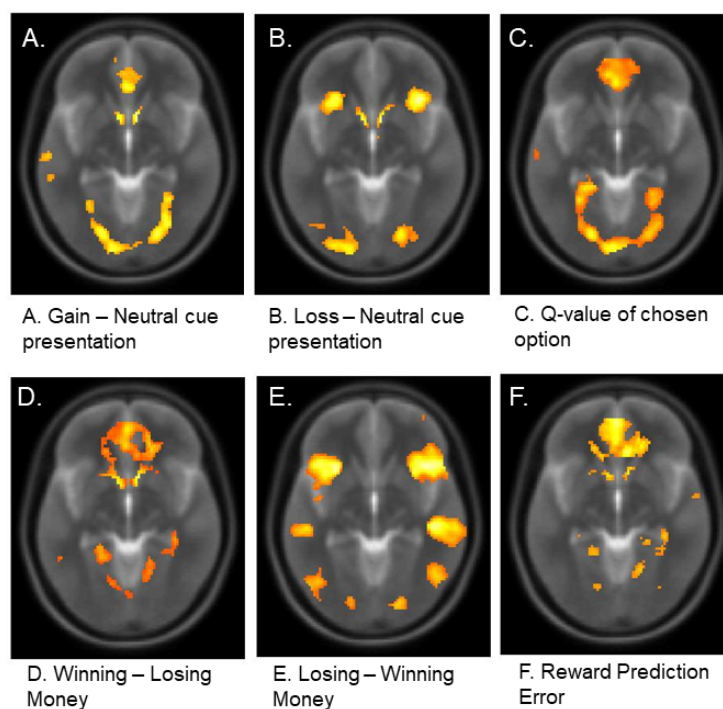


Figure 4-7: Neural activation in response to choice (A-C) and outcome (D-F) in task. Neural activation at cue presentation (A-C) and at outcome presentation (D-F) across all subjects shown in the axial plane at an uncorrected threshold $p < 0.001$ with a cluster extent of 10 contiguous voxel (for illustration, not inference, purposes only).

4.4.5 Left ventral striatal reward bias at cue onset in gene carriers

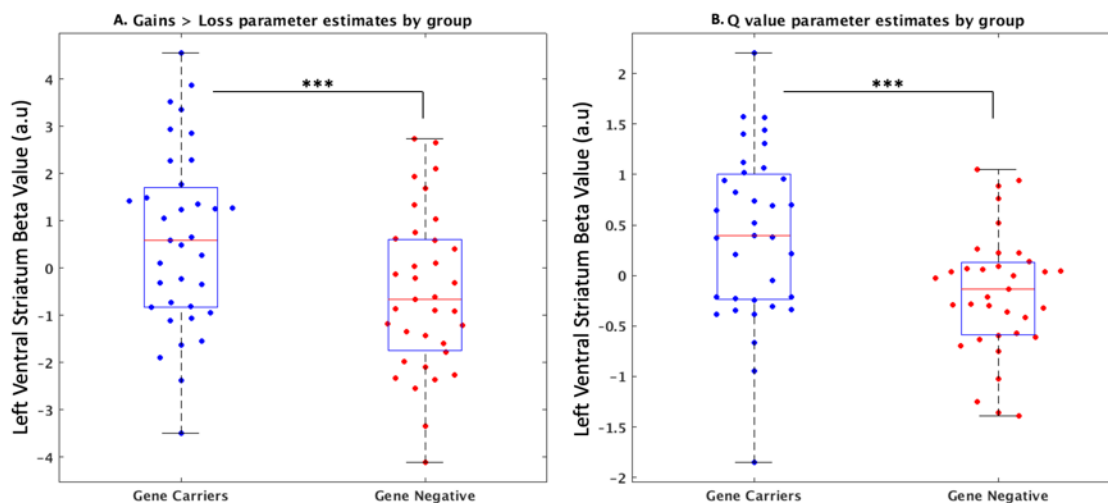


Figure 4-8: Left ventral striatum beta values for reward bias contrasts, by group. Individual left ventral striatum parameter estimates by subject in each group for (A) Gain cue minus Loss Cue activity and (B) Q-value regressor *** group difference with significance of $p < 0.005$ after adjusting for effects of age, gender and handedness.

In order to assess for a difference in neural reward bias between groups, I first identified reward-responsive regions in the left and right ventral striatum and medial PFC. I identified significant clusters of fMRI activity in these three regions from voxels which survived FWE correction across the whole brain, across all subjects at a threshold of $p < 0.05$, when contrasting activity associated with either winning money as compared to losing money or, at gain cue presentation as compared to loss cue presentation. Clusters in the left and right ventral striatum, bounded by an anatomical mask, and medial PFC were extracted and used to complete a region of interest analysis that is unbiased with respect to group (see Methods). Parameter values were averaged over all voxels in each ROI.

Adjusting for covariates of age, gender and handedness I assessed whether mean parameter estimates in these regions were greater in gene carriers than controls in two 'reward bias' contrasts. Firstly, at cue presentation I assessed activity in the ROIs when comparing gain cue presentation to loss cue presentation. As is shown in Table (4-2), striatal activity is associated with both gain and loss cue presentation as compared to neutral stimuli. As such, in this subtractive contrast, parameter estimates should be close to zero if activity evoked by gain and loss cues are equivalent. More positive estimates in one group signifies greater activity in gains relative to losses and I hypothesised this would occur in

gene carriers. Likewise, at outcome presentation I compared activity for winning compared to losing money. More positive parameter estimates in one group signify a bias in activity towards winning as compared to losing. I compared parameter estimates between groups in these two contrasts, hypothesising greater activity in gene carriers than controls. To account for testing these two contrasts in three ROIs (left and right ventral striatum and medial PFC) I used a Bonferroni threshold of $p < 0.008$.

At cue presentation, I found that the gene carrier cohort, compared to the control participants, showed enhanced left ventral striatal response comparing gain cue presentation to loss cue presentations ($t = 2.79$, $p_{\text{uncorrected}} = 0.003$). This effect was not seen in the right ventral striatum ($t = 0.4$, $p_{\text{uncorrected}} = 0.34$) or the medial PFC ($t = 0.87$, $p_{\text{uncorrected}} = 0.20$). Individual participant parameter estimates by group are shown in Fig. 4-8(A). To ensure these results were not influenced by the choice of ROI, a 6mm spherical mask was created in the left ventral striatum at the co-ordinates described by Pessiglione *et al* (2006) (Pessiglione *et al.*, 2006). Results using this ROI showed the same difference between groups ($t = 2.06$, $p = 0.02$).

No significant differences between groups were seen at outcome presentation, comparing winning money to losing money in any of the three ROIs (LVS: $t = 0.94$, $p = 0.17$, RVS: $t = 1.05$, $p = 0.15$, mPFC: $t = 0.28$, $p = 0.39$).

4.4.6 Ventral striatal reward bias seen in striatal response to model-derived value estimates

In a complementary analysis I compared activity in the three ROIs using regressors extracted from the computational model namely the value estimate for the chosen option, *the Q-value*, and the reward prediction error (δ), the difference between received and expected reward. These two regressors were used as parametric modulators of cue and outcome presentation, respectively. The Q-value regressor tracks the value of the chosen stimulus in both gain and loss frames – as such, neural activity positively associated with this regressor should show increased activity in gain frame, when Q-values are positive, and reduced activity in the loss frame, when Q-values are negative. Similarly, neural activity associated with the RPE regressor will increase in response to rewarding outcomes but decrease in response to

losses, as predicted by the learning model. Here, I use these regressors as sensitive complementary probes to the model-free fMRI analysis above to assess for a reward bias difference between groups. In both contrasts, more positive parameter estimates reflect a wider difference in neural activity between gains and losses in the cue and outcome phases of the task, for Q-value and RPE respectively. I hypothesised this would occur in the gene carrier group as compared to controls and as before I considered a Bonferroni threshold of $p < 0.008$ to be significant.

In keeping with the model-free analysis, computational fMRI analysis showed that the gene positive cohort compared to the control subjects had higher parameter estimates associated with the Q-value regressor in the left ventral striatum ($t = 3.32$, $p_{\text{uncorrected}} = 0.0007$) but not the right striatum ($t = 0.51$, $p_{\text{uncorrected}} = 0.31$) or the medial PFC ($t = 1.22$, $p_{\text{uncorrected}} = 0.11$). Using the independent ROI derived from the literature, as above, the left ventral striatum showed the same differences between groups ($t = 2.37$, $p = 0.01$). Individual parameter estimates by group are shown in Fig. 4-8(B). I found no evidence of a difference in the betas associated with reward prediction error related activity in the gene carrier cohort in any of the three ROIs (LVS: $t = 0.12$, $p = 0.45$, RVS: $t = -0.06$, $p = 0.47$, mPFC: $t = -0.46$, $p = 0.68$).

4.4.7 More robust response to loss cues in controls:

To display this reward bias, either gene carriers should show a greater response to gain cues than controls or the controls should display greater response to loss cues than gene carriers, or both. Post hoc, using the unbiased task-defined left ventral striatum ROI, I tested these hypotheses by comparing valence cue onsets to neutral cue onsets. Gene carriers did not show an enhanced striatal response comparing gain cues to neutral cues ($t = 0.91$, $p_{\text{uncorrected}} = 0.18$); however, controls did show significantly increased response to loss cues than neutral cues ($t = 1.91$, $p_{\text{uncorrected}} = 0.03$). This suggests that striatal representation of loss cues may be driving the reward bias effect described above.

I should add that during the review process for publication, reviewers suggested additionally controlling for caudate volume and depressive symptoms. I re-ran the above analyses with these

additional covariates and found the same, if not slightly more robust, findings indicating these differences were not the result of depressive symptoms or subtle differences in caudate volume.

4.4.8 Neural reward bias not correlated with disease burden score:

Neither the parameter estimates in the gain versus loss contrast ($r = -0.02$, $p = 0.89$), nor the Q value parameter estimates ($r = -0.11$, $p = 0.53$) in the gene carrier group correlated with disease burden score.

4.5 Discussion

In this study, we (myself and the HD-YAS team) recruited a cohort of healthy HD gene carriers estimated to be 25 years from onset, based on age and CAG length, and found that neural activity in response to stimulus valence and value was significantly different from matched controls in the striatum. No group differences were seen in behaviour, cognitive scores or caudate volumes. Taken together, these findings suggest that changes in the fronto-striatal value networks may occur very early in the life of HD gene carrier; however, these changes are not sufficient to manifest as behavioural differences, 25 years before motor onset. To my knowledge, these findings are the earliest reported functional imaging differences between HD gene carrier and controls.

In a behavioural study, Palminteri *et al* (2012) reported an asymmetry between gain and loss learning, a ‘reward bias’, in HD gene carriers approximately 10 years from motor onset (Palminteri *et al.*, 2012). Although they did not collect fMRI data, they found that these behavioural differences may be driven by computational differences at the choice phase with HD gene carrier making noisier decisions in the loss frame. These findings are wholly in keeping with my fMRI findings. I also found a difference between the groups at the choice phase with some evidence that this difference is mediated by impaired loss cue representation in the ventral striatum. I found no difference at outcome, or in behavioural analysis. As both studies used the same task, the neural changes identified here may be antecedent to the behavioural and computational changes identified by Palminteri *et al* (2012) and may be predicted to occur in this cohort in approximately 15 years. These findings also raise three further possibilities.

Firstly, they suggest a window exists in which functional neural changes occur in HD gene carriers, before measurable atrophy and corresponding behavioural changes. Secondly, these findings may be in keeping with early dysfunction of the indirect pathway in HD gene carriers, which, as discussed in detail in the thesis Introduction, is lost at a greater rate in HD and thought to contribute to loss learning and avoidance (Albin *et al.*, 1992; Collins and Frank, 2014; Hikida *et al.*, 2010, 2013; Waldvogel *et al.*, 2015; Zalocusky *et al.*, 2016). Finally, this study adds to the growing body of evidence that suggests

limbic and reward processing may be amongst the most sensitive and early cognitive markers of HD (Bora et al., 2016; Enzi et al., 2012; Henley et al., 2012; Palminteri et al., 2012; Stout et al., 2011).

Although neurodegeneration in HD is described as moving along a dorso-ventral gradient, several observations and empirical findings suggest that ventral or limbic striatal function is disrupted earlier rather than later in the disease (Waldvogel et al., 2012). Clinically, there is considerable psychiatric morbidity in both pre-manifest and early stage disease (Martinez-Horta et al., 2016). Amongst the cognitive measures used in premanifest HD, disrupted emotional processing and reward processing appear to be particularly sensitive to early disease again suggestive of early ventral or limbic dysfunction (Bora et al., 2016; Enzi et al., 2012; Henley et al., 2012; Labuschagne et al., 2013; Palminteri et al., 2012). Neuroimaging connectivity studies show that striato-prefrontal connectivity is disrupted in premanifest cohorts (McColgan et al., 2017b). Furthermore, HD participants approximately 9 years from onset show disturbed neuronal activation in the left ventral striatum related to valence discrimination in a non-learning task (Enzi et al., 2012). Taken together with my findings, changes in ventral striatal function may therefore be some of the earliest changes associated with carrying the HD gene.

The need for fMRI to detect differences between my groups also does not support the hypothesis that gross neurodevelopmental changes in the striatal reward system are associated with carrying the HD gene (Wiatr et al., 2018). In previous work, HD gene carriers showed behaviourally manifest differences from matched controls in the task I use here (Palminteri et al., 2012). Moving much further away in time, to 25 years before predicted onset, I found little evidence that the altered neural activity within the nodes of the fronto-striatal network is associated with robust behavioural impairment. Assuming the same fronto-striatal nodes bear the neurodevelopmental cost of carrying the HD gene, it does not appear that this cost is sufficient to yield functional or behavioural impairment, at least in this cohort. This does not mean that microstructural or more fine grain functional differences may occur secondary to carrying the HD gene however, this is not the focus of my study. Indeed, in the larger HD-YAS study, neurofilament-light chain was shown to be elevated in HD gene carriers 25 years from onset suggesting

possibly active, albeit relatively subtle, neurodegeneration is occurring in this cohort (Scahill et al., 2020).

It has also been hypothesised, secondary to disinhibition resulting from the loss of striatal MSNs, that dopaminergic signalling in HD follows an inverted U-shape in which low levels of dopamine are found later in HD whereas increased dopamine signalling is found earlier in the disease (Chen et al., 2013). In keeping with this model, using a reversal learning task, Nickchen *et al* (2017) reported the loss of RPE signalling in the left VS of manifest HD patients, especially those more severely affected (Nickchen et al., 2016). Pharmacological induction of a hyperdopaminergic state using this task has been shown to enhance RPE signalling; however, I found no differences between the HD gene carrier group and controls in striatal RPE activity to suggest exaggerated dopamine signalling (Pessiglione et al., 2006; Voon et al., 2011). It may be however, that the HD gene carriers group was too far from onset for dopamine dysregulation to manifest as measurable differences in BOLD activity.

I believe this study has a number of strengths. We successfully recruited a unique cohort of HD gene carriers estimated to be over two decades from motor onset and a well-matched cohort of control participants. I was able to demonstrate that these groups were not significantly different in tests traditionally sensitive to HD. I used a task with existing data in HD patients and gene carriers closer to onset to allow us to better interpret my results and was able to replicate canonical results from the literature. Given both prior literature and my hypotheses I restricted group comparison to a limited number of regions. ROIs were defined using task data to identify voxels which showed hypothesis relevant activity. Although task derived, a stringent statistical threshold was used to identify these clusters to limit the inclusion of false positive voxels. These regions were identified based on shared activity across both groups and so were not biased to group differences. I also then ran a confirmatory analysis with a spherical ROI at independently reported co-ordinates and found the same group differences.

I also acknowledge that this study has the following limitations that to consider. My study design was cross-sectional and not powered to determine whether the effect that I found progresses as participants grow closer to disease onset. Although I lack longitudinal data existing published HD data using this

task may serve as an indicator of how task performance may change as the disease progresses. I also do not claim that these findings clearly represent disease per se; however, in conjunction with published data from the same task, I believe that my findings are likely to be antecedent of reward processing deficits which may emerge later. Recent work, from HD-YAS, has shown the disease related change particularly in fluid biomarkers can also be found at this point (Scahill et al., 2020). Unlike previous work, I also only found differences in fMRI data and not behavioural data. Firstly, given that effect sizes for behavioural differences on cognitive tasks diminish in gene carriers further from disease onset, gross behavioural differences in the HD gene carriers may have been surprising (Paulsen, 2011). It is important to highlight however, that lack of behavioural differences in this paradigm may also be related to task difficulty. Behavioural difference in reward learning may be seen this far from clinical onset with more challenging learning tasks.

4.6 Conclusions

Here, I demonstrate that healthy HD gene carriers approximately 25 years from motor onset, show an exaggerated striatal response to gain predicting cues as compared to loss predicting cues in a computational fMRI study. This difference between gene carriers and matched controls was also seen in striatal activity related to the predicted value of choice derived from a reinforcement learning computational model. These results suggest that aberrant neural coding of valence and value may be one of the earliest features of carrying the HD gene occurring decades from onset. These changes are not accompanied with robust behavioural changes suggesting an important window exists – where neural changes occur in HD gene carriers but before these changes drive potentially hard to recover behavioural impairment.

For the purposes of this thesis, this Chapter also serves as an important bridge to the two remaining chapters. In the remaining data chapters, I turn to my hypothesis that involvement of the *direct* basal ganglia pathway contributes to the development of apathy in HD. As described in the Introduction, this hypothesis is in part based on computational models of basal ganglia functions like the OPAL model (Collins and Frank, 2014). It is worth, therefore, considering the results from this Chapter with a

particular focus on this model. As a reminder, OPAL is an extended actor-critic model in which critic reward prediction errors signalled by dopamine, drive opponent effects on the value of choosing and not choosing an action by asymmetrically modulating the weights of the direct and indirect pathway respectively. As described in the Introduction the update value equations for the direct pathway (G) and the indirect pathway (N) are given by these Hebbian update rules:

Equation (4-6):

$$1. G_a(t + 1) = G_a(t) + [\alpha_G G_a(t)] \times \delta_t$$

$$2. N_a(t + 1) = N_a(t) + [\alpha_N N_a(t)] \times -\delta_t$$

Presynaptic activity from the cortex determines the action value (a) being learned, dopamine modulation is signalled by the δ and post-synaptic activity with the striatal pathways is represented by the actor weights (α_G and α_N). In the case of learning from gains, such learning is driven by positive prediction errors. In this situation, the value of the G actor would dramatically increase while the value of the N actor decreases rapidly due to the three-factor Hebbian implementation of OPAL (as the degree of change in the value of G or N is proportional to the current value of G or N respectively). In the case of learning from losses, the opposite effect occurs – the N actor value rapidly increases whilst the G actor value rapidly decreases. In this study, I found no difference in the BOLD activation corresponding in reward prediction error signal. I did, however, find that at the time of choice, there was a greater asymmetry in striatal activation between gains and losses, with the HD gene carriers showing a reward bias and with some evidence of reduced activity in the loss frame.

Let us assume that within a striatal voxel BOLD is proportional to the sum of G and N from the model above i.e., the neurovascular response is proportional to values/activity in both the direct and indirect pathway MSNs. During gain learning, in response to positive prediction errors, the G value of the most rewarding stimulus dramatically increases whilst the N value tends to 0. Likewise, in the loss frame, driven by negative prediction errors the N value for the worst symbol dramatically increases whereas the G value for that symbol tends to 0. Under these assumptions, BOLD activity in the gain frame may be hypothesised to be driven by the large G value for choosing the best symbol and in the loss frame

by the large N value for avoiding the worst symbol. If both pathways, G being direct and N being indirect, are functional one would not expect a significant gain bias. However, if the indirect pathway is dysfunctional or damaged as may be the case in the HD gene carriers, we may expect to see an exaggerated response to gains *versus* losses, driven by a weaker representation of losses. This model prediction matches well with my findings. As the disease progresses with more significant loss in the indirect pathway, this model would predict that HD gene carriers become worse at loss learning, and this has also been shown by Palminteri *et al* (2012).

These results are not direct proof of these models; however, they support the idea that these models can be used to meaningfully make predictions about HD from computational models of basal ganglia function. In a similar vein, the following two chapters focus more squarely on apathy in HD making predictions of epidemiological and neuroimaging data based on involvement of the direct pathway in HD, the role it plays in these models and apathy

Chapter 5: Relationship between distinct motor signs and apathy in Huntington's disease: clues to mechanism.

5.1 Abstract:

Apathy, the loss of goal-directed behaviour and motivation, is a disabling yet poorly understood psychiatric symptom often found in Huntington's disease (HD). Motor signs in HD are thought to represent dysfunction in the direct and indirect striatal pathways, which facilitate and inhibit movement, respectively. These pathways are also implicated in facilitating and inhibiting motivated behaviour. I therefore predicted that signs of direct pathway dysfunction including bradykinesia would be associated with greater apathy whereas signs of indirect pathway dysfunction including chorea would be associated with lower apathy. I built linear mixed models, using data from 2608 patients with manifest HD from the ENROLL-HD database, to characterise the relationship between apathy and motor signs while controlling for demographic and clinical covariates. I found that bradykinesia was associated with greater apathy ($\beta = 0.15$, CI: 0.11 to 0.19, $p < 0.001$), whereas chorea was associated with lower apathy ($\beta = -0.11$, CI: -0.16 to -0.07, $p < 0.001$) in this large cohort. By comparison, neither rigidity nor dystonia showed statistically significant relationships with apathy. In separate models, I found that slower finger tapping ($\beta = 0.08$, CI: 0.04 to 0.13, $p < 0.001$) and slower cognitive processing ($\beta = 1.47$, CI: 1.10 to 1.84, $p < 0.0001$) were associated with greater apathy. Our findings suggest that a shared process underlies the development of apathy and motor signs in HD. A common substrate might be the disruption of striatal pathways that gate movement, decisions, and motivated behaviour.

5.2 Introduction:

In the final two data chapters I turn directly to the pathophysiology of apathy in HD. Apathy is a highly prevalent, disabling yet poorly understood symptom found in a range of neuropsychiatric disorders (Le Heron et al., 2017; Salamone et al., 2015a). In Huntington's disease (HD), apathy is common and associated with poor quality of life, reduced functional capacity and disease progression (Bates et al., 2015; Duijn et al., 2014; Fritz et al., 2018; Hamilton et al., 2003; Jacobs et al., 2018; Lehericy et al., 2005; Tabrizi et al., 2013; Thompson et al., 2012). Currently there are limited effective treatments for apathy in HD, partly as the pathophysiology of apathy in HD is poorly understood (Gelderblom et al., 2017; Krishnamoorthy and Craufurd, 2011).

As reviewed in the Introduction to this thesis, there is limited consistent translational evidence regarding the underlying pathophysiology of apathy in HD; however there is clear and consistent epidemiological evidence. Apathy in HD has been shown to (1) occur very commonly, affecting nearly all patients with HD, (2) is common even in the early stages of the disease and (3) shows a tight connection with disease progression (van Duijn et al., 2014; Martinez-Horta et al., 2016; Tabrizi et al., 2013; Thompson et al., 2012). On the basis of these observations, neuropathology in HD, models of striatal functions – as outlined in Chapter 1 – I hypothesised that the ratio of disruption to the direct, versus indirect, pathway cells of the striatum drives a proportion of the apathy seen in HD.

This hypothesis was challenging to test – not least because there are no clear *in vivo* quantitative measurements of direct and indirect pathway function to my knowledge. In the next chapter, I will use functional imaging data to model these pathways; however in this chapter I present an indirect approach of testing my hypothesis. I leverage pathophysiological models of motor signs in HD to make predictions of data from a large multi-national epidemiological study – ENROLL-HD.

HD is a remarkably complex disorder. Leaving aside the florid and disabling psychiatric and cognitive features, the motor phenotype of HD is varied and complicated (Bates et al., 2015; McColgan and Tabrizi, 2018). Although classically considered hyperkinetic, HD presents with a range of movement signs aside from chorea. Intriguingly, alongside disinhibited movements bradykinesia and akinesia are

also common and co-morbid with hyperkinetic signs. The balance between chorea and hypokinesia has been described as being “determined individually” (Roos, 2010). For the purposes of this chapter, these two neurological features of HD are of particular relevance because of pathophysiological models which suggest that chorea and bradykinesia map onto *indirect* and *direct* pathway dysfunction respectively.

In a seminal theoretical perspective, Albin *et al* (1989) noted that enkephalin stained neurons projecting from the striatum were affected earlier in HD than neurons containing substance P, indirect and direct pathway neurons respectively (Albin *et al.*, 1989). They argued that loss of these neurons increased inhibition of the subthalamic nucleus (STN) and resulted in disinhibition of thalamocortical projections. In reverse, they argued that Parkinsonian features manifest as a result of over activity of the indirect pathway secondary to either degeneration of the direct pathway, or hypodopaminergic states. At the time this model was highly influential. Prior to this, before the function of the opponent pathways was known, the prevailing model of HD pathophysiology was that overall striatal cell loss resulted in inhibition and corruption of motor programmes leading to chaotic hyperkinetic signs (Penney and Young, 1983). As I described in Chapter 1, while now the two-pathway model appears simplistic given further anatomical and physiological advances, there is evidence supporting the two-pathway model as a useful approximation to striatal function (Calabresi *et al.*, 2014a).

Given the prevalence of apathy in HD and its strong associations with disease progression I hypothesised that apathy in HD may be a psychiatric manifestation of the same core striatal pathology that generates motor signs. Aside from motor control, the pathways of the striatum have been implicated in the computation and expression of goal directed behaviour (Haber, 2016; Schultz, 2016) Furthermore, it has been argued that the opponent pathways in the basal ganglia may act to gate the choice of instrumental or rewarding action (Collins and Frank, 2014; Frank, 2011; Haber and Knutson, 2009).

On this basis I predicted that apathy would be more commonly associated with motor symptoms of reduced initiation, such as bradykinesia, possibly indicative of direct pathway dysfunction. In contrast, I predicted that apathy would be less associated with signs of motor disinhibition, such as chorea,

associated with indirect pathway dysfunction. Alternatively, to assess whether apathy in HD was a manifestation of a pseudo-Parkinsonian syndrome perhaps related to striatal dopamine depletion I also assessed whether rigidity in HD was also associated with apathy. Under this hypothesis, it may be predicted that apathy would be associated with bradykinesia and rigidity, but not chorea.

To test these hypotheses whilst accounting for wide inter-individual variation in clinical presentation, psychiatric co-morbidities and medication use, I used detailed longitudinal data from the multinational ENROLL-HD study, the largest cohort of HD patients available.

For the work presented here, I am indebted to Dr. Ahmed Aziz who both introduced me to the ENROLL dataset and wrote code to extract relevant variables from the ENROLL-HD database. I conceived this study, based on the hypotheses above, and analysed the extracted data using the models I describe below. Of course, this chapter would not have been possible without the ENROLL study and the team behind this multinational collaborative effort.

5.3 Methods:

5.3.1 Participants:

Data from ENROLL-HD, a prospective multinational observational study of HD was retrieved on the 17th November 2017 (Landwehrmeyer et al., 2017). Alongside demographic variables and genetic status, standardised neurological, cognitive and neuropsychiatric measures are available for all participants. For this analysis data from patients with manifest HD (n = 2608 unique patients with a total of 5647 observations) were included. For more information regarding ENROLL-HD please see Methods chapter.

5.3.2 Statistical analysis with mixed effects models:

As per the analysis from Chapter 3; in this chapter, I adopted a linear mixed effects model for the analysis of the ENROLL-HD data. In standard linear models, such as those described in Chapter 4, variance in dependent variable is explained by the estimation of an intercept term, followed by a series of fixed coefficients for each explanatory variable with the addition of some noise, which is assumed to be drawn randomly from a distribution. Mixed effects models expand on this framework by introducing another type of variable to the model, namely random effects. Mixed models take the form:

Equation (5-1):

$$Y = \beta X + bZ + \varepsilon$$

Where Y is the dependent variable, X is the fixed-effects design matrix, Z is the random effects design matrix, β are the fixed effect coefficients and b are the random effect coefficients. Unlike the fixed effect coefficients, the b values are thought to be drawn from normal probability distribution.

These random effects specify that fixed effects may vary randomly based on the clustering of the data. For example, let us consider an example in which we are sampling longitudinal data, y , from N subjects and only have one independent variable. In this case alongside the group-level β coefficient explaining the slope of the overall relationship between x and y , that the data may be better modelled by accounting

for clustering of data from each subject. We may therefore estimate a different intercept and a different slope for each subject – these would be considered random effects. The observations from each subject are then considered to be a linear combination of the fixed effects estimated across all subjects plus the relevant random effects estimated for that subject. So, for subject n , their dependent variable at a given time (y_{in}) would be estimated as follows:

Equation (5-2):

$$y_{in} = \beta_0 + \beta_1 x_{in} + b_{0n} + b_{1n} x_{in} + \varepsilon$$

Where β_0 is the fixed effect intercept estimated across all subjects, β_1 is the fixed effect coefficient estimated across all subjects, b_{0n} is the *random intercept* calculated for subject n and finally, b_{1n} is the random slope estimated for subject n . Like the error term ε , the various random effects across subjects, b , are thought to be drawn from a normal distribution with mean 0. Aside from specifying the random effects which may occur in the model, mixed models can also estimate the correlations in repeated measures within a subject through the specification of the variance-covariance matrix. There are a range of possible structures which can be specified; however, it is also possible to leave an unstructured matrix in which the variance-covariance structure is estimated. Mixed models are estimated based on maximum likelihood techniques – in essence, maximising the conditional probability of observing the data given the estimated parameters.

In the case of ENROLL-HD, much like the example above, we are collecting repeated measurements from each participant. Each subject may have a different baseline level of apathy to begin with and data from each of their visits is likely to be highly correlated and influenced by how much time has elapsed between visits. Using a mixed model it is possible to specify this structure and as a result more accurately estimate the true relationship between the fixed effects, motor signs, and our dependent variable, apathy. Aside from specifying clustering by subject, in this study a random slope terms for age was used to account for the correlation between the repeated measurements for each subject (van der Burg et al., 2017).

The primary outcome was a measure of behavioural apathy administered as part of the Problem Behaviour Assessment scale (PBA) (Kingma et al., 2008). This item was a composite of both severity and frequency of apathy, ranging from 0-16. Based on the distribution of model residuals, apathy scores were transformed using a square-root transformation.

Motor signs included in the model as the fixed effects were bradykinesia, chorea and rigidity items from the Unified Huntington's Disease Rating Scale (UHDRS) (Huntington Study Group., 1996). The bradykinesia score is rated by clinician from 0-4, measuring slowing of spontaneous action. The chorea and dystonia scores were determined as the mean score, from 0-4, across all body regions. Rigidity scores were calculated as the mean rigidity as in both upper limbs (0-4).

Covariates included in this model were age, gender, mutant CAG repeat size, disease duration, scores on PBA-depression item, cognitive performance and the current or previous use of psychotropic medications. A summary score of cognitive performance was used in this analysis based on a principal component analysis of the core cognitive measures in the ENROLL-HD study (including Symbol Digit Modality Test – total correct in 90s, Stroop word, colour naming and interference – total correct in 45s and verbal category fluency in 60s). The first principal component (PC1) accounted for 79.3% of the variance and was included in this analysis to summarise cognitive performance.

For the second analysis reported here, bradykinesia was replaced with the measure of finger tapping speed taken at each assessment. This scored between 0 and 4, 0 representing > 15 taps/5 secs and a score of 4 representing gross impairment with 0-2 taps/5 secs. This score is measured in both hands. For this analysis the mean performance was used with higher score indicating slower voluntary finger tapping. For the final analysis, cognitive processing speed during Stroop word naming and colour naming was calculated as the sum of colours or words named (correctly, or incorrectly) in 45 seconds, divided by the maximum possible, 200.

Data variables were extracted from the ENROLL-HD dataset using R and MATLAB. The linear mixed models were fit using MATLAB 2017 using the *fitlme* function. Residual diagnostics are shown in supplementary data at the end of this Chapter indicating that model residuals formed a near normal

distribution. An unstructured variance–covariance matrix was used, and the model was fit using a maximum likelihood method to allow for model comparison (Magezi, 2015). Although this procedure may generate the best fitting parameter, model estimation itself does not defend against model fitting. For this, model comparison is required. Like in all of the other Chapters, I used a model comparison metric in here which incapsulates Occam’s Razor. In this chapter, I have adopted the Akaike Information Criteria (AIC).

The AIC is calculated as follows:

Equation (5-3):

$$AIC = 2k - 2\ln(\hat{L})$$

Where k represents the number of parameters in the model and L represents that maximum likelihood value for the model. In this way AIC can also be considered as complexity minus goodness of fit. The smaller the AIC, the better in terms of model comparison. It is also possible to compare the likelihood of competing models using a Likelihood ratio test. In this Chapter I use these methods to justify the inclusion of the motor signs in the model.

5.4 Results

5.4.1 Sample characteristics:

n = 2608	First visit	STD	Last visit	STD	p-value of difference
Mutant CAG length	43.8	3.51			
Gender (F%)	47%				
Age	50.9	12.01	54.1	12.17	
Duration	2.7	3.64	5.95	4.15	
Total functional capacity (TFC)	9.43	2.96	7.44	3.48	<0.001
Apathy	3.16	4.17	4.07	4.72	0.007
Depression	5.56	6.78	5.17	6.4	0.003
Cognitive performance	0.44	1.86	-0.15	2.09	<0.001
Bradykinesia	1.03	1.01	1.56	1.18	<0.001
Chorea	0.98	0.61	1.18	0.71	<0.001
Rigidity	0.51	0.66	0.77	0.83	<0.001
Dystonia	0.38	0.60	0.66	0.81	<0.001

Table 5-1: Sample characteristics including change in clinical variables used in the model between first and last available visit. P-values show the statistical significance of non-parametric (Wilcoxon) paired differences between first and last visit. Participants showed progression on all measures considered except depression.

The mean sample characteristics for first and last visits included in the analysis are shown in Table 1. At the first visit, partial non-parametric (Spearman) correlation analysis showed that apathy was associated with reduced total functional capacity (TFC) ($\rho = -0.30$, $p < 0.0001$) controlling for the effects of age, gender, CAG length, motor score and cognitive impairment.

5.4.2 Relationship between apathy in HD and motor signs

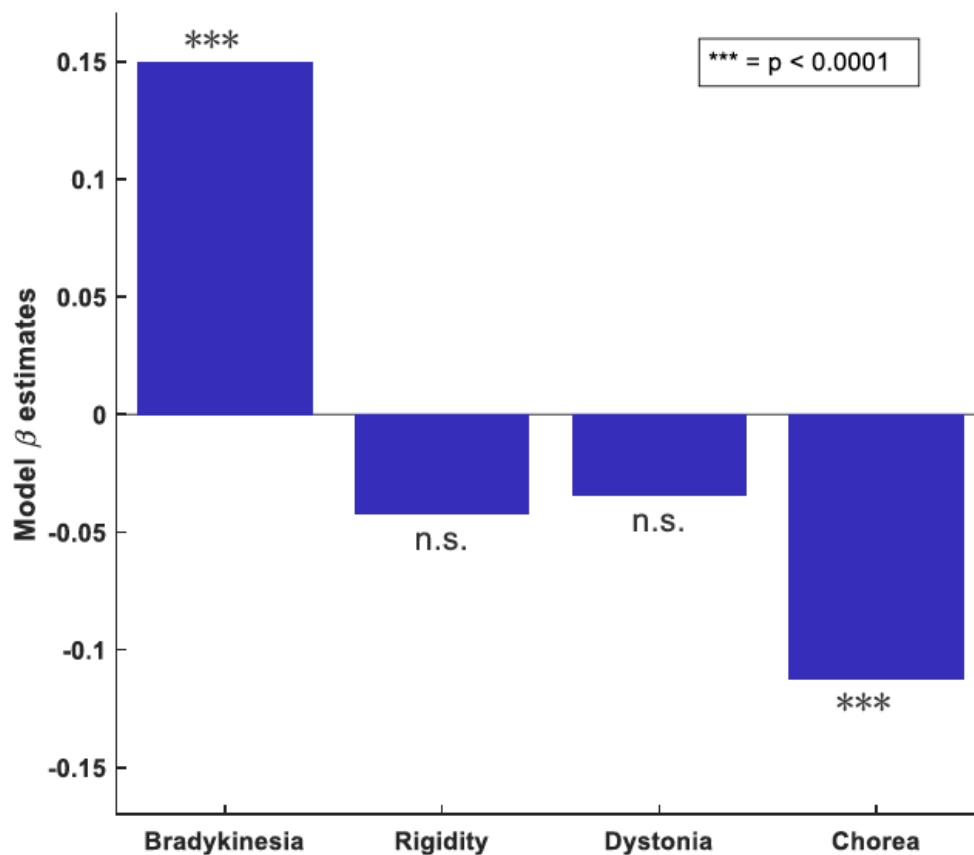


Figure 5-1: Relationship between apathy in HD and four common motor signs (n = 2608). *** represents $p < 0.001$, n.s. represent non-significant result.

As hypothesised, both bradykinesia and chorea significantly predicted apathy severity, with opposite effects (Fig. 5-1) after adjusting for the effects of age, gender, CAG length, depression, cognitive performance, duration of illness and medication use. While higher bradykinesia score was associated with more severe apathy ($\beta = 0.15$, CI: 0.11 to 0.19, $p < 0.001$), higher chorea was associated with lower apathy scores ($\beta = -0.11$, CI: -0.07 to -0.16, $p < 0.001$). There were significant effects for depression ($\beta = 0.06$, CI: 0.06 to 0.07, $p < 0.001$), cognitive performance ($\beta = -0.14$, CI: -0.11 to -0.16, $p < 0.001$), antipsychotic use ($\beta = 0.40$, CI: 0.31 to 0.47, $p < 0.001$), SSRI ($\beta = 0.15$, CI: 0.08 to 0.23, $p < 0.001$), other classes of antidepressants ($\beta = 0.12$, CI: 0.04 to 0.20, $p < 0.01$) and tetrabenazine ($\beta = 0.1$, CI: 0.003 to 0.2, $p = 0.04$). In this model, rigidity ($\beta = -0.04$, CI: -0.09 to 0.007, $p = 0.09$), dystonia ($\beta =$

-0.03, CI: -0.08 to 0.02, $p = 0.2$) and disease duration ($\beta = 0.001$, CI: -0.008 to 0.01, $p = 0.82$) were not found to have significant main effects. Removing motor signs from the model substantially increased the model AIC (Model 1: 17261, Model 2 (no motor): 17381, difference = 120) and the Likelihood Ratio Test strongly supported the inclusion of motor signs ($\chi^2(4) = 127.8$, $p < 0.0001$).

5.4.3 Finger tapping speed and apathy

A related objective measure of movement speed is the UHDRS maximum finger tapping speed recorded over 5 seconds. In this analysis, the bradykinesia item in the model as described above was replaced with the participants' average finger tapping score. In keeping with the above analysis, slow finger tapping speed showed a significant positive main effect ($\beta = 0.09$, CI: 0.04 to 0.13, $p = 0.001$) after controlling for covariates described. These results suggest that a simple bedside test of movement speed is associated with apathy severity in HD. Finger tapping score was also strongly correlated with clinician rated bradykinesia ($\rho = 0.55$, $p < 0.001$ at Visit 1).

5.4.4 Cognitive processing speed and apathy:

Given these results, I asked whether apathy in HD was also associated with a more domain-general slowing. In the above model, apathy was strongly associated with worse cognitive performance however, this score reflects reduced processing speed and increased cognitive errors. To assess processing speed, whilst not penalising participants for making errors, I chose to assess the relationship between apathy and total number of colours and words named in the Stroop naming tests, including errors. I found a strong negative relationship between this measure of faster cognitive processing and apathy scores ($\beta = -1.47$, CI: -1.10 to -1.83, $p < 0.0001$). This score does not penalise for impaired limb motor function, cognitive control and requires minimal memory or attention. A lower score on this measure therefore represents fewer total colours or words named in 45 seconds. In this model I replaced the cognitive composite score in the model above with this measure of cognitive processing speed, controlled for the effects of motor signs with the addition of dysarthria score.

5.4.5 Discussion:

The pathophysiology of apathy in HD is poorly understood and there are limited treatment options. Using a large, well-characterised cohort of patients with manifest HD, I found that both bradykinesia and chorea were significantly associated with apathy however their effects were in opposite directions. Bradykinesia was associated with greater apathy whereas chorea was associated with lower apathy. Rigidity and dystonia in HD were not significantly associated with apathy. I also show that finger tapping, a related simple bedside test of bradykinesia was associated with higher apathy scores. Finally, apathy in HD was also associated with slowed cognitive processing suggesting that it may be part of a domain general slowing or impaired gating phenomenon. Beyond these main findings, these data also demonstrate that depression, psychotropic medication use, and cognitive impairment are associated with apathy severity.

This analysis raises both interesting theoretical questions and potentially important clinical implications. Firstly, these data suggest that the presence of significant in clinic bradykinesia should prompt enquiry about apathy symptoms given the reduced quality of life and increased care burden associated with apathy (Banaszkiewicz et al., 2012; Fritz et al., 2018; Jacobs et al., 2018). Secondly, beyond the motor symptoms, these results clearly indicate an association between depression, psychotropic medication, cognitive impairment and apathy. This suggests that apathy in HD is a complex construct with neurological, psychiatric, cognitive and iatrogenic components. This complex aetiology may also be an explanation for the relatively small strength of the associations I report here. Finally, as described earlier in this thesis, apathy is hard to treat in HD. If these findings support the hypothesis that there may be shared pathophysiology between bradykinesia and apathy in HD, novel treatments for bradykinesia may also be beneficial for apathy.

Theoretically, to explain the results presented here, any hypothesised pathophysiological process should be able to account for the inverse relationships between apathy and bradykinesia as compared to apathy and chorea. This is alongside the existing epidemiological observations about apathy, namely that it is common in HD, can occur early in the disease and tracks closely with disease progression (van Duijn

et al., 2014; Martinez-Horta et al., 2016; Tabrizi et al., 2013; Thompson et al., 2012). As I have outlined above, I completed this analysis as an indirect method testing my hypothesis that the ratio of disruption to the direct, versus indirect, pathways of striatum drives a proportion of the apathy seen in HD (see Chapter 1). Based on the theoretical and empirical evidence outlined in Chapter 1, it is intuitive to find a positive relationship between apathy and bradykinesia, possibly caused by direct pathway involvement and a negative relationship between apathy and chorea, a clinical marker of indirect pathway function.

Although the associations reported in this Chapter are in line with my hypothesis, the relevance of these results is of course entirely dependent on the pathophysiology of motor signs themselves. Although this model of pathophysiology is well established in the literature (Albin et al., 1989, 1990; Waldvogel et al., 2015), it is important to highlight that empirical evidence for this model of chorea and bradykinesia is limited. Regarding functional imaging, to my knowledge only one PET study, by Esmailzadeh *et al* (2011), demonstrated that striatal D2-R binding measured via the binding of [11C]FLB-457 was inversely correlated with chorea (Esmailzadeh et al., 2011; Pagano et al., 2016). As with many PET studies however, this finding should be caveated with the fact that this study included only 9 participants. Aside from this result, there is limited *in vivo* evidence of changes in basal ganglia connectivity and the motor features in HD. This is the topic and aim of the following, and final, data chapter of my thesis. It is also worth highlighting that D2-antagonists, such as antipsychotics are commonly used for the management of chorea in keeping with the idea of an *indirect pathway* model of chorea (Coppen and Roos, 2017). By comparison, to my knowledge, there are no studies demonstrating the involvement of the *direct* pathway in bradykinesia in HD and, unfortunately, treatments for bradykinesia are limited with few drugs targeting D1 specifically.

Dopaminergic innervation of the striatum also controls the balance of these pathways and plays an important role in action initiation and vigour (Beierholm et al., 2013; Hamid et al., 2015; Ikemoto et al., 2015; Mohebi et al., 2019; Niv et al., 2007; Salamone et al., 2015c). An alternative hypothesis therefore is that apathy in HD forms part of a pseudo-Parkinsonian syndrome related to dopamine depletion. Changes to the dopaminergic system are seen in HD and it has been suggested that in later

disease stages dopamine depletion may occur, although the relationship between HD and dopamine is complex (Cepeda et al., 2014; Chen et al., 2013). In order to assess whether apathy in HD was related to the development of such a syndrome we also assessed the relationship between apathy, rigidity and bradykinesia. Rigidity in HD shares clinical features with the rigidity found in Parkinson's disease, namely a sustained resistance to movement (Roos, 2010). In this analysis apathy in HD was not associated with rigidity. This of course does not exclude a dopaminergic mechanism, and this may still be a significant contributing factor; however, with the other results presented here it could be argued that striatal loss and dysfunction in specific cell populations may better explain these findings. It should also be noted that Reiner and Deng (2018) argue, based on neuropathological studies of loss of dopamine neurons in HD as compared to Parkinson's disease, that it is "unlikely that the dopaminergic input loss to MSN in late HD by itself is great enough to have a symptomatic impact, but in combination with MSN loss could exert effects".

I should once again state that these hypotheses are not directly tested here as there is currently limited scope to quantify these pathways *in vivo*. In this chapter proxy measures, such as motor signs, are used to provide useful clues to basal ganglia connectivity. It may also be argued that the sample used here is weighted towards participants who are in the early to moderate stages of the disease. It is possible that severe dopamine dysregulation, with resulting apathy, may be a feature of late disease and not captured in this dataset. I also did not find a relationship between apathy and dystonia in my analysis. Although considered a *hyperkinetic* sign, the pathophysiology of dystonia is less well conceptualised than chorea and not easily explained by the disrupted striatal pathway model (van de Zande et al., 2017). As compared to chorea, dystonia is thought to involve cerebellar and cortical structures as well as the basal ganglia and in HD it has been hypothesised that disrupted striatal interneuron function may be more significant in the generation of dystonia as compared to asymmetrical striatal pathway degeneration (Reiner et al., 2013).

I further predicted that if the pathophysiology of apathy and bradykinesia overlap due to disrupted striatal gating, apathy in HD may also be associated with reduced speed of cognitive processing as basal ganglia are also thought to contribute to cognitive processing (Haber, 2016). Using a measure that does

not penalise for errors, impaired cognitive control and limb motor impairment I found that apathy in HD was strongly associated with reduced cognitive processing speed. This analysis, combined with the motor findings suggest that apathy in HD may be, in part, a manifestation of a domain-general slowing or impaired gating phenomenon.

At the time of completing this analysis, these associations had not previously been reported, although others have made similar predictions by comparing diseases with different motor characteristics. When comparing progressive-supranuclear palsy (PSP) with choreic patients with HD, Litvan *et al* (1998) found a similar relationship between apathy and motor signs as choreic patients reported significantly fewer symptoms of apathy as compared to hypokinetic patients with PSP (Litvan *et al.*, 1998). As quantification of basal ganglia pathway connectivity *in vivo* is not established there is limited imaging data available to test this hypothesis directly. In previous HD studies, apathy has been shown to be associated with motor severity and, in smaller samples, increased apathy in patients with more severe hypokinesia has been reported (Fritz *et al.*, 2018; Reedeker *et al.*, 2010; Sousa *et al.*, 2018a).

More recently, in a very similar analysis to the one presented here, Julayanont *et al* (2020) studied 3505 patients from the ENROLL database and classified them as chorea-dominant, parkinsonism-dominant and mixed-motor based on motor scores based on the balance of their motor features. Like the results found here, this group also showed that apathy (and depressive) symptoms were higher in the ‘parkinsonism-dominant group’ as compared to the ‘chorea-dominant group’. Unlike the analysis shown here, the parkinsonism-dominant group in Julayanont *et al* (2020) consisted of those patients with a wider range of symptoms including bradykinesia, rigidity and postural instability.

The primary strength of this analysis is the use of a large well characterised cohort of patients with HD. The use of ENROLL-HD data enabled us to assess the relationship between apathy and motor symptoms whilst accounting for phenotypic variation and multiple potential confounders. The analysis presented also uses multiple measurements from the same individual to increase the power of the statistical model. This, however, does not mean that we can infer a causal or temporal relationship between our variables of interest. Given the inexorable degenerative nature of HD, there is less data from patients further into disease and therefore the findings reported here are most generalisable to

early-moderate stage HD. This is an important limitation as the nature of apathy in HD is likely to change as the disease progresses. In later stage disease cognitive impairment is marked and neurodegeneration occurs in almost all parts of the brain (Waldvogel et al., 2015). It should also be noted that the apathy measure used in this study is relatively simple as compared to other, fine-grained, apathy scales used throughout this thesis. I am unable to distinguish the subtypes of apathy in this analysis such as cognitive, emotional or social for example (Ang et al., 2017; Le Heron et al., 2017; Levy and Dubois, 2006b). The scale used within the PBA maps closest to the concept of behavioural apathy however, should be viewed as a general apathy assessment (Thompson et al., 2002). The PBA is described further in the Methods Chapter.

5.4.6 Conclusion:

This analysis suggests that the processes driving distinct motor symptoms in HD may provide clues to the processes driving hard-to-treat psychiatric symptoms such as apathy. A common substrate and possible target for this shared mechanism is the disruption of specific striatal pathways that gate actions, decisions and motivated behaviour.

Much like the previous Chapter, it was encouraging to see the associations reported here fit theoretically within the predictions made by computational models of the basal ganglia. Moving forward, I built on these results by developing a method which measures the connectivity within the basal ganglia circuit. Using this novel approach, I ask whether apathy scores in HD are associated with specific changes in basal ganglia connectivity, in keeping with direct pathway changes.

5.4.7 Supplementary figures:

5.4.8 Model (1) diagnostics: square root apathy and motor signs

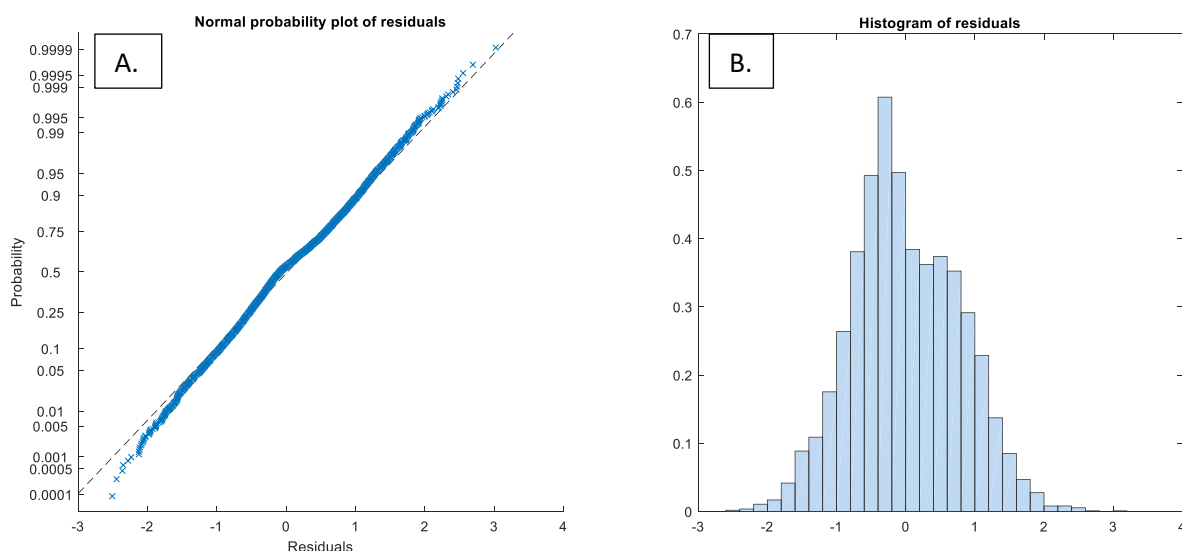


Figure 5-2: Supplementary figure showing the distribution of the residuals from the linear model assessing the relationship between apathy and motor signs. (A) shows the residuals as blue crosses overlaid on top of a dashed lined representing the probability expected for the residuals assuming a normal distribution. (B) shows that residuals as a frequency distribution.

5.4.9 Model (2) diagnostics: square root apathy and finger tapping

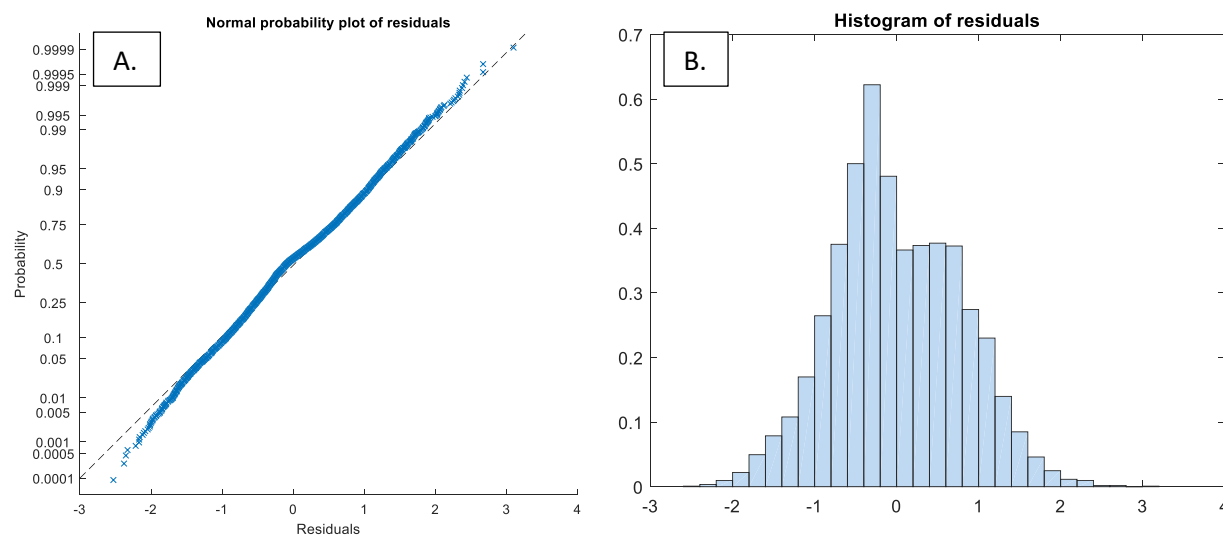


Figure 5-3 Supplementary figure showing the distribution of the residuals from the linear model assessing the relationship between apathy and finger tapping . (A) shows the residuals as blue crosses overlaid on top of a dashed lined representing the probability expected for the residuals assuming a normal distribution. (B) shows that residuals as a frequency distribution.

5.4.10 Model (3): square root apathy and processing speed

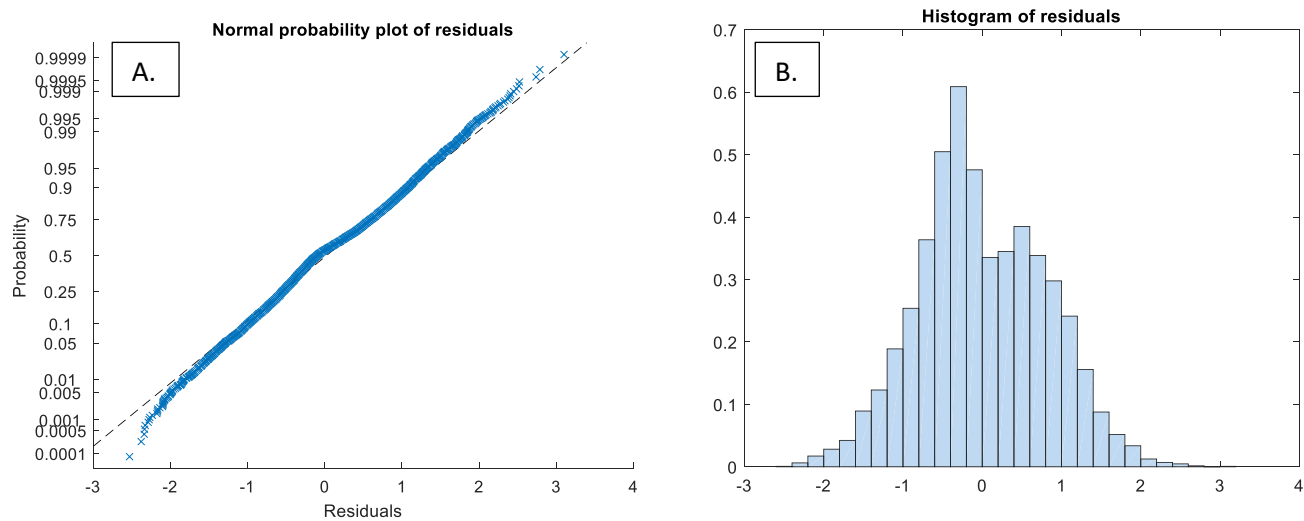


Figure 5-4: Supplementary figure showing the distribution of the residuals from the linear model assessing the relationship between apathy and cognitive processing speed. (A) shows the residuals as blue crosses overlaid on top of a dashed lined representing the probability expected for the residuals assuming a normal distribution. (B) shows that residuals as a frequency distribution.

Chapter 6: Imbalanced basal ganglia connectivity is associated with motor deficits and apathy in Huntington's disease: First evidence from human *in vivo* neuroimaging

6.1 Abstract:

The gating of movement is thought to depend on activity within the cortico-striato-thalamic loops. Within these loops, emerging from the cells of the striatum, run two opponent pathways – the *direct* and *indirect* pathway. Both are complex and polysynaptic but the overall effect of activity within these pathways is to encourage and inhibit movement respectively. In Huntington's disease (HD), the preferential early loss of striatal neurons forming the indirect pathway is thought to lead to disinhibition of basal ganglia networks giving rise to the characteristic motor features of the condition. But early HD is also associated with apathy, a failure to engage in goal-directed movement. I hypothesised that in HD, motor signs and apathy may be correlated with unique changes in basal ganglia connectivity driven by indirect and direct pathway dysfunction, respectively. Using a Bayesian technique for estimating dynamic *effective* connectivity within the basal ganglia, I tested both of these hypotheses *in vivo* for the first time in a large cohort of patients with prodromal HD using functional neuroimaging data. I used spectral dynamic causal modelling of resting state fMRI data to model effective connectivity in a model of these cortico-striatal pathways. I did not test this hypothesis directly. Instead, I used an advanced Bayesian approach by combining Parametric Empirical Bayes with an automated Bayesian Model Reduction procedure. This approach generated and compared a large number of competing models using a data driven approach. With this fully Bayesian approach, associations between clinical measures and connectivity parameters emerge *de novo* from the data. I found very strong evidence (posterior probability > 0.99) to support both of my hypotheses. More severe motor signs in HD were associated with altered connectivity in the indirect pathway connectivity and by comparison, apathy was associated with changes in the direct pathway connectivity of our model. The empirical evidence I provide here is the first *in vivo* demonstration that imbalanced basal ganglia connectivity may play an important role

in the pathogenesis of some of the commonest and most disabling features of HD, and may have important implications for therapeutics.

6.2 Introduction:

As described in the Introduction to this thesis, Huntington's disease (HD) is an autosomal dominant neurodegenerative condition caused by a triplet repeat expansion in the *huntingtin* gene on chromosome 4 (Bates et al., 2015; MacDonald et al., 1993). While the aetiology of HD is clear, the pathogenesis of many of the core clinical motor, cognitive and behavioural features of HD remain to be established. Although later in disease HD affects almost the entire brain, early degeneration of the striatum is canonical of this disorder both pathologically and on structural imaging (Tabrizi et al., 2012; Waldvogel et al., 2012; Wilson et al., 2018a).

The striatum, however, is not a homogenous structure (Graybiel and Grafton, 2015). As the input node to the basal ganglia, it has a complex anatomy. The medium spiny neurons (MSNs) of the striatum form a wide range of compartments and pathways (Calabresi et al., 2014b; Crittenden and Graybiel, 2011; Graybiel and Grafton, 2015). For HD, this anatomical complexity is of relevance because the disorder does not affect all striatal MSN populations equally (Tippett et al., 2007; Waldvogel et al., 2015). Cortico-striatal connections, which are topographically arranged, form the input to the striatum (Haber, 2016; Haber and Knutson, 2009). These cortical projections synapse with MSN populations that fall into two key groups – those forming the *direct* and the *indirect* pathway (Albin et al., 1989; DeLong, 1990b). They form unique and complex polysynaptic connections with other basal ganglia structures, such as the globus pallidus, subthalamic nucleus and substantia nigra (Calabresi et al., 2014b).

Overall, these two pathways form opponent channels that regulate thalamic control over cortical activation. In the motor system the activity of the direct pathway encourages movement whereas the indirect pathway activity inhibits or reduces movement (Bateup et al., 2010; Freeze et al., 2013; Kravitz et al., 2010). Although all MSNs are susceptible to degeneration in HD, those of the indirect pathway appear more susceptible earlier in the disease (Albin et al., 1992; Deng et al., 2004; Waldvogel et al., 2015). Based on these observations it has been hypothesised that changes in connectivity caused by damage to the indirect pathway would be associated with the emergence of motor signs in HD which

are characterised by erratic, noisy and disinhibited movements such as chorea, dystonia, in-coordination and jerky eye movements (Albin et al., 1992; McColgan and Tabrizi, 2018). Despite the widespread reference to this hypothesis, I know of no direct *in vivo* evidence supporting it. This is in part because *in vivo* assessment of basal ganglia connectivity is challenging.

Establishing the role of altered basal ganglia connectivity in the pathogenesis of HD may also have a wider clinical relevance beyond simply understanding motor signs. Alongside the motor features of the condition, HD is associated with a marked psychiatric phenotype and the focus of this thesis is apathy. As a reminder, although associated with a range of psychiatric disturbances, there appears to be a unique relationship between HD and the development of apathy (van Duijn et al., 2014). Apathy, the loss of motivation and goal-directed behaviour, is highly prevalent in HD (Duijn et al., 2014). Its pathogenesis is poorly understood and treatments are lacking (Gelderblom et al., 2017; Krishnamoorthy and Craufurd, 2011). Apathy in HD also tracks closely with disease progression even in premanifest and prodromal cohort (Tabrizi et al., 2013). As it is associated with significant morbidity and functional decline there is an urgent need to try and understand the pathogenesis of apathy in HD (Jacobs et al., 2018).

I hypothesised that like motor signs, some degree of apathy in early HD may also be a feature of basal ganglia pathway dysregulation. However, unlike motor signs, I hypothesised that apathy may instead arise from involvement of the *direct* basal ganglia pathway. This hypothesis is explained in detail in the Introduction to this thesis; however, I will summarise the main arguments again here. As described above, later in disease, both direct and indirect pathway MSNs are known to be affected in HD. Here I propose that in peri-manifest patients, early involvement of the direct pathway may contribute to the development of apathy. I base this hypothesis on two strands of evidence. Firstly, as alluded to above, activation of direct pathway MSNs is thought to encourage free operant movement (Bateup et al., 2010; Freeze et al., 2013; Kravitz et al., 2010). The lack of free-operant action initiation is characteristic feature of behavioural apathy and disruption to the direct pathway may hamper this final stage of goal-directed behaviour – the expression of action (Levy and Dubois, 2006b; Robert et al., 2009; Thompson et al., 2002). Secondly, computational models of basal ganglia function propose that as a result of the

physiological asymmetry in dopamine receptor expression, these pathways not only play opponent roles in motor expression but in value-based decision making (Collins and Frank, 2014; Frank, 2011; Franklin and Frank, 2015; Rubin, 2017). Dopaminergic inputs from the midbrain to the striatum are thought of as coding a range of computational parameters including opportunity cost, state value and in phasic dopamine signalling the reward prediction error (Hamid et al., 2015; Niv et al., 2007; Pessiglione et al., 2006; Schultz, 2016; Schultz et al., 1997). Common to all these theories is that higher levels of dopamine approximate to a richer environment or state. Computational models of striatal pathways therefore argue that via D1 and D2 receptors on the direct and indirect pathways respectively, higher levels of dopamine increase the activity of the direct pathway and reduce the activity in the indirect pathway by shifting their cortico-striatal synaptic weights (Collins and Frank, 2014; Franklin and Frank, 2015). Given the link between dopamine and higher value or reward, these models suggest that the activity and synaptic weights of the cells in the direct pathway come to represent the value of taking an action. Therefore, not only will dysfunction in this pathway disrupt the machinery necessary to take goal-directed action but may also impair the neural representations of reasons to take an action. I hypothesised that these two processes may therefore contribute to the development of apathy in early HD.

In the two preceding Chapters we have seen some evidence that striatal pathway function may be relevant to motivated behaviour in HD gene carriers. In Chapter 4, I assessed striatal activation in a gain and loss reinforcement learning task in a cohort of gene carriers decades from onset. At this point in disease, neuropathological evidence would suggest that if there is pathology at this stage, the indirect pathway MSNs are most likely to bear the cost. The computational models I reference above make the argument that cells in this pathway may serve a useful role in accruing reasons *not* to take an action or “No-Go”. With this in mind, as predicted, I found a wider asymmetry between gains and losses in the striatum of HD gene carriers, even 25 years from onset, than controls. Reward maximisation, a key component of my working goal of motivated behaviour, requires optimal learning in both gain and loss settings and, although I found no behavioural differences in my cohort, it is possible that the fMRI findings I report in Chapter 4 are antecedent of behavioural changes, with impaired loss learning seen

in HD gene carriers approximately 10 years from onset (Palminteri et al., 2012). Although not directly related to apathy, this study demonstrated that meaningful predictions could be made from computational models of basal ganglia function to motivated behaviour in HD, even if I was not able to quantify those pathways directly. Moving from motivated behaviour in the pre-manifest phase of HD, in Chapter 5 I leveraged models of the pathophysiology of motor signs in HD in a large early-mid stage HD population to ask whether apathy severity was associated with motor signs purportedly associated with direct pathway involvement. As described above, disruption to this pathway on the one hand disrupts the mechanisms of action initiation however, reinforcement learning models of the basal ganglia also propose that cells within this pathway accrue neural representations to take an action. Furthermore, given the hypothesised role of the indirect pathway, I predict the reverse relationship between apathy and signs associated with indirect pathway involvement. Although the effects were modest, I found, in a large cohort of manifest HD participants, a positive relationship between apathy and bradykinesia and a negative relationship with chorea.

In summary, in the preceding chapter I have presented evidence which is in keeping with the idea that imbalance basal ganglia pathway connectivity and function may be relevant to motivated behaviour in HD. In this Chapter I aim to test this hypothesis more directly using functional imaging data. Before testing my hypothesis about apathy, I first wanted to establish whether using this approach could find evidence to support the widely held theory that the emergence of motor signs in HD would be associated with altered indirect pathway connectivity. After testing this I move onto my novel hypothesis that apathy in early HD may be associated with change in direct pathway connectivity.

To test these hypotheses, I used an *in vivo* technique to model direct and indirect pathway connectivity change. Multiple anatomical and functional properties separate these pathways but canonically, they are distinguished by change in activity that they *cause* within the thalamic nuclei. Within a neuroimaging framework, this causal connectivity is described as *effective connectivity* (Friston, 2011). Here I leverage the difference in both anatomical and effective connectivity between the two pathways to test our key hypotheses. To study effective connectivity, I use a Bayesian framework known as *dynamic causal modelling (DCM)* to build a simplified model of our pathways of interest (Friston et

al., 2003, 2017; Kahan and Foltynie, 2013; Stephan et al., 2010). I based our study design on previous work in Parkinson's disease (PD) but using several technological advances to test my hypotheses (Kahan et al., 2014a). Firstly, I use *spectral* DCM for resting state fMRI (rsfMRI) to infer connectivity parameters in the pathways of interest as opposed to stochastic DCM (Friston et al., 2014b; Razi et al., 2015). Spectral DCM performs better than stochastic DCM, used in the previous PD study, in terms of accuracy and identifying group differences and associations (Razi et al., 2015). Secondly, I used Parametric Empirical Bayes (PEB) at the group level (Friston et al., 2016b). Parametric Empirical Bayes (PEB) framework for DCM models examines how individual (within-subject) connections relate to between subject factors. This approach uses the posterior probability distribution from each subject's unique DCM — both the expected strength value and the associated uncertainty — to inform the group-level results (such as the group means and the role of clinical variables). Lastly, I used Bayesian Model Reduction (BMR) to perform Bayesian model comparison to test our hypotheses (Friston et al., 2016b; Zeidman et al., 2019a, 2019b). Unlike previous studies which relied on a user specified model space comprising of relatively few models (or hypotheses) to test, here I used BMR which has the advantage of creating the models for the data in an automated manner. BMR prunes away associations between connectivity parameters and between-subject variables (such as apathy) based purely on model evidence, or *free energy*. As such, the relationship between clinical variables and basal ganglia connectivity parameters must arrive *de novo* from the data itself.

Using this approach, I demonstrate in a large cohort of patients with peri-manifest HD from the TRACK-ON HD study, (Klöppel et al., 2015) that motor signs and apathy in HD are associated with unique basal ganglia connectivity profiles. Furthermore, I found that as hypothesised, higher motor scores were associated with connectivity changes in the indirect pathway components, whereas higher apathy scores were associated with direct pathway connectivity changes. The contents of this chapter have been submitted for peer-review publication.

6.3 Methods:

6.3.1 Sample:

Data collected as part of the TRACK-ON HD were used in this analysis as previously described (Klöppel et al., 2015). For this analysis data from the third (and last) TRACK-ON visit were used, when variance in motor scores is the highest. Participants aged below 18 or over 65 were not recruited and participants with major psychiatric, neurological, medical disorder or history of head injury were excluded. Participants with the HD mutation all had greater than or equal to 40 CAG repeats and a disease burden score of greater than 250 at baseline. The study was approved by the local ethics committees and all participants gave written informed consent according to the Declaration of Helsinki. Sample characteristics are described in Table 1. Of 102 scans which passed quality control, two participants were excluded for antipsychotic use. A further 6 participants who were left-handed were excluded leaving data from 94 HD gene carriers in the peri-manifest phase of the disease in this study. Although group differences were not the focus of this study, data from 85 right-handed control participants was also used to replicate baseline network connectivity as described below. Left handed participants (6% of total participants) were excluded, to minimise effects of laterality as analysis were carried out unilaterally with ROIs placed across all participants in the left motor network. This approach was also taken by Klöppel *et al* (2015) to minimise differences in laterality of connectivity within the motor network.

6.3.2 Clinical outcomes:

Two primary outcomes were used in this study – Unified Huntington’s Disease Rating total motor score (TMS) and the self-rated Baltimore apathy scale (BAS) (Chatterjee et al., 2005; 1996). The motor score assesses the severity of 31 common neurological features such as chorea, dystonia, bradykinesia and oculomotor signs. The maximum score possible is 124. Due to the early stage of disease in these patients, and the relatively mild motor signs in the cohort (mean score 10.5 - see Table 1), the total motor score was used as opposed to specific subscales which would be underpowered. The BAS

consists of 14 items with scores ranging from 0-42 where a higher score represents a higher degree of apathy. Self-rated apathy scores were used for this analysis. Self and carer rated apathy have good interrater reliability especially in the absence of significant cognitive impairment (Baake et al., 2018b; Chatterjee et al., 2005; Mason and Barker, 2015). To control for the effects of depression, Beck Depression Inventory scores (BDI) were used as a covariate in the apathy analysis (Mestre et al., 2016).

6.3.3 MRI data acquisition:

3T MRI data were acquired at four sites; London, Paris, Leiden and Vancouver. T1-weighted image volumes were acquired using a 3D MPRAGE acquisition sequence as described by Kloppel *et al* (2015). Over the four sites, two different scanner systems were used: Philips Achieva at Leiden and Vancouver and Siemens TIM Trio at London and Paris. For resting state fMRI, whole-brain volumes were acquired at a repetition time (TR) of 3s using a T_2^* -weighted echo planar imaging (EPI) sequence with the following parameters: echo time 30ms, field of view 212mm, flip angle 80°, 48 slices in ascending order (slice thickness: 2.8 mm, gap: 1.5 mm, in plane resolution 3.3×3 mm) and bandwidth of 1906 Hz/Px. In total 165 volumes were acquired over 8:20 min followed by field map acquisition.

6.3.4 MRI pre-processing:

MRI image pre-processing and quality control were as described in Kloppel *et al* (2015) and I did not repeat these processes in this analysis (Klöppel et al., 2015). In brief, the first four EPI images were discarded to allow for steady state equilibrium. Images were realigned and underwent inhomogeneity correction where field maps were available. EPI images were co-registered to anatomical images and normalised to MNI space. Data was smoothed with a 6mm full-width at half-maximum Gaussian kernel. Data underwent significant quality control as described by Kloppel *et al* (2015). Manual QC along with the use of ArtRepair and tsdiffana were used to assess for significant movement before pre-processing. In the supplementary material at the end of this chapter, I have presented plots detailing in-scanner movement as summarise by the “framewise displacement”. This metric, as described by Power *et al* (2014) represents the sum of the values of the derivatives of the six movement parameters. In the

supplementary I present the cumulative framewise displacement, over the entire scan by group and by clinical variables – motor score and apathy score in HD. Overall, there was a weak correlation between motor score and in-scanner movement ($r = 0.37$, $p < 0.01$) however there was no association with apathy ($r = 0.11$, $p = 0.28$). This is to be expected given the nature of the disorder however, despite this there were no group difference between the HD gene carriers and controls in terms of in-scanner movement (as show in Supplementary). Motor regressors were used to control for the effect of movement in the analysis below.

6.3.5 Analysis of resting state data:

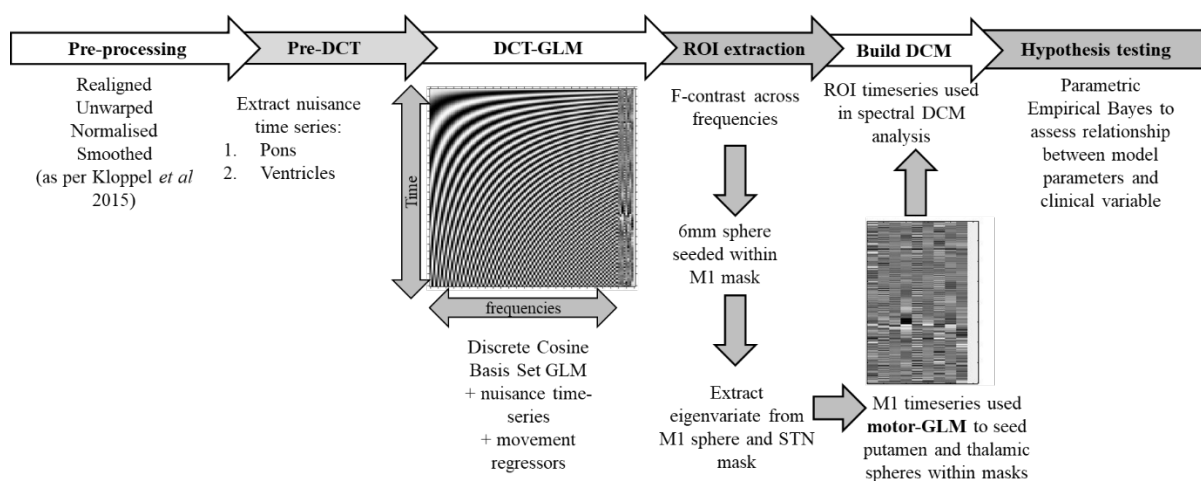


Figure 6-1: Summary of the resting state fMRI analysis pipeline used in this study

A summary schematic of the pipeline used to analyse the rsfMRI data is shown in Fig. (6-1). For this analysis, timeseries were extracted from four pre-defined regions of interest (ROIs) to make up the motor basal ganglia loop - the motor cortex, motor thalamus, motor putamen and the sub-thalamic nucleus (STN). With the exception of the subthalamic nucleus, timeseries were extracted from spheres seeded within anatomical masks defined in a standard space. An anatomical mask of Brodmann's Area 4 from Wake Forest University Atlas was used to define the motor cortex (Maldjian *et al.*, 2003). The motor putamen and motor thalamus masks were defined from probabilistic connectivity atlases with a threshold of 50% probability (Behrens *et al.*, 2003; Tziortzi *et al.*, 2014). The STN was not manually defined in this study. Instead, a mask made available by Keuken *et al* (2013) was used (Keuken *et al.*,

2013). This mask, defined in MNI space, was derived from the accurate high-resolution delineation of STN using 7T imaging, also assessing the impact of age. Based on the sample characteristics in this study (mean age 45.5 +/- 8.9), the mask for middle-aged individuals was used again with a conservative threshold of >50% probability. Given the size of this structure and the spatial resolution of functional imaging, the timeseries extracted may also contain signal from adjacent structures.

6.3.6 Resting state fMRI modelling with GLM:

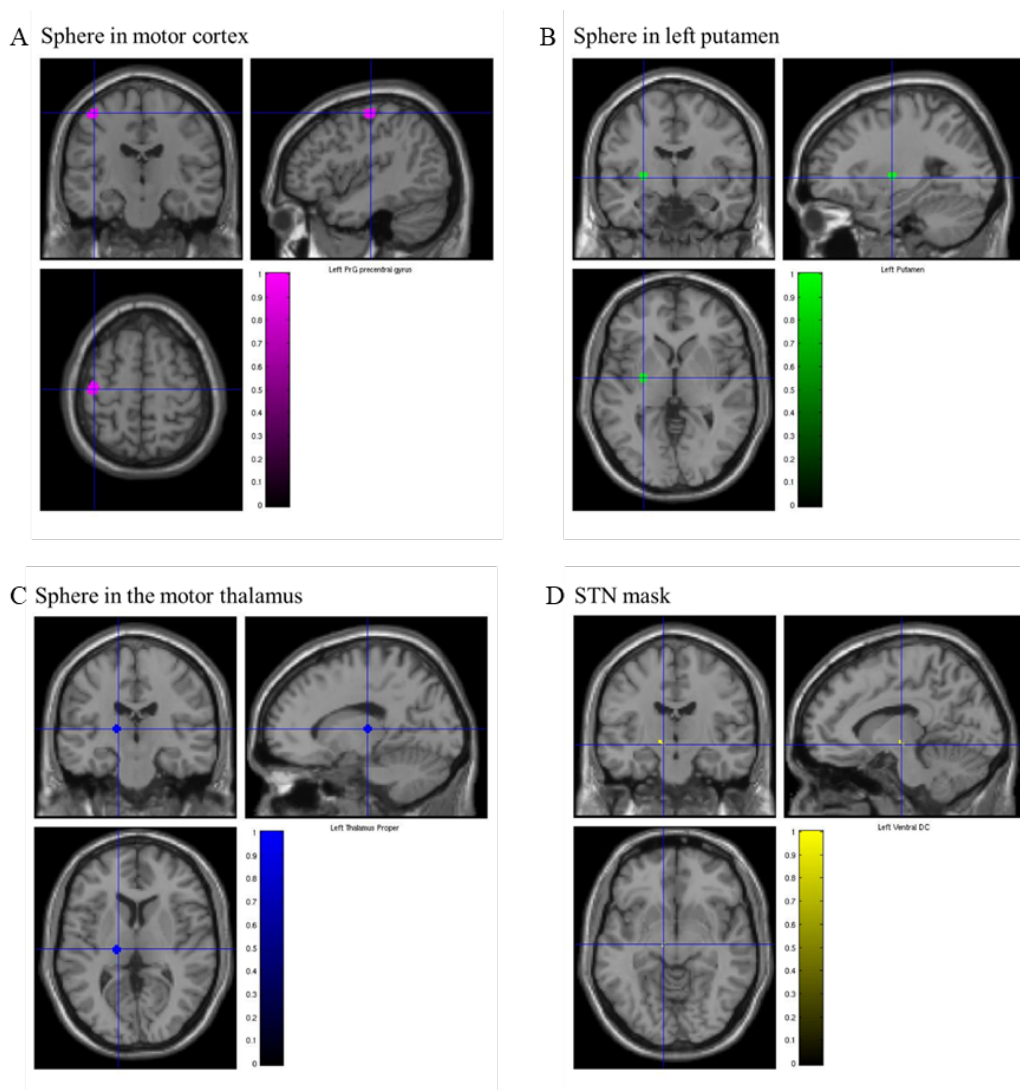


Figure 6-2: Region of interest locations for an example subject: (A) Shows the 6mm sphere, in pink, seeded within BA4 mask for motor cortex used to extract timeseries data (B & C) 4mm sphere seeded within motor putamen (B, in green) and thalamic (C, in blue) masks used to extract timeseries data. (D) No sphere was seeded within the STN – the entire mask, in yellow, was used to extract timeseries data. Masks are shown in coronal, sagittal and axial planes with SPM neuromorphometric labels shown for the crosshair location confirming locations. In all cases, spheres are superimposed on canonical single subject T1 image available in SPM.

Using the pre-processed scans, a dummy GLM was created to extract nuisance time series from the pons and ventricles. To better model resting state low frequency fluctuations, I then used a discrete cosine transform (DCT). In summary, this approach consists of 189 cosine basis functions modelling frequencies in the typical resting state range of 0.0078-0.1Hz (Biswal et al., 1995; Deco et al., 2011; Fox and Raichle, 2007; Fransson, 2005; Kahan et al., 2014b). I created a GLM containing these DCT regressors as well as the nuisance timeseries extracted as described above alongside six movement regressors.

An F-contrast was used over the DCT frequencies to identify regions that showed resting state activity that correlated with the motor cortex. Based on this contrast, within the BA4 mask, a 6mm sphere was placed at the location which showed the highest activity in the frequencies of interest. From this sphere the principal eigenvariate (adjusting for head movements and nuisance timeseries) was extracted. This procedure summarises the timeseries from all of the voxels in the sphere into one representative timeseries for the ROI. The variance explained by the eigenvariate in the M1 ROI had a mean of 67% with a variance of +/- 11.5%. The principle eigenvariate from the entire sub-thalamic nucleus mask was also extracted as above with variance explained mean of 87% with a variance of +/- 4.3%. The timeseries extracted from the motor cortex was then used to determine the location of 4mm sphere placed within the motor putamen and motor thalamic masks. The centre of these spheres was placed within each mask, at the co-ordinates that showed the strongest correlation with the M1 timeseries regressor. The principal eigenvariate was extracted from these spheres controlling for the same confounders showing variance explained with a mean of 76% (variance: +/-8.6) and 77.3% (variance: +/-8.4) in the putamen and thalamus respectively. Example ROIs are shown in Fig. 6-2. Example timeseries extracted from these ROIs is shown in Fig 6-3.

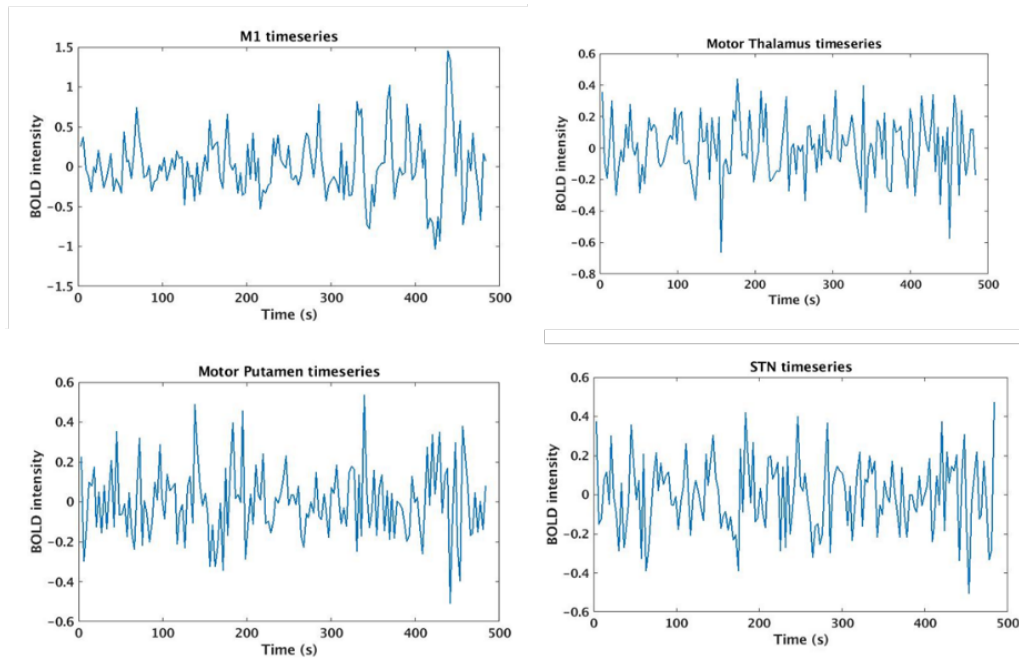


Figure 6-3: Example summary timeseries from four ROIs from one participant. Timeseries represent the principle eigenvariate of activity within voxels within each ROI shown in Fig. 6-2

6.3.7 Dynamic causal modelling and specification of the connectivity matrix

Based on previously published work, I used a simplified circuit representing the direct, indirect and hyperdirect pathway (Kahan et al., 2014b) as shown in Fig. (6-4). Here I do not model connections involving the globus pallidus, instead I use simplified circuit involving motor cortex, putamen, thalamus and STN as described by Kahan *et al* (2014). A forward connection from M1 to motor putamen represents the input to the network from the motor cortex. Motor putamen was modelled as having two forward connections – one connecting it to the motor thalamus, forming the direct pathway, and a second connection linking it to the STN, the first component of the indirect pathway. The STN was modelled as having a further connection to the thalamus, forming the second connection within the indirect pathway. A further direct connection between the cortex and the STN was specified representing the hyperdirect pathway. These basal ganglia pathways are shown as a schematic in Fig. (6-5). In this work, the globus pallidus structures are not modelled. This approach was also adopted by Kahan *et al* (2014). In part this approach was adopted to minimise potential overlap between nodes and to limit model complexity whilst, we argue, retaining the key features of the network. Inclusion of the globus pallidus segments would have necessitated the inclusion of multiple small adjacent nodes from

which to extract neural data. Furthermore, although perhaps more anatomically accurate, the inclusion of these nodes would not have added much more clarity to the results. Both the direct and indirect pathways drive activity in the globus pallidus; however, it is the driving effective connectivity between the striatum and thalamus which defines the function of the direct pathway and the inhibition of the thalamus via the STN which defines the indirect pathway. These aspects are modelled using our approach. We accept this approach has limitations and it must be stated that the connectivity we model must be driven by, unmodelled, activity in the globus pallidus.

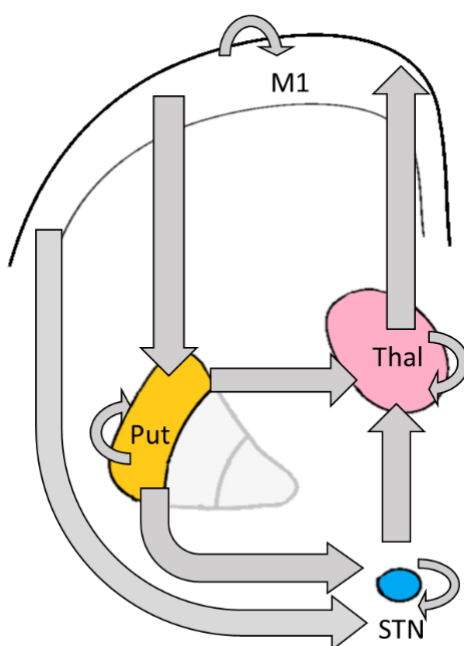


Figure 6-4: Schematic of the DCM A-matrix used in this study. Arrows looping back to the same node represent inhibitory self-connections specified in the DCM. The grey arrows describe the 'A' matrix in the DCM

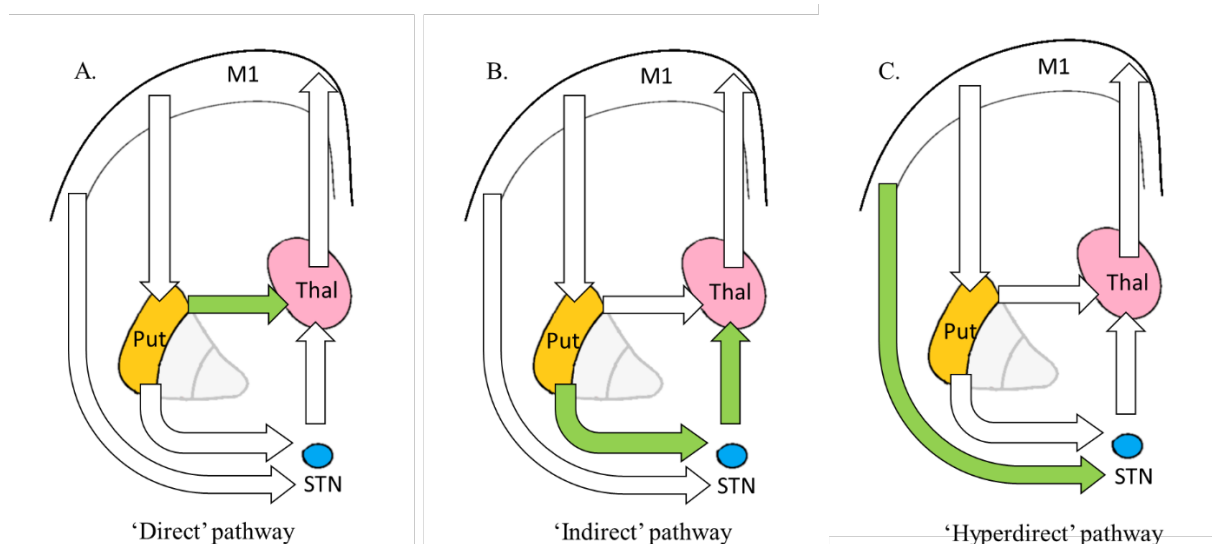


Figure 6-5: This model generates simplified representations of three pathways of interest – the direct, indirect and hyper-direct pathway. The direct pathway (A) is composed of the connection between putamen and thalamus. The indirect pathway components (B) are the putamen-STN connection and the STN-thalamic connection. Finally, the hyper-direct pathway (C) composes of a connection from the motor cortex to the STN.

Having specified this network, or *A-matrix*, I used spectral dynamic causal modelling (DCM) packaged as part of SPM12 to infer effective connectivity parameters. As described above, in this project I was explicitly interested in the causal relationship between nodes of the basal ganglia, i.e. how striatal activity causes changes in thalamic activity. This form of neuronal connectivity is referred to as *effective connectivity*.

DCM for resting state is centred around two functions – a neuronal state function and an observation function. In the neuronal state equation, the *change* of neuronal states is thought of as a function of the current state of that node, any exogenous inputs to the node (such as sensory stimulation – absent from rsfMRI) and the parameters governing the effective connectivity between nodes. These effective connectivity parameters, and their relationship with motor score and apathy, are of interest here. The simplified basal ganglia connectivity matrix described above, or the *A-matrix*, determines the modelled connections between the nodes. For example, when estimating neuronal connectivity, the DCM considers thalamic activity to be driven only by striatal and STN activity and not M1 activity because a pre-specified connection is absent. M1 may influence the thalamus in the DCM however, only indirectly via the striatum or STN. The goal of DCM is therefore to fit the connectivity parameters based on the fMRI data from each subject, according to the specified *A-matrix*. Of course, fMRI data

itself is a measure of the BOLD response and not neuronal activation. The true neuronal state is unknown and therefore we seek to infer these *hidden neuronal states* from BOLD activity. In DCM, BOLD is assumed to be neuronal state activity transformed via a haemodynamic response function (plus some noise). This transformation is called the observation equation which itself contains a series of parameters governing neuro-vascular coupling.

In task fMRI, task events can be thought to drive neuronal activity; however this is clearly lacking in resting state activity. As such, DCM for resting state encounters a thorny problem – how to successfully model the resting timeseries, as shown in Fig 6-5, without any clear driving input. The first solution to this problem was called *stochastic* DCM and was used by Kahan *et al* (2014). In stochastic DCM, endogenous stochastic fluctuations in neuronal activity are modelled as driving activity within the network in the absence of inputs. This, however, raises a problem when inverting from BOLD to neuronal activity – not only are the effective connectivity parameters unknown but the endogenous stochastic neuronal fluctuations are unknown, or hidden. This means the during the inversion from the BOLD timeseries stochastic DCM estimates of both effective connectivity parameters and endogenous fluctuations, both of which are unknown and contribute to the neuronal state activity.

Spectral DCM simplifies this process by inverting the DCM in the frequency domain. By this I mean the time series is converted into the distribution of frequencies which makes up that time series. More specifically, spectral DCM uses BOLD data to compute the *cross-spectra* between brain regions – this is the frequency domain equivalent of cross-correlation between timeseries, which is used to estimate connectivity. Spectral DCM is therefore much more efficient because instead of estimating the time series, and the stochastic fluctuations driving the neuronal state throughout the scan, it uses the cross-spectra to estimate the covariance between brain regions which is assumed to be time-invariant. This assumption is reasonable for resting state fMRI in which it is assumed that nothing is perturbing the system and makes the modelling of effective connectivity significantly faster (Friston *et al.*, 2014b). It has been shown that this approach is more accurate at recovering parameters and estimated second-level effects such as group differences (Razi *et al.*, 2015). In this analysis, I do not specify the valence of the connections between nodes and allowed these to be estimated from the data. The positive

connectivity value refers to an excitatory connection whereas negative connectivity value refers to an inhibitory influence.

In order to find each subjects DCM parameters from the BOLD data – each subject’s DCM is inverted. This means that each subject’s parameters are estimated to best explain the data. As we have seen in every data chapter so far, parameter estimation and model fitting must follow Occam’s Razor by balancing accuracy and complexity. In previous chapters metrics such as the Bayesian Information Criterion and Akaike Information Criterion have been used to compare models. In both cases, models are rewarded for goodness of fit but penalised for model complexity.

In the case of DCM, the models are inverted based on their *free energy*. DCM is based around Bayesian statistical principles with the aim of parameter estimation being to maximise the *log model evidence*. This is the probability of seeing the BOLD data given a model m , or $\ln p(Y|m)$. This is challenging however, as the calculation of log model evidence relies on *marginalising* or averaging over all model parameters. Given the large parameter space in models such as DCM, marginalising over parameters to compute model evidence rapidly becomes intractable. One approach to computing the model evidence is to use sampling techniques such as Markov Chain Monte Carlo (MCMC). Alternatively, as implemented in SPM, one can approximate the model evidence calculated using a metric known as *free energy*. The derivation of free energy is complex and beyond the scope of this Chapter; however, a few fundamental properties of free energy are pertinent to this investigation. Firstly, free energy approximates the lower bound on model evidence meaning that maximising free energy is equivalent to maximising model evidence (the evidence of the model given the data). This means when fitting parameters, parameters which maximise free energy are most probable, given the data. It also means that when comparing models, models with the highest free energy are most probable, given the data. Secondly, much like other statistics of model comparison, free energy consists of an accuracy component and a complexity component. The accuracy component is capturing how the simulated BOLD activity correspond to the actual data. The complexity element in free energy, captures the difference between the estimated parameters and their priors and also accounts for parameter covariance.

When a DCM is inverted, free energy is used to score the model evidence for model comparison and to output the probability density of parameters which maximises free energy. In this way, DCM parameter estimation outputs not only the expected value but the associated uncertainty. The process for fitting models using maximisation of free energy is known as Variational Laplace.

6.3.8 Parametric empirical Bayes (PEB)

The DCMs specified above were fit and estimated for each participant separately using Variational Laplace. The DCMs performed well explaining 83.1% of the variance of the fMRI data (variance: +/- 9.7% in the patient cohort (and 83.8% +/-8.4%) in the control cohort). Inference on clinical scores was performed using Parametric Empirical Bayes (PEB) (Friston et al., 2016b). This is a between-subjects Bayesian model that models how connections at the individual level, such as connectivity parameters, relate to between subject factors, such as motor score. In more detail – PEB can be thought of as a series of hierarchical equations which I describe below, summarised largely from an excellent pair of reviews by Zeidman *et al* (2019) (Zeidman et al., 2019a, 2019b):

Equation (6-1):

$$\begin{aligned}
 1. \quad y_i &= \zeta(\theta_i^{(1)}) + X^{(1)}\beta_i + \epsilon_i^{(1)} \\
 2. \quad \theta^{(1)} &= X^{(2)}\theta_i^{(2)} + \epsilon^{(2)} \\
 3. \quad \theta^{(2)} &= \mu + \epsilon^{(2)}
 \end{aligned}$$

In Equation (6.1.1), y_i represents the fMRI data from a participant. It is thought of as being a function of $\epsilon_i^{(1)}$ observation noise, “uninteresting” effects such as mean signal ($X^{(1)}\beta_i$) and, most importantly for our purposes, ζ a DCM of neural activity which contains parameters θ_i^1 . These are the connectivity parameters between the nodes of the GLM estimated for each subject. Equation (6.1.2) states that these subject level parameters are themselves thought of as being generated by a GLM including a design matrix $X^{(2)}$ and population level parameters θ^2 (and noise $\epsilon^{(2)}$) which have a prior expected value (μ), as described in Equation (6.1.3). The design matrix in Equation (2) contains all of the relevant between subject factors which are thought to lead to inter-subject variability in the DCM parameter. In the case

of this experiment, this includes motor score and apathy however, also important confounds such as gender and age. Each subject's parameters are therefore considered to deflections from the group level parameter (θ^2), or *random effects* for that subject, based on the values of the design matrix for that subject. For example, the model may assume that x is the expected value of the connection between the striatum and the thalamus of my model. At the next level, an individual subjects striato-thalamic connection strength would be given by the effect of, for example motor score, age and gender, on this population value or $x_i = \beta_{TMS} * x + \beta_{age} * x + \beta_{gender} * x$. The model would then assume that the BOLD signal from that individual is produced as a result of that individual having x_i connection strength between the striatum and the thalamus. In this model, it is important to note that all between-subject variables specified in $X^{(2)}$ are assumed to have an effect on all connections in the DCM, the within subject factors:

Equation (6-2):

$$X^{(2)} = X_{between} \otimes X_{within}$$

Where \otimes being the Kronecker tensor product. This is the default approach of PEB as implemented in SPM.

Based on this system of equations, the joint probability of the data, subject level parameters and groups parameter, $P(Y, \theta^{(1)}, \theta^{(2)})$ can be considered in three tiers: (1) What is the probability of a subjects fMRI data given the estimated DCM parameters? (2) What is probability of the estimated DCM parameters given the design matrix and the group level parameters? (3) And finally, what is the probability of the group priors? Mathematically this can be expressed as (again, adapted from Zeidman *et al* (2019)):

Equation (6-3):

$$P(Y, \theta^{(1)}, \theta^{(2)}) = \sum_i \ln p(y_i | \theta^{(1)}) + \ln p(\theta^{(1)} | \theta^{(2)}) + \ln p(\theta^{(2)})$$

Where Y represents all the data across subjects, $\theta^{(1)}$ represents DCM parameter across all subjects and finally $\theta^{(2)}$ represents the population parameters.

This hierarchical PEB model can now be inverted to yielded using Variational Laplace method to maximise *free energy* as described above. At the DCM level, this approach was used to optimise the fit of parameters and calculate an approximation of, the lower bound, of the model evidence for each subject's DCM. In PEB, this approach is used to provide an approximation of the model evidence at a group level, while estimating the group level parameters $\theta^{(2)}$ – both in terms of expected value and uncertainty.

6.3.9 Hypothesis testing with Bayesian model reduction.

In order to test my hypotheses, I combined Parametric Empirical Bayes, the hierarchical model described above, with *Bayesian Model Reduction* (BMR) procedure (Zeidman et al., 2019a, 2019b). As described above, before completing Bayesian Model reduction, the model estimated using PEB is one in which all between-subject variables influence all connections to the A-matrix. This is a full or parent model. To test my hypotheses however, we must determine whether clinical variables such as apathy or motor score show a specific pattern of association with connections in the A-matrix. BMR achieves this by testing whether reduced models, in which clinical variables do not influence specific connections for example, perform better in terms of free energy. Although the initial PEB procedure and the estimation of the complete model is computationally demanding, it has been shown that the free energy of nested models within the parent model can be computed without re-estimation or inversion – rather analytically from the estimation of the parent model (Friston and Penny, 2011; Friston et al., 2016). This means that the estimation of the free energy of nested models occurs incredibly quickly. For the purposes of this study, this advantage of BMR allowed me to test my hypotheses in a data driven manner.

As the free energy of nested models can be calculated quickly, BMR can complete a greedy search of a very large model space by scoring and comparing the free energy of each reduced model rapidly.

BMR attempts to discard parameters from the second level GLM ($X^{(2)}$) if they do not contribute to the model free energy. If the free energy decreases, the parameter is not discarded. Using this approach, based only on the free energy of the nested models, BMR would attempt to remove, for example, the effect of total motor score on striato-thalamic connectivity or apathy on striato-STN connectivity unless it contributed to the model free energy.

Given the number of between and within subject variables in the second level GLM the number of nested models is potentially very large. In order to summarise the results from BMR an accepted procedure is known as Bayesian Model Averaging (BMA). In BMA, in the final greedy search iteration, the parameters from the best 256 reduced models from this search procedure are then averaged, weighted by their model evidence. As a result, the final parameter estimates are not heavily influenced by models with high levels of uncertainty. Estimates of parameter strength are outputted along with the posterior probability of the parameters being non-zero. In this chapter I only report connections which have a posterior probability of >0.99 indicating a very strong probability that the parameter is non-zero.

This procedure outputs group average DCM parameters and the group average second level GLM parameters. Parameters within the DCMs themselves represent the rate of change in activity in the afferent node, measured in Hz, caused by activity in the efferent node. As elegantly described by Kahan *et al* (2014), they can be thought of as the “sensitivity” of the target node to the source (Kahan *et al.*, 2014a). In turn, the second level parameters describe the influence of between-subject parameters on DCM parameters.

In the motor score analysis, the PEB models controlled for age, gender and scanner type (as opposed to site) alongside testing for the effect of total motor score on DCM parameters. The effect of total motor score and depressive scores were then additionally controlled for in analyses of apathy, alongside the demographic factors described above. Group comparison was not the focus of this study however data from control participants was used to replicate the baseline connectivity profile (as shown in Supplementary Material at the end of this Chapter). Regressors were mean centred allowing the interpretation of the first covariate of the model to be the average connectivity weights in the network.

Having estimated the effect of clinical co-variates on connection strengths at a group level, it remains unclear how clinically relevant these findings are. One approach available in SPM is to complete a leave-one-out cross validation procedure. In this approach, one subject's data is excluded and the PEB model is estimated. The co-variates of the left-out subject, such as motor score, are then predicted based on the estimated PEB model and that subject's DCM parameters. This procedure is iterated across all subjects and in the end, the estimated parameters, and compared to the actual parameters by means of a correlation coefficient. Such a procedure describes the predictive validity of the connectivity strength from a new patient (Zeidman et al., 2019b).

6.4 Results:

6.4.1 Sample demographics:

	Gene carriers (n = 94)
Age (mean +/- std)	45.5 (+/- 8.9)
% female	50%
Mean CAG repeat length	43.1 (+/- 2.3)
TMS	10.5 (+/- 8.5)
Apathy score	10.9 (+/- 6.0)
Depressive scores	6.6 (+/-6.8)
Number by scanner type (Siemens/Philips)	52/42

Table 6-1: Sample demographics consisted of 94 HD gene carriers who underwent resting state fMRI as part of the TRACK-ON study. Apathy measured using the Baltimore Apathy Scale (BAS). Depressive symptoms measured using the Beck Depression Inventory (BDI). Spread of TMS and apathy scores in supplementary figures

Our sample consisted of HD gene carriers and controls recruited into the TRACK-ON study who had both clinical and neuroimaging data available at visit 3. This cohort is peri-manifest with 34 of 94 patients having been diagnosed with early HD and the remainder in the premanifest phase. In the early-stage HD cohort, the mean Total Motor Score (TMS) was 17.9 (+/- 9.2). Spread of apathy and TMS scores are in this cohort of peri-manifest gene carriers is shown in Fig. 6-6.

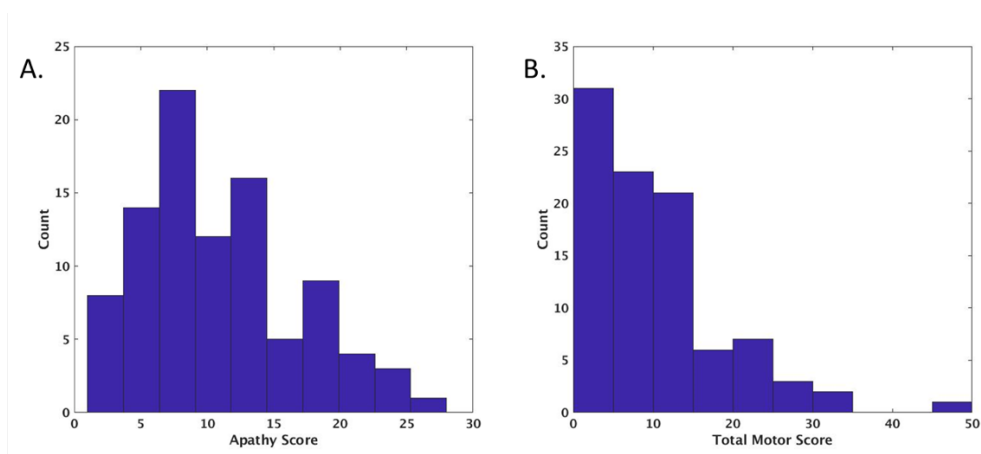


Figure 6-6: A. Spread of apathy scores in the peri-manifest HD cohort as measured by the Baltimore Apathy Scale. Scores on this scale range from 0-42 with higher scores representing higher self-reported apathy. B. Spread of the Total Motor Score in the peri-manifest cohort as measured by the UHDRS total motor score. Scores on this scale range from 0-124. Relatively low scores in this cohort indicate early and premanifest disease.

6.4.2 Average connectivity parameters show a network suppressing motor cortex activity

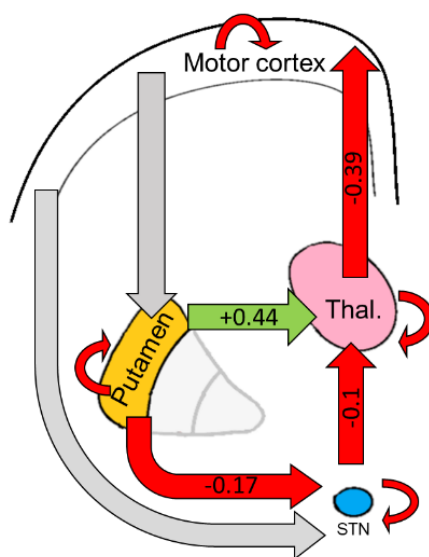


Figure 6-7: Schematic showing the average parameter values in the modelled network, across all 94 HD subjects, for between node connections. Red arrows indicate suppression of activity, green arrows indicate excitation and grey arrows indicate non-significant connections. Coloured arrows represent connections with a posterior probability of >0.99 for being greater than 0. Overall, the network activity shows a suppression of M1 activity which may be expected given that subjects are explicitly trying to remain still. Negative self-connections are shown as curved arrows looping back to the node – their values are described in Supplementary Table 1 as the end of the chapter.

During data collection, participants are explicitly asked to stay still across the scanning session. In keeping with this, average connectivity parameters show active suppression of the driving input from the motor cortex (see Fig. 6-7). Striato-thalamic connection was found to be excitatory (0.43, 95% confidence interval (CI) 0.37- 0.50 Hz, posterior probability (pp) > 0.99) whereas subthalamic-thalamic (-0.1 Hz, 95% CI: -0.15 to -0.04 Hz, pp > 0.99) and striato-subthalamic were found to be inhibitory (-0.17 Hz, 95% CI: -0.24 to -0.11 pp > 0.99). The net output from this system via the thalamo-cortical connection was to suppress motor activity (-0.39 Hz, 95% CI:-0.47 to -0.31 Hz, pp > 0.99). These data are shown in a schematic in Fig. 6-7, with green arrows representing excitation, red arrows representing inhibition and grey arrows representing non-significant connectivity. This connectivity profile was also demonstrated in a cohort of control participants (n = 85) from the same study as shown in Fig. 6-9 (supplementary section). All connectivity parameters for both groups are shown in Supplementary Table 6-2.

6.4.3 Altered connectivity in components of the indirect pathway associated with total motor score

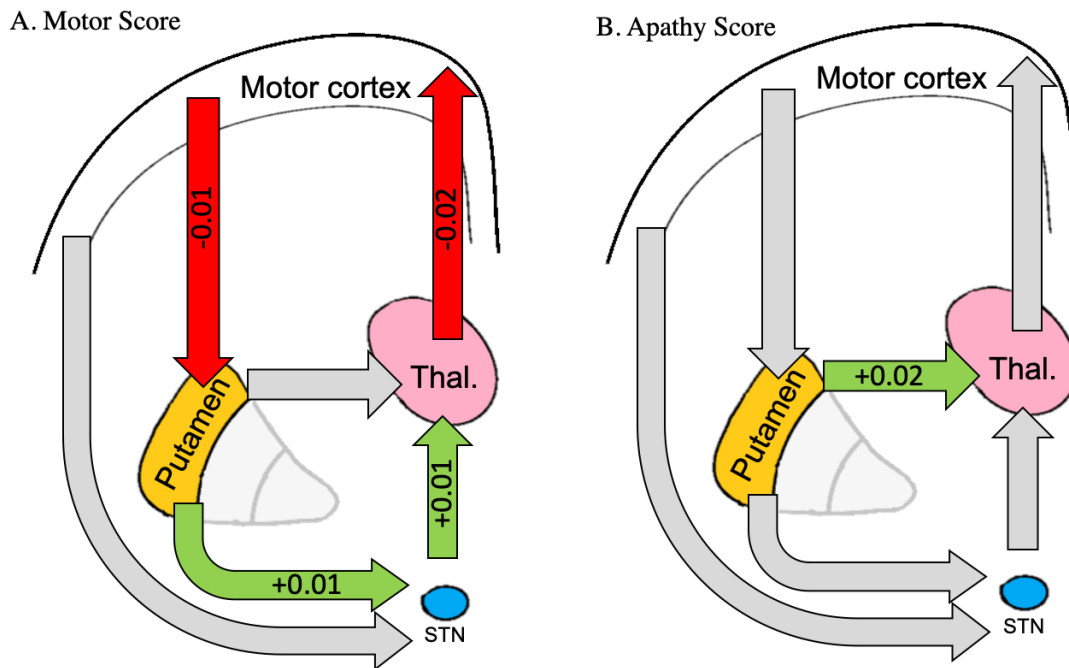


Figure 6-8: Association between inter-node connectivity parameters and (A) Total Motor Score and (B) Baltimore Apathy Score. Green and red arrows indicate which connections were found to be associated with clinical variable with >99% posterior probability using Parametric Empirical Bayes (PEB) and BMR. Grey arrows show connections from connectivity matrix not found to be associated with clinical scores. Green arrows represent evidence of a positive relationship between connection strength and clinical scores, whereas red arrows represent a negative relationship between clinical score and connection strength. 95% confidence intervals are given in the text below.

Across the group, total motor score (TMS) was positively associated with changes in coupling in the two components of the indirect pathway - striato-STN (0.013, 95% CI: 0.005 to 0.021, $pp > 0.99$) and STN-thalamic (0.011, 95% CI: 0.005 to 0.018, $pp > 0.99$). This is shown schematically in Fig. 6-8A. TMS was also negatively associated with cortico-striatal connectivity (-0.009, 95% CI: -0.014 to -0.004, $pp > 0.99$) and thalamo-cortical connectivity (-0.019, 95% CI: -0.030 to -0.009, $pp > 0.99$). TMS was positively associated with STN self-connection (0.01, 95% CI: 0.006 to 0.016, $pp > 0.99$). These are normalised beta values with no units. No association between TMS and change in the striato-thalamic connectivity was seen. The weights from two components of the indirect pathway (striato-STN and STN-thalamus) predicted TMS ($r = 0.17$, $p = 0.047$) in a leave one-out-cross validation analysis.

6.4.4 Altered connectivity in components of the direct pathway connectivity associated with apathy in gene carrier cohort

By comparison, controlling for the effect of TMS and depression, total apathy score was positively associated with changes in striato-thalamic connection (0.022, 95% CI 0.014 to 0.03, $p > 0.99$). This is shown schematically in Fig. 6-8B. Apathy was also negatively associated with STN self-inhibition (-0.013, 95% CI: -0.018 to -0.007, $p > 0.99$). Although these results indicate that strong evidence for this effect exists at a group level, weights of the striato-thalamic connection were not strong enough to predict individual apathy scores in a leave-one-out cross validation analysis ($p = 0.30$).

Please note that raw parameter estimates and their associations with motor and apathy scores are shown in the Supplementary material below for interest. Of note, although an F-contrast was used to seed the ROIs, there is no evidence of bimodal distribution of parameter estimates.

6.5 Discussion:

In this study, I show *in vivo*, that motor signs and apathy in Huntington's disease (HD) are associated with unique profiles of altered effective connectivity within basal ganglia pathways. I found strong evidence at a group level that higher motor scores in a large cohort of peri-manifest HD patients were associated with altered coupling in the indirect pathway components of our model. I found no associations with altered coupling in the direct, striato-thalamic, pathway component of our model suggesting, that imbalanced pathway changes are critical to the emergence of motor signs.

Beyond motor signs however, apathy in HD is prevalent in both prodromal and manifest groups. Although common, the pathophysiology of apathy in HD is unknown and as a result treatments are lacking (Banaszkiewicz et al., 2012; van Duijn et al., 2014). Given the prevalence of apathy in HD, the propensity of HD to damage cells that constitute the basal ganglia pathways and the proposed role these cells play in the expression of goal-directed behaviour, I hypothesised that like motor signs, apathy in HD would also be associated with altered connectivity in the basal ganglia. Unlike motor signs however, I hypothesised specifically that apathy in HD may be the result of the disruption to the direct pathway of my model. Activity in the direct pathway drives free-operant action initiation – a feature commonly lacking in apathy as described in Chapter 3 (Freeze et al., 2013; Le Heron et al., 2018c; Kravitz et al., 2010). As described at length in the Introduction, computational models of basal ganglia function argue that, via dopaminergic learning signals, the direct pathway cells effectively accrue the value of taking an action (Collins and Frank, 2014; Frank, 2011; Franklin and Frank, 2015). Impaired connectivity within this pathway may therefore disrupt both the striatal machinery necessary to take goal-directed actions and the neural representations of reasons to take those actions. In keeping with this hypothesis, and unlike motor signs, I identified that apathy scores in prodromal HD may be associated with changes only in striato-thalamic connectivity within our model.

The connectivity profile I detected associated with motor signs suggested less inhibition in the striato-STN and STN-thalamic components of our model whereas apathy was associated with increased

coupling between putamen and thalamus. Although my hypothesis is based on rate-coding models of striatal function like OPAL, given the limitation of interpreting BOLD signals I do not interpret our results as demonstrating of more or less activity in the cell populations I hypothesised. Instead, I simply report evidence that motor signs and apathy were associated with unique basal ganglia connectivity profiles. These findings may represent a range of pathological processes such as altered rating coding, synaptic dysfunction or altered basal ganglia synchrony.

To test my hypotheses, I used data from a large cohort of HD gene carriers who were expressly recruited around the time of motor onset. Many motor signs in HD are not actively elicited and occur at rest – as such, resting state data has considerable ecological validity in trying to understand these features of the disease. In order to analyse this data, used *spectral* DCM which has been shown to have several benefits when analysing resting state data (Friston et al., 2014b; Razi et al., 2015). Using this technique, I found a network whose net output was to reduce activity in the motor cortex. There is little existing data, to my knowledge, with which to compare these results but this profile was similarly found in a control cohort in a separate analysis. Secondly, I tested the relationship between clinical variables and connections within the network using an advanced Bayesian, approach (Friston et al., 2016b; Zeidman et al., 2019a, 2019b). Group level analysis was completed using a hierarchical Bayesian procedure known as Parametric Empirical Bayes followed by an automated Bayesian Model Reduction.

Using Bayesian model reduction procedure, many competing models were compared and only those with the strongest evidence survived. As described in the Methods section of this chapter, this procedure uses an automated greedy search retaining only parameters in the second level GLM which contribute to model free-energy (Friston et al., 2016b; Zeidman et al., 2019b). In this manner, aside from specifying the A-matrix and the variables of interest, I did not specify my hypotheses. As such, my *a priori* hypotheses were confirmed *de novo* from the data itself. It was through this automated procedure that the direct pathway components were found to be related to apathy and the indirect pathway components were found to be related to total motor score.

In both analyses, I found very strong evidence to support our main hypotheses at a group level. In subsequent analyses I asked whether individual clinical scores could be predicted by the weights of the

connections identified at the group level in an out of sample leave-one-out cross validation procedure. For motor signs, I found that the weights of the striato-STN and the STN-thalamus could significantly predict motor scores. This was not the case for apathy scores, as direct pathway weights could not predict apathy scores in the leave one out procedure.

These modest effect sizes seen in both analyses are perhaps unsurprising. Firstly, in both cases I am sampling from a small region of each structure and it is unlikely that all clinical change can be attributed to such a restricted region of interest. Secondly, many neural changes are associated with HD and the pathogenesis of both motor signs and psychiatric symptoms are likely to be biologically heterogeneous (Vonsattel et al., 2011; Waldvogel et al., 2015). In the case of apathy in particular, multiple neurological mechanisms may contribute to the development of apathy in HD such as white matter changes, involvement of cortical structures or indeed the involvement of other striatal compartments, such as striosomes, which we are unable to currently resolve with *in vivo* imaging (Gregory et al., 2015b; Martínez-Horta et al., 2018b; McColgan et al., 2017a; Tippett et al., 2007; Waldvogel et al., 2012). I therefore do not claim, based on the data presented here that changes in connectivity that I present are sufficient to generate clinical features. Rather, I argue that changes in basal ganglia connectivity may contribute to their development in patients with very early HD.

Before concluding I would like to highlight a few important caveats to the work presented here. The model used in this study, as the A-matrix, was a simplified model of the relevant basal ganglia circuits (Calabresi et al., 2014a; Haber, 2016). Modelling the true extent of the anatomical complexity within basal ganglia circuits is currently intractable with *in vivo* imaging and therefore any attempt to do so requires simplification (Nelson and Kreitzer, 2014). At the core of our model, also used by Kahan *et al* (2014), is a connection through which striatal activity can drive thalamic activity directly or via a secondary, indirect, route in order to change thalamic connectivity (Kahan et al., 2014b). I found that these pathways excited and inhibited thalamic activity respectively. On this basis I described them as the *direct* and *indirect* pathways in our model. It is important to highlight that I cannot confirm they represent activity in the MSNs as I hypothesise. Although a simplification, I believe this model

sufficiently captures the principal dynamics of the network as relevant to the hypotheses I am testing, whilst also limiting model complexity.

Finally, due to the size of the regions I was interested in, especially the subthalamic nucleus, partial volume effects are difficult to avoid. However, it should be noted that the data extracted from these regions largely conformed to the pattern of activity expected for this system at rest namely, reduction of motor cortical activity, striato-thalamic excitation and thalamic inhibition via the indirect pathway. In comparison, previous work treated the STN as a hidden node, meaning that activity from the region is simulated by the model based on *a priori* expected connectivity (Dirkx et al., 2017; Kahan et al., 2014a). Whilst avoiding partial volume effects, this approach has the key limitation that the model itself must infer the timeseries from a key node in the network as opposed to modelling data taken from the region itself, the approach taken in this study.

In terms of experimental design, I adopted a cross-sectional design. A longitudinal study would give a clearer understanding of the changes that drive the emergence of these features however this approach has a number of challenges. Given the slow rate at which clinical features evolve in HD, it is unlikely that longitudinal analysis over a few years would have sufficient power to detect changes in our areas of interest. Instead, I compared across participants with a wide variance in relevant clinical features. I hypothesise that similar results would be obtained longitudinally if sampled over a sufficiently long time period. Of course, this longitudinal approach is also challenging as the emergence of more florid movement signs limits the quality of the scans and increases the probability of the use of medications which reduce movements. By comparison, this cohort was in the very earliest stages of manifest disease with low motor scores (peri-manifest disease stage). This meant that very few participants needed to be excluded due to anti-dopaminergic medication use and secondly, participants were able to tolerate fMRI imaging. The principal limitation of this dataset is that signs and symptoms were mild. As a result, it was not possible to adopt a more fine-grained analysis of specific motor subscales as this would be underpowered.

6.6 Conclusions:

In summary therefore, I demonstrate using resting state fMRI neuroimaging data that changes in the connectivity of the basal ganglia motor loop is associated with motor sign severity and apathy in HD. Using a simplified model of canonical basal pathways, I show that motor score severity was associated with altered connectivity in the indirect pathway components of our model whereas apathy in prodromal HD was associated with changes in direct pathway connectivity.

6.7 Supplementary analysis:

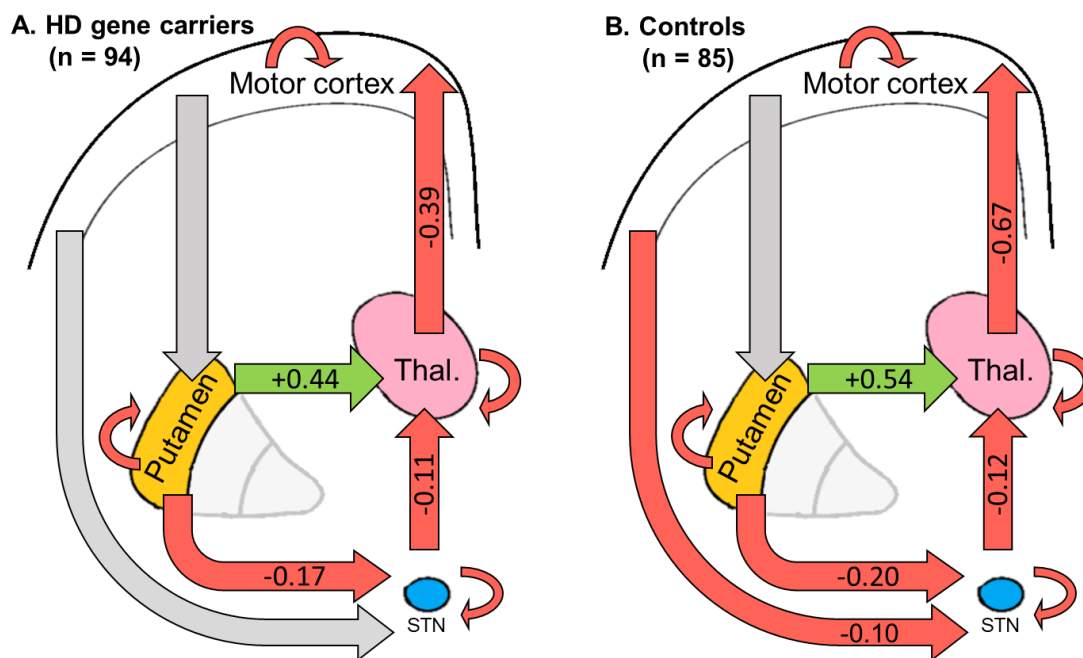


Figure 6-9: Average coupling estimates show an active inhibition of M1 in HD gene carriers and controls (model included TMS, age, gender and scanner type as covariates). This connectivity profile was replicated in a cohort of control participants (model included age, gender and scanner type). Parameter estimates with 95% CI and posterior probabilities are show in Supplementary Table 1 for both groups.

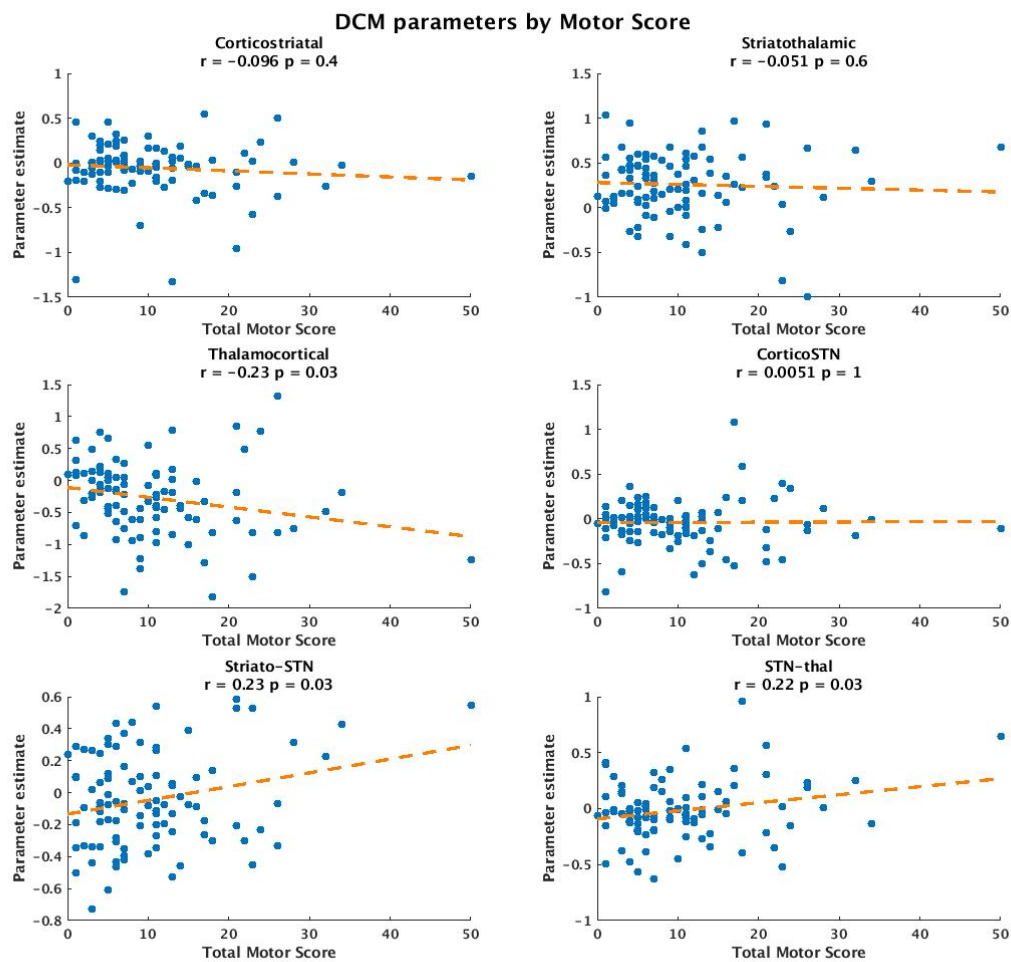


Figure 6-10: Association between inter-node connectivity parameters and Total Motor Score – individual parameter estimates shown for each HD participant. r represents correlation coefficient. Significant correlations occurred in mostly the same pathways identified using hierarchical modelling.

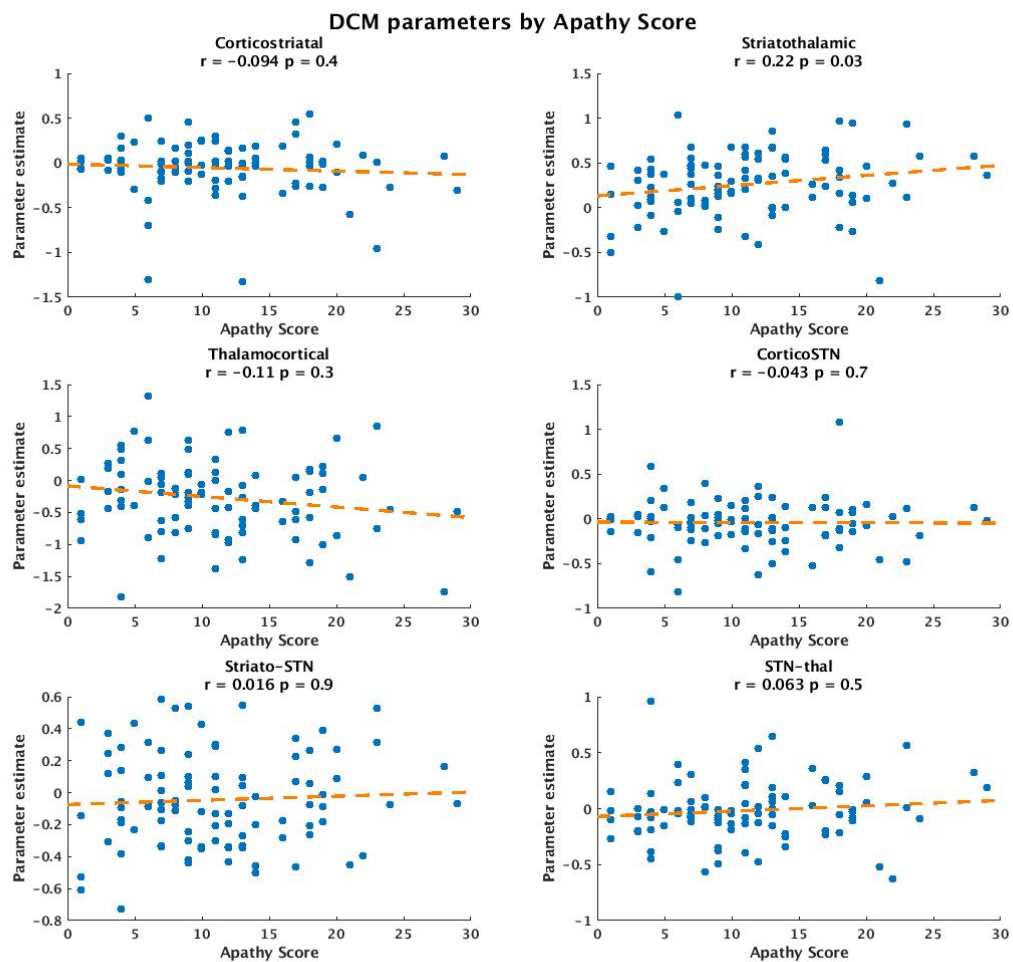


Figure 6-11: Association between inter-node connectivity parameters and apathy scores showing individual parameter estimates for each HD participant. r represents correlation coefficient. Significant correlations occurred in the same pathways identified using hierarchical modelling.

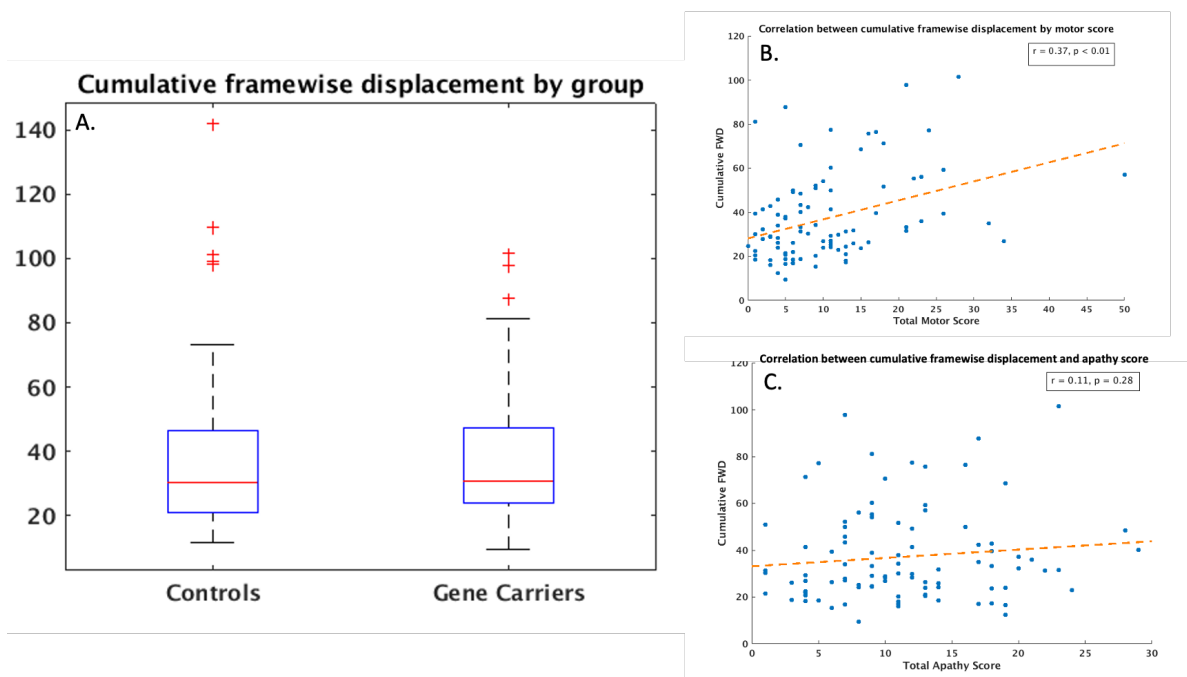


Figure 6-12: Cumulative framewise displacement (sum of framewise displacement (FWD in mm)) during scans was not significantly different between controls and HD gene carriers ($p > 0.05$). Within gene carrier cohort, FWD showed mild correlation with motor scores ($r = 0.37$, $p < 0.01$) however no correlation with apathy scores ($p > 0.05$).

Connection	Gene carriers (n = 94)				Controls			
	Mean value (Hz)	Lower 95% CI	Upper 95% CI	Post. prob	Mean value (Hz)	Lower 95% CI	Upper 95% CI	Post. prob
M1 to motor putamen	0.00	0.00	0.00	0.00	-0.04	-0.10	0.01	0.73
M1 to STN mask	-0.05	-0.12	0.01	0.79	-0.10	-0.15	-0.05	1.00
Putamen to STN mask	-0.17	-0.24	-0.11	1.00	-0.20	-0.26	-0.14	1.00
Putamen to motor thalamus	0.44	0.37	0.50	1.00	0.54	0.47	0.62	1.00
STN to motor thalamus	-0.10	-0.15	-0.05	1.00	-0.12	-0.17	-0.07	1.00
Thalamus to M1	-0.39	-0.47	-0.30	1.00	-0.67	-0.77	-0.58	1.00
Self-connections								
M1 self-connection	0.48	0.40	0.56	1.00	0.64	0.59	0.70	1.00
Putamen self-connection	1.16	1.11	1.22	1.00	1.08	1.02	1.15	1.00
STN self-connection	1.17	1.13	1.22	1.00	1.12	1.08	1.16	1.00
Thalamus self-connection	1.17	1.11	1.23	1.00	1.28	1.23	1.33	1.00

Table 6-2: Comparison of baseline connectivity parameters in the motor network in gene carriers and controls. Both groups show the same overall pattern of effective connectivity (as shown in Supplementary Fig 5) which is suggestive that the motor cortex activity is being suppressed at rest. Positive values of self-connections reflect the degree of self-inhibition. Gene carrier values derive from a model including motor score, age, gender and scanner type. Control values derive from a model including age, gender and scanner type.

Chapter 7: Conclusions:

In this thesis I have adopted a computational framework to study motivated behaviour and apathy. Apathy remains one of the most disabling and poorly treated symptoms in neuropsychiatry. By adopting this approach, I sought to understand apathy across three theoretical levels – namely, the computational, algorithmic and at the level of neural implementation. Much of the work in this thesis centres around Huntington’s disease (HD) in which apathy is common and debilitating. I used the known pathophysiology of HD to constrain my hypotheses at the level of neural implementation – focussing largely in this thesis on the effect of HD on striatal anatomy and pathways. At the “top”, computational level, I proposed that the goal of motivated behaviour was the maximisation of net rewards, per unit time, gained through self-initiated behaviour. In the middle, bridging these two levels I used reinforcement learning (RL) as the algorithmic framework to link the computational to the neural levels. RL is suited well to sit between these layers as the overarching goal of RL is not dissimilar to my hypothesised computational goal of motivated behaviour and, secondly, numerous neural signals, such as phasic dopamine signalling, have been shown to correlate well with latent variables in RL models, such as the reward prediction framework. With this as my theoretical starting point, I tested a range of related hypotheses.

In Chapter 3, I considered the implications of the opportunity cost model of free-operant action initiation latency for motivated behaviour and apathy. Opportunity cost represents the amount of net reward which may be lost, per unit time, if action is not taken. As such opportunity cost could be used to optimise free-operant action initiation. In Chapter 3, I designed and built a novel behavioural task in which opportunity cost is manipulated while participants are given free choice as to when they may emit responses. Using this design, replicated in two studies in different settings, I show that the choice of free-operant action initiation is highly influenced by changes in opportunity cost – both for rewarding and non-rewarding actions. Furthermore, given the relevance of free-operant action initiation to apathy, I predicted that sensitivity to changes in opportunity cost within my task would predict apathy scores. This prediction is derived from the algorithmic opportunity cost model. In the model, changes in

motivational states influence timing of actions by driving up the opportunity cost across the environment. I hypothesised that motivated individuals, as compared to apathetic individuals, would behave in a similar manner – acting as if opportunity cost was high throughout the task, irrespective of local task fluctuations. I replicate this effect in both experiments; however, this finding must be caveated with the note that in the online replication sample this effect was only seen in the younger half of the cohort. I also show in this chapter, in a third experiment, that this task can be adapted for use in patients with manifest HD and a similar association between apathy and opportunity cost may apply in HD. I have updated this task to a smartphone format for large scale data collection and to probe the relationship between opportunity cost and mood.

In Chapter 4, I switch focus to learning to optimise behaviour from gains and losses and how this process may be disrupted in participants who are decades from the onset of HD. Leveraging predictions made by existing literature and RL models of the basal ganglia function, I completed an fMRI experiment in which 35 HD gene carriers, approximately 25 years from onset, and 35 well-matched control participants completed a gains and losses RL task in an MRI scanner. Based on the RL models of basal ganglia function, which suggest that early dysfunction of the indirect pathway may impair loss learning, I predicted that HD gene carriers in this experiment would show a “reward bias” – either better performance in gain learning versus loss learning or an exaggerated neural response to gains versus losses. I did not find a behavioural difference, although this is perhaps expected given how many decades these participants were from disease onset. I did however find evidence of a neural reward bias in the ventral striatum, possibly driven by impaired loss learning. Not only does this finding match the predictions from the RL basal ganglia models but it also fits well with empirical findings from HD gene carriers nine years from onset, in the same task, who show impaired loss learning behaviourally. These findings represent the earliest functional neuroimaging difference between HD gene carriers and controls.

In Chapter 5, I present the first of two chapters probing the pathophysiology of apathy in HD. In this chapter I use the large multi-national study, ENROLL-HD, to investigate how apathy in HD is related to motor signs in HD. Based on pathophysiological models of HD, chorea is believed to represent that

involvement of the indirect basal ganglia pathway whereas bradykinesia in HD may represent the involvement of the direct pathway in HD. I predicted, based on empirical data and theoretical models, that the involvement of the direct pathway in HD may be associated with the development of apathy in HD. I therefore predicted that apathy would be associated with higher levels of bradykinesia but not chorea. This was indeed the relationship that I uncovered in this sample. Beyond this, I demonstrated that medications, depression and cognitive impairment may also contribute to apathy in HD. These findings reinforce the idea that apathy is likely the end product of multiple pathophysiological processes, especially in complex diseases like HD, however striatal pathway changes may drive a component of the apathy seen in HD.

Based on the findings in Chapter 5, in my final data chapter, I used resting state fMRI and dynamic causal modelling to model connectivity in the basal ganglia in a cohort of patients with peri-manifest HD. Using this approach, my model contained approximations to the connectivity of the indirect and direct pathway. I was able to test two hypotheses – firstly that the emergence of motor signs in HD was indeed related to changes in the connectivity of the indirect pathway and then secondly, my novel hypothesis that apathy in HD would be related to changes in the connectivity of the direct pathway. It should be stated however, that I did not directly test these hypotheses. By using Parametric Empirical Bayes and an automated Bayesian model reduction procedure, I was able to see whether evidence for these hypotheses emerged from the data itself. Using this approach, I found evidence to support both of these hypotheses. The relationship between motor signs and changes in indirect pathway connectivity was stronger than that of the apathy and direct pathway relationship as indirect pathway connectivity strength was able to predict motor score in a cross-validation procedure; however, this was not the case for apathy. Given that I have already shown that apathy in HD is a multi-factorial problem in Chapter 5, this is perhaps not surprising. This limitation notwithstanding, I believe that the data in this chapter represent the first neuroimaging evidence of that association between changes in basal ganglia connectivity and both motor signs and apathy.

Each chapter contains its own discussion of the results and I will not therefore dwell on the strengths and limitations of the methods or experiments here.

I will firstly discuss how this work could be extended going forward. In Chapter 3, I outline pilot results from a trial of the fisherman game in HD patients. Aside from increasing the sample size, it is my intent to complete a more robust computational description of apathy in HD but including a range of tasks alongside the fisherman. These would include learning from gains and losses and an effort discounting paradigm. This approach would offer not just sensitivity to opportunity cost, but measures of value learning, decision making noise, reward sensitivity and effort sensitivity. My hypothesis that direct pathway involvement contributes to apathy early in the disease course and models of pathway function like OPAL allow us to make specific predictions in all of these tests. Firstly, I would predict that apathy in HD is accompanied by impaired gain learning, as opposed to loss learning which I would predict in all patients with HD. Secondly, I do not predict that effort sensitivity would correlate with apathy but rather impaired reward sensitivity. Finally, as described in Chapter 3 – I would predict that apathetic HD patients would show increased sensitivity to externally cued opportunity cost.

In a broader theoretical work, I would like to extend my work in opportunity cost by exploring its relationship with mood. Recent work has shown that momentary subjective mood may be a function of recent reward prediction errors. As alluded to in the introduction and Chapter 3, within the average reward RL literature temporal difference learning can be used to update average reward value estimates. As opportunity cost derives from the average reward signal, I believe it is worth exploring whether the psychomotor features of depression – typically slowing and effortful action, may be related to prediction errors related to average reward updating.

Returning to my neural hypothesis that the ratio of the direct and indirect pathway cell population are related to motivational status – an alternative approach would be to consider the problem across species. If the fisherman task, and other tasks in the computational battery, could be adapted for use in other animals, performance of the tasks can be compared across humans and various animal models – such as those with HD, those with pathway specific ablations and perhaps most powerfully those with optogenetic stimulation. While again not direct evidence, if similar robust and reproducible behavioural

signals occur across clinical samples and in animal with known pathway dysfunction – this approach may offer power evidence in support of this idea.

I will conclude this thesis by considering the strengths and limitations of the computational approach as a whole. Firstly, the greatest strength is the powerful theoretical bridge this approach offers to developing hypotheses about psychiatric symptoms across various levels of explanation. I believe that beyond the mathematical exterior the computational approach to neuropsychiatry actually requires us to ask almost philosophical questions of psychiatric phenomena, for example, not only what motivation is but *why* it needs to exist. From this starting position, mathematical algorithms can be used, not only to intimidate early career researchers, but to explicitly lay out mechanistic hypotheses for both behaviour and brain simultaneously. Finally, another strength certainly in neuropsychiatry, is that neural hypotheses constrained by disease pathophysiology can be used to constrain the theoretical layers above.

It is perhaps clichéd to cite George Box when considering the limitation of computational psychiatry but there is no escaping the saying that “all models are wrong, but some are useful”. While above I have detailed how this approach is useful, it is also worth highlighting where computational psychiatry may go wrong. At the heart of the problem, I believe, is the issue of Occam’s razor and model comparison. Although the approach above can be used to make theoretical jumps from neurons to psychology, it must be noted that our resolution diminishes significantly when moving from the neural to the psychological or behavioural. Behaviour is a gross aggregated output driven by a range of complex neural processes. If we use behaviour, or psychological measures, to guide our choice of algorithmic models then Occam’s razor will punish the complex models if they offer no extra explanatory power. As discussed in this thesis, this philosophical principle is elegantly embedded in most statistical measures used for model comparison. This then leads to a challenging problem for computational psychiatry: algorithmic models which may be most biophysically realistic are very unlikely to emerge as the “best” models because of the sheer number of parameters which must be fit while using behavioural data to fit them. Perhaps one solution to this problem is to fit algorithms simultaneously to behaviour and contemporaneous neural data; however, this is work which must be left for the future.

Therefore, while RL provides a bridging algorithmic framework in this thesis, it is not necessarily implemented by the brain. RL algorithms may capture behaviour and neural signals at a certain degree of resolution; however, moving to an algorithmic understanding of true neural complexity remains a significant challenge. This problem perhaps becomes most acute when attempting to use a computational framework to make novel pharmacological hypotheses.

A computational approach to motivated behaviour is, therefore, not without its limitations. However, I hope that the work presented in this thesis demonstrates how such an approach may be used to develop novel hypotheses for hard-to-treat symptoms like apathy.

I conclude with thanks – to my family, the colleagues and friends I met over the last four years, my supervisors, my funders and not least, the participants in my various studies.

Publications:

Published/Accepted:

Nair, A., Johnson, E.B., Gregory, S., Osbourne-Crowley, K., Zeun, P., Scahill, R.I., Lowe, J., Papoutsis, M., Palminteri, S., Rutledge, R.B., Rees, G., Tabrizi, S.J. Aberrant striatal value representation in Huntington's disease gene carriers 25 years before onset. *Biological Psychiatry CNI* (2021); *in press*

Nair A, Rutledge RB, Mason L. Under the Hood: Using Computational Psychiatry to Make Psychological Therapies More Mechanism-Focused. *Front Psychiatry*. 2020 Mar 18;11:140.

Scahill, R. I.*, Zeun P.*, Osborne-Crowley K., Johnson E.B., Gregory S., Parker C., Lowe J., **Nair A. et al.** Biological and clinical characteristics of gene carriers far from predicted onset in the Huntington's disease Young Adult Study (HD-YAS): a cross-sectional analysis. *Lancet Neurol* 2020; 19(6): 502-512.

Osborne-Crowley K, Andrews SC, Labuschagne I, **Nair A**, Scahill R, Craufurd D, Tabrizi SJ, Stout JC; TRACK-HD Investigators. Apathy Associated with Impaired Recognition of Happy Facial Expressions in Huntington's Disease. *J Int Neuropsychol Soc*. 2019 May;25(5):453-461

Under peer-review:

Nair, A., Niyogi, R. K., Shang, F., Tabrizi, S. J., Rees, G., & Rutledge, R. (2020). Opportunity cost determines action initiation latency and predicts apathy. Preprint available on PsyArXiv: [10.31234/osf.io/d9pgz](https://doi.org/10.31234/osf.io/d9pgz)

Nair A, Razi A., Gregory S., Rutledge R., Tabrizi S.J.*, Rees, G.* (2021) Imbalanced basal ganglia connectivity is associated with motor deficits and apathy in Huntington's disease: First evidence from human in vivo neuroimaging.

Zeun, P., McColgan, P., Dhollander, T., Gregory, S., Johnson, E.B., Papoutsis, M., Nair, A., Scahill, R.I., Rees, G., Tabrizi, S.J. and the TrackOn-HD and HD-YAS Investigators. Timing and specificity of basal ganglia white matter loss in premanifest Huntington's disease.

Gregory, S., Wijeratne, P., Osborne-Crowley, K., Johnson, E.B., Zeun, P., Scahill, R.I., Lowe, J., Nair, A., O'callaghan, C., Langle, C., Papoutsis, M., Estevez-Fraga, C.E., Fayer, K., Alexander, D., Robbins, T.W., Sahakian, B.J., Tabrizi, S.J., Rees, G. Neural connectivity as a substrate for behavioural compensation in premanifest Huntington's disease. Under peer review.

Johnson, E.B., Parker, C., Scahill, R.I., Gregory, S., Papoutsis, M., Zeun, P., Osborne-Crowley, K., Lowe, J., Nair, A., Estevez-Fraga, C., Fayer, K., Rees, G., Zhang, G., Tabrizi, S.J. and the HD-YAS Investigators. Iron and myelin as markers of early microstructural brain changes in premanifest Huntington's disease

References:

- Albin, R.L., Young, A.B., and Penney, J.B. (1989). The functional anatomy of basal ganglia disorders. *Trends Neurosci.* *12*, 366–375.
- Albin, R.L., Reiner, A., Anderson, K.D., Penney, J.B., and Young, A.B. (1990). Striatal and nigral neuron subpopulations in rigid Huntington's disease: Implications for the functional anatomy of chorea and rigidity-akinesia. *Ann. Neurol.* *27*, 357–365.
- Albin, R.L., Reiner, A., Anderson, K.D., Dure, L.S., Handelin, B., Balfour, R., Whetsell, W.O., Penney, J.B., and Young, A.B. (1992). Preferential loss of striato-external pallidal projection neurons in presymptomatic Huntington's disease. *Ann. Neurol.* *31*, 425–430.
- Alexander, G.E., DeLong, M.R., and Strick, P.L. (1986). Parallel Organization of Functionally Segregated Circuits Linking Basal Ganglia and Cortex. *Annu. Rev. Neurosci.* *9*, 357–381.
- Andreasen, N.C. (1982). Negative Symptoms in Schizophrenia: Definition and Reliability. *Arch. Gen. Psychiatry* *39*, 784–788.
- Andrews, S.C., Langbehn, D.R., Craufurd, D., Durr, A., Leavitt, B.R., Roos, R.A., Tabrizi, S.J., and Stout, J.C. (2020). Apathy predicts rate of cognitive decline over 24 months in premanifest Huntington's disease. *Psychol. Med.*
- Ang, Y.-S., Lockwood, P., Apps, M.A.J., Muhammed, K., and Husain, M. (2017). Distinct Subtypes of Apathy Revealed by the Apathy Motivation Index. *PLoS One* *12*, e0169938.
- Arias-Carrián, O., Stamelou, M., Murillo-Rodríguez, E., Menéndez-Gonzalez, M., and Pöppel, E. (2010). Dopaminergic reward system: A short integrative review. *Int. Arch. Med.* *3*, 24.
- Atkinson, J.W. (John W. (1964). *An introduction to motivation*, (New York [etc.]: Van Nostrand).
- Attwell, D., and Iadecola, C. (2002). The neural basis of functional brain imaging signals. *Trends Neurosci.* *25*, 621–625.
- Averbeck, B.B., Lehman, J., Jacobson, M., and Haber, S.N. (2014). Estimates of projection overlap and zones of convergence within frontal-striatal circuits. *J. Neurosci.* *34*, 9497–9505.
- Ayers, E., Shapiro, M., Holtzer, R., Barzilai, N., Milman, S., and Verghese, J. (2017). Symptoms of apathy independently predict incident frailty and disability in community-dwelling older adults. *J. Clin. Psychiatry* *78*, e529–e536.
- Baake, V., Coppen, E.M., van Duijn, E., Dumas, E.M., van den Bogaard, S.J.A., Scahill, R.I., Johnson, H., Leavitt, B., Durr, A., Tabrizi, S.J., et al. (2018a). Apathy and atrophy of subcortical brain structures in Huntington's disease: A two-year follow-up study. *NeuroImage Clin.* *19*, 66–70.
- Baake, V., van Duijn, E., and Roos, R.A.C. (2018b). Huntington's Disease Gene Expansion Carriers Are Aware of Their Degree of Apathy. *J. Neuropsychiatry Clin. Neurosci.* *30*, 183–187.
- Banaszkiewicz, K., Sitek, E.J., Rudzińska, M., Sołtan, W., Sławek, J., and Szczudlik, A. (2012). Huntington's disease from the patient, caregiver and physician's perspectives: three sides of the same coin? *J. Neural Transm.* *119*, 1361–1365.
- Bates, G.P., Dorsey, R., Gusella, J.F., Hayden, M.R., Kay, C., Leavitt, B.R., Nance, M., Ross, C. a., Scahill, R.I., Wetzell, R., et al. (2015). Huntington disease. *Nat. Rev. Dis. Prim.* *1*, 1–21.
- Bateup, H.S., Santini, E., Shen, W., Birnbaum, S., Valjent, E., Surmeier, D.J., Fisone, G., Nestler, E.J., and Greengard, P. (2010). Distinct subclasses of medium spiny neurons differentially regulate striatal motor behaviors. *Proc. Natl. Acad. Sci. U. S. A.* *107*, 14845–14850.

- Baudic, S., Maison, P., Dolbeau, G., Boissé, M.-F., Bartolomeo, P., Dalla Barba, G., Traykov, L., and Bachoud-Lévi, A.-C. (2006). Cognitive impairment related to apathy in early Huntington's disease. *Dement. Geriatr. Cogn. Disord.* *21*, 316–321.
- Beaulieu, J.M., Espinoza, S., and Gainetdinov, R.R. (2015). Dopamine receptors - IUPHAR review 13. *Br. J. Pharmacol.* *172*, 1–23.
- Behrens, T.E.J., Johansen-Berg, H., Woolrich, M.W., Smith, S.M., Wheeler-Kingshott, C.A.M., Boulby, P.A., Barker, G.J., Sillery, E.L., Sheehan, K., Ciccarelli, O., et al. (2003). Non-invasive mapping of connections between human thalamus and cortex using diffusion imaging. *Nat. Neurosci.* *6*, 750–757.
- Beierholm, U., Guitart-Masip, M., Economides, M., Chowdhury, R., Düzel, E., Dolan, R., and Dayan, P. (2013). Dopamine Modulates Reward-Related Vigor. *Neuropsychopharmacology* *38*, 1495–1503.
- Biswal, B., Yetkin, F.Z., Haughton, V.M., and Hyde, J.S. (1995). Functional connectivity in the motor cortex of resting human brain using echo-planar MRI. *Magn. Reson. Med.* *34*, 537–541.
- Bleuler, E. (1950). *Dementia praecox or the group of schizophrenias.* (International Universities Press.).
- Bonnelle, V., Veromann, K.R., Burnett Heyes, S., Lo Sterzo, E., Manohar, S., and Husain, M. (2015). Characterization of reward and effort mechanisms in apathy. *J. Physiol. Paris* *109*, 16–26.
- Bonnelle, V., Manohar, S., Behrens, T., and Husain, M. (2016). Individual Differences in Premotor Brain Systems Underlie Behavioral Apathy. *Cereb. Cortex* *26*, 807–819.
- Bora, E., Velakoulis, D., and Walterfang, M. (2016). Social cognition in Huntington's disease: A meta-analysis. *Behav. Brain Res.* *297*, 131–140.
- Botvinick, M., Ritter, S., Wang, J.X., Kurth-Nelson, Z., Blundell, C., and Hassabis, D. (2019). Reinforcement Learning, Fast and Slow. *Trends Cogn. Sci.* *23*, 408–422.
- Le Bouc, R., Rigoux, L., Schmidt, L., Degos, B., Welter, M.-L., Vidailhet, M., Daunizeau, J., and Pessiglione, M. (2016). Computational Dissection of Dopamine Motor and Motivational Functions in Humans. *J. Neurosci.* *36*, 6623–6633.
- Brett, M., Penny, W., and Kiebel, S. (2003). *An Introduction to Random Field Theory.*
- van der Burg, J.M.M., Gardiner, S.L., Ludolph, A.C., Landwehrmeyer, G.B., Roos, R.A.C., and Aziz, N.A. (2017). Body weight is a robust predictor of clinical progression in Huntington disease. *Ann. Neurol.* *82*, 479–483.
- Calabresi, P., Picconi, B., Tozzi, A., Ghiglieri, V., and Di Filippo, M. (2014a). Direct and indirect pathways of basal ganglia: a critical reappraisal. *Nat. Neurosci.* *17*, 1022–1030.
- Calabresi, P., Picconi, B., Tozzi, A., Ghiglieri, V., and Di Filippo, M. (2014b). Direct and indirect pathways of basal ganglia: a critical reappraisal. *Nat. Publ. Gr.* *17*.
- Camacho, M., Barker, R.A., and Mason, S.L. (2018). Apathy in Huntington's Disease: A Review of the Current Conceptualization. *J. Alzheimer's Dis. Park.* *08*, 1–9.
- Cepeda, C., Murphy, K.P.S., Parent, M., and Levine, M.S. (2014). The Role of Dopamine in Huntington's Disease. *Prog. Brain Res.* *211*, 235–254.
- Cerovic, M., D'Isa, R., Tonini, R., and Brambilla, R. (2013). Molecular and cellular mechanisms of dopamine-mediated behavioral plasticity in the striatum. *Neurobiol. Learn. Mem.*
- Chakravarthy, V.S., Joseph, D., Bapi, R.S., Joseph, D., and Bapi, R.S. (2010). What do the basal ganglia do? A modeling perspective. *Biol Cybern* *103*, 237–253.
- Charnov, E.L. (1976). Optimal foraging theory: the marginal value theorem. *Theor. Popul. Biol.* *9*, 129–136.
- Chase, H.W., Kumar, P., Eickhoff, S.B., and Dombrovski, A.Y. (2015). Reinforcement learning models and their neural correlates: An activation likelihood estimation meta-

- analysis. *Cogn. Affect. Behav. Neurosci.* *15*, 435–459.
- Chatterjee, A., Anderson, K.E., Moskowitz, C.B., Hauser, W.A., and Marder, K.S. (2005). A comparison of self-report and caregiver assessment of depression, apathy, and irritability in Huntington's disease. *J Neuropsychiatry Clin Neurosci* *17*, 378–383.
- Chen, J.Y., Wang, E.A., Cepeda, C., and Levine, M.S. (2013). Dopamine imbalance in Huntington's disease: A mechanism for the lack of behavioral flexibility. *Front. Neurosci.* *7*, 1–14.
- Chowdhury, R., Guitart-Masip, M., Lambert, C., Dayan, P., Huys, Q., Düzel, E., and Dolan, R.J. (2013). Dopamine restores reward prediction errors in old age. *Nat. Neurosci.* *16*, 648–653.
- Clarke, D.E., Van Reekum, R., Simard, M., Streiner, D.L., Freedman, M., and Conn, D. (2007). Apathy in dementia: An examination of the psychometric properties of the Apathy Evaluation Scale. *J. Neuropsychiatry Clin. Neurosci.* *19*, 57–64.
- Collins, A.G.E., and Frank, M.J. (2014). Opponent actor learning (OpAL): Modeling interactive effects of striatal dopamine on reinforcement learning and choice incentive. *Psychol. Rev.* *121*, 337–366.
- Coppen, E.M., and Roos, R.A.C. (2017). Current Pharmacological Approaches to Reduce Chorea in Huntington's Disease. *Drugs* *77*, 29–46.
- Craufurd, D., Thompson, J.C., and Snowden, J.S. (2001). Behavioral changes in Huntington Disease - PubMed. *Neuropsychiatry Neuropsychol Behav Neurol*.
- Crittenden, J.R., and Graybiel, A.M. (2011). Basal Ganglia Disorders Associated with Imbalances in the Striatal Striosome and Matrix Compartments. *Front. Neuroanat.* *5*, 59.
- Cui, G., Jun, S.B., Jin, X., Pham, M.D., Vogel, S.S., Lovinger, D.M., and Costa, R.M. (2013). Concurrent activation of striatal direct and indirect pathways during action initiation. *Nature* *494*, 238–242.
- Daniel, R., and Pollmann, S. (2014). A universal role of the ventral striatum in reward-based learning: evidence from human studies. *Neurobiol. Learn. Mem.* *114*, 90–100.
- Daw, N.D. (2009). Trial-by-trial data analysis using computational models. 1–26.
- Daw, N.D. (2013). 16: Advanced Reinforcement Learning (Elsevier Inc.).
- Daw, N.D., and Tobler, P.N. (2013). 15: Value Learning through Reinforcement: The Basics of Dopamine and Reinforcement Learning (Elsevier Inc.).
- Daw, N.D., O'Doherty, J.P., Dayan, P., Seymour, B., and Dolan, R.J. (2006). Cortical substrates for exploratory decisions in humans. *Nature* *441*, 876–879.
- Daw, N.D., Gershman, S.J., Seymour, B., Dayan, P., and Dolan, R.J. (2011). Model-based influences on humans' choices and striatal prediction errors. *Neuron* *69*, 1204–1215.
- Dayan, P., and Niv, Y. (2008). Reinforcement learning : The Good , The Bad and The Ugly. *Curr. Opin. Neurobiol.* *18*, 185–196.
- Deco, G., Jirsa, V.K., and McIntosh, A.R. (2011). Emerging concepts for the dynamical organization of resting-state activity in the brain. *Nat. Rev. Neurosci.* *12*, 43–56.
- Delmaire, C., Dumas, E.M., Sharman, M.A., van den Bogaard, S.J.A., Valabregue, R., Jauffret, C., Justo, D., Reilmann, R., Stout, J.C., Craufurd, D., et al. (2013). The structural correlates of functional deficits in early huntington's disease. *Hum. Brain Mapp.* *34*, 2141–2153.
- DeLong, M.R. (1990a). Primate models of movement disorders of basal ganglia origin. *Trends Neurosci.* *13*, 281–285.
- DeLong, M.R. (1990b). Primate models of movement disorders of basal ganglia origin. *Trends Neurosci.* *13*, 281–285.
- DeLong, M., and Wichmann, T. (2009a). Update on models of basal ganglia function and dysfunction. *Parkinsonism Relat. Disord.* *15*, S237–S240.
- DeLong, M., and Wichmann, T. (2009b). Update on models of basal ganglia function and

dysfunction. *Park. Relat. Disord.* 15, S237.

Deng, Y., P., Albin, R., L., Penney, J., B., Young, A., B., Anderson, K., D., and Reiner, A. (2004). Differential loss of striatal projection systems in Huntington's disease: A quantitative immunohistochemical study. *J. Chem. Neuroanat.* 27, 143–164.

Deniau, J.M., Mailly, P., Maurice, N., and Charpier, S. (2007). The pars reticulata of the substantia nigra: a window to basal ganglia output. *Prog. Brain Res.* 160, 151–172.

Desouza, C. V., Padala, P.R., Haynatzki, G., Anzures, P., Demasi, C., and Shivaswamy, V. (2012). Role of apathy in the effectiveness of weight management programmes. *Diabetes, Obes. Metab.* 14, 419–423.

Dirkx, M.F., den Ouden, H.E.M., Aarts, E., Timmer, M.H.M., Bloem, B.R., Toni, I., and Helmich, R.C. (2017). Dopamine controls Parkinson's tremor by inhibiting the cerebellar thalamus. *Brain* 140, 721–734.

Djousse, L., Knowlton, B., Hayden, M., Almqvist, E.W., Brinkman, R., Ross, C., Margolis, R., Rosenblatt, A., Durr, A., Dode, C., et al. (2003). Interaction of normal and expanded CAG repeat sizes influences age at onset of Huntington disease. *Am. J. Med. Genet. Part A* 119A, 279–282.

Doll, B.B., Simon, D.A., and Daw, N.D. (2012). The ubiquity of model-based reinforcement learning. *Curr. Opin. Neurobiol.* 22, 1075–1081.

Dorsey, E.R., Beck, C.A., Darwin, K., Nichols, P., Brocht, A.F.D., Biglan, K.M., and Shoulson, I. (2013). Natural history of Huntington disease. *JAMA Neurol.* 70, 1520–1530.

Doya, K., and Kimura, M. (2013). 17: The Basal Ganglia, Reinforcement Learning, and the Encoding of Value (Elsevier Inc.).

Drew, P.J. (2019). Vascular and neural basis of the BOLD signal. *Curr. Opin. Neurobiol.*

Duijn, E. Van, Craufurd, D., Hubers, A.A.M., Giltay, E.J., Bonelli, R., Rickards, H., Anderson, K.E., Walsem, M.R. Van, Mast, R.C. Van Der, Orth, M., et al. (2014).

Neuropsychiatric symptoms in a European Huntington's disease cohort (REGISTRY). 1411–1418.

van Duijn, E., Craufurd, D., Hubers, A.A.M., Giltay, E.J., Bonelli, R., Rickards, H., Anderson, K.E., van Walsem, M.R., van der Mast, R.C., Orth, M., et al. (2014).

Neuropsychiatric symptoms in a European Huntington's disease cohort (REGISTRY). *J. Neurol. Neurosurg. Psychiatry* 85, 1411–1418.

Van Duijn, E., Reedeker, N., Giltay, E.J., Roos, R.A.C., and Van Der Mast, R.C. (2010). Correlates of apathy in Huntington's disease. *J. Neuropsychiatry Clin. Neurosci.* 22, 287–294.

Dumas, E.M., van den Bogaard, S.J.A., Middelkoop, H.A.M., and Roos, R.A.C. (2013). A review of cognition in Huntington's disease. *Front. Biosci. (Schol. Ed.)* 5, 1–18.

Eddy, C.M., Parkinson, E.G., and Rickards, H.E. (2016). Changes in mental state and behaviour in Huntington's disease. *The Lancet Psychiatry* 3, 1079–1086.

Enzi, B., Edel, M.A., Lissek, S., Peters, S., Hoffmann, R., Nicolas, V., Tegenthoff, M., Juckel, G., and Saft, C. (2012). Altered ventral striatal activation during reward and punishment processing in premanifest Huntington's disease: A functional magnetic resonance study. *Exp. Neurol.* 235, 256–264.

Esmaeilzadeh, M., Farde, L., Karlsson, P., Varrone, A., Halldin, C., Waters, S., and Tedroff, J. (2011). Extrastriatal dopamine D2 receptor binding in Huntington's disease. *Hum. Brain Mapp.* 32, 1626–1636.

Fervaha, G., Foussias, G., Agid, O., and Remington, G. (2014). Motivational and neurocognitive deficits are central to the prediction of longitudinal functional outcome in schizophrenia. *Acta Psychiatr. Scand.* 130, 290–299.

Foussias, G., and Remington, G. (2010). Negative symptoms in schizophrenia: avolition and Occam's razor. *Schizophr. Bull.* 36, 359–369.

- Fox, M.D., and Raichle, M.E. (2007). Spontaneous fluctuations in brain activity observed with functional magnetic resonance imaging. *Nat. Rev. Neurosci.* *8*, 700–711.
- Frank, M.J. (2011). Computational models of motivated action selection in corticostriatal circuits. *Curr. Opin. Neurobiol.* *21*, 381–386.
- Frank, M.J., and Badre, D. (2012). Mechanisms of hierarchical reinforcement learning in corticostriatal circuits 1: Computational analysis. *Cereb. Cortex* *22*, 509–526.
- Frank, M.J., Seeberger, L.C., and O'Reilly, R.C. (2004). By carrot or by stick: Cognitive reinforcement learning in Parkinsonism. *Science* (80-.). *306*, 1940–1943.
- Franklin, N.T., and Frank, M.J. (2015). A cholinergic feedback circuit to regulate striatal population uncertainty and optimize reinforcement learning. *Elife* *4*, 1–29.
- Fransson, P. (2005). Spontaneous low-frequency BOLD signal fluctuations: An fMRI investigation of the resting-state default mode of brain function hypothesis. *Hum. Brain Mapp.* *26*, 15–29.
- Freeborough, P.A., Fox, N.C., and Kitney, R.I. (1997). Interactive algorithms for the segmentation and quantitation of 3-D MRI brain scans. *Comput. Methods Programs Biomed.* *53*, 15–25.
- Freeze, B.S., Kravitz, A. V., Hammack, N., Berke, J.D., and Kreitzer, A.C. (2013). Control of Basal Ganglia Output by Direct and Indirect Pathway Projection Neurons. *J. Neurosci.* *33*, 18531–18539.
- Friston, K.J. (2011). Functional and Effective Connectivity: A Review. *Brain Connect.* *1*, 13–36.
- Friston, K., Brown, H.R., Siemerkus, J., and Stephan, K.E. (2016a). The dysconnection hypothesis (2016). *Schizophr. Res.* *176*, 83–94.
- Friston, K.J., Harrison, L., and Penny, W. (2003). Dynamic causal modelling.
- Friston, K.J., Stephan, K.E., Montague, R., and Dolan, R.J. (2014a). Computational psychiatry: The brain as a phantastic organ. *The Lancet Psychiatry* *1*, 148–158.
- Friston, K.J., Kahan, J., Biswal, B., and Razi, A. (2014b). A DCM for resting state fMRI. *Neuroimage* *94*, 396–407.
- Friston, K.J., Litvak, V., Oswal, A., Razi, A., Stephan, K.E., van Wijk, B.C.M., Ziegler, G., and Zeidman, P. (2016b). Bayesian model reduction and empirical Bayes for group (DCM) studies. *Neuroimage* *128*, 413–431.
- Friston, K.J., Preller, K.H., Mathys, C., Cagan, H., Heinzle, J., Razi, A., and Zeidman, P. (2017). Dynamic causal modelling revisited. *Neuroimage*.
- Fritz, N.E., Boileau, N.R., Stout, J.C., Ready, R., Perlmutter, J.S., Paulsen, J.S., Quaid, K., Barton, S., McCormack, M.K., Perlman, S.L., et al. (2018). Relationships Among Apathy, Health-Related Quality of Life, and Function in Huntington's Disease. *J. Neuropsychiatry Clin. Neurosci.* *30*, 194–201.
- Garrison, J., Erdeniz, B., and Done, J. (2013). Prediction error in reinforcement learning: A meta-analysis of neuroimaging studies. *Neurosci. Biobehav. Rev.* *37*, 1297–1310.
- Gelderblom, H., Wüstenberg, T., McLean, T., Mütze, L., Fischer, W., Saft, C., Hoffmann, R., Süßmuth, S., Schlattmann, P., van Duijn, E., et al. (2017). Bupropion for the treatment of apathy in Huntington's disease: A multicenter, randomised, double-blind, placebo-controlled, prospective crossover trial. *PLoS One* *12*, e0173872.
- Ghosh, R., and Tabrizi, S.J. (2018). Clinical Features of Huntington's Disease. In *Advances in Experimental Medicine and Biology*, pp. 1–28.
- Graybiel, A.M. (2000). The Basal ganglia. *Curr. Biol.* *10*, R509–R511.
- Graybiel, A.M., and Grafton, S.T. (2015). The Striatum: Where Skills and Habits Meet. *Cold Spring Harb. Perspect. Biol.* *7*, a021691.
- Green, L., Myerson, J., and Ostaszewski, P. (1999). Discounting of delayed rewards across the life span: Age differences in individual discounting functions. *Behav. Processes* *46*, 89–

96.

- Gregory, S., Scahill, R.I., Seunarine, K.K., Stopford, C., Zhang, H., Zhang, J., Orth, M., Durr, A., Roos, R.A.C., Langbehn, D.R., et al. (2015a). Neuropsychiatry and White Matter Microstructure in Huntington's Disease. *J. Huntingtons. Dis.* *4*, 239–249.
- Gregory, S., Scahill, R.I., Seunarine, K.K., Stopford, C., Zhang, H., Zhang, J., Orth, M., Durr, A., Roos, R.A.C., Langbehn, D.R., et al. (2015b). Neuropsychiatry and White Matter Microstructure in Huntington's Disease. *J. Huntingtons. Dis.* *4*, 239–249.
- Guitart-Masip, M., Beierholm, U.R., Dolan, R., Duzel, E., and Dayan, P. (2011). Vigor in the Face of Fluctuating Rates of Reward: An Experimental Examination. *J. Cogn. Neurosci.* *23*, 3933–3938.
- Haber, S.N. (2011). Neuroanatomy of Reward: A View from the Ventral Striatum.
- Haber, S.N. (2016). Corticostriatal circuitry. *Dialogues Clin. Neurosci.* *18*, 7–21.
- Haber, S.N., and Knutson, B. (2009). The Reward Circuit: Linking Primate Anatomy and Human Imaging. *Neuropsychopharmacology* *35*, 4–26.
- Haber, S.N., Fudge, J.L., and McFarland, N.R. (2000). Striatonigrostriatal pathways in primates form an ascending spiral from the shell to the dorsolateral striatum. *J. Neurosci.* *20*, 2369–2382.
- Hamid, A.A., Pettibone, J.R., Mabrouk, O.S., Hetrick, V.L., Schmidt, R., Vander Weele, C.M., Kennedy, R.T., Aragona, B.J., and Berke, J.D. (2015). Mesolimbic dopamine signals the value of work. *Nat. Neurosci.* *19*, 117–126.
- Hamilton, J.M., Salmon, D.P., Corey-Bloom, J., Gamst, A., Paulsen, J.S., Jerkins, S., Jacobson, M.W., and Peavy, G. (2003). Behavioural abnormalities contribute to functional decline in Huntington's disease. *J. Neurol. Neurosurg. Psychiatry* *74*, 120–122.
- Hauser, T.U., Eldar, E., and Dolan, R.J. (2017). Separate mesocortical and mesolimbic pathways encode effort and reward learning signals. *Proc. Natl. Acad. Sci.* 201705643.
- Heath, C.J., O'Callaghan, C., Mason, S.L., Phillips, B.U., Saksida, L.M., Robbins, T.W., Barker, R.A., Bussey, T.J., and Sahakian, B.J. (2019). A Touchscreen Motivation Assessment Evaluated in Huntington's Disease Patients and R6/1 Model Mice. *Front. Neurol.* *10*, 858.
- Heeger, D.J., Huk, A.C., Geisler, W.S., and Albrecht, D.G. (2000). Spikes versus BOLD: What does neuroimaging tell us about neuronal activity? *Nat. Neurosci.* *3*, 631–633.
- Henley, S.M.D., Novak, M.J.U., Frost, C., King, J., Tabrizi, S.J., and Warren, J.D. (2012). Emotion recognition in Huntington's disease: A systematic review. *Neurosci. Biobehav. Rev.* *36*, 237–253.
- Le Heron, C., Apps, M.A.J., and Husain, M. (2017). The anatomy of apathy: A neurocognitive framework for amotivated behaviour. *Neuropsychologia*.
- Le Heron, C., Apps, M.A.J., and Husain, M. (2018a). The anatomy of apathy: A neurocognitive framework for amotivated behaviour. *Neuropsychologia* *118*, 54–67.
- Le Heron, C., Plant, O., Manohar, S., Ang, Y.-S., Jackson, M., Lennox, G., Hu, M.T., and Husain, M. (2018b). Distinct effects of apathy and dopamine on effort-based decision-making in Parkinson's disease. *Brain* *141*, 1455–1469.
- Le Heron, C., Apps, M., and Husain, M. (2018c). The anatomy of apathy: A neurocognitive framework for amotivated behaviour.
- Le Heron, C., Holroyd, C.B., Salamone, J., and Husain, M. (2019). Brain mechanisms underlying apathy. *J. Neurol. Neurosurg. Psychiatry* *90*, 302–312.
- Hikida, T., Kimura, K., Wada, N., Funabiki, K., and Nakanishi, S. (2010). Distinct Roles of Synaptic Transmission in Direct and Indirect Striatal Pathways to Reward and Aversive Behavior. *Neuron* *66*, 896–907.
- Hikida, T., Yawata, S., Yamaguchi, T., Danjo, T., Sasaoka, T., Wang, Y., and Nakanishi, S. (2013). Pathway-specific modulation of nucleus accumbens in reward and aversive behavior via selective transmitter receptors. *Proc. Natl. Acad. Sci. U. S. A.* *110*, 342–347.

- Hillman, E.M.C. (2014). Coupling mechanism and significance of the BOLD signal: A status report. *Annu. Rev. Neurosci.* *37*, 161–181.
- Hirano, Y., Stefanovic, B., and Silva, A.C. (2011). Spatiotemporal evolution of the functional magnetic resonance imaging response to ultrashort stimuli. *J. Neurosci.* *31*, 1440–1447.
- Honrath, P., Dogan, I., Wudarczyk, O., Görlich, K.S., Votinov, M., Werner, C.J., Schumann, B., Overbeck, R.T., Schulz, J.B., Landwehrmeyer, B.G., et al. (2018). Risk factors of suicidal ideation in Huntington’s disease: literature review and data from Enroll-HD. *J. Neurol.* *265*, 2548–2561.
- Howes, O.D., and Nour, M.M. (2016). Dopamine and the aberrant salience hypothesis of schizophrenia. *World Psychiatry* *15*, 3–4.
- Huhn, M., Nikolakopoulou, A., Schneider-Thoma, J., Krause, M., Samara, M., Peter, N., Arndt, T., Bäckers, L., Rothe, P., Cipriani, A., et al. (2019). Comparative efficacy and tolerability of 32 oral antipsychotics for the acute treatment of adults with multi-episode schizophrenia: a systematic review and network meta-analysis. *Lancet* *394*, 939–951.
- Hull, C.L. (1943). *Principles of behavior: an introduction to behavior theory.* (Oxford, England: Appleton-Century).
- Huntington, G. (1872). On Chorea.
- Huntington Study Group. (1996). Unified Huntington’s disease rating scale: Reliability and consistency. *Mov. Disord.* *11*, 136–142.
- Husain, M., and Roiser, J.P. (2017). Neuroscience of apathy and anhedonia : a transdiagnostic approach. *Nat. Rev. Neurosci.* 1–26.
- Huys, Q.J.M., Cruickshank, A., and Seriès, P. (2014). Reward-Based Learning, Model-Based and Model-Free. In *Encyclopedia of Computational Neuroscience*, (Springer New York), pp. 1–10.
- Huys, Q.J.M., Maia, T. V, and Frank, M.J. (2016). Computational psychiatry as a bridge from neuroscience to clinical applications. *Nat. Neurosci.* *19*, 404–413.
- Ikemoto, S., Yang, C., and Tan, A. (2015). Basal ganglia circuit loops, dopamine and motivation: A review and enquiry. *Behav. Brain Res.* *290*, 17–31.
- Jacobs, M., Hart, E.P., and Roos, R.A.C. (2018). Cognitive Performance and Apathy Predict Unemployment in Huntington’s Disease Mutation Carriers. *J. Neuropsychiatry Clin. Neurosci.* *30*, 188–193.
- Jenkinson, M. (2018). Introduction to neuroimaging analysis.
- Jenkinson, M., Chappell, M., Bijsterbosch, J., and Winkler, A. (2018). *An Introduction to Neuroimaging Analysis: General Linear Model for Neuroimaging* .
- Joel, D., Niv, Y., and Ruppin, E. (2002). Actor-critic models of the basal ganglia: new anatomical and computational perspectives. *Neural Networks* *15*, 535–547.
- Johnson, E.B., Gregory, S., Johnson, H.J., Durr, A., Leavitt, B.R., Roos, R.A., Rees, G., Tabrizi, S.J., and Scahill, R.I. (2017). Recommendations for the Use of Automated Gray Matter Segmentation Tools: Evidence from Huntington’s Disease. *Front. Neurol.* *8*, 519.
- Kachian, Z.R., Cohen-Zimmerman, S., Bega, D., Gordon, B., and Grafman, J. (2019). Suicidal ideation and behavior in Huntington’s disease: Systematic review and recommendations. *J. Affect. Disord.* *250*, 319–329.
- Kahan, J., and Foltynie, T. (2013). Understanding DCM: Ten simple rules for the clinician. *Neuroimage* *83*, 542–549.
- Kahan, J., Urner, M., Moran, R., Flandin, G., Marreiros, A., Mancini, L., White, M., Thornton, J., Yousry, T., Zrinzo, L., et al. (2014a). Resting state functional MRI in Parkinson’s disease: The impact of deep brain stimulation on “effective” connectivity. *Brain* *137*, 1130–1144.
- Kahan, J., Urner, M., Moran, R., Flandin, G., Marreiros, A., Mancini, L., White, M., Thornton, J., Yousry, T., Zrinzo, L., et al. (2014b). Resting state functional MRI in

- Parkinson's disease: the impact of deep brain stimulation on 'effective' connectivity. *Brain* 137, 1130–1144.
- Kapur, S. (2003). Psychosis as a state of aberrant salience: A framework linking biology, phenomenology, and pharmacology in schizophrenia. *Am. J. Psychiatry* 160, 13–23.
- Katzell, R.A., and Thompson, D.E. (1990). Work Motivation: Theory and Practice. *Am. Psychol.* 45, 144–153.
- Kawaguchi, Y., Wilson, C.J., Augood, S.J., and Emson, P.C. (1995). Striatal interneurons: chemical, physiological and morphological characterization. *Trends Neurosci.* 18, 527–535.
- Kempnich, C.L., Andrews, S.C., Fisher, F., Wong, D., Georgiou-Karistianis, N., and Stout, J.C. (2018). Emotion recognition correlates with social-neuropsychiatric dysfunction in huntington's disease. *J. Int. Neuropsychol. Soc.* 24, 417–423.
- Keuken, M.C., Bazin, P.-L., Schafer, A., Neumann, J., Turner, R., and Forstmann, B.U. (2013). Ultra-High 7T MRI of Structural Age-Related Changes of the Subthalamic Nucleus. *J. Neurosci.* 33, 4896–4900.
- Kingma, E.M., van Duijn, E., Timman, R., van der Mast, R.C., and Roos, R.A.C. (2008). Behavioural problems in Huntington's disease using the Problem Behaviours Assessment. *Gen. Hosp. Psychiatry* 30, 155–161.
- Klein-Flügge, M.C., Kennerley, S.W., Saraiva, A.C., Penny, W.D., and Bestmann, S. (2015). Behavioral Modeling of Human Choices Reveals Dissociable Effects of Physical Effort and Temporal Delay on Reward Devaluation. *PLoS Comput. Biol.* 11.
- Klein-Flügge, M.C., Kennerley, S.W., Friston, K., and Bestmann, S. (2016). Neural signatures of value comparison in human cingulate cortex during decisions requiring an effort-reward trade-off. *J. Neurosci.* 36, 064105.
- Klöppel, S., Gregory, S., Scheller, E., Minkova, L., Razi, A., Durr, A., Roos, R.A.C.C., Leavitt, B.R., Papoutsis, M., Landwehrmeyer, G.B., et al. (2015). Compensation in Preclinical Huntington's Disease: Evidence From the Track-On HD Study. *EBioMedicine* 2, 1420–1429.
- Kolling, N., Behrens, T.E.J., Mars, R.B., and Rushworth, M.F.S. (2012). Neural Mechanisms of Foraging. *Science* 336, 91–95.
- Konstantakopoulos, G., Ploumpidis, D., Oulis, P., Patrikelis, P., Soumani, A., Papadimitriou, G.N., and Politis, A.M. (2011). Apathy, cognitive deficits and functional impairment in schizophrenia. *Schizophr. Res.* 133, 193–198.
- Krause, M., Zhu, Y., Huhn, M., Schneider-Thoma, J., Bighelli, I., Nikolakopoulou, A., and Leucht, S. (2018). Antipsychotic drugs for patients with schizophrenia and predominant or prominent negative symptoms: a systematic review and meta-analysis. *Eur. Arch. Psychiatry Clin. Neurosci.* 268, 625–639.
- Kravitz, A. V., Freeze, B.S., Parker, P.R.L., Kay, K., Thwin, M.T., Deisseroth, K., and Kreitzer, A.C. (2010). Regulation of parkinsonian motor behaviours by optogenetic control of basal ganglia circuitry. *Nature* 466, 622–626.
- Kreitzer, A.C. (2009). Physiology and Pharmacology of Striatal Neurons.
- Kremer, B., Goldberg, P., Andrew, S.E., Theilmann, J., Telenius, H., Zeisler, J., Squitieri, F., Lin, B., Bassett, A., Almqvist, E., et al. (1994). A Worldwide Study of the Huntington's Disease Mutation: The Sensitivity and Specificity of Measuring CAG Repeats. *N. Engl. J. Med.* 330, 1401–1406.
- Krishnamoorthy, A., and Craufurd, D. (2011). Treatment of Apathy in Huntington's Disease and Other Movement Disorders. *Curr. Treat. Options Neurol.* 13, 508–519.
- Kusurkar, R.A., Ten Cate, T.J., Vos, C.M.P., Westers, P., and Croiset, G. (2013). How motivation affects academic performance: A structural equation modelling analysis. *Adv. Heal. Sci. Educ.* 18, 57–69.
- Labuschagne, I., Jones, R., Callaghan, J., Whitehead, D., Dumas, E.M., Say, M.J., Hart, E.P., Justo, D., Coleman, A., Dar Santos, R.C., et al. (2013). Emotional face recognition deficits

and medication effects in pre-manifest through stage-II Huntington's disease. *Psychiatry Res.* *207*, 118–126.

Lanciego, J.L., Luquin, N., and Obeso, J.A. (2012). Functional neuroanatomy of the basal ganglia. *Cold Spring Harb. Perspect. Med.* *2*, a009621.

Landwehrmeyer, G.B., Fitzer-Attas, C.J., Giuliano, J.D., Gonçalves, N., Anderson, K.E., Cardoso, F., Ferreira, J.J., Mestre, T.A., Stout, J.C., and Sampaio, C. (2017). Data Analytics from Enroll-HD, a Global Clinical Research Platform for Huntington's Disease. *Mov. Disord. Clin. Pract.* *4*, 212–224.

Langbehn, D., Brinkman, R., Falush, D., Paulsen, J., Hayden, M., and International Huntington's Disease Collaborative Group (2004). A new model for prediction of the age of onset and penetrance for Huntington's disease based on CAG length. *Clin. Genet.* *65*, 267–277.

Langbehn, D.R., Hayden, M.R., Paulsen, J.S., Group, the P.-H.I. of the H.S., and and the PREDICT-HD Investigators of the Huntington Study Group (2010). CAG-Repeat Length and the Age of Onset in Huntington Disease (HD): A Review and Validation Study of Statistical Approaches. *Am J Med Genet B Neuropsychiatr Genet.* *153B*.

Ledig, C., Heckemann, R.A., Hammers, A., Lopez, J.C., Newcombe, V.F.J., Makropoulos, A., Lötjönen, J., Menon, D.K., and Rueckert, D. (2015). Robust whole-brain segmentation: Application to traumatic brain injury. *Med. Image Anal.* *21*, 40–58.

Lee, J.M., Ramos, E.M., Lee, J.H., Gillis, T., Mysore, J.S., Hayden, M.R., Warby, S.C., Morrison, P., Nance, M., Ross, C.A., et al. (2012). CAG repeat expansion in Huntington disease determines age at onset in a fully dominant fashion. *Neurology* *78*, 690–695.

Lehéricy, S., Benali, H., Van de Moortele, P.-F., Péligrini-Issac, M., Waechter, T., Ugurbil, K., and Doyon, J. (2005). Distinct basal ganglia territories are engaged in early and advanced motor sequence learning. *Proc. Natl. Acad. Sci. U. S. A.* *102*, 12566–12571.

Levy, R., and Dubois, B. (2006a). Apathy and the Functional Anatomy of the Prefrontal Cortex–Basal Ganglia Circuits. *Cereb. Cortex* *16*, 916–928.

Levy, R., and Dubois, B. (2006b). Apathy and the functional anatomy of the prefrontal cortex-basal ganglia circuits. *Cereb. Cortex* *16*, 916–928.

Leys, C., Ley, C., Klein, O., Bernard, P., and Licata, L. (2013). Journal of Experimental Social Psychology Detecting outliers : Do not use standard deviation around the mean , use absolute deviation around the median. 4–6.

Lindquist, M.A., and Mejia, A. (2015). Zen and the art of multiple comparisons. *Psychosom. Med.* *77*, 114–125.

Litvan, I., Paulsen, J.S., Mega, M.S., and Cummings, J.L. (1998). Neuropsychiatric assessment of patients with hyperkinetic and hypokinetic movement disorders. *Arch. Neurol.* *55*, 1313–1319.

Liu, X., Hairston, J., Schrier, M., and Fan, J. (2011). Common and distinct networks underlying reward valence and processing stages: A meta-analysis of functional neuroimaging studies. *Neurosci. Biobehav. Rev.* *35*, 1219–1236.

Logothetis, N.K., Pauls, J., Augath, M., Trinath, T., and Oeltermann, A. (2001). Neurophysiological investigation of the basis of the fMRI signal. *Nature* *412*, 150–157.

MacDonald, M.E., Ambrose, C.M., Duyao, M.P., Myers, R.H., Lin, C., Srinidhi, L., Barnes, G., Taylor, S.A., James, M., Groot, N., et al. (1993). A novel gene containing a trinucleotide repeat that is expanded and unstable on Huntington's disease chromosomes. *Cell* *72*, 971–983.

Macpherson, T., Morita, M., and Hikida, T. (2014). Striatal direct and indirect pathways control decision-making behavior. *Front. Psychol.* *5*, 1301.

Magezi, D.A. (2015). Linear mixed-effects models for within-participant psychology experiments: an introductory tutorial and free, graphical user interface (LMMgui). *Front.*

Psychol. 6, 2.

Mahadevan, S. (1996). Average reward reinforcement learning: foundations, algorithms, and empirical results. *Mach. Learn.* 22, 159–195.

Maldjian, J.A., Laurienti, P.J., Kraft, R.A., and Burdette, J.H. (2003). An automated method for neuroanatomic and cytoarchitectonic atlas-based interrogation of fMRI data sets. *Neuroimage* 19, 1233–1239.

Malone, I.B., Leung, K.K., Clegg, S., Barnes, J., Whitwell, J.L., Ashburner, J., Fox, N.C., and Ridgway, G.R. (2015). Accurate automatic estimation of total intracranial volume: a nuisance variable with less nuisance. *Neuroimage* 104, 366–372.

Mandal, P.K., Mahajan, R., and Dinov, I.D. (2012). Structural brain atlases: Design, rationale, and applications in normal and pathological cohorts. *J. Alzheimer's Dis.*

Mann, R.S. (1991). Apathy: A Neuropsychiatric Syndrome.

Marin, R.S. (1991). Apathy: A Neuropsychiatric Syndrome. *J. Neuropsychiatr.* 3, 243–254.

Marin, R.S., Biedrzycki, R.C., and Firinciogullari, S. (1991). Reliability and validity of the Apathy Evaluation Scale. *Psychiatry Res.* 38, 143–162.

Marr, D. (1982). *Vision: a computational investigation into the human representation and processing of visual information* (MIT Press).

Martindale, J., Berwick, J., Martin, C., Kong, Y., Zheng, Y., and Mayhew, J.E.W. (2005). Long duration stimuli nonlinearities in the neural-haemodynamic coupling. *J. Cereb. Blood Flow Metab.* 25, 651–661.

Martinez-Horta, S., Perez-Perez, J., van Duijn, E., Fernandez-Bobadilla, R., Carceller, M., Pagonabarraga, J., Pascual-Sedano, B., Campolongo, A., Ruiz-Idiago, J., Sampedro, F., et al. (2016). Neuropsychiatric symptoms are very common in premanifest and early stage Huntington's Disease. *Parkinsonism Relat. Disord.* 25, 58–64.

Martínez-Horta, S., Perez-Perez, J., Sampedro, F., Pagonabarraga, J., Horta-Barba, A., Carceller-Sindreu, M., Gomez-Anson, B., Lozano-Martinez, G.A., Lopez-Mora, D.A., Camacho, V., et al. (2018a). Structural and metabolic brain correlates of apathy in Huntington's disease. *Mov. Disord.* 33, 1151–1159.

Martínez-Horta, S., Perez-Perez, J., Sampedro, F., Pagonabarraga, J., Horta-Barba, A., Carceller-Sindreu, M., Gomez-Anson, B., Lozano-Martinez, G.A., Lopez-Mora, D.A., Camacho, V., et al. (2018b). Structural and metabolic brain correlates of apathy in Huntington's disease. *Mov. Disord.*

Mason, S., and Barker, R.A. (2015). Rating Apathy in Huntington's Disease: Patients and Companions Agree. *J. Huntingtons. Dis.* 4, 49–59.

Mason, S.L., Daws, R.E., Soreq, E., Johnson, E.B., Scahill, R.I., Tabrizi, S.J., Barker, R.A., and Hampshire, A. (2018). Predicting clinical diagnosis in Huntington's disease: An imaging polymarker. *Ann. Neurol.* 83, 532–543.

McClure, S.M., Berns, G.S., and Montague, P.R. (2003). Temporal prediction errors in a passive learning task activate human striatum. *Neuron* 38, 339–346.

McColgan, P., and Tabrizi, S.J. (2018). Huntington's disease: a clinical review. *Eur. J. Neurol.* 25, 24–34.

McColgan, P., Razi, A., Gregory, S., Seunarine, K.K., Durr, A., Ac, R., Leavitt, B.R., Scahill, R.I., Clark, C.A., Langbehn, D.R., et al. (2017a). Structural and functional brain network correlates of depressive symptoms in Premanifest Huntington's disease. *Hum. Brain Mapp.* 38, 2819–2829.

McColgan, P., Seunarine, K.K., Gregory, S., Razi, A., Papoutsis, M., Long, J.D., Mills, J.A., Johnson, E., Durr, A., Roos, R.A., et al. (2017b). Topological length of white matter connections predicts their rate of atrophy in premanifest Huntington's disease. *JCI Insight* 2.

McLauchlan, D.J., Lancaster, T., Craufurd, D., Linden, D.E.J., and Rosser, A.E. (2019). Insensitivity to loss predicts apathy in huntington's disease. *Mov. Disord.* 34, 1381–1391.

- Mestre, T.A., van Duijn, E., Davis, A.M., Bachoud-Lévi, A.C., Busse, M., Anderson, K.E., Ferreira, J.J., Mahlknecht, P., Tumas, V., Sampaio, C., et al. (2016). Rating scales for behavioral symptoms in Huntington's disease: Critique and recommendations. *Mov. Disord.* *31*, 1466–1478.
- Mestre, T.A., Forjaz, M.J., Mahlknecht, P., Cardoso, F., Ferreira, J.J., Reilmann, R., Sampaio, C., Goetz, C.G., Cubo, E., Martinez-Martin, P., et al. (2018). Rating Scales for Motor Symptoms and Signs in Huntington's Disease: Critique and Recommendations. *Mov. Disord. Clin. Pract.* *5*, 111–117.
- Mohebi, A., Pettibone, J.R., Hamid, A.A., Wong, J.M.T., Vinson, L.T., Patriarchi, T., Tian, L., Kennedy, R.T., and Berke, J.D. (2019). Dissociable dopamine dynamics for learning and motivation. *Nature* *570*, 65–70.
- Mukamel, R., Gelbard, H., Arieli, A., Hasson, U., Fried, I., and Malach, R. (2005). Neuroscience: Coupling between neuronal firing, field potentials, and fMRI in human auditory cortex. *Science* (80-.). *309*, 951–954.
- Naarding, P., Janzing, J.G.E., Eling, P., van der Werf, S., and Kremer, B. (2009). Apathy Is Not Depression in Huntington's Disease. *J. Neuropsychiatr.* *21*, 266–270.
- Nair, A., Rutledge, R.B., and Mason, L. (2020). Under the Hood : Using Computational Psychiatry to Make Psychological Therapies More. *11*, 1–7.
- Nambu, A., Tokuno, H., and Takada, M. (2002). Functional significance of the cortico-subthalamo-pallidal “hyperdirect” pathway. *Neurosci. Res.* *43*, 111–117.
- Nelson, A.B., and Kreitzer, A.C. (2014). Reassessing Models of Basal Ganglia Function and Dysfunction. *Annu. Rev. Neurosci.* *37*, 117–135.
- Niccolini, F., and Politis, M. (2014). Neuroimaging in Huntington's disease. *World J. Radiol.* *6*, 301–312.
- Nickchen, K., Boehme, R., del Mar Amador, M., Hälbig, T.D., Dehnicke, K., Panneck, P., Behr, J., Prass, K., Heinz, A., Deserno, L., et al. (2016). Reversal learning reveals cognitive deficits and altered prediction error encoding in the ventral striatum in Huntington's disease. *Brain Imaging Behav.* 1–11.
- Niv, Y. (2007). The effects of motivation on habitual instrumental behaviour.
- Niv, Y., Daw, N.D., and Dayan, P. (2005). How fast to work: Response vigor, motivation and tonic dopamine. *Adv. Neural Inf. Process. Syst.* *18* (NIPS 2005) 1019–1026.
- Niv, Y., Daw, N.D., Joel, D., and Dayan, P. (2007). Tonic dopamine: Opportunity costs and the control of response vigor. *Psychopharmacology (Berl).* *191*, 507–520.
- Noonan, M.P., Kolling, N., Walton, M.E., and Rushworth, M.F.S. (2012). Re-evaluating the role of the orbitofrontal cortex in reward and reinforcement. *Eur. J. Neurosci.* *35*, 997–1010.
- O'Doherty, J., Dayan, P., Schultz, J., Deichmann, R., Friston, K., and Dolan, R.J. (2004). Dissociable Roles of Ventral and Dorsal Striatum in Instrumental Conditioning. *Science* (80-.). *304*, 452–454.
- O'Doherty, J.P., Dayan, P., Friston, K., Critchley, H., and Dolan, R.J. (2003). Temporal difference models and reward-related learning in the human brain. *Neuron* *38*, 329–337.
- Ogawa, S., Lee, T.M., Kay, A.R., and Tank, D.W. (1990). Brain magnetic resonance imaging with contrast dependent on blood oxygenation. *Proc. Natl. Acad. Sci. U. S. A.* *87*, 9868–9872.
- P. Murphy, K. (1991). *Machine Learning: A Probabilistic Perspective*.
- De Paepe, A.E., Sierpowska, J., Garcia-Gorro, C., Martinez-Horta, S., Perez-Perez, J., Kulisevsky, J., Rodriguez-Dechicha, N., Vaquer, I., Subira, S., Calopa, M., et al. (2019). White matter cortico-striatal tracts predict apathy subtypes in Huntington's disease. *NeuroImage Clin.* *24*, 101965.
- Pagano, G., Niccolini, F., and Politis, M. (2016). Current status of PET imaging in Huntington's disease. *Eur. J. Nucl. Med. Mol. Imaging* *43*, 1171–1182.

- Pagonabarraga, J., Kulisevsky, J., Strafella, A.P., and Krack, P. (2015). Apathy in Parkinson's disease: Clinical features, neural substrates, diagnosis, and treatment. *Lancet Neurol.* *14*, 518–531.
- Palminteri, S., Justo, D., Jauffret, C., Pavlicek, B., Dauta, A., Delmaire, C., Czernecki, V., Karachi, C., Capelle, L., Durr, A., et al. (2012). Critical Roles for Anterior Insula and Dorsal Striatum in Punishment-Based Avoidance Learning. *Neuron* *76*, 998–1009.
- Paoli, R.A., Botturi, A., Ciammola, A., Silani, V., Prunas, C., Lucchiari, C., Zugno, E., and Caletti, E. (2017). Neuropsychiatric Burden in Huntington's Disease. *Brain Sci.* *7*.
- Papoutsis, M., Labuschagne, I., Tabrizi, S.J., and Stout, J.C. (2014). The cognitive burden in Huntington's disease: Pathology, phenotype, and mechanisms of compensation. *Mov. Disord.* *29*, 673–683.
- Paulsen, J.S. (2011). Cognitive impairment in Huntington disease: diagnosis and treatment. *Curr. Neurol. Neurosci. Rep.* *11*, 474–483.
- Paulsen, J.S., and Long, J.D. (2014). Onset of Huntington's disease: can it be purely cognitive? *Mov. Disord.* *29*, 1342–1350.
- Penney, J.B., and Young, A.B. (1983). SPECULATIONS ON THE FUNCTIONAL ANATOMY OF BASAL GANGLIA DISORDERS.
- Penny, W., Friston, K., Ashburner, J., Kiebel, S., and Nichols, T. (2007). *Statistical Parametric Mapping: The Analysis of Functional Brain Images* (Elsevier Ltd).
- Perry, D.C., and Kramer, J.H. (2015). Reward processing in neurodegenerative disease. *Neurocase* *21*, 120–133.
- Pessiglione, M., Seymour, B., Flandin, G., Dolan, R.J., and Frith, C.D. (2006). Dopamine-dependent prediction errors underpin reward-seeking behaviour in humans. *Nature* *442*, 1042–1045.
- Pezzulo, G., Rigoli, F., and Friston, K.J. (2018). Hierarchical Active Inference: A Theory of Motivated Control. *Trends Cogn. Sci.* *xx*, 1–13.
- Poldrack, R.A., Nichols, T., and Mumford, J. (2011). *Handbook of Functional MRI Data Analysis* (Cambridge University Press).
- Puterman, M.L. (2005). *Markov decision processes : discrete stochastic dynamic programming* (Wiley-Interscience).
- Raichle, M.E. (1998). Behind the scenes of functional brain imaging: A historical and physiological perspective. *Proc. Natl. Acad. Sci. U. S. A.* *95*, 765–772.
- Razi, A., Kahan, J., Rees, G., and Friston, K.J. (2015). Construct validation of a DCM for resting state fMRI. *Neuroimage* *106*, 1–14.
- Reedeker, N., Van Der Mast, R.C., Giltay, E.J., Van Duijn, E., and Roos, R.A.C. (2010). Hypokinesia in Huntington's disease co-occurs with cognitive and global dysfunctioning. *Mov. Disord.* *25*, 1612–1618.
- Reiner, A., and Deng, Y.-P. (2018). Disrupted striatal neuron inputs and outputs in Huntington's disease. *CNS Neurosci. Ther.* *24*, 250–280.
- Reiner, A., Shelby, E., Wang, H., Demarch, Z., Deng, Y., Guley, N.H., Hogg, V., Roxburgh, R., Tippett, L.J., Waldvogel, H.J., et al. (2013). Striatal parvalbuminergic neurons are lost in Huntington's disease: implications for dystonia. *Mov. Disord.* *28*, 1691–1699.
- Robert, P., Onyike, C.U., Leentjens, A.F.G., Dujardin, K., Aalten, P., Starkstein, S., Verhey, F.R.J., Yessavage, J., Clement, J.P., Drapier, D., et al. (2009). Proposed diagnostic criteria for apathy in Alzheimer's disease and other neuropsychiatric disorders. *Eur. Psychiatry* *24*, 98–104.
- Roos, R.A.C. (2010). Huntington's disease: A clinical review. *Orphanet J. Rare Dis.* *5*, 40.
- Ross, C. a, Aylward, E.H., Wild, E.J., Langbehn, D.R., Long, J.D., Warner, J.H., Scahill, R.I., Leavitt, B.R., Stout, J.C., Paulsen, J.S., et al. (2014a). Huntington disease: natural history, biomarkers and prospects for therapeutics. *Nat. Rev. Neurol.* *10*, 204–216.

- Ross, C.A., Aylward, E.H., Wild, E.J., Langbehn, D.R., Long, J.D., Warner, J.H., Scahill, R.I., Leavitt, B.R., Stout, J.C., Paulsen, J.S., et al. (2014b). Huntington disease: natural history, biomarkers and prospects for therapeutics. *Nat. Rev. Neurol.* *10*, 204–216.
- Rothkirch, M., Tonn, J., Köhler, S., and Sterzer, P. (2017). Neural mechanisms of reinforcement learning in unmedicated patients with major depressive disorder. *Brain* *140*, 1147–1157.
- Rüb, U., Vonsattel, J.P. V, Heinsen, H., and Korf, H.-W. (2015). The Neuropathology of Huntington's disease: classical findings, recent developments and correlation to functional neuroanatomy. *Adv. Anat. Embryol. Cell Biol.* *217*, 1–146.
- Rubin, J.E. (2017). Computational models of basal ganglia dysfunction: the dynamics is in the details. *Curr. Opin. Neurobiol.* *46*, 127–135.
- Rutledge, R.B., Dean, M., Caplin, A., and Glimcher, P.W. (2010). Testing the reward prediction error hypothesis with an axiomatic model. *J Neurosci* *30*, 13525–13536.
- Rutledge, R.B.B., Smittenaar, P., Zeidman, P., Brown, H.R.R., Adams, R.A.A., Lindenberger, U., Dayan, P., and Dolan, R.J.J. (2016). Risk Taking for Potential Reward Decreases across the Lifespan. *Curr. Biol.* *26*, 1–6.
- Salamone, J.D., Koychev, I., Correa, M., and Mcguire, P. (2015a). Neurobiological basis of motivational deficits in psychopathology. *Eur. Neuropsychopharmacol.* *25*, 1225–1238.
- Salamone, J.D., Pardo, M., Yohn, S.E., López-Cruz, L., SanMiguel, N., and Correa, M. (2015b). Mesolimbic Dopamine and the Regulation of Motivated Behavior. In *Current Topics in Behavioral Neurosciences*, (Springer Verlag), pp. 231–257.
- Salamone, J.D., Pardo, M., Yohn, S.E., López-Cruz, L., SanMiguel, N., and Correa, M. (2015c). Mesolimbic Dopamine and the Regulation of Motivated Behavior. In *Current Topics in Behavioral Neurosciences*, pp. 231–257.
- Scahill, R.I., Hobbs, N.Z., Say, M.J., Bechtel, N., Henley, S.M.D., Hyare, H., Langbehn, D.R., Jones, R., Leavitt, B.R., Roos, R.A.C., et al. (2013). Clinical impairment in premanifest and early Huntington's disease is associated with regionally specific atrophy. *Hum. Brain Mapp.* *34*, 519–529.
- Scahill, R.I., Andre, R., Tabrizi, S.J., and Aylward, E.H. (2017). Structural imaging in premanifest and manifest Huntington disease. In *Handbook of Clinical Neurology*, (Elsevier B.V.), pp. 247–261.
- Scahill, R.I., Zeun, P., Osborne-Crowley, K., Johnson, E.B., Gregory, S., Parker, C., Lowe, J., Nair, A., O'Callaghan, C., Langley, C., et al. (2020). Biological and clinical characteristics of gene carriers far from predicted onset in the Huntington's disease Young Adult Study (HD-YAS): a cross-sectional analysis. *Lancet Neurol.* *19*, 502–512.
- Schmidt, L., Braun, E.K., Wager, T.D., and Shohamy, D. (2014). Mind matters: placebo enhances reward learning in Parkinson's disease. *Nat. Neurosci.* *17*, 1793–1797.
- Schonberg, T., Daw, N.D., Joel, D., and O'Doherty, J.P. (2007). Reinforcement Learning Signals in the Human Striatum Distinguish Learners from Nonlearners during Reward-Based Decision Making. *J. Neurosci.* *27*, 12860–12867.
- Schulte, J., and Littleton, J.T. (2011). The biological function of the Huntingtin protein and its relevance to Huntington's Disease pathology. *Curr. Trends Neurol.* *5*, 65–78.
- Schultz, W. (2015). Neuronal Reward and Decision Signals: From Theories to Data. *Physiol. Rev.* *95*, 853–951.
- Schultz, W. (2016). Reward functions of the basal ganglia. *J. Neural Transm.* *123*, 679–693.
- Schultz, W., Dayan, P., Montague, P.R., Deichmann, R., Friston, K., and Dolan, R.J. (1997). A neural substrate of prediction and reward. *275*.
- Sellers, J., Ridner, S.H., and Claassen, D.O. (2020). A Systematic Review of Neuropsychiatric Symptoms and Functional Capacity in Huntington's Disease. *J. Neuropsychiatry Clin. Neurosci.* *32*, 109–124.

- Shen, W., Flajolet, M., Greengard, P., and Surmeier, D.J. (2008). Dichotomous dopaminergic control of striatal synaptic plasticity. *Science* (80-.). *321*, 848–851.
- Shen, W., Plotkin, J.L., Francardo, V., Ko, W.K.D., Xie, Z., Li, Q., Fieblinger, T., Wess, J., Neubig, R.R., Lindsley, C.W., et al. (2015). M4 Muscarinic Receptor Signaling Ameliorates Striatal Plasticity Deficits in Models of L-DOPA-Induced Dyskinesia. *Neuron* *88*, 762–773.
- Snowden, J.S. (2017). The Neuropsychology of Huntington’s Disease. *Arch. Clin. Neuropsychol.* 1–12.
- Soares, J.M., Magalhães, R., Moreira, P.S., Sousa, A., Ganz, E., Sampaio, A., Alves, V., Marques, P., and Sousa, N. (2016). A Hitchhiker’s guide to functional magnetic resonance imaging. *Front. Neurosci.* *10*, 515.
- Sockeel, P., Dujardin, K., Devos, D., Denève, C., Destée, A., and Defebvre, L. (2006). The Lille apathy rating scale (LARS), a new instrument for detecting and quantifying apathy: validation in Parkinson’s disease. *J. Neurol. Neurosurg. Psychiatry* *77*, 579–584.
- Sousa, M., Moreira, F., Jesus-Ribeiro, J., Marques, I., Cunha, F., Canário, N., Freire, A., and Januário, C. (2018a). Apathy Profile in Parkinson’s and Huntington’s Disease: A Comparative Cross-Sectional Study. *Eur. Neurol.* *79*, 13–20.
- Sousa, M., Moreira, F., Jesus-Ribeiro, J., Marques, I., Cunha, F., Canário, N., Freire, A., and Januário, C. (2018b). Apathy Profile in Parkinson’s and Huntington’s Disease: A Comparative Cross-Sectional Study. *Eur. Neurol.* *79*, 13–20.
- Staddon, J.E.R., and Cerutti, D.T. (2003). Operant Conditioning. *Annu. Rev. Psychol.* *54*, 115–144.
- Starkstein, S.E. (2000). Apathy and Withdrawal. *Int. Psychogeriatrics* *12*, 135–137.
- Starkstein, S.E., Petracca, G., Chemerinski, E., and Kremer, J. (2001). Article Syndromic Validity of Apathy in Alzheimer’s Disease.
- Starkstein, S.E., Jorge, R., Mizrahi, R., and Robinson, R.G. (2006). A prospective longitudinal study of apathy in Alzheimer’s disease. *J. Neurol. Neurosurg. Psychiatry* *77*, 8–11.
- Stephan, K.E., Penny, W.D., Moran, R.J., den Ouden, H.E.M., Daunizeau, J., and Friston, K.J. (2010). Ten simple rules for dynamic causal modeling. *Neuroimage* *49*, 3099–3109.
- Stern, A.F. (2014). The Hospital Anxiety and Depression Scale. *Occup. Med. (Chic. Ill.)*. *64*, 393–394.
- Stout, J.C., Paulsen, J.S., Queller, S., Solomon, A.C., Whitlock, K.B., Campbell, J.C., Carlozzi, N., Duff, K., Beglinger, L.J., Langbehn, D.R., et al. (2011). Neurocognitive signs in prodromal Huntington disease. *Neuropsychology* *25*, 1–14.
- Surmeier, D.J., Ding, J., Day, M., Wang, Z., and Shen, W. (2007). D1 and D2 dopamine-receptor modulation of striatal glutamatergic signaling in striatal medium spiny neurons. *Trends Neurosci.* *30*, 228–235.
- Sutton, R.S. (1988). Learning to predict by the methods of temporal differences. *Mach. Learn.* *3*, 9–44.
- Sutton, R.S., and Barto, A.G. (2012). Reinforcement learning. *Learning* *3*, 322.
- Sutton, R.S., and Barto, A.G. (2018). Reinforcement Learning : An Introduction (The MIT Press).
- Sutton, R.S., Precup, D., and Singh, S. (1999). Between MDPs and semi-MDPs: A framework for temporal abstraction in reinforcement learning.
- Tabrizi, S.J., Scahill, R.I., Durr, A., Roos, R.A.C., Leavitt, B.R., Jones, R., Landwehrmeyer, G.B., Fox, N.C., Johnson, H., Hicks, S.L., et al. (2011). Biological and clinical changes in premanifest and early stage Huntington’s disease in the TRACK-HD study: The 12-month longitudinal analysis. *Lancet Neurol.*
- Tabrizi, S.J., Reilmann, R., Roos, R.A.C., Durr, A., Leavitt, B., Owen, G., Jones, R., Johnson, H., Craufurd, D., Hicks, S.L., et al. (2012). Potential endpoints for clinical trials in

- premanifest and early Huntington's disease in the TRACK-HD study: analysis of 24 month observational data. *Lancet Neurol.* *11*, 42–53.
- Tabrizi, S.J., Scahill, R.I., Owen, G., Durr, A., Leavitt, B.R., Roos, R.A., Borowsky, B., Landwehrmeyer, B., Frost, C., Johnson, H., et al. (2013). Predictors of phenotypic progression and disease onset in premanifest and early-stage Huntington's disease in the TRACK-HD study: analysis of 36-month observational data. *Lancet Neurol.* *12*, 637–649.
- Tabrizi, S.J., Leavitt, B.R., Landwehrmeyer, G.B., Wild, E.J., Saft, C., Barker, R.A., Blair, N.F., Craufurd, D., Priller, J., Rickards, H., et al. (2019). Targeting Huntingtin Expression in Patients with Huntington's Disease. *N. Engl. J. Med.* *380*, 2307–2316.
- Thompson, J.C., Snowden, J.S., Craufurd, D., and Neary, D. (2002). Behavior in Huntington's Disease. *J. Neuropsychiatry Clin. Neurosci.* *14*, 37–43.
- Thompson, J.C., Harris, J., Sollom, A.C., Cheryl Stopford, M.L., Howard, E., Julie Snowden, Mbc.S., and Craufurd, D. (2012). Longitudinal Evaluation of Neuropsychiatric Symptoms in Huntington's Disease.
- Tippett, L.J., Waldvogel, H.J., Thomas, S.J., Hogg, V.M., Roon-Mom, W. Van, Synek, B.J., Graybiel, A.M., Faull, R.L.M., van Roon-Mom, W., Synek, B.J., et al. (2007). Striosomes and mood dysfunction in Huntington's disease. *Brain* *130*, 206–221.
- Treadway, M.T., Bossaller, N.A., Shelton, R.C., and Zald, D.H. (2012). Effort-based decision-making in major depressive disorder: A translational model of motivational anhedonia. *J. Abnorm. Psychol.* *121*, 553–558.
- Tziortzi, A.C., Haber, S.N., Searle, G.E., Tsoumpas, C., Long, C.J., Shotbolt, P., Douaud, G., Jbabdi, S., Behrens, T.E.J., Rabiner, E.A., et al. (2014). Connectivity-based functional analysis of dopamine release in the striatum using diffusion-weighted MRI and positron emission tomography. *Cereb. Cortex* *24*, 1165–1177.
- Vonsattel, J.P.G., Keller, C., and Cortes Ramirez, E.P. (2011). Huntington's disease - neuropathology (Elsevier B.V.).
- Voon, V., Pessiglione, M., Brezing, C., Gallea, C., Hubert, H., Dolan, R.J., and Hallett, M. (2011). Mechanisms underlying dopamine-mediated reward bias in compulsive behaviors. *Neuron* *65*, 1–14.
- Waldvogel, H.J., Kim, E.H., Thu, D.C. V, Tippett, L.J., and Faull, R.L.M. (2012). New perspectives on the neuropathology in Huntington's disease in the human brain and its relation to symptom variation. *J. Huntingtons. Dis.* *1*, 143–153.
- Waldvogel, H.J., Kim, E.H., Tippett, L.J., Vonsattel, J.G., and Faull, R.L.M. (2015). The Neuropathology of Huntington's Disease. *Curr Top. Behav Neurosci* 33–80.
- Wallis, J.D., and Rushworth, M.F.S. (2013). *22: Integrating Benefits and Costs in Decision Making* (Elsevier Inc.).
- Walton, M.E., and Bouret, S. (2019). What Is the Relationship between Dopamine and Effort? *Trends Neurosci.* *42*, 79–91.
- Weiskopf, N., Hutton, C., Josephs, O., and Deichmann, R. (2006). Optimal EPI parameters for reduction of susceptibility-induced BOLD sensitivity losses: A whole-brain analysis at 3 T and 1.5 T. *Neuroimage* *33*, 493–504.
- Wiatr, K., Szlachcic, W.J., Trzeciak, M., Figlerowicz, M., and Figiel, M. (2018). Huntington Disease as a Neurodevelopmental Disorder and Early Signs of the Disease in Stem Cells. *Mol. Neurobiol.* *55*, 3351–3371.
- Wigert, B.E.N., Ph, D., Harter, J.I.M., Ph, D., Sheehan, C., Streur, J., Boyle, E.O., Cooper, S., Sutton, R., Dvorak, N., et al. (2017). Re-Engineering Performance Management.
- Wild, E.J., and Tabrizi, S.J. (2017). Therapies targeting DNA and RNA in Huntington's disease. *Lancet Neurol* *16*, 837–847.
- Wilson, R.C., and Niv, Y. (2015). Is Model Fitting Necessary for Model-Based fMRI? *PLOS Comput. Biol.* *11*, e1004237.

- Wilson, H., Dervenoulas, G., and Politis, M. (2018a). Structural Magnetic Resonance Imaging in Huntington's Disease. In *International Review of Neurobiology*, pp. 335–380.
- Wilson, R.P., Colizzi, M., Bossong, M.G., Allen, P., Kempton, M., Abe, N., Barros-Loscertales, A.R., Bayer, J., Beck, A., Bjork, J., et al. (2018b). The Neural Substrate of Reward Anticipation in Health: A Meta-Analysis of fMRI Findings in the Monetary Incentive Delay Task. *Neuropsychol. Rev.* 28, 496–506.
- van Wouwe, N.C., Kanoff, K.E., Claassen, D.O., Richard Ridderinkhof, K., Hedera, P., Harrison, M.B., and Wylie, S.A. (2016). The Allure of High-Risk Rewards in Huntington's disease. *J. Int. Neuropsychol. Soc.* 22, 426–435.
- Yager, L.M., Garcia, A.F., Wunsch, A.M., and Ferguson, S.M. (2015). The ins and outs of the striatum: Role in drug addiction. *Neuroscience* 301, 529–541.
- Zaitsev, M., Akin, B., LeVan, P., and Knowles, B.R. (2017). Prospective motion correction in functional MRI. *Neuroimage* 154, 33–42.
- Zalocusky, K.A., Ramakrishnan, C., Lerner, T.N., Davidson, T.J., Knutson, B., and Deisseroth, K. (2016). Nucleus accumbens D2R cells signal prior outcomes and control risky decision-making. *Nature* 531, 642–646.
- van de Zande, N.A., Massey, T.H., McLauchlan, D., Pryce Roberts, A., Zutt, R., Wardle, M., Payne, G.C., Clenaghan, C., Tijssen, M.A.J., Rosser, A.E., et al. (2017). Clinical characterization of dystonia in adult patients with Huntington's disease. *Eur. J. Neurol.* 24, 1140–1147.
- Zeidman, P., Jafarian, A., Corbin, N., Seghier, M.L., Razi, A., Price, C.J., and Friston, K.J. (2019a). A guide to group effective connectivity analysis, part 1: First level analysis with DCM for fMRI. *Neuroimage* 200, 174–190.
- Zeidman, P., Jafarian, A., Seghier, M.L., Litvak, V., Cagnan, H., Price, C.J., and Friston, K.J. (2019b). A guide to group effective connectivity analysis, part 2: Second level analysis with PEB. *Neuroimage* 200, 12–25.
- Zuccato, C., and Cattaneo, E. (2016). The Huntington's Paradox. *Sci. Am.* 315, 56–61.
- Zuccato, C., Valenza, M., and Cattaneo, E. (2010). Molecular mechanisms and potential therapeutical targets in Huntington's disease. *Physiol. Rev.* 90, 905–981.
- (1996). Unified Huntington's disease rating scale: Reliability and consistency. *Mov. Disord.* 11, 136–142.

Chapter 8: Appendix

8.1 HD-YAS Eligibility Criteria

8.1.1 Inclusion criteria

- a. Are 18-40 years of age, inclusive; and
- b. Are capable of providing informed consent and
- c. Are capable of complying with study procedures and

For the Healthy Control group, participants eligible are persons who meet the following criteria:

- d. Have no known family history of Huntington's disease (family control or community control) *; or
- e. Have known family history of Huntington's disease but have been tested for the huntingtin gene CAG expansion and are not at genetic risk for Huntington's disease (CAG < 36) (gene negative).

For the Young Adult Premanifest Huntington's disease group, participants eligible are persons who meet the additional following criteria:

- f. Do not have clinical diagnostic motor features of Huntington's disease, defined as Unified Huntington's Disease Rating Scale (UHDRS) Diagnostic Confidence Score1 < 4; and
- g. Have CAG expansion ≥ 40 and
- h. A disease burden score (DBS) ≤ 240 **

* Family controls were partners or spouses of someone either with the Huntington's disease gene or at risk of Huntington's disease due to having a 1st degree relative with Huntington's disease. Community controls were either friends of someone with

246

or at risk of Huntington's disease, or from the wider Huntington's disease community recruited via advertisement through Huntington's disease support groups.

** The rationale for this DBS cut-off is that this boundary corresponds approximately to >18 years to estimated disease onset according to the Langbehn formula.

8.1.2 Exclusion criteria

- a. Current use of investigational drugs or participation in a clinical drug trial within 30 days prior to study visit; or
- b. Current intoxication, drug or alcohol abuse or dependence; or
- c. If using any antidepressant, psychoactive, psychotropic or other medications or nutraceuticals used to treat Huntington's disease, the use of inappropriate (e.g., non-therapeutically high) or unstable dose within 30 days prior to study visit; or
- d. Significant medical, neurological or psychiatric co-morbidity likely***, in the judgment of the Principal Investigator, to impair participant's ability to complete essential study procedures; or
- e. Predictable non-compliance as assessed by the Principal Investigator; or
- f. Inability or unwillingness to undertake any of the essential study procedures; or g. Needle phobia; or
- h. Contraindication to MRI, including, but not limited to, MR-incompatible pacemakers, recent metallic implants, foreign body in the eye or other indications, as assessed by a standard pre-MRI questionnaire; or
- i. Pregnant (as confirmed by urine pregnancy test); or
- j. Claustrophobia, or any other condition that would make the subject incapable of undergoing an MRI.

For the optional cerebrospinal fluid (CSF) collection only

- k. Needle phobia, frequent headache, significant lower spinal deformity or major surgery; or
 - l. Antiplatelet or anticoagulant therapy within the 14 days prior to sampling visit, including but not limited to:
aspirin, clopidogrel, dipyridamole, warfarin, dabigatran, rivaroxaban and apixaban; or
 - m. Clotting or bruising disorder; or
 - n. Screening blood test results outside the clinical laboratory's normal range for the following: white cell count, neutrophil count, lymphocyte count, haemoglobin (Hb), platelets, prothrombin time or activated partial thromboplastin time; or
 - o. Screening blood test results for C-reactive protein $>2\times$ upper limit of normal; or
 - p. Exclusion during history or physical examination, final decision to be made by the Principal Investigator; including but not limited to:
 - i any reason to suspect abnormal bleeding tendency, e.g. easy bruising, petechial rash; or
 - ii any reason to suspect new focal neurological lesion, e.g. new headache, optic disc swelling, asymmetric focal long tract signs; or
 - iii any other reason that, in the clinical judgment of the operator or the Principal Investigator, it is felt that lumbar puncture is unsafe.
- *** Comorbidities are assessed for during an interview asking about current and previous medical and drug history. The T1 weighted MRI brain was reviewed by an experienced consultant neuroradiologist and CSF white and red cell counts were also reviewed to further ensure absence of neurological comorbidity.

8.2 TrackOn Eligibility Criteria

8.2.1 Inclusion Criteria

Written informed consent must be obtained from the participant, who must agree to all the assessments. In addition:

1. All participants should be able to tolerate MRI and sample donation
2. Participants will be either
 - a. Control participant
 - i. An existing control participant previously enrolled in TRACK-HD
 - ii. A newly recruited control participant who is either
 - Partner/spouse of a participant, not at risk of HD (note these participants will not have CAG repeat testing)
 - HD Normal repeat length sibling or HD normal repeat length control volunteer
 - b. Premanifest gene carrier
 - An existing premanifest gene carrier previously enrolled in TRACK-HD
 - A newly recruited premanifest gene carrier with:
 - Positive genetic test with CAG repeat length ≥ 40 and
 - Burden of pathology score (CAG-35.5) \times age >250

8.2.2 Exclusion Criteria

1. Stage 1 (UHDRS diagnostic confidence score of 4) or greater at time of enrolment, unless previously enrolled as a premanifest participant in TRACK-HD
2. Less than 18 years of age
3. More than 65 years of age (unless previously enrolled in TRACK-HD)

4. Major psychiatric disorder at time of enrolment
5. Concomitant significant neurological disorder
6. Concomitant significant medical illness
7. Unsuitability for MRI, e.g. claustrophobia, metal implants
8. Unwillingness to donate blood
9. History of significant head injury
10. Predictable non-compliance by drug and/or alcohol abuse
11. Significant hand injuries that preclude either writing or rapid computerized responding
12. Participant in Predict-HD
13. Currently participating in a clinical drug trial